DISS. ETH NO. 24542

Transport and evolution of terrestrial organic carbon signals along the Danube River basin

A thesis submitted to attain the degree of

DOCTOR OF SCIENCES of ETH ZÜRICH

(Dr. Sc. ETH Zürich)

presented by

Chantal Valérie Freymond
MSc in Environmental Geosciences, University of Basel
born on April 16, 1986
citizen of Basel-Stadt, Switzerland

accepted on the recommendation of

Prof. Dr. Timothy I. Eglinton, examiner
Dr. Ir. Francien Peterse, co-examiner
Dr. Maarten Lupker, co-examiner
Prof. Dr. Thomas Bianchi, external-examiner

-2018-

Summary

Rivers are the main land-to-ocean transport mechanism for transfer of particulate organic carbon (OC) mobilized on the continents to the ocean. Steady deposition and burial of terrigenous OC on continental margins act as a net sink for carbon, including that additionally mobilized by human intervention in the global carbon cycle. At the same time, valuable and continuous archives of environmental conditions on the continents are built up through the accumulation of sediment in front of river systems. However, the evolution of OC as it moves through river basins from biological source to the depositional sink, and the corresponding timescales of this carbon transfer are not well constrained. In this thesis, these questions are addressed with a detailed basin-wide investigation of the Danube River system, the second largest river basin in Europe. River sediment was collected along the Danube mainstem from headwaters to the Black Sea and at 12 tributaries close to their confluences with the Danube. The fine fraction (<63 μm) of this sediment was analyzed for sedimentological parameters (mineralogy, grain size, mineral-specific surface area), as well as the abundances, distributions and isotopic compositions (^{13}C, ^{14}C) of bulk OC and specific biomarker compounds. Branched glycerol dialkyl glycerol tetraethers (brGDGTs) were evaluated as indicators of soil-derived OC, whereas long-chain leaf wax fatty acids (FAs) and lignin phenols served as markers for higher plant-derived OC. Total OC, FA and brGDGT concentrations normalized to mineral-specific surface area show a systematic decrease of 70–80% along the course of the Danube, suggesting significant reduction in OC loading due to either degradation or dilution with a high-surface-area but low-OC source such as loess, which occurs extensively in the middle and lower Danube basin. The evolving characteristics of brGDGT distributions as well as plant wax FA stable isotopic signatures suggest significant inputs of locally-derived OC to the sediment load along the course of the Danube river mainstem. A mixing model including bulk OC $\delta^{13}C$ and ^{14}C further reveals that soil is the main contributor of OC in fluvial sediments throughout the basin, however, the contribution from loess increases from the middle to the lower basin, accounting for up to 37% of OC close to the river terminus at the Black Sea. The integrated transport or residence time of total OC and higher plant derived OC in the Danube is determined to be 2,130 and 2,790 years, respectively. Assuming these ages correspond to average residence times, model calculations that take into account accompanying changes in OC loading imply that complete degradation would occur with transport time >2,700 years. These calculations suggest that the majority of the upstream OC signal would be degraded by the time it reaches the terminus of the river. It is concluded that the combined effect of loss due to degradation and loess OC addition leads to the observed decrease in OC and biomarker loadings as well as to the gradual aging trend along the river. Additionally to the longitudinal investigation of river sediment along the Danube, an in-depth study of the bulk and molecular

composition of suspended particulate matter in depth profiles across a river cross-section close to the outflow of the Danube was performed. Instantaneous OC and biomarker fluxes to the Black Sea were determined with this 'picket-fence' approach. Comparing brGDGT and FA-derived proxies and bulk and compound-specific stable isotope values from suspended matter in the cross-section to sediment deposited on riverbanks reveals that the fine fraction of freshly deposited sediment on riverbanks may serve as a proxy for the suspended particulate matter in a well mixed river such as the Danube. The finding that about 8 kg particulate OC per second are discharged by the Danube underlines the importance of global riverine OC export as a transport mechanism for terrestrial OC to the ocean. Further, this thesis shows that the OC load in a river evolves during transport, and highlights the importance of provenance studies and consideration of continental residence times for robust interpretation of paleo-environmental signals preserved in sedimentary records.

Zusammenfassung

Flüsse stellen den wichtigsten Transportmechanismus für den Transfer von partikulärem organischen Kohlenstoff dar, welcher von den Kontinenten zu den Ozeanen transportiert wird. Die kontinuierliche Deposition von organischem Kohlenstoff auf Kontinentalrändern ist eine aktive Senke für Kohlenstoff aus natürlichen Quellen und Kohlenstoff, der durch anthropogenes Eingreifen in den globalen Kohlenstoffkreislauf zusätzlich mobilisiert wurde. Gleichzeitig entstehen durch die kontinuierliche Sedimentakkumulation vor Flussmündungen wertvolle Archive mit Informationen über kontinentale Umweltbedingungen. Aus diesen Gründen gibt es zahlreiche offene Fragen zur Entwicklung der Zusammensetzung des organischen Kohlenstoffs während des fluviatilen Transports von seiner biologischen Quelle zur Ablagerung sowie zu der Transportdauer. In der vorliegenden Dissertation werden diese Fragen anhand einer detaillierten Untersuchung über das gesamte Einzugsgebiet der Donau als zweitgrössten Fluss Europas behandelt. Vom Oberlauf bis zur Mündung ins Schwarze Meer wurden entlang des Donauhauptarms und an 12 Zuflüssen Flusssedimente beprobt. Die Feinfraktion des Sedimentes (<63 μm) wurde auf sedimentologische Parameter (Mineralogie, Korngrössenverteilung, Mineraloberfläche) und das Vorkommen, sowie bezüglich der strukturellen und Isotopen-Zusammensetzung (^{13}C, ^{14}C) von Gesamtkohlenstoff und spezifischen Biomarkern untersucht. Bakterielle Membranlipide (brGDGTs) wurden als Indikatoren für aus Böden stammenden organischen Kohlenstoff bestätigt und verwendet. Weiter wurden langkettige Fettsäuren von Pflanzenwachsen und Lignin Phenole als Marker für Kohlenstoff von höheren Pflanzen genutzt. Somit konnten die Konzentrationen des Gesamtkohlenstoffes, der Fettsäuren und der brGDGTs auf die Mineraloberfläche normalisiert und ein systematischer Rückgang von 70–80% entlang der Donau vermerkt werden. Dieser signifikante Rückgang der 'Beladung' der Mineraloberflächen mit organischem Kohlenstoff kann entweder durch den Abbau von organischem Material oder der Verdünnung durch Sediment mit hoher Mineraloberfläche, aber tiefem Kohlenstoffgehalt verursacht werden. Eine solche Sedimentquelle könnte feinkörniger Löss darstellen, der im mittleren und unteren Donaubecken vermehrt vorkommt. Die sich ändernde Zusammensetzung von brGDGTs und stabilen Pflanzenwachsisotopen entlang der Donau deuten auf eine signifikante Zufügung von lokalem organischen Kohlenstoff zur Sedimentfracht des Donauhauptarmes hin. Mit einem aus Gesamtkohlenstoff $\delta^{13}C$ und ^{14}C bestehendem Mischmodell, konnte gezeigt werden, dass der Boden die Hauptquelle von organischem Kohlenstoff im Flusssediment entlang des gesamten Donauverlaufs darstellt. Im Verlauf nimmt der Lössanteil im mittleren und unteren Donaubecken zu und erreicht ein Maximum von 37% des organischen Kohlenstoffs im Flusssediment an der Mündung zum Schwarzen Meer. Die integrierten Transportzeiten von organischem Gesamtkohlenstoff und spezifischem Pflanzen-Kohlenstoff wurden auf 2'130 und 2'790 Jahre berechnet. Basierend auf der Annahme,

dass diese zwei Transportzeiten die durchschnittliche Verweildauer darstellen, wurde unter Berücksichtigung des Rückgangs der Beladung der Mineraloberflächen die Transportzeit modelliert, nach der der gesamte organischen Kohlenstoff abgebaut ist, wodurch ein Ergebnis von >2'700 Jahre ermittelt werden konnte. Diese Berechnung deutet darauf hin, dass die Mehrheit des organischen Kohlenstoffs aus den oberen Bereichen des Einzugsgebietes abgebaut ist, bevor sie das Schwarze Meer erreicht. Es ergibt sich das Fazit, dass der kombinierte Effekt von Abbau von organischem Material und Zufügen von Löss zu dem gemessenen Rückgang der Mineraloberflächenbeladung mit organischem Gesamtkohlenstoff und Biomarkern sowie dem graduellen Alterungstrend entlang der Donau führt. Zusätzlich zu der Untersuchung von Flusssedimenten entlang der Donau wurde anhand von Tiefenprofilen über einen Flussquerschnitt die Zusammensetzung von organischem Gesamtkohlenstoff und Biomarkern in Suspension gehaltenem partikulären Sediment in der Donau nahe der Mündung zum Schwarzen Meer untersucht. Mit dieser detaillierten Untersuchung wurden Zeitpunkt-spezifische Abflüsse von organischem Gesamt-kohlenstoff und Biomarkern berechnet. Weiterhin wurde die Zusammensetzung von brGDGTs und Pflanzenwachsen sowie die organischen Gesamtkohlenstoff- und Biomarker-spezifischen Isotopenwerte in suspendiertem Sediment im Flussquerschnitt mit dem am Ufer abgelagerten Flusssediment verglichen. So konnte gezeigt werden, dass die Feinfraktion von frisch abgelagerten Ufersedimenten die organische Zusammensetzung von suspendiertem Sediment in einem gut durchmischten Fluss wie der Donau angemessen repräsentiert. Die Erkenntnis, dass ca. 8 kg partikulärer organischer Kohlenstoff pro Sekunde von der Donau ins Schwarze Meer exportiert werden, zeigt die Bedeutung von Flüssen für den Transport des organischen Kohlenstoffes von den Kontinenten in die Ozeane. Darüber hinaus legt diese Dissertation dar, dass sich die Zusammensetzung von organischem Kohlenstoff in Flusssedimenten während des Transports verändert. Dadurch wird auf die Bedeutung von Studien zu Kohlenstoffquellen für Flusssedimente und die Berücksichtigung der Verweildauer auf Kontinenten für eine aussagekräftige Interpretation von Sedimentablagerungen hingewiesen.

Table of Contents

Chapter 1

Introduction

1.1 Motivation and main objectives

In the Anthropocene, the era of climate change and anthropogenic perturbations of natural processes, a better understanding of the carbon cycle, including reservoir sizes, interactions and corresponding carbon sources and sinks, is key for future climate predictions and politics. Rivers form a crucial link between terrigenous and oceanic carbon pools, exporting 200 megatonnes (Mt) particulate organic carbon (POC) and 19,000 Mt sediment yearly (Milliman and Farnsworth, 2011; Galy et al., 2015). Even though carbon burial efficiency on continental margins is generally low (Burdige, 2005), organic carbon discharged by rivers and buried in ocean sediments comprises an important sink of carbon additionally mobilized by fossil fuel burning and land use change. However, sources of organic carbon (OC) buried in front of river mouths, its fate as it is transported along the land ocean continuum, and corresponding residence times within drainage basins remains unclear, and is a topic of recent research (Diefendorf and Freimuth, 2017). Better understanding of OC sources, transport mechanisms and times also helps to more precisely interpret the sedimentary archive full of information on continental climate building up with continuous deposition and burial of terrigenous sediment on continental margins.

In this thesis, a detailed investigation of sediments along the course of a major modern river system is carried out to assess the evolution of the OC composition from the headwaters to its terminus. With the help of organic markers specific to higher plants and soil bacteria, constraints are placed on the sources of organic carbon to Danube River sediments and their residence times in the catchment. Finally, the organic carbon signal that eventually reaches the delta and instantaneous fluxes of organic carbon and biomarkers to the Black Sea are determined and compared to corresponding signals reported in Black Sea surface sediments.

1.2 Thoughts on the global carbon cycle

The carbon cycle has emerged as an important and pressing topic in society and politics since the influence of elevated greenhouse gas concentrations on the global climate has been recognized. The atmospheric CO_2 concentration exceeded 400 ppm in 2015, and is now at levels that are higher than during the past several million years (Graven, 2016). The atmosphere with its short turnover time is a small carbon reservoir compared to the largest reservoirs, namely sedimentary rocks, the ocean and soils (Drenzek, 2007), and is therefore sensitive to changes in other carbon reservoirs. Anthropogenic perturbations, mainly fossil fuel combustion and land use change, have significantly increased the carbon fluxes and created short-cuts between reservoirs, resulting in a dramatic rise in atmospheric CO_2 since the industrial revolution. The oceans and the biosphere take up large amounts of carbon emitted during fossil fuel burning. However, vegetation and

soil as a natural carbon sink are nearly neutralized due to losses caused by land use change (Graven, 2016). Rivers act as a net carbon sink, transferring carbon from faster cycling terrigenous carbon pools to ocean sediments, where carbon may be sequestered indefinitely (Berner, 1982).

1.3 Rivers as transport mechanism for organic carbon

Rivers are basin integrators, discharging erosional material from the entire catchment (Viers et al., 2009). However, what seems to be true for conservative elements is probably not applicable to organic carbon.

Organic carbon in river sediments is a complex mixture of components derived from different sources. Soils are generally seen as a main contributor (e.g. Gordon and Goni, 2003), itself being a complex mixture of fresh plant litter and soil fauna, pre-aged and petrogenic organic carbon. Degradation and soil formation processes alter the OC composition by preferential removal of (labile) compounds while other processes such as the formation of aggregates and organo-mineral associations serve to stabilize organic matter for centuries to millennia (von Lützow et al., 2006). Through soil erosion and mass-wasting events, soil organic carbon is mobilized and eventually introduced to a river system. Modern sources of carbon to a river include fresh plant material, added to rivers by surface runoff, or autochthonous organic matter from within-river autotrophic and heterotrophic biomass production. Petrogenic carbon input results from the erosion of sedimentary rocks and anthropogenic inputs (e.g., fossil fuel or petrochemical contaminants). Organic carbon is subject of ongoing consumption and degradation processes along the course of the river, and therefore undergoes alteration throughout its transport from terrigenous source to the depositional sink, both on the continent and further during cross-shelf transport (Blair et al., 2004). This complex interplay between diverse sources and processes renders it challenging to constrain the origin, fate, and dynamics, of carbon within river drainage basins.

1.4 Organic carbon stabilization mechanisms

OC in soils and sediments has been found to be often associated with the mineral phase (Blair and Aller, 2012; Doetterl et al., 2015). Sorption to mineral surfaces, mainly to clay-sized phyllosilicates with large and reactive surfaces, is a result of chemical interactions (e.g. cation bridging, Van der Waals forces) and occlusion in aggregates and fine pores. This mineral association reduces the availability of OC to decomposers and slows down degradation (Keil and Mayer, 2014). The OC-rich fine fraction as well as the free light fraction (i.e. plant debris) are preferentially eroded and transported across the landscape compared to coarser mineral grains with low OC content (Doetterl et al.,

2016). In rivers, the hydrodynamic behavior of particles, driven by density, size and shape, further influences suspension and deposition and therefore transport (Blair and Aller, 2012), resulting in preferential transportation of the fine fraction.

Positive correlations of OC and fine-grained minerals and therefore mineral specific surface area (SA) were found in soils and ocean sediments (Keil and Mayer, 2014). Therefore, a typical OC/SA ratio range was defined for river suspended sediment dominated continental margin deposits (Blair and Aller, 2012). However, the timescale of organo-mineral association persistence in general and especially the fate of OC in soil derived organo-mineral associations in rivers are unclear because of possible weathering of the mineral matrix in aquatic environments and aggregate break up (Blair and Aller, 2012; Doetterl et al., 2016).

1.5 Radiocarbon dating

The radioactive ^{14}C isotope is naturally produced by cosmic rays in the upper atmosphere (Schuur et al., 2016). After oxidation to CO_2, ^{14}C enters the biosphere through primary production and has been used as a tracer in the global carbon cycle. ^{14}C decays with a half-life of 5,730 years, enabling dating of organic compounds after death of the source organism back to ~50,000 years. Human activities, i.e. nuclear bomb testing in the early 1960s and fossil fuel burning, alter the ^{14}C content in the atmosphere significantly, which needs to be taken into account when dating organic material (Schuur et al., 2016).

Radiocarbon dating of soil OC is for example used to determine the turnover time in soils and to study soil carbon dynamics in general, since the soil OC pool is expected to play a key role as carbon source and/or sink with changing climate (Trumbore, 2009; Graven, 2016). A further application is to use the significantly increased atmospheric ^{14}C of the so-called "bomb spike" to investigate fluxes between different carbon reservoirs (Trumbore, 2009). These diverse applications make radiocarbon a powerful tool to constrain carbon dynamics. However, investigating on a bulk scale has its limitations due to the various carbon sources that range from modern to 'radiocarbon dead'. An additional layer of information can therefore be added through compound-specific dating of specific molecules.

1.6 Biomolecular markers

Biomarkers are organic molecules, generally consisting of a distinctive carbon skeleton, with covalently bound hydrogen atoms and often a functional group (e.g., acid, ketone or alcohol). Important characteristics of biomarkers are their recalcitrance against decomposition during transportation, sedimentation and early diagenesis in addition to their abundance and source specificity (e.g., for Bacteria, Archaea and eukaryotes including higher plants; Peters et al., 2005). Specific to source organism and physiological function, biomarkers encode information about environmental conditions under which they were produced. In this thesis, three different groups of biomarkers are used to trace the origin and fate of terrigenous organic carbon within the catchment and transport along a major river system.

1.6.1 Plant wax fatty acids

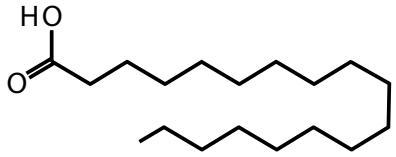

Figure 1.1. Plant wax fatty acid.

Surfaces of higher land plants are usually covered by a waxy layer, which helps the plant to regulate its water balance and serves as protection against mechanical damage, fungal and insect attack and UV radiation. Plant waxes consist of alkanes, alcohols and fatty acids amongst other molecules (Eglinton and Hamilton, 1967; Eglinton and Eglinton, 2008). In this thesis, the focus lays on long chain plant wax fatty acids (FA) with chain lengths of 24–32 carbon atoms due to their specificity to higher plants, high abundance in Danube sediments and insensitivity to anthropogenic (fossil carbon) inputs that for example can impact long chain alkane signatures. FA signals are characterized according to the abundance and distribution of different chain lengths, e.g. average chain lengths (ACL) and carbon preference index (CPI).

Stable carbon and hydrogen (H) isotope ratios contain detailed information about the plant type and its environment. The $\delta^{13}C$ value of FAs depends on the CO_2 used for biomass synthesis and the photosynthetic pathway of the source plant. Most temperate plants, including trees, shrubs and grasses use the C3 pathway to fix carbon during photosynthesis, resulting in distinct $\delta^{13}C$ values compared to C4 plants that predominantly grow in warmer and dryer regions. $\delta^{2}H$ values of FAs reflect the isotopic composition of the plant available water that changes with elevation and distance from the ocean, and isotopic fractionation driven by plant physiological and environmental parameters like water availability and accordingly stress (Sachse et al., 2012).

A further layer of information is added with the radiocarbon composition of FAs. A constant $^{14}C/^{12}C$ ratio in equilibrium with the atmosphere is prevailed within living organisms. With death and stop of constant cell renewal, the ^{14}C content starts to

decrease with a half-life of 5,730 years. Due to its temporal aspect, FA ^{14}C, as well as bulk sediment ^{14}C, can be used to disentangle different OC sources in river sediments (e.g. Marwick et al., 2015; Tao et al., 2015).

1.6.2 BrGDGTs as soil markers

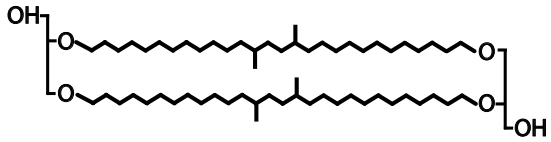

Figure 1.2. BrGDGT representative.

Branched glycerol dialkyl glycerol tetraethers (brGDGTs) are a relatively newly identified (Sinninghe Damsté et al., 2000) but widely studied group of biomarker compounds with great potential for palaeoclimatology (e.g. Weijers et al., 2007; Sinninghe Damsté et al., 2012). BrGDGTs are membrane lipids, most likely of heterotrophic bacteria in soils and peat (Weijers et al., 2009; Sinninghe Damsté et al., 2011) and have been found to also be produced in lakes and rivers (Tierney and Russell, 2009; De Jonge et al., 2014b). The molecular structure of their carbon skeleton shows adaptations to environmental conditions in the way that the incorporation of varying amounts of methyl groups ('branches') and rings was found to correlate with mean annual air temperature and soil pH (De Jonge et al., 2014a).

In this thesis, brGDGTs are used as markers for soil organic carbon input to river sediments since the contribution of in-river production has shown to be minor (see chapter 2) and to trace the soil OC signal along the Danube River.

1.6.3 Lignin phenols

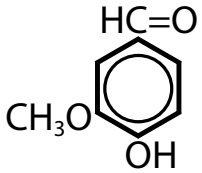

Figure 1.3. Lignin phenol representative.

Lignin is a macromolecule synthesized by vascular plants to give stability and structure to cells. The abundance of different phenols in this macromolecule refers to the composition of the vegetation cover (gymnosperm vs. angiosperm and woody vs. non-woody vegetation) and the degree of decomposition (Hedges and Mann, 1979; Hedges et al., 1988).

Here, the abundance of total lignin as specific marker for plant derived OC, in addition to FAs and brGDGTs, is set in context with sedimentological parameters to better constrain OC transport mechanisms along the Danube (see chapter 3).

1.7 The Danube River

1.7.1 An international river

The Danube River is an international river that crosses or borders nine countries, with eleven more countries that lie partially within its catchment (Figure 1.4; Miklós, 2010). Common interests like flood protection, water quality, power production and inland navigation connect these countries. To face and coordinate common challenges and goals, international collaboration is important and started early (in 1948, coordination of inland water navigation started; Schiller et al., 2010), resulting for example in the publication of the Hydrological Monograph of the Danube and its Catchment in 1986 (UNESCO, 1986). The International Commission for the Protection of the Danube River (ICPDR) is a key association working on the sustainable development and use of the Danube and its tributaries, including intense research and monitoring (www.icpdr.org). Full Danube survey cruises with an international scientific crew from various fields (water quality, pollutants, ecology, invasive alien species, hydromorphology, etc.) took place in 2001, 2007 and 2013. Besides this, annual reports are published and data from monitoring stations are collected in a common database (https://danubis.icpdr.org). The Danube Commission is an international intergovernmental organization responsible for the navigation on the Danube, which is a main waterway for commercial vessels (http://www.danubecommission.org).

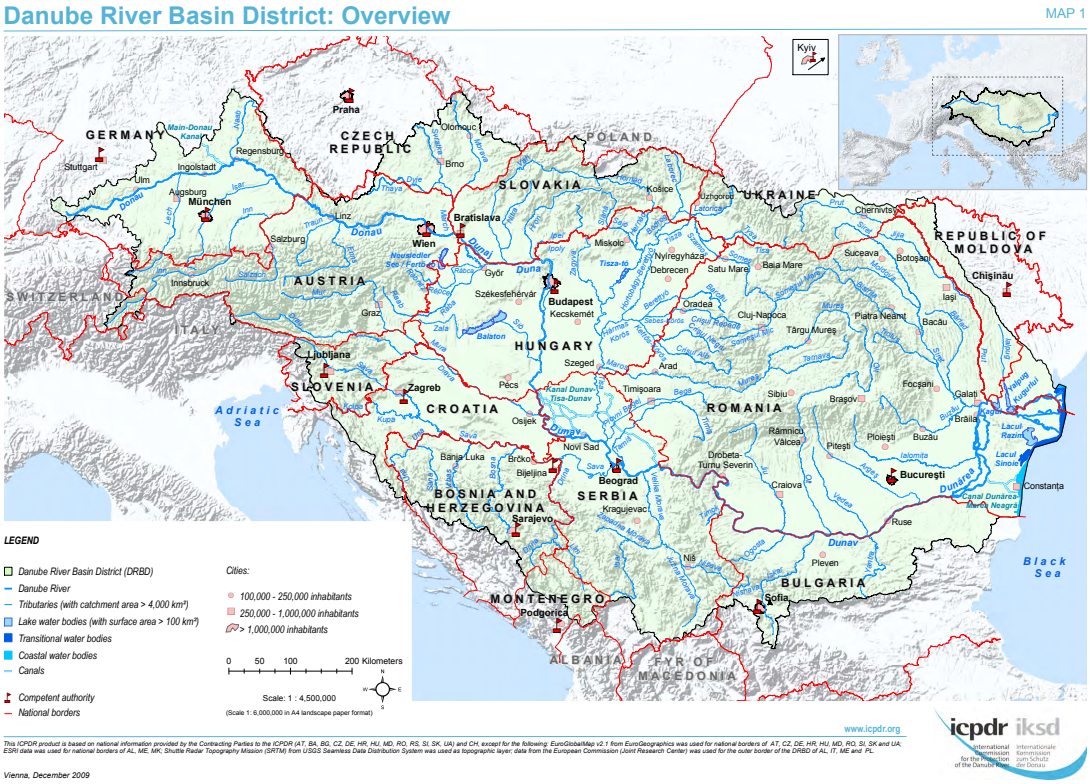

Figure 1.4. Overview map of the Danube River basin from 2009, including 19 countries sharing the Danube basin. Today, including the Kosovo there are 20 Danube countries (www.icpdr.org).

1.7.2 Historical overview

The Danube played an important role as migration pathway and frontier throughout the history of human settlement and migration in Europe (Sommerwerk et al., 2009). Excavations of mammoth hunters in Austria from about 25,000 BC represent the earliest indices of human occupation in the Danube region. Later on, from about 8,500 BC, permanent settlements of fishers and hunters were located in the Iron Gate gorge and around today's Belgrade. At about the same time, Anatolian farmers migrated and expanded in Europe most likely along the Danube. Later on, between 750–500 BC, the upper Danube valley was completely populated by the Celts and also parts of the middle basin were under Celtic influence at their largest expansion. East and southeast of this region, the Greek culture, amongst others, was active. Most of this region became part of the Roman Empire, which used the Danube as frontier where they built the 'Limes' and many fortifications that developed to large cities (e.g. Regensburg, Salzburg, Linz, Vienna, Budapest; Sommerwerk et al., 2009). From the 14th century on, portions of the middle and lower Danube basin were part of the Ottoman Empire for about 500 years. After the Second World War, the Danube basin was politically divided by the Iron Curtain until its opening in 1989.

Human influence on the Danube region started early. At the peak of the Roman Empire about 2,000 yr BP, deforestation reached about 30% in the upper basin, and in the lower basin, significant deforestation started at about 1,000 AD. With increasing land use, the sediment load in the Danube increased, and together with industrial and domestic waste water discharge leading to eutrophication of the Black Sea (Giosan et al., 2012). The Danube and its tributaries, mainly in the upper reaches where the elevation gradient is steeper, are extensively used for hydropower production. More than 70 dams were built along the Danube mainstem and its main tributaries. The largest hydropower plants are the Iron Gate I and II, situated within the Iron Gate Gorge in the Carpathian Mountains, reducing the sediment load of the Danube by about 50% (McCarney-Castle et al., 2012). The Danube was used as waterway since the Greek dynasty and developed to a major inland waterway for commercial navigation which was underlined with the opening of the Rhine-Main-Danube Canal in 1992 (Sommerwerk et al., 2009). With increased navigation, dredging and canalization came up. For navigation and flood protection, the flow path of the Danube was shortened significantly (Habersack et al., 2016). Today, flood protection for events of a 100-year occurrence interval is achieved in most of the upper and middle basin with additional levee construction.

1.7.3 The Danube as study area

The Danube as the second largest river basin in Europe, covering about 8% of the European continent, is a major river system globally and main supplier of terrigenous sediment to the Black Sea (Panin and Jipa, 2002). Its size and general west-east orientation, preventing the Danube from crossing major climate zones, make the Danube an ideal system to study mid latitude riverine organic carbon transport. Still, the climate within the catchment does change due to the diverse relief and in general from an Atlantic climate with high precipitation and mild winters in the upper basin to a more continental climate with less precipitation and cold and dry winters in the lower basin. The Danube is widely studied and well monitored as it plays an important role in inland water navigation, hydropower production and flood hazard risk for about 100 million people living in its catchment. Due to intense international collaborations, a wealth of background information on hydrological and ecological data is available. The reasons why the Danube is so well studied are also the main challenges in studying the organic carbon transfer from source to sink. The long history of human perturbations turned the Danube into a well-managed river system and renders it impossible to study natural conditions and processes. However, as is, the Danube basin is a good example of today's environment in the Anthropocene.

1.8 Thesis outline

Results from this PhD project are structured in four main chapters:

In **chapter 2**, a detailed investigation of the brGDGT composition in river sediments along the Danube River is shown. With proxy values following the local conditions of the sampling site, it is suggested that the brGDGT signal exported by the Danube is mainly a lower basin signal.

In **chapter 3**, OC and biomarker loadings on mineral surface area are investigated in river sediments throughout the catchment and ranges for typical river sediment biomarker loadings are suggested. The decreasing loadings imply significant loss of OC and/or dilution of the signal with local OC poor sediment.

In **chapter 4**, bulk and compound-specific stable and radiocarbon isotopes of river sediments are discussed in the context OC sources, evolution of the signal from the headwater to the Black Sea and the temporal aspect of pre-ageing, transport and residence time.

In **chapter 5**, suspended sediment OC and biomarker composition from depth profiles in a river cross-section close to the Black Sea are analyzed, extrapolated to the river cross-section and compared to the composition of river sediments deposited on the riverbank. Combined concentration and water discharge data are used to derive instantaneous OC and biomarker fluxes.

References

Berner, R.A. (1982) Burial of organic-carbon and pyrite sulfur in the modern ocean - its geochemical and environmental significance. *American Journal of Science* 282, 451–473.

Blair, N.E. and Aller, R.C. (2012) The fate of terrestrial organic carbon in the marine environment. *Annual Review of Marine Science* 4, 401–423.

Blair, N.E., Leithold, E.L. and Aller, R.C. (2004) From bedrock to burial: The evolution of particulate organic carbon across coupled watershed-continental margin systems. *Marine Chemistry* 92, 141–156.

Burdige, D.J. (2005) Burial of terrestrial organic matter in marine sediments: A re-assessment. *Global Biogeochemical Cycles* 19.

De Jonge, C., Hopmans, E.C., Zell, C.I., Kim, J.H., Schouten, S. and Sinninghe Damsté, J.S. (2014a) Occurrence and abundance of 6-methyl branched glycerol dialkyl glycerol tetraethers in soils: Implications for palaeoclimate reconstruction. *Geochimica et Cosmochimica Acta* 141, 97–112.

De Jonge, C., Stadnitskaia, A., Hopmans, E.C., Cherkashov, G., Fedotov, A. and Sinninghe Damsté, J.S. (2014b) In situ produced branched glycerol dialkyl glycerol tetraethers in suspended particulate matter from the Yenisei River, Eastern Siberia. *Geochimica et Cosmochimica Acta* 125, 476–491.

Diefendorf, A.F. and Freimuth, E.J. (2017) Extracting the most from terrestrial plant-derived n-alkyl lipids and their carbon isotopes from the sedimentary record: A review. *Organic Geochemistry* 103, 1–21.

Doetterl, S., Berhe, A.A., Nadeu, E., Wang, Z.G., Sommer, M. and Fiener, P. (2016) Erosion, deposition and soil carbon: A review of process-level controls, experimental tools and models to address C cycling in dynamic landscapes. *Earth-Science Reviews* 154, 102–122.

Doetterl, S., Stevens, A., Six, J., Merckx, R., Van Oost, K., Pinto, M.C., Casanova-Katny, A., Munoz, C., Boudin, M., Venegas, E.Z. and Boeckx, P. (2015) Soil carbon storage controlled by interactions between geochemistry and climate. *Nature Geoscience* 8, 780–783.

Drenzek, N.J. (2007) The temporal dynamics of terrestrial organic matter transfer to the oceans: Initial assessment and application. PhD thesis, WHOI.

Eglinton, G. and Hamilton, R.J. (1967) Leaf epicuticular waxes. *Science* 156, 1322-1335.

Eglinton, T.I. and Eglinton, G. (2008) Molecular proxies for paleoclimatology. *Earth and Planetary Science Letters* 275, 1–16.

Galy, V., Peucker-Ehrenbrink, B. and Eglinton, T. (2015) Global carbon export from the terrestrial biosphere controlled by erosion. *Nature* 521, 204–207.

Giosan, L., Coolen, M.J.L., Kaplan, J.O., Constantinescu, S., Filip, F., Filipova-Marinova, M., Kettner, A.J. and Thom, N. (2012) Early anthropogenic transformation of the Danube-Black Sea system. *Scientific Reports* 2, 1–6.

Gordon, E.S. and Goni, M.A. (2003) Sources and distribution of terrigenous organic matter delivered by the Atchafalaya River to sediments in the northern Gulf of Mexico. *Geochimica et Cosmochimica Acta* 67, 2359–2375.

Graven, H.D. (2016) The carbon cycle in a changing climate. *Physics Today* 69, 48–54.

Habersack, H., Hein, T., Stanica, A., Liska, I., Mair, R., Jager, E., Hauer, C. and Bradley, C. (2016) Challenges of river basin management: Current status of, and prospects for, the river Danube from a river engineering perspective. *Science of The Total Environment* 543, 828–845.

Hedges, J.I., Blanchette, R.A., Weliky, K. and Devol, A.H. (1988) Effects of fungal degradation on the CuO oxidation-products of lignin - a controlled laboratory study. *Geochimica et Cosmochimica Acta* 52, 2717–2726.

Hedges, J.I. and Mann, D.C. (1979) Characterization of plant-tissues by their lignin oxidation-products. *Geochimica et Cosmochimica Acta* 43, 1803–1807.

Keil, R.G. and Mayer, L.M. (2014) Mineral matrices and organic matter, in: Turekian, K.K. (Ed.), Treatise on geochemistry (second edition). Elsevier, Oxford, pp. 337–359.

Marwick, T.R., Tamooh, F., Teodoru, C.R., Borges, A.V., Darchambeau, F. and Bouillon, S. (2015) The age of river-transported carbon: A global perspective. *Global Biogeochemical Cycles* 29, 122–137.

McCarney-Castle, K., Voulgaris, G., Kettner, A.J. and Giosan, L. (2012) Simulating fluvial fluxes in the Danube watershed: The 'Little Ice Age' versus modern day. *Holocene* 22, 91–105.

Miklós, D. (2010) History and results of the hydrological co-operation of the countries sharing the Danube catchment (1971-2008), in: Mitja, B. (Ed.), Hydrological processes of the Danube River basin. Perspectives from the danubian countries. Springer, Dordrecht, Netherlands, pp. 1–24.

Milliman, J. and Farnsworth, K. (2011) Runoff, erosion, and delivery to the coastal ocean, in: River discharge to the coastal ocean: A global synthesis. Cambridge University Press, Cambridge.

Panin, N. and Jipa, D. (2002) Danube river sediment input and its interaction with the north-western Black Sea. *Estuarine Coastal and Shelf Science* 54, 551–562.

Peters, K.E., Walters, C.C. and Moldowan, J.M. (2005) The biomarker guide. 1 biomarkers and isotopes in the environment and human history (second edition). Cambridge University Press, Cambridge, UK.

Sachse, D., Billault, I., Bowen, G.J., Chikaraishi, Y., Dawson, T.E., Feakins, S.J., Freeman, K.H., Magill, C.R., McInerney, F.A., van der Meer, M.T.J., Polissar, P., Robins, R.J., Sachs, J.P., Schmidt, H.L., Sessions, A.L., White, J.W.C., West, J.B. and Kahmen, A. (2012) Molecular paleohydrology: Interpreting the hydrogen-isotopic composition of lipid biomarkers from photosynthesizing organisms. *Annual Review of Earth and Planetary Sciences* 40, 221–249.

Schiller, H., Miklós, D. and Sass, J. (2010) The Danube River and its basin physical characteristics, water regime and water balance, in: Mitja, B. (Ed.), Hydrological processes of the Danube River basin. Perspectives from the danubian countries. Springer, Dordrecht, Netherlands, pp. 25–77.

Schuur, E.A.G., Trumbore, S.E., Druffel, E.R.M., Southon, J.R., Steinhof, A., Taylor, R.E. and Turnbull, J.C. (2016) Radiocarbon and the global carbon cycle, in: Schuur, E.A.G., Druffel, E.R.M., Trumbore, S.E. (Eds.), Radiocarbon and climate change. Springer, Switzerland.

Sinninghe Damsté, J.S., Hopmans, E.C., Pancost, R.D., Schouten, S. and Geenevasen, J.A.J. (2000) Newly discovered non-isoprenoid glycerol dialkyl glycerol tetraether lipids in sediments. *Chemical Communications*, 1683–1684.

Sinninghe Damsté, J.S., Ossebaar, J., Schouten, S. and Verschuren, D. (2012) Distribution of tetraether lipids in the 25-ka sedimentary record of Lake Challa: Extracting reliable tex86 and mbt/cbt palaeotemperatures from an equatorial African lake. *Quaternary Science Reviews* 50, 43–54.

Sinninghe Damsté, J.S., Rijpstra, W.I.C., Hopmans, E.C., Weijers, J.W.H., Foesel, B.U., Overmann, J. and Dedysh, S.N. (2011) 13,16-dimethyl octacosanedioic acid (iso-diabolic acid), a common membrane-spanning lipid of acidobacteria subdivisions 1 and 3. *Applied and Environmental Microbiology* 77, 4147–4154.

Sommerwerk, N., Hein, T., Schneider-Jacoby, M., Baumgartner, C., Ostojic, A., Sieber, R., Bloesch, J., Paunovic, M. and Tockner, K. (2009) The Danube River basin, in: Tockner, K., Robinson, C.T., Uehlinger, U. (Eds.), Rivers of Europe. Elsevier Science, London, pp. 59–112.

Tao, S.Q., Eglinton, T.I., Montluçon, D.B., McIntyre, C. and Zhao, M.X. (2015) Pre-aged soil organic carbon as a major component of the Yellow River suspended load: Regional significance and global relevance. *Earth and Planetary Science Letters* 414, 77–86.

Tierney, J.E. and Russell, J.M. (2009) Distributions of branched GDGTs in a tropical lake system: Implications for lacustrine application of the mbt/cbt paleoproxy. *Organic Geochemistry* 40, 1032–1036.

Trumbore, S. (2009) Radiocarbon and soil carbon dynamics. *Annual Review of Earth and Planetary Sciences* 37, 47–66.

UNESCO (1986) Die Donau und ihr Einzugsgebiet: Eine hydrologische Monographie. UNESCO, International Hydrological Programme, Bayerisches Landesamt für Wasserwirtschaft, Bratislava.

Viers, J., Dupre, B. and Gaillardet, J. (2009) Chemical composition of suspended sediments in world rivers: New insights from a new database. *Science of the Total Environment* 407, 853–868.

von Lützow, M., Kögel-Knabner, I., Ekschmitt, K., Matzner, E., Guggenberger, G., Marschner, B. and Flessa, H. (2006) Stabilization of organic matter in temperate soils: Mechanisms and their relevance under different soil conditions - a review. *European Journal of Soil Science* 57, 426–445.

Weijers, J.W.H., Panoto, E., van Bleijswijk, J., Schouten, S., Rijpstra, W.I.C., Balk, M., Stams, A.J.M. and Sinninghe Damsté, J.S. (2009) Constraints on the biological source(s) of the orphan branched tetraether membrane lipids. *Geomicrobiology Journal* 26, 402–414.

Weijers, J.W.H., Schefuss, E., Schouten, S. and Sinninghe Damsté, J.S. (2007) Coupled thermal and hydrological evolution of tropical Africa over the last deglaciation. *Science* 315, 1701–1704.

Chapter 2

Branched GDGT signals in fluvial sediments of the Danube River basin: Method comparison and longitudinal evolution

Chantal V. Freymond[a], Francien Peterse[a,b], Lorena V. Fischer[a]
Florin Filip[c,d], Liviu Giosan[e] and Timothy I. Eglinton[a]

[a] Geological Institute, ETH Zurich, Switzerland
[b] Geochemistry, Utrecht University, Netherlands
[c] Department of Geography, University of Bucharest, Romania
[d] Fabrica de Cercetare, Romania
[e] Woods Hole Oceanographic Institution, USA

Published in *Organic Geochemistry* 103, 88–96, 2017
Corrigendum: *Organic Geochemistry* 105, 37–38, 2017

Abstract

Abundances and distributional changes of branched glycerol dialkyl glycerol tetraethers (brGDGTs) in fluvially influenced sediments are used in various paleoclimate studies to reconstruct variations in soil export, continental air temperature and soil pH in corresponding river basins. For accurate interpretation of these records, it is important to understand the provenance and the evolution of biomarker signals as they move through the river system. Here we investigate the brGDGT composition of modern river sediments of the Danube River, the second largest river in Europe. BrGDGT-based mean annual air temperature and soil pH parallel the actual values of air temperature and soil pH from the upper to the lower basin, showing that signals predominantly reflect local as opposed to basin-wide environmental conditions. Furthermore, data generated using the recently developed method with improved chromatography, separating the 6-methyl-isomers from the 5-methyl-isomers, was compared with that resulting from the conventional method. We show that the temperatures and pH values reconstructed using the data obtained by improved chromatography best resemble the local environmental conditions throughout the Danube River basin. Our results highlight the importance of in-depth studies within river systems to better understand the provenance of biomarker signals in fluvially derived sedimentary archives.

2.1 Introduction

Branched glycerol dialkyl glycerol tetraethers (brGDGTs; Figure 2.1) are promising biomarkers to reconstruct paleo-environmental conditions on land (Weijers et al., 2007a; Bendle et al., 2010; Sinninghe Damsté et al., 2012; Sanchi et al., 2014, 2015). These lipids occur widely in soils and peats around the globe (Weijers et al., 2004, 2007b; Peterse et al., 2012; Ding et al., 2015). In addition to being found in soils, brGDGTs are also produced in rivers and lakes (e.g., Tierney and Russell, 2009; Weber et al., 2015). Although identifying the organisms producing brGDGTs has proven challenging, brGDGTs are likely to be membrane lipids derived from heterotrophic bacteria (Oppermann et al., 2010; Weijers et al., 2010; Huguet et al., 2013). Certain cultured *Acidobacteria* have been found to produce the tetra-methylated brGDGT Ia (Sinninghe Damsté et al., 2011), however, other bacterial strains synthesizing brGDGTs cannot be excluded and the exact source organism(s) of brGDGTs remain(s) elusive.

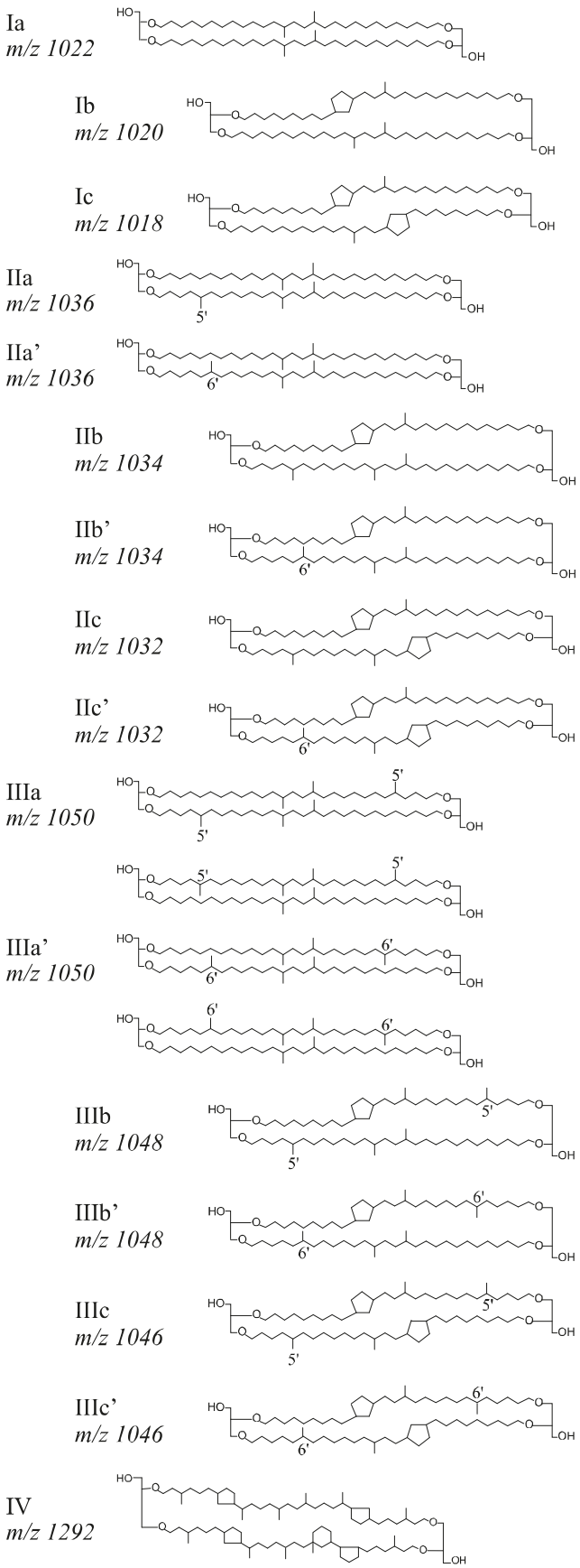

Figure 2.1. Molecular structures of the branched and isoprenoid GDGTs measured in this study (De Jonge et al., 2014a).

In general, bacteria modify their composition of cell membrane lipids for optimal function under given environmental conditions such as temperature (that influences membrane flexibility) and pH (which has an influence on the proton gradient across the cell membrane) (Weijers et al., 2007b; Sinninghe Damsté et al., 2011). Hence, variations in lipid composition can correspond to an adaptation mechanism of the microorganisms to changing environmental conditions, but can also result from changes in the microbial community composition, that are reflected in the diversity of lipids encountered (Prado et al., 1988; Suutari and Laakso, 1992; Sinninghe Damsté et al., 2011, 2014). This physiological adaptation and associated variation in biomarker lipids provides the foundation for molecular proxies to reconstruct parameters such as mean annual air temperature (MAAT) and the soil pH from the relative distributions of different brGDGTs (Figure 2.1) (Weijers et al., 2007b; De Jonge et al., 2014a). The brGDGTs occur with varying amounts of (a) four to six methyl groups ('branches'), a feature that can be summarized by the methylation index of branched tetraethers (MBT) that correlates to mean annual air temperature and to a lesser extent to soil pH and (b) the incorporation of up to two cyclopentane moieties, expressed as the cyclization index of branched tetraethers (CBT) that co-varies with soil pH (Weijers et al., 2007b; Peterse et al., 2012). Upon soil erosion and subsequent river runoff and discharge, brGDGTs may serve as tracers of terrestrial organic matter, delivering continental climate information to shelf sediments. The relative amount of brGDGTs compared to that of crenarchaeol, an isoprenoidal GDGT produced by Thaumarchaeota that are abundant in the open ocean, is quantified by the branched to isoprenoid tetraether (BIT) index (Hopmans et al., 2004) and is used to identify soil inputs to marine sediments. The BIT index is also applicable to some freshwater systems since crenarchaeol is also produced in lacustrine environments (Schouten et al., 2013). However, the presence of crenarchaeol in soils, and the production of brGDGTs in aquatic environments may at times complicate the interpretation of the BIT index as indicator of soil input (Schouten et al., 2013).

Regardless, application of these proxies has resulted in records of continental paleotemperatures and past soil pH within river basins, on the assumption that the brGDGT load exported by the river to shelf sediments represents an integrated signal of the catchment area (Weijers et al., 2007a; Bendle et al., 2010; Sanchi et al., 2014). However, this assumption and simplification remains largely untested as the source region and transport history of exported organic carbon is not well constrained for many river systems. For example, the distribution of brGDGTs could potentially be influenced by hydrodynamic sorting or microbial reworking during fluvial transport. Furthermore, the finding that brGDGTs may also be produced in aquatic environments complicates the interpretation of proxy-based temperature, pH, and BIT records, as this *in situ* contribution may affect or overprint the original soil-derived brGDGT signature in a river (e.g., Tierney and Russell, 2009; Buckles et al., 2014; De Jonge et al., 2014b; Zell

et al., 2014). Finally, certain brGDGT peaks have co-eluting isomers in the initial chromatographic method used to analyze brGDGTs –recognizable in the chromatogram as shoulders on the peaks– complicating peak integration and thus contributing to an error in the reconstructed environmental parameter. A recently refined chromatographic method using different columns now enables the separation of these shoulder peaks (De Jonge et al., 2014a; Hopmans et al., 2016), which were found to be brGDGT isomers with a methyl group at the α6 and/or ω6 instead of the α5 and/ or ω5 position (Figure 2.1) (De Jonge et al., 2013), and shown to correlate with soil pH (De Jonge et al., 2014a; Xiao et al., 2015) and soil moisture content (Dang et al., 2016). Subsequent recalibration of the MAT and pH transfer functions for the global soil calibration data set resulted in improved correlations, reducing the residual mean error on brGDGT-based temperatures and soil pH from 5 °C to 4.6 °C and from 0.8 to 0.5, respectively (Peterse et al., 2012; De Jonge et al., 2014a). Using the new chromatography method, De Jonge et al. (2014b) revealed that 6-methyl brGDGTs dominated the brGDGTs in suspended particulate matter (SPM) carried by the Yenisei River. Similarly, Weber et al. (2015) identified a novel isomer of brGDGT-IIIa with methylations on the 5 and 6' positions in a suite of Swiss lakes. The absence of this compound in surrounding soils and its distinct $\delta^{13}C$ signature confirm the production of brGDGTs in aquatic environments. Hence, in addition to the improved accuracy, the novel chromatography method may also provide information on possible contributions of *in situ* produced brGDGTs when used in studies tracing fluvial transport of soil organic matter.

In this study, a detailed basin-wide investigation of the brGDGT composition of modern fluvial sediments along the Danube River is undertaken. In order to understand the composition, provenance, and transport history of the brGDGT signal that is finally exported to the Black Sea, the changes in brGDGT abundances and distributions were examined from headwater tributaries to the Danube delta. Furthermore, data obtained using the "classic" GDGT measurement method and soil calibration (Schouten et al., 2007; Peterse et al., 2012) are compared with those using the method with improved chromatography (De Jonge et al., 2014a; Hopmans et al., 2016) to assess the potential of the latter method to identify the contribution of aquatic production to the total brGDGT pool present in river sediment deposits.

2.2 Site description

The Danube River (Figure 2.2A) is the largest river of the European Union (catchment area: 801,463 km^2; length: 2,850 km). With its source in the Black Forest, southern Germany, and its terminus in the Black Sea, the Danube has a general west to east orientation, and can be divided into three geographic regions: the upper basin from the source to the Gate of Devin (transverse valley between the Eastern Alps and the Little

Carpathians) east of Vienna (border Austria/Slovakia), the middle basin from the Gate of Devin to the Iron Gates reservoir where the Danube cuts the Carpathian Mountains, and the lower basin downstream of the Iron Gates (Figure 2.2A). The upper basin is influenced by an Atlantic climate with high precipitation, whereas dry and cold winters and higher temperatures in summer are typical for the continental climate that characterizes the eastern part of the basin (ICPDR, 2005). The southwest, i.e., the Drava and Sava catchments, is partly influenced by a Mediterranean climate with less precipitation in summer (ICPDR, 2005; McCarney-Castle et al., 2012). In short, mean annual air temperature in the upper, middle, lower basin, and the delta is 6.7 °C, 8.8 °C, 9.2 °C, 10.7 °C, mean annual precipitation is 1,012 mm, 792 mm, 605 mm, and 432 mm, mean suspended solids are 27.5 mg/L, 29.0 mg/L, 43.7 mg/L, and 36.1 mg/L (Tockner et al., 2009), and the average soil pH is 6.4, 6.3, 6.7, and 5.1 (Figure 2.2B), respectively. The Danube basin has experienced a long history of human influence since the Neolithic as agriculture spread into Europe along the river and its tributaries. Deforestation started early in the upper basin, and reached around 30% during the peak of the Roman Empire. In the lower basin, deforestation rapidly increased after 1,000 years AD, resulting in enhanced soil erosion and suspended sediment load (Giosan et al., 2012). With subsequent industrialization, inorganic nitrogen and phosphorus load increased, leading to eutrophication of the river, floodplains and the Black Sea (Kideys, 2002; Giosan et al., 2012). Training and damming of the Danube and its tributaries started in the 1870s. Following the construction of the largest hydropower dams, Iron Gate I (1972) and Iron Gate II (1986) downstream of the Carpathian Mountains, the sediment load of the lower Danube basin was reduced by approximately 50% (McCarney-Castle et al., 2012).

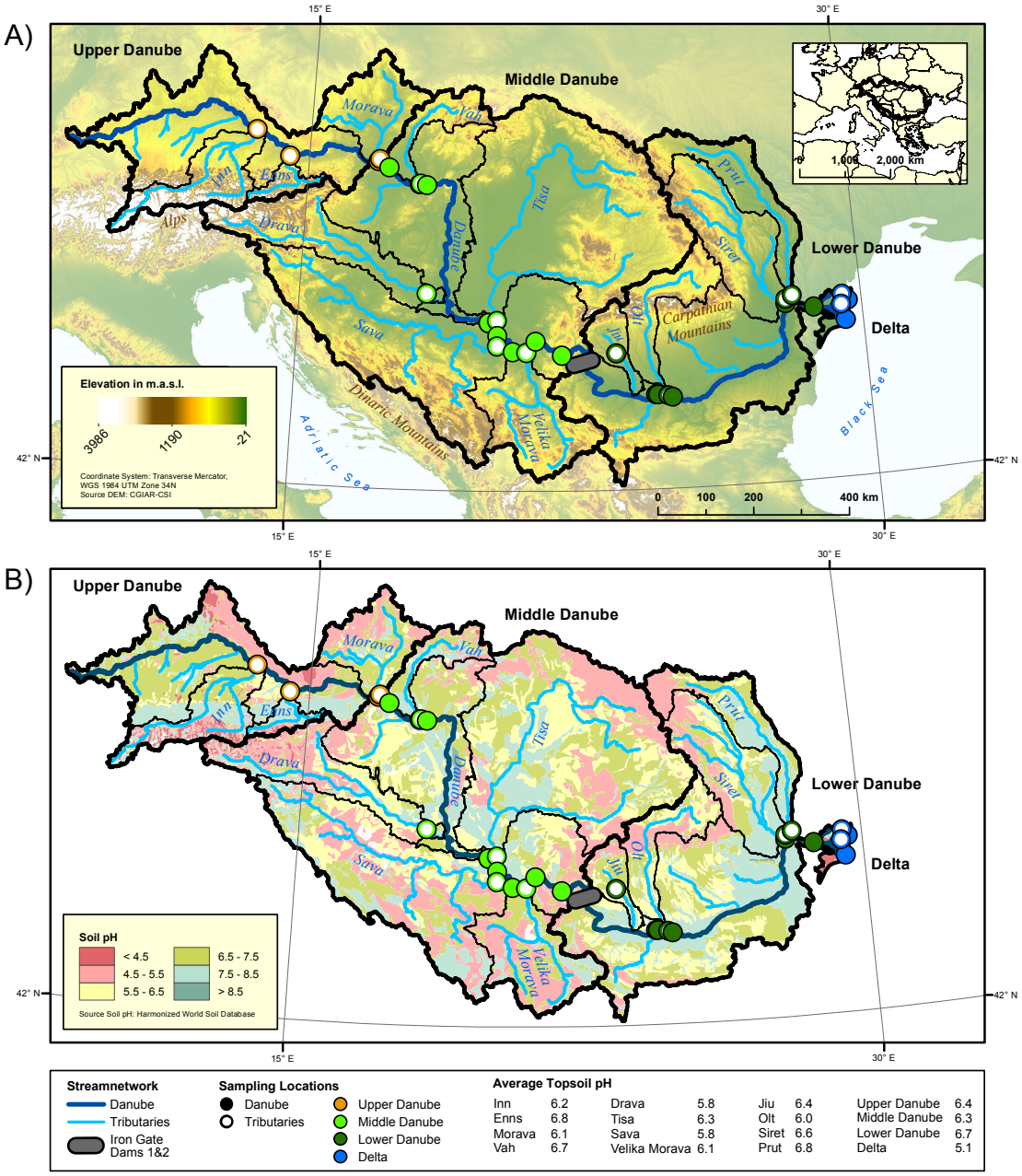

Figure 2.2. (A) The Danube River catchment. Sampling locations are shown as closed symbols for the Danube main branch and open middle, lower basin and delta indicated in orange, light green, dark green and blue, respectively. The border of the drainage basin is borders of the sub-basins. Tributary catchments borders are shown in thin black lines. The locations of two Iron Gate dams are indicated as a single gray bar. (B) Top soil pH map of Eastern Europe covering the Danube catchment. Data from the Harmonized World Soil Database (HWSD, 2012).

2.3 Methods

2.3.1 Sampling

Along a stretch of more than 2,200 km, river sediments were collected from the flanks of the river at 15 sites along the Danube mainstream and of the 12 largest tributaries between Passau (Germany) and the Black Sea (Figure 2.2; Supplementary Tables B.2) during May and June 2013. "River sediment" is defined here as recently accumulated sediment from the riverbank or in very calm and shallow water deposited during decreasing water level following the last high water event. The fine fraction (<63 μm) of this river sediment is considered to represent an integrated signal of the SPM of the river during the deposition period.

Notably, during the sampling campaign, a heavy rain event impacted central Europe with precipitation of up to >100 mm within three days for large parts of the upper basin. This corresponds to more than 100% of the average May precipitation (Grams et al., 2014) and caused a 100-year flood event in the upper and middle basin (ICPDR, 2014). High water levels and flood deposits of mostly coarse sandy sediments complicated the sampling and rendered it impossible to find freshly deposited fine-grained river sediments at several planned locations in the upper and middle basin.

Nevertheless, river sediments were collected from the following tributaries: Inn, Enns, Morava, Vah, Drava, Tisa, Sava, Velika Morava, Jiu, Olt, Siret and Prut (n = 12; Figure 2.2). Corresponding sediments from the Danube mainstream (n = 15) were collected immediately before and within ~5 km after the confluence of these tributaries and the mainstream, from sites with quiescent hydrodynamic conditions where fine-grained sediment (~<1 mm grain size) accumulated. At every location where fine sediment was available, approximately 2 kg of surface sediment was transferred to zip-lock bags. The sediment samples were kept frozen until further treatment in the laboratory at ETH Zürich.

2.3.2 Sample processing and extraction

Bulk river sediments were wet sieved with milliQ water over 200 μm and 63 μm sieves on a shaking table. The resulting <63 μm fraction was freeze-dried and kept frozen until subsequent sample work-up.

30–50 g of dry <63 μm bank sediments were microwave-extracted with dichloromethane/methanol (DCM/MeOH, 9:1, v:v, 25 min at 100 °C). A 5% aliquot of the resulting total lipid extract (TLE) was saponified with KOH in MeOH (0.5 M, 2 h at 70 °C) to allow for analysis of other biomarkers (e.g., fatty acids) in the same extract. After the addition of 5 mL MilliQ water with NaCl the neutral phase was back-extracted with hexane (Hex) and further separated by eluting over a 1% deactivated SiO_2 column into: (1) an apolar fraction with Hex:DCM (9:1, v:v) and (2) a polar fraction (containing the GDGTs) with DCM:MeOH (1:1, v:v). The GDGT fraction was dissolved in

Hex/isopropanol (Hex/IPA, 99:1, v:v) and passed over 0.45 µm PTFE filters. For quantification, 0.115 µg of an internal C_{46} GDGT standard (Huguet et al., 2006) was added.

2.3.3 GDGT analysis

2.3.3.1 The classic HPLC–APCI–MS method

The GDGT fractions were dissolved in Hex:IPA (99:1, v:v) and analyzed at ETH Zürich using a Agilent 1260 High Performance Liquid Chromatograph with Atmospheric Pressure Chemical Ionization coupled to a quadrupole Mass Spectrometer (HPLC–APCI–MS) according to Schouten et al. (2007). GDGTs were separated over a Grace Prevail cyano column (150 mm × 2.1 mm, 3 µm), preceded with a guard column with the same packing. Injection volume was 10 µL and the flow rate was set to 0.2 mL/min. The samples were eluted for 5 min with 90% Hex, 10% Hex:IPA (9:1, v:v), followed by a linear relative increase in Hex:IPA (9:1, v:v) to 82% Hex, 18% Hex:IPA over 34 min. Between samples, a 10 min back-flush phase with Hex:IPA (9:1, v:v), and a 10 min equilibrium phase with Hex:IPA (99:1, v:v), was set up.

2.3.3.2 The UHPLC–APCI–MS method with improved isomer separation

The GDGT fractions were dissolved in Hex:IPA (99:1, v:v) and separated on a Ultra High Performance Liquid Chromatograph (Agilent 1290) coupled to an Agilent 6310 quadrupole Mass Spectrometer (UHPLC–APCI–MS) at Utrecht University. Two silica Waters Acquity UPLC HEB Hilic (1.7 µm, 2.1 × 150 mm) columns, preceded by a guard column of the same material, were used for separation of the GDGTs. The injection volume was set to 10 µL and the flow rate to 0.2 mL/min. The samples were eluted with 82% Hex, 18% Hex:IPA (9:1, v:v) for 25 min, followed by a linear gradient to 70% Hex, 30% Hex:IPA (9:1, v:v), for 25 min, and then to 100% Hex:IPA (9:1 v:v) in 30 min. Each run was followed by a 20 min equilibration phase (Hopmans et al., 2016). Both HPLC systems were operated in selected ion mode (SIM). The following $[M+H]^+$ ions were detected: *m/z* 1292, 1050, 1048, 1046, 1036, 1034, 1032, 1022, 1020, 1018 and 744 for the internal standard. Molecular structures corresponding to the *m/z* values are depicted in Figure 2.1.

2.3.4 Proxy calculation

GDGT-based proxies were calculated using the following equations for data generated using the classic method. Apparent shoulders were generally cut off during the integration step.

(2.1) BIT = (Ia + IIa + IIIa)/(Ia + IIa + IIIa + Cren) (Hopmans et al., 2004)

(2.2) MBT' = (Ia + Ib + Ic)/(Ia + Ib + Ic + IIa + IIb + IIc + IIIa) (Peterse et al., 2012)

(2.3) CBT = -log[(Ib + IIb)/(Ia + IIa)] (Weijers et al., 2007b)

(2.4) pH = 7.90 – 1.97 × CBT (r^2 = 0.70; RMSE = 0.8) (Peterse et al., 2012)

(2.5) MAT = 0.81 – 5.67 × CBT + 31.0 × MBT' (r^2 = 0.59, RMSE = 5.0 °C) (Peterse et al., 2012)

For the data generated using the method with improved chromatography, the following transfer functions were used to calculate the proxy values:

(2.6) BIT = (IIIa + IIIa' + IIa + IIa' + Ia)/(IIIa + IIIa' + IIa + IIa' + Ia + Cren) (Hopmans et al., 2004; De Jonge et al., 2015)

Fractional abundance of each compound:

(2.7) rel-x = x/(Ia + Ib + Ic + IIa + IIa' + IIb + IIb' + IIc + IIc' + IIIa + IIIa' + IIIb + IIIb' + IIIc + IIIc'),

where x stands for one of the brGDGTs.

(2.8) CBT' = $\log_{10}$[(rel-Ic + rel-IIa' + rel-IIb' + rel-IIc' + rel-IIIa' + rel-IIIb' + rel-IIIc')/(rel-Ia + rel-IIa + rel-IIIa)] (De Jonge et al., 2014a)

(2.9) MAT_{mr} = 7.17 + (17.1 × rel-Ia) + (25.9 × rel-Ib) + (34.4 × rel-Ic) – (28.6 × rel-IIa) (r^2 = 0.68, RMSE = 4.6 °C) (De Jonge et al., 2014a)

(2.10) pH = 7.15 + 1.59 × CBT' (r^2 = 0.85, RMSE = 0.52) (De Jonge et al., 2014a)

(2.11) IR = (IIa' + IIb' + IIc' + IIIa' + IIIb' + IIIc')/(IIa + IIb + IIc + IIIa + IIIb + IIIc + IIa' + IIb' + IIc' + IIIa' + IIIb' + IIIc') (De Jonge et al., 2015)

2.3.5 Average soil pH calculation

The soil pH map was downloaded from the Harmonized World Soil Database (HWSD, 2012) and imported to ArcGIS (version 10.2.2). The pH value for each layer (originally representing a range of 1 pH unit) was set to the mean value (e.g., the layer pH 4.5–5.5 was set to pH 5). The average soil pH value (calculated with the function 'Zonal Statistics Table') for each Danube sampling location was calculated from the catchment area that lays in between the considered location and the one more upstream. First, the drainage area for the considered location was calculated, which includes the entire catchment upstream of this point. Then, the drainage area for the sampling location upstream of the considered location was calculated in the same way. The intermediate area was finally obtained by subtracting the catchment area from each other (downstream minus upstream location). Average intermediate area pH was chosen for comparison with brGDGT-derived pH values because it represents the local soil contributions. Average soil pH values for tributary sampling locations represent the average of the entire tributary catchment area.

2.4 Results

2.4.1 Classic method

Chromatograms from the classic method show clear shoulders on the brGDGT-IIIa, IIIb and IIIc peaks that correspond to the 5-methyl (left shoulder) and the 6-methyl (right shoulder) isomers. These 6-methyl shoulders are often comparable in size as the presumed 5-methyl brGDGT-IIIa, IIIb and IIIc peaks, respectively (Supplementary Figure A.2.1). No shoulders, and thus no isomers were visible for the peaks corresponding to brGDGT IIa–c.

The brGDGT-derived temperatures based on brGDGTs measured with the classic method and transfer functions of Peterse et al. (2012) are in the same range for the upper and middle basin (Figure 2.3A, Supplementary Table B.2.1), and increase after the Iron Gates reservoir. Reconstructed MAT values for the Danube plus tributaries range from 4.9 °C to 10.9 °C (average MAT = 7.3 °C, n = 32) and from 4.9 °C to 8.5 °C (average MAT = 7.1 °C, n = 18) only for sampling locations in the Danube mainstream (Figure 2.3A, Supplementary Table B.2.1). Calculated soil pH values after Peterse et al. (2012) based on this method tend to increase from 6.7 to 7.5 (average pH = 7.2, n = 32) for the Danube plus tributaries and from 7.0 to 7.4 (average pH = 7.2, n = 18) only for the Danube locations (Figure 2.3A, Supplementary Table B.2.1). Corresponding BIT index values including the tributaries range from 0.81 to 0.95 with an average of 0.90 (n = 32), and from 0.83 to 0.94 with an average of 0.90 (n = 18) excluding the tributaries (Figure 2.3A, Supplementary Table B.2.1).

2.4.2 Method with improved chromatography

Using the improved chromatography method with two silica columns, all six 6-methyl isomers (IIIa'–IIIc' and IIa'–IIc') were detected and appeared clearly separated from the 5-methyl isomers in every chromatogram, in similar abundance as the 5-methyl brGDGTs (Supplementary Figure A.2.1).

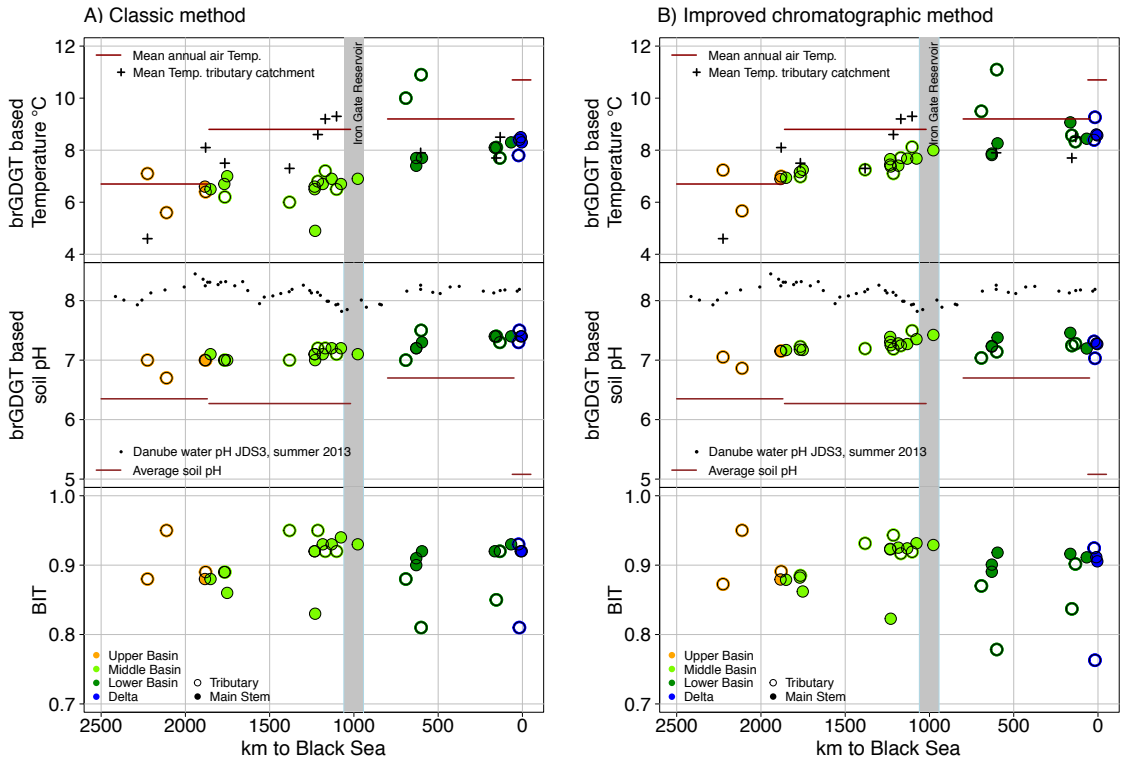

Figure 2.3. Figure from corrigendum: Freymond et al. (2017), OC 105 (2017) 37-38. Br-GDGT based mean annual air temperature, soil pH and BIT index determined by (A) the classic method and (B) the method with improved chromatography. Open circles are sampling locations at tributaries; closed circles are sampling locations at the Danube mainstream. Symbol colors correspond to those in Figure 2.2. The vertical gray bar shows the location of the Iron Gate reservoir. Actual mean annual air temperatures of sub-basins and tributary catchments are from Tockner et al. (2009); Danube water pH is from the Joint Danube Survey 3, Summer 2013 (JDS3, 2013); for average soil pH see Figure 2.2B.

Reconstructed temperatures (Figure 2.3B, Supplementary Table B.2.3) range from 5.7 °C to 11.1 °C (average MAT_{mr} = 7.9 °C, n = 32) for the Danube plus tributaries, and steadily increase from 6.9 °C to 9.1 °C (average MAT_{mr} = 7.8 °C, n = 18) for the Danube mainstream excluding tributary sampling locations (Figure 2.3B, Supplementary Table B.2.3). Average MAT_{mr} values for the sub-basins are 6.7 °C, 7.4 °C, 8.8 °C and 8.7 °C for the upper, middle, lower basin and the delta, respectively. Calculated soil pH values after De Jonge et al. (2014a) are between 6.9 and 7.5 (average pH = 7.2, n = 32) and between 7.2 and 7.5 (average pH = 7.3, n = 18) excluding tributaries (Figure 2.3B, Supplementary Table B.2.3). The BIT values of the Danube mainstream and tributaries (n = 32) show consistently high values, ranging from 0.76 to 0.95 with an average of 0.89 (Figure 2.3B, Supplementary Table B.2.3). The lowest BIT values (0.76 and 0.78) are from an old, unchannelized distributary in the Danube Delta and a tributary in the lower basin (Olt River), respectively. Excluding tributaries, BIT values for the Danube mainstream are between 0.82 and 0.93 with an average value of 0.90 (n = 18) (Figure 2.3B, Supplementary Table B.2.3).

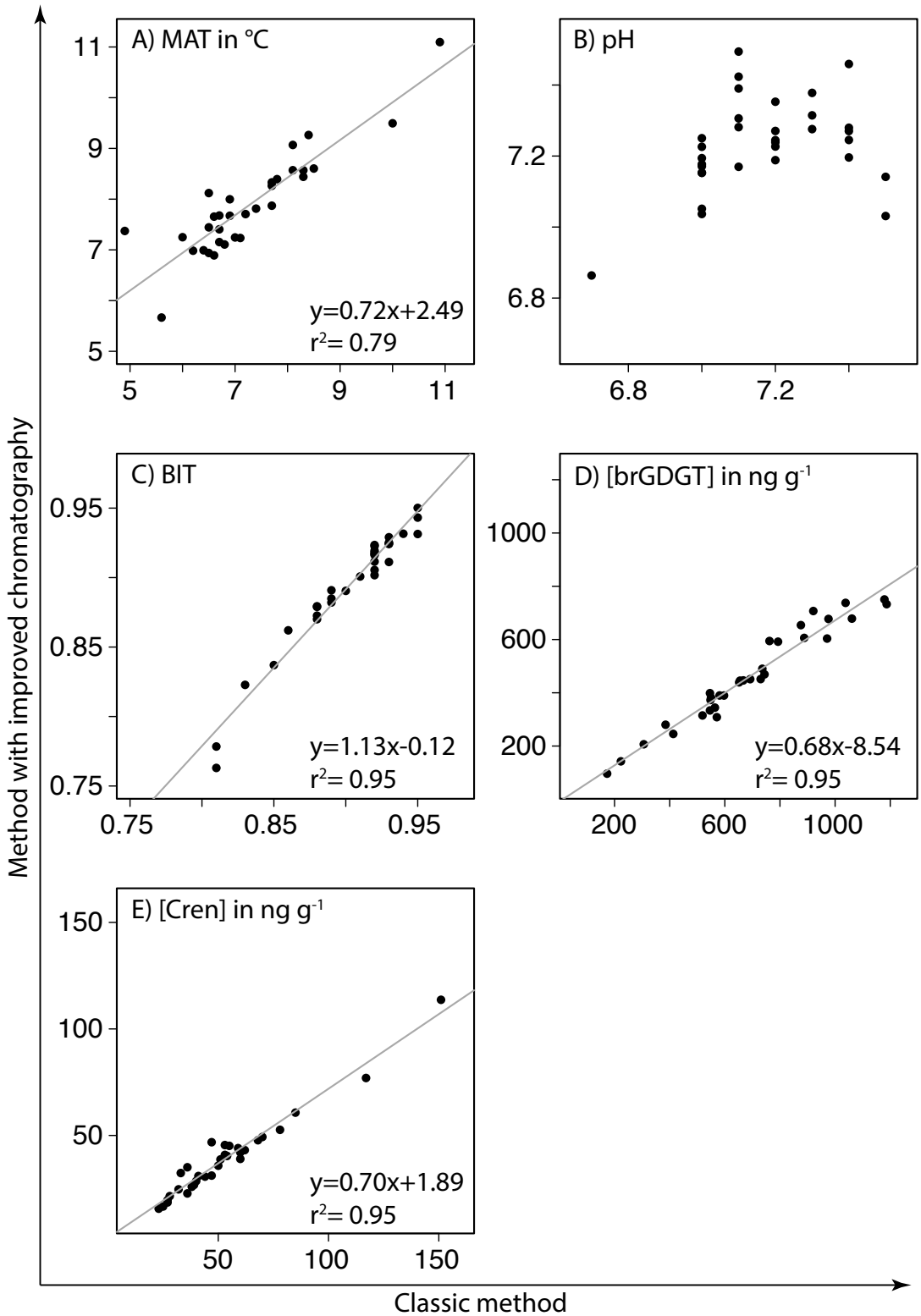

Figure 2.4. Method comparison: (A) brGDGT-based mean annual air temperature, (B) brGDGT-based soil pH, (C) BIT index, (D) summed brGDGT concentration, (E) crenarchaeol concentration of the classic method against the improved chromatographic method.

2.4.3 Method comparison

For a comparison of the two methods, proxy values of the classic method are plotted against those from the improved chromatography method (Figure 2.4A–E). MAT, BIT, total brGDGT concentration, and crenarchaeol concentration show linear correlations with r^2 values of 0.79, 0.95, 0.95 and 0.95, respectively. The improved method generally returns slightly higher MAT values (average +0.6 °C), whereas brGDGT and crenarchaeol concentrations are on average 34% and 26% lower compared to the classic method. Notably, there is no correlation between brGDGT-derived pH values reconstructed using the two methods ($r^2 = 0.09$), although this is likely caused by the limited pH range (0.8; 0.6 pH unit for the classic and the improved chromatography method, respectively) covered by the samples.

2.5 Discussion

2.5.1 Method comparison

The use of the new method revealed the presence of 6-methyl isomers for brGDGT IIa–IIc that were not visible in the chromatograms obtained with the classic method (Supplementary Figure A.2.1). As a consequence, for the latter, these isomers are automatically included during derivation of proxy values (Equations 2.1–2.5).

The brGDGT and crenarchaeol concentrations measured in two different labs (ETH Zürich and Utrecht University) are very similar ($r^2 = 0.95$), albeit with generally lower concentrations measured with the improved chromatography method than with the classic method (Figure 2.4D and E). This may reflect different response factors of the two mass spectrometers used (Schouten et al., 2009) or a greater loss (irreversible binding) to the HPLC column phases with the improved method compared to the classic method because of the higher column surface area. However, with the use of an internal standard, the latter should not be a factor, and indeed consistent BIT values suggest that the data acquired using two different HPLC–MS systems are comparable. Differences in calculated proxy values depending on brGDGT ratios are therefore not considered to result from use of two different HPLC–MS systems.

The brGDGT-derived MAT values from the two methods are linearly correlated (Figure 2.4A), albeit with greater variability ($r^2 = 0.79$) than the BIT index (Figure 2.4C) or GDGT concentrations (Figure 2.4D and E). This variability may be a result of the improved separation of 6-methyl brGDGT isomers. Temperatures from the improved method are slightly higher than temperatures derived from the classic method (on average 0.3 °C, 0.9 °C, 0.3 °C and 0.5 °C for the upper, middle, lower basin, and the delta, respectively; Supplementary Table B.2.1 & B.2.3) and closer to the actual mean annual air temperature (c.f. Tockner et al., 2009; Figure 2.3). The largest difference appears in the middle basin, where MAT_{mr} is on average 0.9 °C higher than MAT.

Indeed, this offset, although it is still a very small offset, coincides with a relative increase in 6-methyl compounds compared to the 5-methyl compounds and therefore higher isomer ratio (Figure 2.5), confirming its presumed influence on MAT reconstruction using the classic method. The influence of 6-methyl brGDGTs does not manifest itself comparing the pH values obtained by the two methods, as the values plot in the same limited range (pH range 6.7–7.5; Figure 2.4B), implying similar reconstructed pH values for the two methods. Nevertheless, soil pH in the Danube catchment is in the range 5.8–6.8 (Figure 2.2B), indicating that both methods record the same offset with actual soil pH.

Overall, we conclude that the separation of 5-methyl and 6-methyl brGDGTs improves the reliability of the generated proxy data for this river system. The subsequent discussion of brGDGT distributions in Danube River sediments therefore focuses exclusively on the results from the new method with improved chromatography.

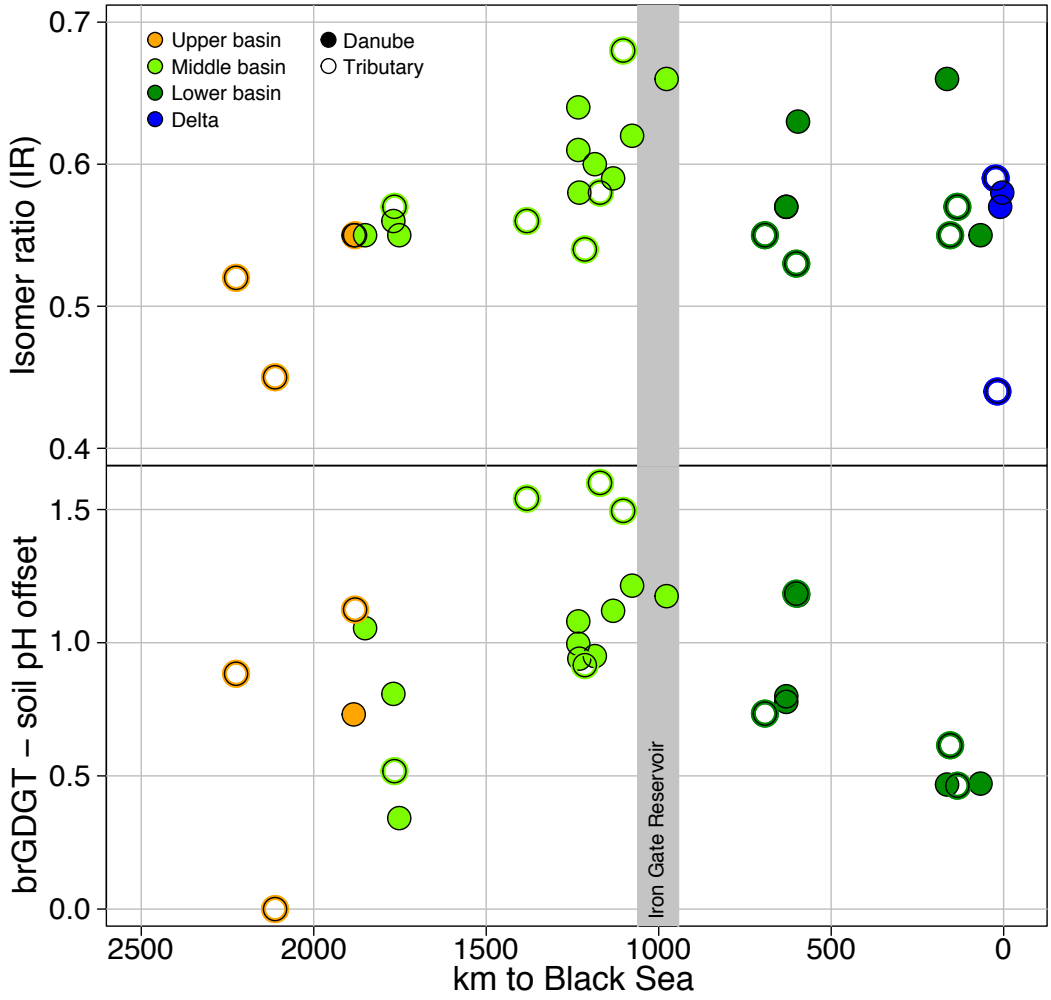

Figure 2.5. Upper panel: isomer ratio (IR) showing the fractional abundance ratio of 6 methyl brGDGTs compared to total penta- and hexamethylated brGDGTs. Lower panel: Offset between brGDGT based pH and actual soil pH along the Danube. Symbol shape and color correspond to those in Figure 2.2.

2.5.2 Evolution of brGDGT distributions along the Danube

The brGDGT composition of Danube River sediments was determined with the goal of exploiting it as a tracer to study the transport of soil-derived material along the course of a major modern river system, with the working assumption that soil is the main source of brGDGTs to the river sediment. Although the range of reconstructed temperatures and pH values is relatively minor (5.4 °C; 0.6 pH; Supplementary Table B.2.3), MAT_{mr} follows the increase in actual air temperature from headwater tributaries in the Alps to the lowlands and the Black Sea (Tockner et al., 2009) (Figure 2.3B). The brGDGT-derived temperatures for the Danube main branch are –except of the upper basin– slightly lower than the actual temperatures (average offset: 0 °C; -1.4 °C; -0.4 °C and -2 °C for the upper, middle, lower basin and delta). Although this offset is well within the calibration error (4.6 °C; De Jonge et al., 2014a), there are two processes that may have contributed to the slight underestimation of MAT_{mr}: First, the sediment collected at a specific location along the river includes sediment from the upstream (cooler) part of the catchment, and will thus result in a lower reconstructed temperature than actual MAAT. This interpretation is supported by the fact that the average MAT_{mr} for the upper basin (6.7 °C) exactly matches with the actual mean annual air temperature (6.7 °C) of that sub-basin. Further, the contribution of an upstream signal is apparent in the middle basin (Figure 2.3B). This river section may have received an exceptional contribution of material from the upper basin due to the 100-year flood event that occurred days before sample collection.

A second explanation is a contribution of *in situ* produced brGDGTs that has altered the soil-derived signal. Upstream of the Iron Gate dams, the offset in reconstructed vs actual MAAT is pronounced (Figure 2.3B). The dams lower the flow velocity and decrease the turbidity of the river, promoting conditions for *in situ* production. A similar scenario has been described to explain brGDGT signals in front of the Three Gorges Dam in the Yangtze River (Yang et al., 2013). It is found that brGDGTs produced in lakes can cause an underestimation of MBT-CBT derived temperatures by up to 10–15 °C compared to that reflected by brGDGTs in catchment soils (Tierney and Russell, 2009; Tierney et al., 2012; Li et al., 2016). Similarly, the brGDGT composition of SPM from the Amazon River resulted in reconstructed MAT that was ~2 °C lower than that reconstructed for soils in the river catchment, and ~5 °C less than actual measurements of MAAT (Zell et al., 2013). Part of such a 'cold bias' may potentially be explained by an increased contribution of the 6-methyl isomers in freshwater systems, as brGDGTs produced in a river would record the generally higher pH of river water compared to that of soils. Using the original chromatography method, the resulting larger contribution of 6-methyl brGDGTs then causes an overestimation of their similarly eluting 5-methyl counterpart, thus introducing the described bias. This suggests that we may use the relative abundance of 6-me brGDGTs as indicator of potential *in situ* production. The new chromatography method and associated transfer

functions (De Jonge et al., 2014a) has the advantage that functions for pH and MAT are independent. Thus, pH-induced *in situ* production should have a smaller effect on MAT reconstruction than when using the classic method.

Changes in the relative contribution of 6-methyl brGDGTs along the Danube are reflected by the isomer ratio (IR). This ratio is indeed slightly higher upstream of the Iron Gates (Figure 2.5), which is consistent with the suggestion of enhanced *in situ* production in this region. However, input of local soil material with a high pH value would have a similar effect. In an attempt to disentangle the contributions of aquatic and soil-derived brGDGTs, we compared brGDGT-based pH and actual soil pH. Depicting the offset between these two pH values reveals a similar picture to that of the IR ratio, with an increased offset in front of the Iron Gate dams (Figure 2.5). The average soil pH in the catchment remains relatively constant (pH = 6.3–6.4 in upper and middle basin), and only slightly increases in the lower basin (average pH = 6.7; Figure 2.2B). BrGDGT-based pH values upstream of the Iron Gate dams deviate from this trend by up to 1.2 pH units, implying that the offset is indeed related to a contribution of aquatic brGDGTs. Nevertheless, the good fit of actual mean air temperature and MAT_{mr} (Figure 2.3) suggests that the influence of in-river production on temperature estimates is relatively minor even in this section of the river.

The largest offset in temperature is found in the delta, where there is a 2.0 °C difference between reconstructed MAT_{mr} and actual MAAT. The delta has a west-east extension of about 80 km and contains an extensive network of small channels and connected shallow lakes, which may promote *in situ* production. However, we speculate that the flow path of the Danube through the delta (~90 km) is insufficient for local inputs to severely overprint the Danube signal that is entering the delta region and exported to the Black Sea. Furthermore, the consistently high BIT index values along the river indicate that the relative proportion of brGDGTs and crenarchaeol remains constant, and therefore points to a single primary source of brGDGTs, likely soil.

2.5.3 Provenance of the GDGT signal

Reconstructions of past continental climate have been based on indices and proxies derived from brGDGT distributions retrieved from paleosol-loess sequences (Peterse et al., 2011, 2014; Zech et al., 2012) and deltaic and river-proximal continental margin sediments (Weijers et al., 2007a; Sanchi et al., 2015). However, constraining the provenance of proxy signals is a prerequisite for accurate reconstruction of environmental conditions in sediment deposits. While certain inorganic and mineralogical properties of fluvial sediments integrate inputs from a river catchment and reflect basin-wide signals (Martin and Meybeck, 1979), organic matter turnover is much faster and therefore the particulate organic matter load that is discharged to the ocean may not carry an average basin-wide signal. Sanchi et al. (2015) reconstructed soil pH variations over the past 40 ka from a sediment core in the northwestern Black Sea

and found a shift from Dnieper-dominated sediments toward a dominant sediment supply from the Danube at ca. 15.5 ka BP. However, this apparent shift in source region of brGDGT signals can only be explained if the alkaline soils (higher pH) from the lower Danube basin serve as the major source to the Black Sea instead of the more acidic soils from the Carpathian Mountains. Our study of modern sediment deposits along the Danube River shows proximal signals of the brGDGT-derived proxies, following local temperature and soil pH, and only a weak influence from upstream sources. Similar conclusions are reported for another large river system, the Yangtze River (Li et al., 2015). The finding of a local, lower basin, signal being exported from the Danube supports the interpretation of Sanchi et al. (2015), but underlines the importance of understanding signal provenance in interpretations of brGDGT-based paleoclimate investigations of fluvially dominated paleoclimate archives. In this context, further within-river investigations are clearly required to understand the evolution and origin of brGDGT and other molecular proxy signals as a function of climate and drainage basin properties.

2.6 Conclusions

The comparison of methods for brGDGT analysis of fluvial sediments undertaken here shows that improved chromatographic separation of pH- and temperature-dependent isomers leads to more accurate reconstruction of local environmental conditions. Applying this new method, we find that longitudinal trends in brGDGT-based mean annual air temperature and soil pH from fluvial sediments within the Danube River basin follow the actual local conditions from headwater tributaries to the Black Sea. Minor contributions from *in situ* derived brGDGTs do not significantly alter the signal derived from local soil inputs. We therefore conclude that the brGDGT signal ultimately exported to the Black Sea emanates from soils within the drainage basin, albeit dominated by inputs from the lower Danube basin.

Acknowledgements

This project was funded by the Swiss National Science Foundation (“CAPS-LOCK”; #200021_140850). We wish to thank everyone who took part in the sampling campaign (Björn Buggle, Marilu Tavagna, Alissa Zuijdgeest, James Saenz, Stefan Eugen Filip, Silvia Lavinia Filip and Mihai). Further acknowledgement goes to Daniel Montluçon, Negar Haghipour (ETH Zürich) and Dominika Kasjaniuk (UU) for laboratory support. This product includes data licensed from International Commission for the Protection of the Danube River (ICPDR) and data from FAO/IIASA/ISRIC/ISS-CAS/ JRC. FP acknowledges ETH Fellowship FEL-36 11-1 and NWO Veni grant 863.13.016 for funding. NWO grant 834.11.006 enabled the purchase of the UHPLC-MS system for GDGT analysis at Utrecht University. This manuscript benefited from reviews by Cindy De Jonge, David Naafs and two anonymous reviewers.

Associate Editor—Sylvie Derenne

References

Bendle, J.A., Weijers, J.W.H., Maslin, M.A., Sinninghe Damsté, J.S., Schouten, S., Hopmans, E.C., Boot, C.S. and Pancost, R.D. (2010). Major changes in glacial and Holocene terrestrial temperatures and sources of organic carbon recorded in the Amazon fan by tetraether lipids. *Geochemistry, Geophysics, Geosystems* 11.

Buckles, L.K., Weijers, J.W.H., Tran, X.M., Waldron, S. and Sinninghe Damsté, J.S. (2014). Provenance of tetraether membrane lipids in a large temperate lake (Loch Lomond, UK): Implications for glycerol dialkyl glycerol tetraether (GDGT)-based palaeothermometry. *Biogeosciences* 11, 5539–5563.

Dang, X.Y., Yang, H., Naafs, B.D.A., Pancost, R.D. and Xie, S.C. (2016). Evidence of moisture control on the methylation of branched glycerol dialkyl glycerol tetraethers in semi-arid and arid soils. *Geochimica et Cosmochimica Acta* 189, 24–36.

De Jonge, C., Hopmans, E.C., Stadnitskaia, A., Rijpstra, W.I.C., Hofland, R., Tegelaar, E. and Sinninghe Damsté, J.S. (2013). Identification of novel penta- and hexamethylated branched glycerol dialkyl glycerol tetraethers in peat using HPLC–MS^2, GC–MS and GC–SMB–MS. *Organic Geochemistry* 54, 78–82.

De Jonge, C., Hopmans, E.C., Zell, C.I., Kim, J.H., Schouten, S. and Sinninghe Damsté, J.S. (2014a). Occurrence and abundance of 6-methyl branched glycerol dialkyl glycerol tetraethers in soils: Implications for palaeoclimate reconstruction. *Geochimica et Cosmochimica Acta* 141, 97–112.

De Jonge, C., Stadnitskaia, A., Hopmans, E.C., Cherkashov, G., Fedotov, A. and Sinninghe Damsté, J.S. (2014b). In situ produced branched glycerol dialkyl glycerol tetraethers in suspended particulate matter from the Yenisei River, Eastern Siberia. *Geochimica et Cosmochimica Acta* 125, 476–491.

De Jonge, C., Stadnitskaia, A., Hopmans, E.C., Cherkashov, G., Fedotov, A., Streletskaya, I.D., Vasiliev, A.A. and Sinninghe Damsté, J.S. (2015). Drastic changes in the distribution of branched tetraether lipids in suspended matter and sediments from the Yenisei River and Kara Sea (Siberia): Implications for the use of brGDGT-based proxies in coastal marine sediments. *Geochimica et Cosmochimica Acta* 165, 200–225.

Ding, S., Xu, Y., Wang, Y., He, Y., Hou, J., Chen, L. and He, J.S. (2015). Distribution of branched glycerol dialkyl glycerol tetraethers in surface soils of the Qinghai-Tibetan Plateau: Implications of brGDGTs-based proxies in cold and dry regions. *Biogeosciences* 12, 3141–3151.

Giosan, L., Coolen, M.J.L., Kaplan, J.O., Constantinescu, S., Filip, F., Filipova-Marinova, M., Kettner, A.J. and Thom, N. (2012). Early anthropogenic transformation of the Danube-Black Sea system. *Scientific Reports* 2.

Grams, C.M., Binder, H., Pfahl, S., Piaget, N. and Wernli, H. (2014). Atmospheric processes triggering the central European floods in June 2013. *Natural Hazards and Earth Systems Sciences* 14, 1691–1702.

Hopmans, E.C., Schouten, S. and Sinninghe Damsté, J.S. (2016). The effect of improved chromatography on GDGT-based palaeoproxies. *Organic Geochemistry* 93, 1–6.

Hopmans, E.C., Weijers, J.W.H., Schefuss, E., Herfort, L., Sinninghe Damsté, J.S. and Schouten, S. (2004). A novel proxy for terrestrial organic matter in sediments based on branched and isoprenoid tetraether lipids. *Earth and Planetary Science Letters* 224, 107–116.

Huguet, A., Gocke, M., Derenne, S., Fosse, C. and Wiesenberg, G.L.B. (2013). Root-associated branched tetraether source microorganisms may reduce estimated paleotemperatures in subsoil. *Chemical Geology* 356, 1–10.

Huguet, C., Hopmans, E.C., Febo-Ayala, W., Thompson, D.H., Sinninghe Damsté, J.S. and Schouten, S. (2006). An improved method to determine the absolute abundance of glycerol dibiphytanyl glycerol tetraether lipids. *Organic Geochemistry* 37, 1036–1041.

HWSD (2012). FAO/IIASA/ISRIC/ISS-CAS/JRC, Harmonized World Soil Database (version 1.2), FAO, Rome, Italy and IIASA, Laxenburg, Austria. <http:// webarchive.iiasa.ac.at/Research/LUC/ External-World-soil-database/HTML/> (date accessed: 04.08.2016).

ICPDR (2005). The Danube River Basin District. Part A – basin-wide overview, in: Schmedtje, U. (Ed.), International Commission for the Protection of the Danube River, ICPDR.

ICPDR (2014). Floods in June 2013 in the Danube River Basin – Brief Overview of Key Events and Lessons Learned.

JDS3 (2013). Danubis, the ICPDR Information System – Danube River Basin Water Quality Database. <http://www.icpdr.org/wq-db> (date accessed: 09.03.2016).

Kideys, A.E. (2002). Fall and rise of the Black Sea ecosystem. *Science* 297, 1482–1484.

Li, J.J., Pancost, R.D., Naafs, B.D.A., Yang, H., Zhao, C. and Xie, S.C. (2016). Distribution of glycerol dialkyl glycerol tetraether (GDGT) lipids in a hypersaline lake system. *Organic Geochemistry* 99, 113–124.

Li, Z.Q., Peterse, F., Wu, Y., Bao, H.Y., Eglinton, T.I. and Zhang, J. (2015). Sources of organic matter in Changjiang (Yangtze River) bed sediments: Preliminary insights from organic geochemical proxies. *Organic Geochemistry* 85, 11–21.

Martin, J.M. and Meybeck, M. (1979). Elemental mass-balance of material carried by major world rivers. *Marine Chemistry* 7, 173–206.

McCarney-Castle, K., Voulgaris, G., Kettner, A.J. and Giosan, L. (2012). Simulating fluvial fluxes in the Danube watershed: The 'Little Ice Age' versus modern day. *Holocene* 22, 91–105.

Oppermann, B.I., Michaelis, W., Blumenberg, M., Frerichs, J., Schulz, H.M., Schippers, A., Beaubien, S.E. and Kruger, M. (2010). Soil microbial community changes as a result of long-term exposure to a natural CO_2 vent. *Geochimica et Cosmochimica Acta* 74, 2697–2716.

Peterse, F., Martinez-Garcia, A., Zhou, B., Beets, C.J., Prins, M.A., Zheng, H.B. and Eglinton, T.I. (2014). Molecular records of continental air temperature and monsoon precipitation variability in East Asia spanning the past 130,000 years. *Quaternary Science Reviews* 83, 76–82.

Peterse, F., Prins, M.A., Beets, C.J., Troelstra, S.R., Zheng, H.B., Gu, Z.Y., Schouten, S. and Sinninghe Damsté, J.S. (2011). Decoupled warming and monsoon precipitation in East Asia over the last deglaciation. *Earth and Planetary Science Letters* 301, 256–264.

Peterse, F., van der Meer, J., Schouten, S., Weijers, J.W.H., Fierer, N., Jackson, R.B., Kim, J.H. and Sinninghe Damsté, J.S. (2012). Revised calibration of the MBT-CBT paleotemperature proxy based on branched tetraether membrane lipids in surface soils. *Geochimica et Cosmochimica Acta* 96, 215–229.

Prado, A., Dacosta, M.S. and Madeira, V.M.C. (1988). Effect of growth temperature on the lipid-composition of 2 strains of *Thermus* sp. *Journal of General Microbiology* 134, 1653–1660.

Sanchi, L., Menot, G. and Bard, E. (2014). Insights into continental temperatures in the northwestern Black Sea area during the Last Glacial period using branched tetraether lipids. *Quaternary Science Reviews* 84, 98–108.

Sanchi, L., Menot, G. and Bard, E. (2015). Environmental controls on paleo-pH at mid-latitudes: A case study from Central and Eastern Europe. *Palaeogeography, Palaeoclimatology, Palaeoecology* 417, 458–466.

Schouten, S., Hopmans, E.C. and Sinninghe Damsté, J.S. (2013). The organic geochemistry of glycerol dialkyl glycerol tetraether lipids: A review. *Organic Geochemistry* 54, 19–61.

Schouten, S., Hopmans, E.C., van der Meer, J., Mets, A., Bard, E., Bianchi, T.S., Diefendorf, A., Escala, M., Freeman, K.H., Furukawa, Y., Huguet, C., Ingalls, A., Menot-Combes, G., Nederbragt, A.J., Oba, M., Pearson, A., Pearson, E.J., Rosell- Mele, A., Schaeffer, P., Shah, S.R., Shanahan, T.M., Smith, R.W., Smittenberg, R., Talbot, H.M., Uchida, M., van Mooy, B.A.S., Yamamoto, M., Zhang, Z.H. and Sinninghe Damsté, J.S. (2009). An interlaboratory study of TEX_{86} and BIT analysis using high-performance liquid chromatography–mass spectrometry. *Geochemistry, Geophysics, Geosystems* 10.

Schouten, S., Huguet, C., Hopmans, E.C., Kienhuis, M.V.M. and Sinninghe Damsté, J.S. (2007). Analytical methodology for TEX_{86} paleothermometry by high-performance liquid chromatography/ atmospheric pressure chemical ionization-mass spectrometry. *Analytical Chemistry* 79, 2940–2944.

Sinninghe Damsté, J.S., Ossebaar, J., Schouten, S. and Verschuren, D. (2012). Distribution of tetraether lipids in the 25-ka sedimentary record of Lake Challa: Extracting reliable TEX86 and MBT/CBT palaeotemperatures from an equatorial African lake. *Quaternary Science Reviews* 50, 43–54.

Sinninghe Damsté, J.S., Rijpstra, W.I.C., Hopmans, E.C., Foesel, B.U., Wust, P.K., Overmann, J., Tank, M., Bryant, D.A., Dunfield, P.F., Houghton, K. and Stott, M.B. (2014). Ether- and ester-bound iso-diabolic acid and other lipids in members of acidobacteria subdivision 4. *Applied and Environment Microbiology* 80, 5207– 5218.

Sinninghe Damsté, J.S., Rijpstra, W.I.C., Hopmans, E.C., Weijers, J.W.H., Foesel, B.U., Overmann, J. and Dedysh, S.N. (2011). 13,16-Dimethyl octacosanedioic acid (iso-diabolic acid), a common membrane-spanning lipid of acidobacteria subdivisions 1 and 3. *Applied and Environment Microbiology* 77, 4147–4154.

Suutari, M. and Laakso, S. (1992). Temperature adaptation in *Lactobacillus fermentum*: Interconversions of oleic, vaccenic and dihydrosterulic acids. *Journal of General Microbiology* 138, 445–450.

Tierney, J.E. and Russell, J.M. (2009). Distributions of branched GDGTs in a tropical lake system: Implications for lacustrine application of the MBT/CBT paleoproxy. *Organic Geochemistry* 40, 1032–1036.

Tierney, J.E., Schouten, S., Pitcher, A., Hopmans, E.C. and Sinninghe Damsté, J.S. (2012). Core and intact polar glycerol dialkyl glycerol tetraethers (GDGTs) in Sand Pond, Warwick, Rhode Island (USA): Insights into the origin of lacustrine GDGTs. *Geochimica et Cosmochimica Acta* 77, 561–581.

Tockner, K., Uehlinger, U. and Robinson, C.T. (2009). Rivers of Europe. Elsevier Science.

Weber, Y., De Jonge, C., Rijpstra, W.I.C., Hopmans, E.C., Stadnitskaia, A., Schubert, C.J., Lehmann, M.F., Sinninghe Damsté, J.S. and Niemann, H. (2015). Identification and carbon isotope composition of a novel branched GDGT isomer in lake sediments: Evidence for lacustrine branched GDGT production. *Geochimica et Cosmochimica Acta* 154, 118–129.

Weijers, J.W.H., Schouten, S., van der Linden, M., van Geel, B. and Sinninghe Damsté, J.S. (2004). Water table related variations in the abundance of intact archaeal membrane lipids in a Swedish peat bog. *FEMS Microbiology Letters* 239, 51–56.

Weijers, J.W.H., Schefuss, E., Schouten, S. and Sinninghe Damsté, J.S. (2007a). Coupled thermal and hydrological evolution of tropical Africa over the last deglaciation. *Science* 315, 1701–1704.

Weijers, J.W.H., Schouten, S., van den Donker, J.C., Hopmans, E.C. and Sinninghe Damsté, J.S. (2007b). Environmental controls on bacterial tetraether membrane lipid distribution in soils. *Geochimica et Cosmochimica Acta* 71, 703–713.

Weijers, J.W.H., Wiesenberg, G.L.B., Bol, R., Hopmans, E.C. and Pancost, R.D. (2010). Carbon isotopic composition of branched tetraether membrane lipids in soils suggest a rapid turnover and a heterotrophic life style of their source organism(s). *Biogeosciences* 7, 2959–2973.

Xiao, W.J., Xu, Y.P., Ding, S., Wang, Y.H., Zhang, X.Y., Yang, H., Wang, G.A. and Hou, J.Z. (2015). Global calibration of a novel, branched GDGT-based soil pH proxy. *Organic Geochemistry* 89–90, 56–60.

Yang, G., Zhang, C.L., Xie, S., Chen, Z., Gao, M., Ge, Z. and Yang, Z. (2013). Microbial glycerol dialkyl glycerol tetraethers from river water and soil near the Three Gorges Dam on the Yangtze River. *Organic Geochemistry* 56, 40–50.

Zech, R., Gao, L., Tarozo, R. and Huang, Y. (2012). Branched glycerol dialkyl glycerol tetraethers in Pleistocene loess-paleosol sequences: Three case studies. *Organic Geochemistry* 53, 38–44.

Zell, C., Kim, J.H., Hollander, D., Lorenzoni, L., Baker, P., Silva, C.G., Nittrouer, C. and Sinninghe Damsté, J.S. (2014). Sources and distributions of branched and isoprenoid tetraether lipids on the Amazon shelf and fan: Implications for the use of GDGT-based proxies in marine sediments. *Geochimica et Cosmochimica Acta* 139, 293–312.

Zell, C., Kim, J.H., Moreira-Turcq, P., Abril, G., Hopmans, E.C., Bonnet, M.P., Sobrinho, R.L. and Sinninghe Damsté, J.S. (2013). Disentangling the origins of branched tetraether lipids and crenarchaeol in the lower Amazon River: Implications for GDGT-based proxies. *Limnology and Oceanography* 58, 343–353.

Appendix A.2 Supplementary information

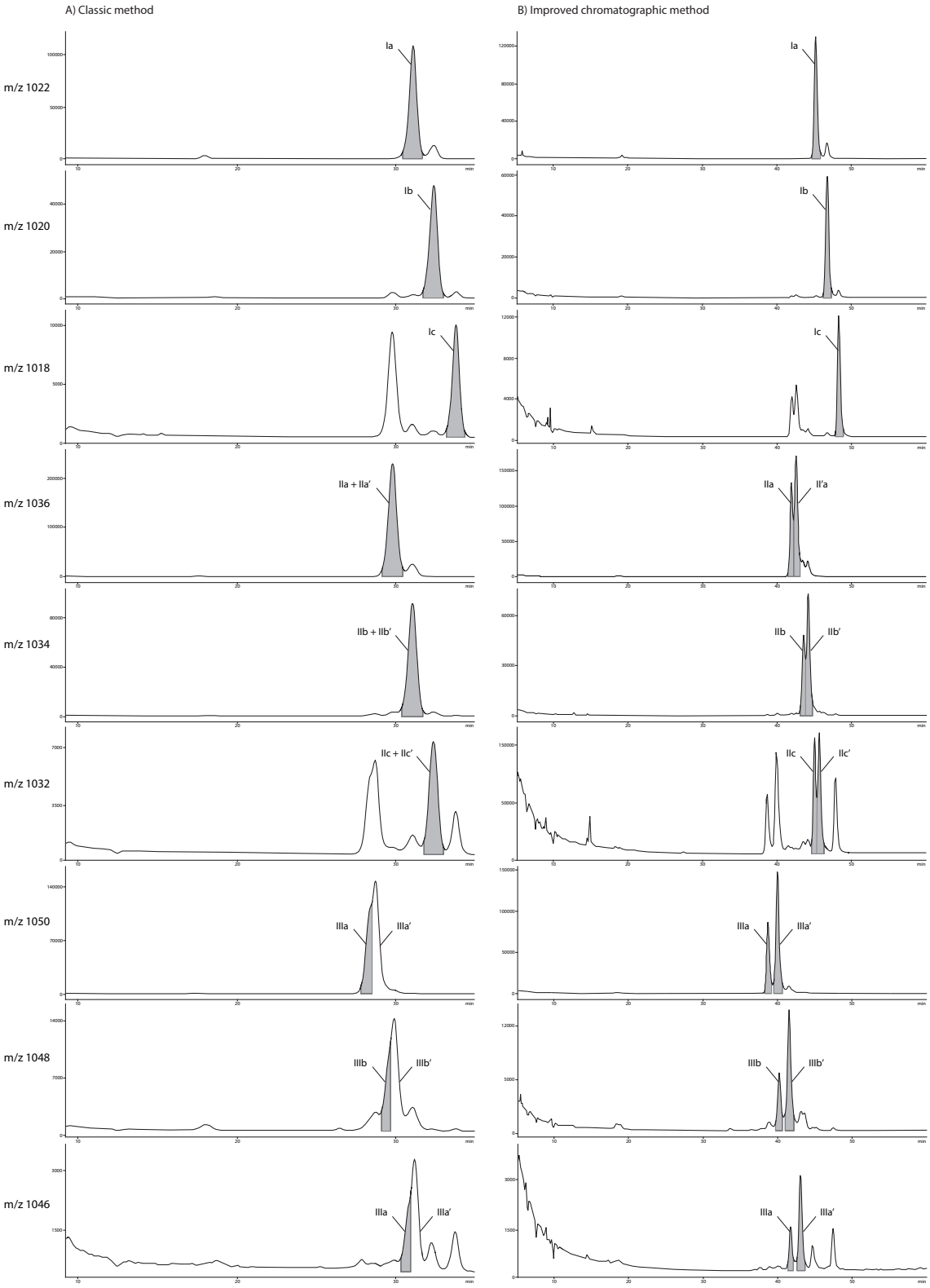

Supplementary figure A.2.1. Chromatograms of the brGDGTs from Danube River sediments upstream of the Iron Gate reservoir measured with A) the classic method, and B) the method with improved chromatography. The grey areas show the peak integration that was used for proxy calculations.

Appendix B.2 Data tables

Table B.2.1. BrGDGT proxies and concentrations determined with the classic method.

			Classic method								
Name	**N**	**E**	**BIT**	**CBT**	**MBT'**	**MAT' [°C]**	**pH'**	**brGDGTs [ng/g]**	**isoGDGTs [ng/g]**	**Cren. [ng/g]**
Inn	48°34'15.0"	13°27'46.7"	0.88	0.45	0.28	7.1	7.0	546	244	60
Enns	48°07'48.3"	14°28'15.1"	0.95	0.62	0.27	5.6	6.7	564	116	23
D up Morava	48°08'45.9"	16°56'00.3"	0.88	0.45	0.27	6.6	7.0	385	189	41
Morava	48°11'10.6"	16°58'38.1"	0.89	0.47	0.27	6.4	7.0	888	430	85
D d Morava	48°01'56.2"	17°14'57.2"	0.88	0.43	0.26	6.5	7.1	692	329	70
D up Vah	47°45'01.0"	18°06'45.3"	0.89	0.46	0.27	6.7	7.0	597	294	60
Vah	47°54'50.5"	18°00'43.6"	0.89	0.45	0.26	6.2	7.0	1187	619	117
D d Vah	47°43'57.7"	18°19'18.2"	0.86	0.43	0.28	7	7.0	548	332	68
Drava	45°41'26.0"	18°24'59.7"	0.95	0.44	0.25	6	7.0	793	364	36
D up Tisa 1	45°10'03.2"	20°04'46.6"	0.92	0.41	0.26	6.6	7.1	581	307	38
D up Tisa 2	45°10'03.2"	20°04'46.6"	0.92	0.41	0.26	6.5	7.1	876	429	55
D up Tisa 3	45°09'54.1"	20°06'34.3"	0.83	0.46	0.22	4.9	7.0	306	165	50
Tisa	45°12'16.4"	20°18'44.7"	0.95	0.35	0.26	6.8	7.2	921	194	33
D up Sava	44°55'24.5"	20°19'16.0"	0.93	0.41	0.26	6.7	7.1	667	394	40
Sava	44°43'24.9"	20°18'34.7"	0.92	0.37	0.27	7.2	7.2	1179	463	78
D d Sava	44°39'56.7"	20°46'48.2"	0.93	0.38	0.27	6.9	7.2	1061	471	62
Velika Morava	44°36'21.0"	21°05'10.6"	0.92	0.4	0.25	6.5	7.1	652	388	44
D d Velika Morava	44°49'01.0"	21°20'04.3"	0.94	0.38	0.26	6.7	7.2	976	383	51
IG reservoir	44°33'06.6"	22°01'42.3"	0.93	0.39	0.27	6.9	7.1	1038	441	59
Jiu	44°34'09.8"	23°27'19.8"	0.88	0.44	0.38	10	7.0	546	204	53
D up Olt 1	43°46'15.5"	24°30'50.2"	0.91	0.35	0.28	7.4	7.2	736	282	54
D up Olt 2	43°46'16.3"	24°30'42.8"	0.9	0.34	0.28	7.7	7.2	655	251	53
Olt	43°44'38.7"	24°46'43.0"	0.81	0.23	0.37	10.9	7.5	173	53	27
D d Olt	43°42'46.3"	24°53'28.3"	0.92	0.32	0.28	7.7	7.3	744	243	47
D up Siret	45°19'22.8"	28°00'07.9"	0.92	0.26	0.28	8.1	7.4	550	185	32
Siret	45°23'56.8"	28°00'41.9"	0.85	0.25	0.28	8.1	7.4	223	100	27
Prut	45°28'15.9"	28°11'53.3"	0.92	0.31	0.28	7.7	7.3	762	147	47
Apex	45°12'55.3"	28°45'10.7"	0.93	0.27	0.29	8.3	7.4	519	169	28
DD18	44°55'08.7"	29°33'24.7"	0.92	0.25	0.29	8.5	7.4	413	136	25
DD9	45°16'44.9"	29°40'28.7"	0.92	0.26	0.29	8.3	7.4	571	202	36
DD11	45°23'53.3"	29°31'48.3"	0.93	0.29	0.28	7.8	7.3	730	244	39
DD5	45°12'55.8"	29°29'03.8"	0.81	0.19	0.28	8.4	7.5	971	428	151

Abbreviations: D: Danube; D up: Danube upstream of...; D d: Danbue downstram of...; IG: Iron Gate; DD: Danube delta

Table B.2.2. Relative abundances of brGDGTs determined with the classic method.

	Classic method								
Name	**rel-Ia**	**rel-Ib**	**rel-Ic**	**rel-IIa**	**rel-IIb**	**rel-IIc**	**rel-IIIa**	**rel-IIIb**	**rel-IIIc**
Inn	0.197	0.067	0.016	0.364	0.134	0.014	0.190	0.014	0.003
Enns	0.205	0.048	0.012	0.392	0.096	0.011	0.225	0.009	0.003
D up Morava	0.186	0.066	0.016	0.398	0.136	0.014	0.172	0.011	0.003
Morava	0.186	0.062	0.014	0.392	0.133	0.013	0.183	0.013	0.003
D d Morava	0.175	0.066	0.016	0.392	0.145	0.015	0.174	0.014	0.003
D up Vah	0.186	0.067	0.016	0.399	0.137	0.014	0.167	0.012	0.003
Vah	0.177	0.063	0.014	0.404	0.141	0.014	0.173	0.012	0.003
D d Vah	0.189	0.069	0.016	0.391	0.145	0.015	0.158	0.014	0.003
Drava	0.167	0.064	0.013	0.368	0.128	0.011	0.226	0.019	0.004
D up Tisa 1	0.175	0.071	0.015	0.412	0.156	0.012	0.147	0.011	0.002
D up Tisa 2	0.170	0.071	0.014	0.402	0.153	0.012	0.165	0.012	0.002
D up Tisa 3	0.169	0.033	0.013	0.421	0.170	0.011	0.169	0.012	0.002
Tisa	0.157	0.082	0.014	0.399	0.165	0.012	0.156	0.013	0.002
D up Sava	0.176	0.072	0.014	0.408	0.154	0.012	0.153	0.010	0.002
Sava	0.174	0.079	0.016	0.393	0.161	0.014	0.147	0.013	0.003
D d Sava	0.169	0.077	0.015	0.397	0.161	0.013	0.154	0.012	0.002
Velika Morava	0.166	0.073	0.012	0.422	0.163	0.013	0.138	0.010	0.003
D d Velika Morava	0.166	0.076	0.014	0.406	0.163	0.012	0.150	0.011	0.002
IG reservoir	0.176	0.074	0.014	0.411	0.167	0.012	0.134	0.011	0.002
Jiu	0.247	0.104	0.022	0.372	0.119	0.015	0.107	0.011	0.002
D up Olt 1	0.169	0.085	0.016	0.393	0.169	0.014	0.136	0.015	0.003
D up Olt 2	0.176	0.087	0.017	0.385	0.166	0.015	0.139	0.012	0.002
Olt	0.208	0.123	0.029	0.324	0.194	0.022	0.082	0.016	0.003
D d Olt	0.172	0.087	0.017	0.382	0.178	0.015	0.131	0.014	0.003
D up Siret	0.166	0.094	0.019	0.369	0.199	0.018	0.119	0.014	0.002
Siret	0.157	0.098	0.020	0.354	0.192	0.021	0.134	0.019	0.005
Prut	0.156	0.100	0.019	0.397	0.172	0.016	0.125	0.013	0.002
Apex	0.165	0.101	0.020	0.365	0.185	0.017	0.129	0.015	0.002
DD18	0.159	0.107	0.022	0.367	0.187	0.018	0.123	0.014	0.002
DD9	0.163	0.101	0.020	0.365	0.188	0.018	0.129	0.014	0.003
DD11	0.160	0.097	0.019	0.387	0.182	0.017	0.124	0.013	0.002
DD5	0.149	0.096	0.030	0.339	0.222	0.022	0.129	0.012	0.001

Table B.2.3. BrGDGT proxies and concentrations determined with the improved chromatography method.

	Method with improved chromatography						
Name	**BIT**	**CBT'**	**MATmr [°C]**	**pH**	**brGDGTs [ng/g]**	**isoGDGTs [ng/g]**	**Cren. [ng/g]**
Inn	0.87	-0.06	7.2	7.1	334	124	39
Enns	0.95	-0.18	5.7	6.9	344	63	16
D up Morava	0.88	0.00	6.9	7.2	280	115	31
Morava	0.89	0.00	7.0	7.2	606	258	61
D d Morava	0.88	0.01	6.9	7.2	451	188	49
D up Vah	0.88	0.02	7.2	7.2	390	170	42
Vah	0.88	0.05	7.0	7.2	733	347	77
D d Vah	0.86	0.01	7.2	7.2	373	197	48
Drava	0.93	0.03	7.2	7.2	592	336	35
D up Tisa 1	0.92	0.15	7.7	7.4	390	194	26
D up Tisa 2	0.92	0.10	7.4	7.3	654	281	45
D up Tisa 3	0.82	0.06	7.4	7.3	207	86	36
Tisa	0.94	0.02	7.1	7.2	707	162	32
D up Sava	0.93	0.08	7.4	7.3	446	263	29
Sava	0.92	0.06	7.7	7.2	750	268	53
D d Sava	0.92	0.08	7.7	7.3	679	300	43
Velika Morava	0.92	0.22	8.1	7.5	439	253	31
D d Velika Morava	0.93	0.13	7.7	7.4	677	260	39
IG reservoir	0.93	0.17	8.0	7.4	738	306	44
Jiu	0.87	-0.07	9.5	7.0	399	146	45
D up Olt 1	0.90	0.06	7.8	7.2	490	177	40
D up Olt 2	0.89	0.05	7.9	7.2	446	157	41
Olt	0.78	-0.01	11.1	7.1	96	19	19
D d Olt	0.92	0.14	8.3	7.4	469	157	31
D up Siret	0.92	0.19	9.1	7.5	382	122	25
Siret	0.84	0.06	8.6	7.2	143	55	20
Prut	0.90	0.08	8.3	7.3	594	104	47
Apex	0.91	0.03	8.4	7.2	315	109	22
DD18	0.91	0.08	8.6	7.3	246	76	17
DD9	0.91	0.08	8.6	7.3	308	107	23
DD11	0.92	0.10	8.4	7.3	451	145	27
DD5	0.76	-0.07	9.3	7.0	604	222	114

Table B.2.4. Relative abundances of brGDGTs determined with the improved chromatography method.

	Method with improved chromatography														
Name	**rel-Ia**	**rel-Ib**	**rel-Ic**	**rel-IIa**	**rel-IIa'**	**rel-Iib**	**rel-IIb'**	**rel-Iic**	**rel-IIc'**	**rel-IIIa**	**rel-IIIa'**	**rel-IIIb**	**rel-IIIb'**	**rel-IIIc**	**rel-IIIc'**
Inn	0.170	0.058	0.014	0.168	0.137	0.052	0.061	0.007	0.006	0.129	0.169	0.008	0.015	0.002	0.004
Enns	0.175	0.042	0.010	0.208	0.118	0.038	0.044	0.006	0.003	0.163	0.171	0.006	0.010	0.002	0.003
D up Morava	0.155	0.055	0.013	0.168	0.153	0.049	0.066	0.006	0.005	0.117	0.185	0.007	0.015	0.002	0.004
Morava	0.155	0.052	0.013	0.161	0.157	0.045	0.063	0.006	0.005	0.128	0.188	0.008	0.015	0.002	0.004
D d Morava	0.148	0.056	0.014	0.164	0.158	0.053	0.069	0.006	0.006	0.119	0.176	0.008	0.016	0.002	0.004
D up Vah	0.160	0.055	0.013	0.162	0.164	0.049	0.066	0.006	0.006	0.109	0.180	0.008	0.015	0.002	0.004
Vah	0.146	0.052	0.012	0.155	0.172	0.051	0.068	0.006	0.005	0.114	0.187	0.009	0.017	0.002	0.004
D d Vah	0.156	0.057	0.014	0.159	0.160	0.053	0.067	0.007	0.006	0.115	0.176	0.009	0.016	0.002	0.004
Drava	0.153	0.061	0.013	0.159	0.170	0.055	0.064	0.006	0.005	0.109	0.181	0.007	0.014	0.001	0.003
D up Tisa 1	0.143	0.058	0.011	0.135	0.194	0.046	0.082	0.005	0.005	0.088	0.204	0.007	0.018	0.001	0.003
D up Tisa 2	0.144	0.059	0.012	0.144	0.183	0.046	0.059	0.005	0.005	0.104	0.212	0.007	0.017	0.001	0.003
D up Tisa 3	0.140	0.068	0.011	0.151	0.188	0.058	0.085	0.004	0.005	0.109	0.156	0.007	0.016	0.001	0.002
Tisa	0.138	0.076	0.013	0.169	0.179	0.062	0.087	0.006	0.005	0.104	0.131	0.009	0.016	0.002	0.003
D up Sava	0.149	0.061	0.012	0.150	0.187	0.049	0.081	0.005	0.005	0.098	0.175	0.007	0.017	0.001	0.003
Sava	0.149	0.067	0.014	0.147	0.177	0.058	0.079	0.005	0.007	0.105	0.162	0.009	0.017	0.002	0.004
D d Sava	0.147	0.067	0.013	0.147	0.182	0.055	0.083	0.005	0.006	0.101	0.164	0.008	0.017	0.002	0.003
Velika Morava	0.137	0.061	0.010	0.116	0.227	0.046	0.089	0.005	0.006	0.080	0.195	0.008	0.017	0.002	0.003
D d Velika Morava	0.140	0.064	0.012	0.139	0.200	0.050	0.088	0.005	0.006	0.093	0.173	0.008	0.017	0.001	0.003
IG reservoir	0.144	0.061	0.012	0.127	0.203	0.046	0.088	0.005	0.006	0.084	0.195	0.007	0.018	0.001	0.004
Jiu	0.221	0.094	0.020	0.160	0.171	0.051	0.058	0.010	0.004	0.072	0.119	0.006	0.010	0.002	0.002
D up Olt 1	0.149	0.075	0.015	0.152	0.179	0.059	0.088	0.006	0.007	0.097	0.143	0.008	0.017	0.002	0.003
D up Olt 2	0.152	0.076	0.015	0.153	0.177	0.058	0.088	0.006	0.007	0.096	0.143	0.008	0.017	0.002	0.003
Olt	0.197	0.119	0.029	0.123	0.160	0.097	0.084	0.011	0.010	0.062	0.080	0.011	0.013	0.003	0.002
D d Olt	0.142	0.073	0.014	0.130	0.193	0.054	0.099	0.006	0.007	0.087	0.163	0.008	0.019	0.002	0.004
D up Siret	0.142	0.083	0.017	0.115	0.194	0.058	0.115	0.006	0.010	0.072	0.152	0.008	0.022	0.001	0.005
Siret	0.141	0.089	0.019	0.139	0.160	0.073	0.099	0.010	0.009	0.098	0.123	0.012	0.020	0.003	0.004
Prut	0.137	0.094	0.019	0.149	0.195	0.073	0.087	0.008	0.008	0.084	0.118	0.008	0.015	0.002	0.002
Apex	0.150	0.092	0.019	0.151	0.146	0.071	0.099	0.008	0.009	0.094	0.128	0.010	0.019	0.002	0.004
DD18	0.138	0.097	0.020	0.144	0.170	0.068	0.100	0.006	0.010	0.089	0.126	0.008	0.018	0.002	0.003
DD9	0.146	0.090	0.018	0.142	0.171	0.064	0.103	0.008	0.009	0.090	0.127	0.009	0.018	0.002	0.004
DD11	0.141	0.086	0.017	0.139	0.188	0.068	0.094	0.007	0.008	0.085	0.137	0.008	0.017	0.002	0.003
DD5	0.136	0.144	0.029	0.173	0.118	0.111	0.090	0.007	0.013	0.087	0.067	0.007	0.014	0.001	0.002

Chapter 3

Evolution of biomolecular loadings along a major river system

Chantal V. Freymond[a], Nicole Kündig[a], Courcelle Stark[a,b], Francien Peterse[a,c], Björn Buggle[a], Maarten Lupker[a], Michael Plötze[d], Thomas M. Blattmann[a], Florin Filip[e,f], Liviu Giosan[g] and Timothy I. Eglinton[a]

[a] Geological Institute, ETH Zurich, Sonneggstrasse 5, 8092 Zürich, Switzerland
[b] Department of Geosciences, Smith College, Northampton, MA 01063, USA
[c] Department of Earth Sciences, Utrecht University, Heidelberglaan 2, 3584 CS Utrecht, Netherlands
[d] Institute for Geotechnical Engineering, ETH Zurich, Stefano-Franscini-Platz 3, 8093 Zürich, Switzerland
[e] Institute for Fluvial and Marine Systems, Str. Olari, Nr. 7, Sector 2, Bucharest, Romania
[f] Fad Smart Technology srl, Sector 2, Bucharest, Romania
[g] Geology & Geophysics Department, Woods Hole Oceanographic Institution, 86 Water Street, Woodshole, MA 02543, USA

Published in *Geochimica et Cosmochimica Acta* 223, 389–404, 2018

Abstract

Understanding the transport history and fate of organic carbon (OC) within river systems is crucial in order to constrain the dynamics and significance of land–ocean interactions as a component of the global carbon cycle. Fluvial export and burial of terrestrial OC in marine sediments influences atmospheric CO_2 over a range of timescales, while river-dominated sedimentary sequences can provide valuable archives of paleoenvironmental information. While there is abundant evidence that the association of organic matter (OM) with minerals exerts an important influence on its stability as well as hydrodynamic behavior in aquatic systems, there is a paucity of information on where such associations form and how they evolve during fluvial transport. Here, we track total organic carbon (TOC) and terrestrial biomarker concentrations (plant wax-derived long-chain fatty acids (FA), branched glycerol dialkyl glycerol tetraethers (brGDGTs) and lignin-derived phenols) in sediments collected along the entire course of the Danube River system in the context of sedimentological parameters. Mineral-specific surface area-normalized biomarker and TOC concentrations show a systematic decrease from the upper to the lower Danube basin. Changes in OM loading of the available mineral phase correspond to a net decrease of 70–80% of different biomolecular components. Ranges for biomarker loadings on Danube River sediments, corresponding to 0.4–1.5 $\mu g_{FA}/m^2$ for long-chain (n-$C_{24–32}$) fatty acids and 17–71 ng_{brGDGT}/m^2 for brGDGTs, are proposed as a benchmark for comparison with other systems. We propose that normalizing TOC as well as biomarker concentrations to mineral surface area provides valuable quantitative constraints on OM dynamics and organo-mineral interactions during fluvial transport from terrigenous source to oceanic sink.

3.1 Introduction

Rivers form a key connection between continental and marine carbon pools, exporting 210 Mt of dissolved organic carbon (DOC) and 170 Mt particulate organic carbon (POC) annually (Ludwig et al., 1996). Marine burial of terrestrial biospheric carbon in fluvially-derived sediments exerts strong control on the atmospheric O_2/CO_2 balance (Burdige, 2005; Berner, 2006), and can yield continuous records of past continental vegetation and climate dynamics. Constraints on the origin and evolution of biospheric organic carbon (OC) signals transported by rivers is a necessary prerequisite for comprehensive understanding of the manner in which past and present variations in the amount and composition of terrestrially-derived OC reaching and accumulating in ocean sediments reflects drainage basin dynamics (Blair et al., 2004).

A major fraction of riverine POC is associated with mineral particles (Keil et al., 1997; Keil and Mayer, 2014), particularly fine-grained minerals (e.g. phyllosilicates) due

to their large surface area (SA) and sorptive capacity (Keil and Mayer, 2014). Close associations between OM and high SA mineral phases are known to develop in soils (Sorensen, 1981; Baldock and Skjemstad, 2000; von Lützow et al., 2006), where the latter have been suggested to serve a stabilizing role, protecting OC from further degradation (von Lützow et al., 2006) and thereby slowing carbon turnover (e.g. Torn et al., 1997; Vogel et al., 2015).

Upon erosion of mineral soils and outcropping rock formations, particulate matter is introduced to and transported within river catchments, and ultimately discharged to the ocean. Due to their hydrodynamic properties, finegrained high-SA minerals predominately contribute to the amount of suspended OC that is transported from land to ocean (Tesi et al., 2016). Several studies report a positive correlation between total organic carbon content (TOC) and SA in river sediments (Keil et al., 1997; Galy et al., 2008; Tao et al., 2015; Vonk et al., 2015) as well as in river-dominated continental margin sediments (e.g., Mayer et al., 1988; Mayer, 1994; Goni et al., 2003; Blair and Aller, 2012). However, few studies have investigated the evolution of OC loadings (TOC/SA ratios) along the axis of a river system. Keil et al. (1997) found no systematic variation in TOC/SA loading on suspended particulate matter among three sampling locations from the lower 1,800 km of the Amazon River and two delta samples, and suggested that suspended sediments transport OC at similar loadings throughout the Amazon catchment. Vonk et al. (2015), on the other hand, observed a decrease in TOC loadings during riverine sediment transport through the Mackenzie delta, coupled with preferential deposition of coarser fractions. A recent synthesis of data from river-dominated continental margin sediments revealed that OC loadings generally fall in the range between 0.4 and 1 mg_{OC}/m^2, with higher (>1 mg_{OC}/m^2) and lower (<0.4 mg_{OC}/m^2) loadings interpreted in terms of shorter and longer oxygen exposure times prior and subsequent to deposition, respectively (Blair and Aller, 2012).

While organo-mineral interactions appear to exert a key influence on OM dynamics in soils, fluvial particles, and river-dominated ocean sediments, the extent to which mineral-associated OM moves conservatively from source to sink, or evolves during transit remains unclear due to other confounding processes that challenge interpretation of these relationships. One complication is that erosion of OC-rich sedimentary rocks adds C that is intrinsic to the particles and unrelated to mineral surface loadings of river sediments. Further, variations in flow conditions and associated hydrodynamic sorting of particles according to grain size and other properties (density, shape) influence the OC concentrations in aquatic sediments, rendering it challenging to evaluate the fate of OM cascading through the soil-river-ocean continuum.

With respect to the latter issue, mineral-specific SA may serve as a promising property against which to normalize OC abundance (Hedges and Keil, 1995; Keil et al., 1997), thereby obviating OC concentration variations driven by hydrodynamic processes. In order to more directly trace the fate of terrestrial OM and quantify

potential changes in loadings, additional diagnostic power is needed. Source-specific biomolecular marker compounds have proven valuable as diagnostic tracers of OM inputs to soils, river and ocean sediments (e.g. Galy et al., 2011; Tesi et al., 2014; Griepentrog et al., 2015), enabling signals of vegetation and soil carbon to be traced free of interference from other carbon sources (e.g., petrogenic inputs, within-river productivity) (Eglinton and Eglinton, 2008; Thevenot et al., 2010; Schouten et al., 2013). As such, biomarker abundances, distributions and isotopic compositions in river-influenced sedimentary sequences now form the basis for numerous paleo-environmental and paleoclimatological studies (e.g., Kastner and Goni, 2003; Schefuss et al., 2005; Weijers et al., 2007; Bendle et al., 2010; Sanchi et al., 2014).

Despite their diagnostic power, our understanding of the mode and efficacy of biomolecular signal transfer from source to sink remains rudimentary. In particular, we presently have limited knowledge of biomarker dynamics within river networks. While there is a growing number of studies of biomolecular loadings in continental margin sediments (e.g. Goni et al., 2013; Bröder et al., 2016a, 2016b; Tesi et al., 2016), corresponding investigations of riverine sediments are currently sparse (Goni et al., 2005; Tao et al., 2015), and have not focused on the longitudinal evolution of biomolecular signals along a river network. Moreover, the evolution of particle loadings of different biomolecular signals within river basins currently remains unexplored.

In this study, we have undertaken a detailed investigation of OM loadings on sediments within a major river system. In addition to TOC loadings, we determined loadings of biomarkers specific to soil (i.e., branched glycerol dialkyl glycerol tetraethers (brGDGTs)) and higher plants (i.e., long-chain plant wax fatty acids (FAs) and lignin phenols) in a suite of Danube River sediments collected from the headwaters to the delta. The observed evolution of TOC and biomarker loadings within the Danube River is discussed in the context of signals ultimately exported to the Black Sea, and more broadly in defining benchmark ranges for biomolecular loadings on river particles.

3.2 Study area

With a length of 2,850 km and a catchment area of 801,500 km^2, the Danube River (Figure 3.1) is the largest river of the European Union. The Danube is sourced from the Black Forest in southern Germany at an elevation of about 1,000 m a.s.l and drains into the Black Sea with an average discharge of 6,500 m^3/s (ICPDR, 2005). The Danube catchment is typically divided into four sub-basins: (1) the upper basin from the source to the Gate of Devin downstream of Vienna at the confluence with the Morava River, where the foothills of the Eastern Alps and the Small Carpathians meet (ICPDR, 2005); (2) the middle basin from the Gate of Devin to the Iron Gate reservoir, where the Danube cuts the Carpathian mountains; (3) the lower basin from the Iron Gates to the

beginning of the delta and (4) the delta region where the Danube mainstream splits into three main arms, forming a large wetland area (675,000 ha; ICPDR, 2005).

The Danube primarily drains the Mesozoic Alpine ranges outcropping crystalline rocks, limestones, flysch and molasse (e.g., Alps, Carpathians, Dinarics and Balkans together with their foothills) and intermountain plains such as the Pannonian and Romanian plains (e.g., Schiller et al., 2010). In addition, mostly crystalline Paleozoic plateaus are located in the upper basin (e.g., Schwarzwald Massif, Bohemian-Moravian Upland) and near the mouth (i.e., Dobrogea). The south-western part of the pre-Paleozoic Russian Platform is drained by Danube tributaries crossing the Moldavian Plateau. Easily erodible loess covers most of the intermountain plains and plateaus especially in the mid and lower parts of the basin (Haase et al., 2007).

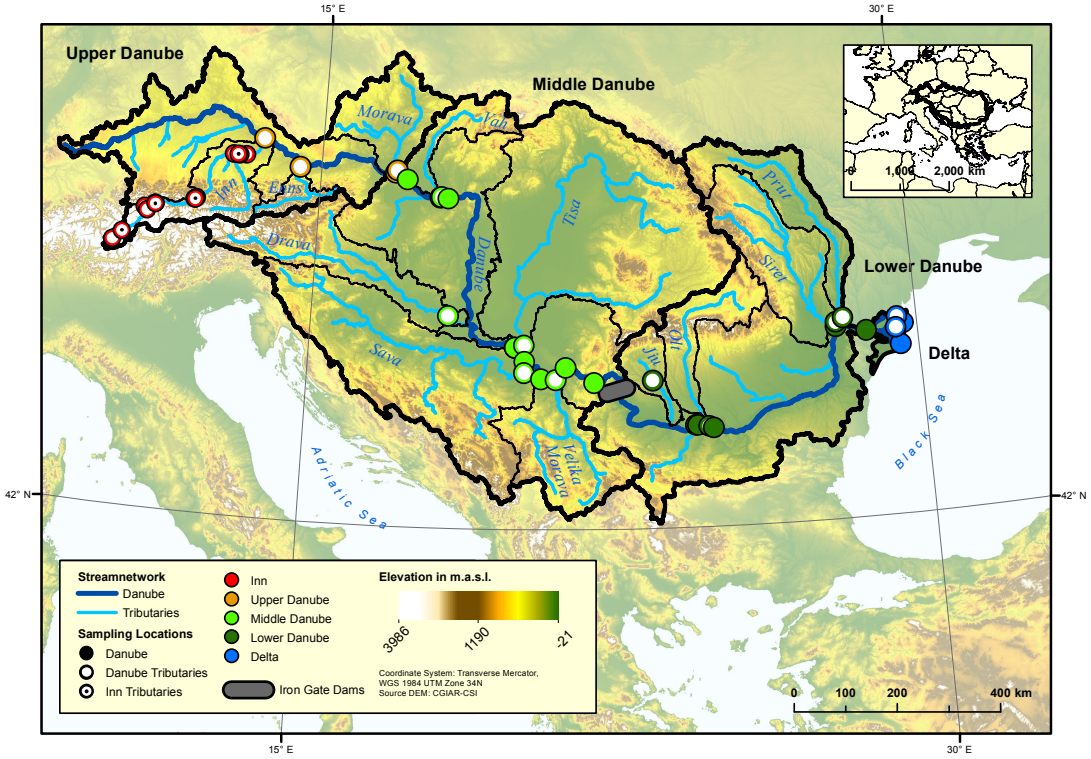

Figure 3.1. The Danube River basin. Thick black lines show the catchment outline as well as the division into upper, middle, lower basin and delta region. Thin black lines are major tributary catchments. The Danube mainstream is shown in dark blue, tributaries in light blue. Sampling locations with a closed symbol correspond to Danube mainstem locations, open symbols to tributary locations. Sampling location colors correspond to sub-basins (orange: upper basin, light green: middle basin, dark green: lower basin, blue: delta). The Inn River, a tributary to the Danube in the upper basin, is shown with open, red symbols, tributaries to the Inn River are shown as open symbols with a black dot.

Mountainous soils in the Danube basin developed on crystalline or Mesozoic limestone bedrock. In high mountainous regions, rock-derived syrozems and leptosols with little humus predominate (Schiller et al., 2010). Below these high altitudes, cambisols and podzol-cambisols occur due to higher temperatures and denser vegetation cover. In low altitudes, deeper soils evolved on loose, Cenozoic sediment and alluvium fills. In river valleys and plains, floodplain soils developed, whereas cambisols, podzol-cambisols and podzols characterize non-flooded areas, and luvisols formed on loess. Chernozems predominate in the plains of the lower Danube basin (Schiller et al., 2010).

3.3 Methods

3.3.1 Sample collection

Detailed sampling of river sediment within the Danube River basin was performed in May and June 2013 and 2014, shortly after the yearly peak in discharge. In 2014, the sampling campaign was extended to include sediment sampling of the Inn River, the largest tributary to the Danube in the upper basin, discharging about 65% more water than the Danube at the confluence. In this study, the term "river sediment" is used for fine-grained sediment (<1 mm grain size) that was recently deposited on the riverbanks or in hydrological quiescent locations in shallow water during decreasing water level of the previous high water event. Coarser and heavy minerals are preferentially deposited during sediment settling (e.g. Garzanti et al., 2009) and therefore, the deposited river sediment mineralogy is likely enhanced in coarse and heavy components compared to the overall suspended load. However, the coarser, denser and lower surface area riverbank sediment also exhibit lower OC concentration compared to actual sampling of suspended sediment (Supplementary Figure A.3.1), most likely resulting in overall comparable OC loadings in suspended- and bank sediments when normalized to surface area. We therefore assume that bank sediment loadings are good representatives of the overall river sediment OC loadings.

Spanning a stretch of ~2,200 km, 20 sites along the Danube mainstem and 12 tributaries were sampled between Passau (Germany) and the Black Sea. The sampling strategy included the collection of one freshly deposited river sediment sample at each of the 12 largest tributaries (Inn, Enns, Morava, Vah, Drava, Tisa, Sava, Velika Morava, Jiu, Olt, Siret, Prut) close to the confluence with the Danube as well as at the Danube mainstem both upstream and 5–10 km downstream of each major tributary confluence. In addition, nine sites along the Inn River and five smaller tributaries to the Inn were sampled in 2014. During the 2013 sampling campaign, a heavy rain event in the upper basin caused a 100-year flood in the upper and middle basin (Blöschl et al., 2013; Grams et al., 2014; ICPDR, 2014). Mostly sandy flood deposits rendered it impossible to find

fine sediment at several planned locations in the upper and middle basin. Moreover, shortly before the second sampling campaign in 2014, another >100-year flood occurred, this time in the lower Sava catchment (ICPDR & ISRBC, 2015). However, this latter event, while locally catastrophic, did not interfere with the sampling. At each sampling location where freshly deposited fine sediment was abundant, ca. 2 kg sediment was collected with a shovel and stored in zip lock bags at -20 °C until further treatment.

3.3.2 Sample treatment, extraction, measurements

3.3.2.1 Samples

For this study, the 32 sediment samples from the Danube sampling in 2013 were analyzed for SA, TOC, FA, lignin-derived phenols, brGDGTs and mineralogy. In addition, 30 samples from the 2014 Danube field campaign were analyzed for SA and TOC, and a subset of samples from 2014 was analyzed for biomarkers (6 FA, 6 lignin phenols, 7 brGDGTs). The 14 Inn River samples were analyzed for SA, TOC, FA, lignin phenols, and brGDGTs (see Supplementary Tables B.3).

3.3.2.2 Sieving

Bulk river sediments were wet sieved with MilliQ water over 200 µm and 63 µm sieves on a shaking table in order to remove coarse particles and organic debris. The resulting <63 µm fraction was freeze-dried and kept frozen until further work-up.

3.3.2.3 Sedimentological parameters

For SA and grain size (GS) measurements, OM in the sediment fine fraction (<63 µm) was removed by combustion (12 h, 450 °C, cool down 40 °C/h). Before SA measurement, samples were degassed under vacuum (>2h, 350 °C) to remove any remaining water. SA was measured with N_2 using the BET method with a 5-point adsorption isotherm (p/p_0 = 0.05–0.3) on a NOVA 4000 surface area analyzer (Keil et al., 1997). For GS distribution measurement, the sediment was dispersed in sodium polyphosphate (1 g/L) overnight and subsequently measured under ultrasonication on a Malvern Mastersizer 2000.

3.3.2.4 Sediment mineralogy

For XRD measurements, 1 g of the <63 µm fraction of Danube 2013 sediments was wet-milled in ethanol to <20 µm using a McCrone Micronising mill. The resulting <20 µm fraction was dried overnight (60 °C) and further powdered and homogenized using a mini mill (Pulverisette 23). Randomly oriented powdered specimens and textured specimens were subsequently prepared. For randomly oriented powder specimens, the powdered material was introduced into a sample holder for packing and forming a flat surface using a razor blade, which minimizes preferential orientation (Zhang et al.,

2003). Textured specimens show enhanced intensity of the basal reflexes of phyllosilicates thereby facilitating their identification following changes in the reflex positions in the XRD pattern after different treatments. The textured specimens were measured in air dry state, after ethylene glycol saturation (stored in ethylene glycol atmosphere at 60 °C for 15 h; for smectite identification) and after combustion (550 °C, 2 h; for kaolinite identification). On a subset of five samples, textured specimens were additionally treated with formamide (measured after 30 min and after 3 h; to distinguish halloysite, kaolinite and chlorite), and with guanidine carbonate (saturated solution; identification of vermiculite). XRD measurements were performed on a Bruker AXS D8 Theta-Theta diffractometer with a SolX detector using Co Kα radiation. The irradiated sample length was holding constant at 18 mm using an automatic θ-compensating divergence slit. Powdered specimens were measured from 2 to 80°2θ with a step size of 0.02° for 4 s/step counting time. Textured specimens were measured from 2 to 30°2θ with step size of 0.02° for 5 s/step. The qualitative phase composition was determined with the software DIFFRACplus (BRUKER AXS). On the basis of the peak position and their relative intensity, the mineral phases were identified in comparison to the PDF-2 database (International Centre for Diffraction Data). Quantification of minerals was achieved with BGMN/AutoQuan software using Rietveld refinement (Bergmann and Kleeberg, 1998).

3.3.2.5 TOC and bulk ^{14}C measurements

Aliquots of the <63 μm sediment fractions were placed in Ag boats and de-carbonated in a desiccator under HCl vapor (60 °C, 3 d), followed by neutralization with NaOH (60 °C, 3 d) (Hedges and Stern, 1984; Komada et al., 2008). The samples together with the silver boats were wrapped in tin boats and TOC was measured on a Vario MICRO cube elemental analyzer (Elementar Analysensysteme GmbH).

For ^{14}C measurement of the 2013 apex sample, the resulting CO_2 from the EA combustion was collected, graphitized with an Automated Graphitisation Equipment system (AGE; Nemec et al., 2010; Wacker et al., 2010) and the ^{14}C contents of the graphite was measured on a MIni radioCArbon DAting System (MICADAS; Synal et al., 2007; Christl et al., 2013). ^{14}C of de-carbonated 2014 sample was measured with an on-line EA-IRMS-AMS system (McIntyre et al., 2016). TOC and bulk ^{14}C were measured at the Laboratory for Ion Beam Physics at ETH Zürich.

3.3.2.6 Lipid analysis

30–50 g of each dry fine-grained (<63 μm) river sediment sample was microwave extracted with dichloromethane/methanol (DCM/MeOH 9:1 v:v, 25 min at 100 °C). The resulting total lipid extract was saponified with KOH in MeOH (0.5 M, 2 h at 70 °C). After the addition of 5 ml MilliQ water with NaCl, a neutral phase was obtained by liquid/liquid extraction with hexane (Hex). An acid fraction was then obtained from the

aqueous phase after acidification to pH 2 with HCl by liquid/liquid extraction with Hex:DCM (4:1 v:v).

Fatty acids (FA): The fatty acids (in the acid fraction) were converted to fatty acid methyl esters (FAMEs) with MeOH:HCl (95:5 v:v, 12–18 h, at 70 °C). The FAME fraction was purified in two steps. First over a SiO_2 column with $NaSO_4$, eluting with (1) Hex, (2) DCM:Hex (2:1 v:v) and (3) DCM. The resulting fraction (2), containing the FAMEs, was passed over an $AgNO_3$–SiO_2 column using (1) DCM and (2) ethyl acetate to remove unsaturated FAMEs. FAMEs were measured on a gas chromatograph with a flame ionization detector (GC-FID; Agilent Technologies 7890A) equipped with an Agilent VF-1 ms column (30 m × 250 µm ID × 0.25 µm film thickness). The temperature program started with a 1 min hold time at 50 °C, followed by a 10 °C/min ramp to 320 °C and a 5 min hold time 320 °C. FAMEs were quantified against an external FAME standard (Supelco, *n*-$C_{4–24}$ even carbon saturated FAMEs) and are reported as long chain FA concentrations (sum *n*-$C_{24–32}$, even C numbers).

brGDGTs: The preparation of a brGDGT fraction from the neutral phase and its subsequent measurement is described in Freymond et al. (2017). The brGDGT concentration data reported here were acquired with the 'classic' method, i.e. without the separation of 5-methyl and 6-methyl brGDGT isomers, using an HPLC-APCI-MS equipped with a Grace Prevail cyano column (150 mm × 2.1 mm, 3 µm) (Schouten et al., 2007; Freymond et al., 2017). This form of data is presented so that all available Danube catchment data, including samples that were not measured with the 'improved chromatography' method, could be used. As shown in Freymond et al. (2017), brGDGT concentrations measured with the two methods correlate strongly (r^2 = 0.95, p-value <0.05), although the 'classic' method gives on average 34% higher values than the 'improved chromatography' method. For proxy calculation see Freymond et al. (2017).

3.3.2.7 Lignin analysis

Lignin phenols were released by microwave-assisted alkaline CuO oxidation (Goni and Montgomery, 2000). In short, about 100 mg cupric oxide, 50 mg ferrous ammonium sulfate, and 100 mg of pre-solvent-extracted fine-grained (<63 µm) sediment sample were combined in ca. 30 ml 2N NaOH solution (deoxygenated with N_2 gas for a minimum of five minutes) in Teflon microwave tubes and the vessels were sealed with a N_2 headspace. The microwave system was run with a 30-min ramp time and 90 min holding at 150 °C. After oxidation, the alkaline solution was siphoned off and the residue rinsed at least three times with NaOH, or until the solution was clear. Then, 10 µL of internal standard (ethylvanillin, trans-cinnamic acid, 1 µg/µL) was added to each sample. The samples were acidified to pH 2 using 37% HCl. Following addition of MilliQ water with NaCl, the phenols were extracted three times with ethyl acetate. To remove water, $NaSO_4$ was added to the vials until it did not clump. The extracts (in ethyl

acetate) were dried under a stream of N_2 and subsequently derivatized with 50 µL of BSTFA and 50 µL pyridine (70 °C, 30 min.).

Lignin phenols were separated and quantified on a GC-FID (Agilent Technologies 7890A) equipped with an Agilent HP-1 ms column (60 m × 250 µm ID × 0.25 µm film thickness). The temperature program was set as follows: after an initial hold time of 1.5 min at 70 °C, temperature was ramped at 30 °C/min to 115 °C, followed by a 3 °C/min ramp to 230 °C, a 40 °C/min ramp to 320 °C and a 10 min hold time at 320 °C. Lignin phenols were quantified against the two internal standards (ethylvanillin to quantify vanillin and syringaldehyde; trans-cinnamic acid to quantify acetovanillone, vanillic acid, acetosyringone, syringic acid, p-coumaric acid, ferulic acid). Concentrations reported in this study correspond to the sum of the eight lignin phenols (acetovanillone, syringaldehyde, vanillic acid, acetosyringone, syringic acid, p-coumaric acid, ferulic acid).

3.3.2.8 Data analysis

The statistic program R (R Core Team, 2014) was used for data analysis and visualization. Relationships between different parameters were assessed by linear regression models where p-values <0.05 were considered to be significant.

3.4 Results

3.4.1 Sediment fine-fraction characteristics

Mineral SA values along the Inn and Danube mainstream (Figure 3.2a) show a linear trend of increasing values, starting from ~3 m^2/g in the upper Inn River basin to 30 m^2/g at the apex of the delta, followed by somewhat lower values within the delta region (delta average: 17 m^2/g). Tributaries follow this trend of increasing values from 2 m^2/g (Inn River tributary in upper Danube basin) to 48 m^2/g (Vedea River in the lower Danube basin) with often slightly higher values than the mainstem, and therefore contribute to the increase in SA in Danube sediments. Median GS (Figure 3.2b) varies from about 6 µm to 25 µm and shows an evolution inverse to SA. Linear regression between SA and GS yields an $r^2 = 0.6$ (p-value <0.05).

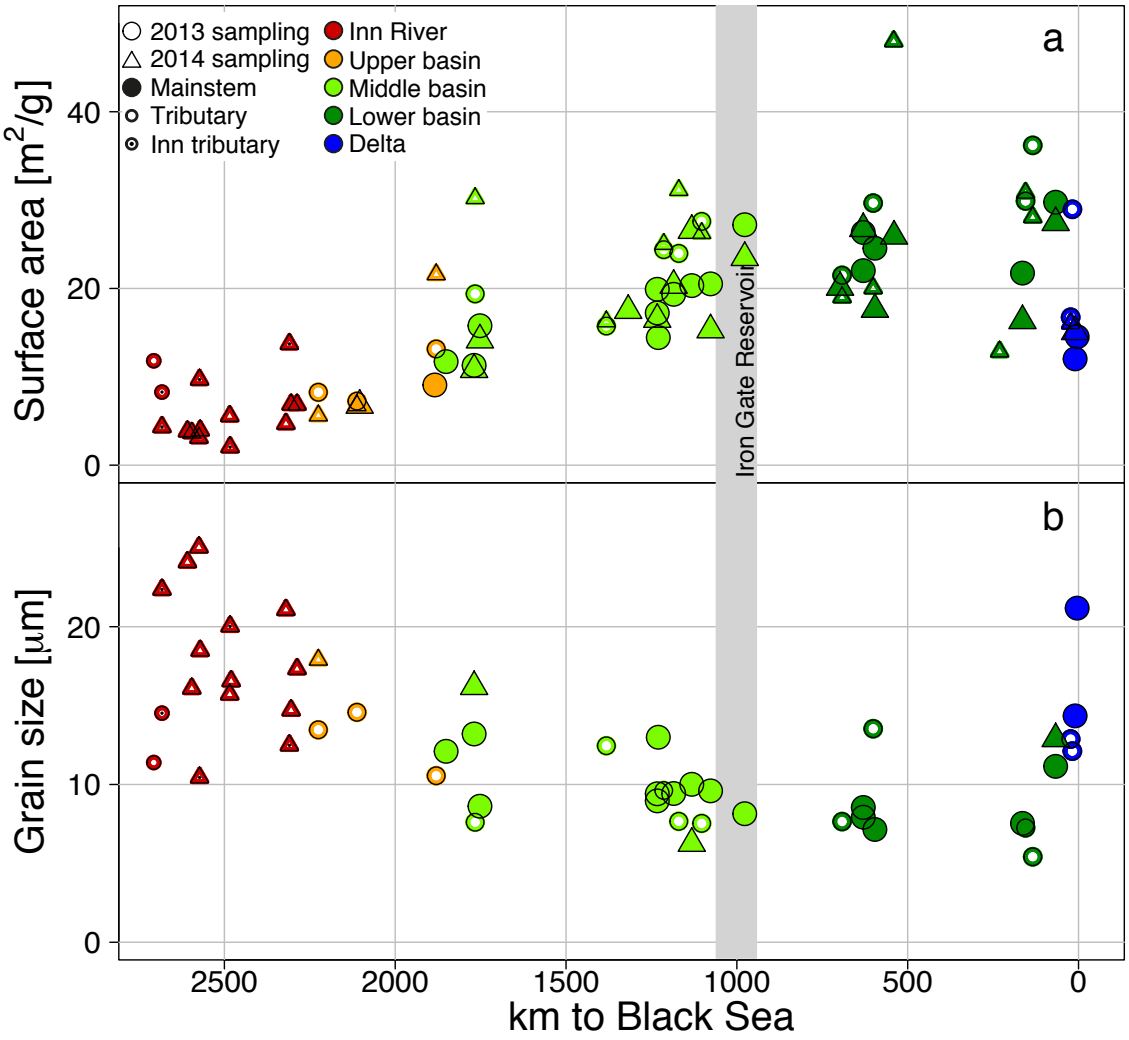

Figure 3.2. (a) Mineral surface area and (b) median grain size along the river. Symbol colors correspond to sub-basins (red: Inn River in the upper basin; orange: upper Danube basin; light green: middle Danube basin; dark green: lower Danube basin; blue: delta region). Circles show samples from 2013, triangles from 2014. Closed symbols correspond to Danube mainstem locations, open symbols to tributary locations. Open red triangles are locations at the Inn mainstem, Inn tributary locations are shown as open symbols with a black dot. The gray bar indicates the location of the Iron Gate reservoir.

Illite and smectite are the phyllosilicates with the largest SA identified in the Danube sediments (BET SA of illite: 20 m^2/g (N_2-BET measurement, Dogan et al., 2007) and smectite: 50–130 m^2/g (N_2-BET measurement, Kaufhold et al., 2010)). The swelling capacity of smectite further increases the available mineral surface area in the interlayer space. The sum of these two minerals (Supplementary Figure A.3.2) increases in the mainstem sediments from 13 wt% of total sediment fine fraction in the upper Danube basin to 25 wt% at the beginning of the Iron Gate Reservoir, and 30 wt% downstream of the reservoir, followed by a decrease to 15 wt% at the mouth of the river. Illite + smectite content of the tributaries follow this evolution, and range from 6 wt% to 33 wt%. Due to their similar evolution along the river, illite + smectite content exhibits a significant correlation with sediment SA (r^2 = 0.62, p-value <0.05; Supplementary Figure A.3.2 and

Figure 3.2a). Kaolinite content shows a similar evolution along the Danube to that of illite + smectite, with increasing values from the upper basin to the beginning of the lower basin, followed by a decrease towards the delta. However, the kaolinite content is lower than illite and smectite, ranging from 0 to 8% (Supplementary Table B.3.3). On a weight basis, the adsorption capacity of phyllosilicates increases in the order of kaolinite < illite < smectite (Saidy et al., 2013; Nguyen and Marschner, 2016; Singh et al., 2016), especially in the pH range of Danube River water of about 8 (JDS3, 2013; Chotzen et al., 2016), rendering illite + smectite the main drivers in the sorption of OC in Danube sediments. Quantitative data for all minerals are listed in Supplementary Table B.3.3.

The most common sediment pretreatment for SA measurements in environmental and geological studies involves the removal of OM either by wet chemical oxidation (e.g. Keil et al., 1994; Mayer, 1994; Ransom et al., 1998) or thermal treatment (e.g. Bao et al., 2016; Coppola et al., 2007; Wakeham et al., 2009). OM removal eliminates a low-density component from the sample, which exhibits a low nitrogen-based SA (mostly <1 m^2/g, less frequently 1–20 m^2/g; Chiou et al., 1990; Pennell et al., 1995). The removal of this component leads to a concentration of the mineral mass, which results in an increase or decrease in the mass-normalized mineral SA. Thermal treatment at low temperatures (≤150 °C) results in a decrease in mineral SA (Kaufhold et al., 2010; Valter and Plötze, 2013). Generally, this loss of mineral SA is observed for various phyllosilicates over a continuous range of temperatures (<600 °C; e.g. Noyan et al., 2006; Plesingerova et al., 2011). Most studies reporting thermally-treated mineral SA data have heated sediment samples at 350 °C. A concern is the efficacy of OM removal at 350 °C due to the formation of charred residues (Masiello, 2004; Wakeham et al., 2009) and thermally recalcitrant OM components (i.e. petrogenic carbon; Hemingway et al., 2017). Chars may exhibit variable and potentially high SA (>50 m^2/g; e.g. Downie et al., 2009) and lead to an overestimate of the mineral SA (Wakeham et al., 2009). The lithogenic nature of the fluvial sediment samples at hand warranted a higher temperature treatment (450 °C) to ameliorate this effect. While results from the present study are internally consistent, caution should be exercised in comparison of SA across studies that have employed different methods and investigated different matrices.

3.4.2 TOC, fatty acid, brGDGT and lignin concentrations

TOC values of Inn and Danube mainstem sediments (Figure 3.3a) increase from 0.25% in the Inn basin to 2.04% in the Iron Gate reservoir and show a decrease after the dam to 0.50% at the mouth. Tributaries follow the same trend and range between 0.40% and 2.30%.

Long-chain FA (n-$C_{24–32}$), as well as brGDGT and lignin concentrations (Figures 3.4a, 3.5a and 3.6a) correlate with TOC (Figure 3.3a) (r^2 = 0.54; 0.46 and 0.51, respectively; p-values <0.05), and show similar evolution patterns along the Danube to that of TOC with low values along the Inn River, concentration maxima upstream of the

Iron Gate dam and decreasing values towards the Black Sea (Figures 3.3a, 3.4a, 3.5a and 3.6a). Long-chain FA (n-C_{24-32}) concentrations range from 1.8 to 30.1 $\mu g/g_{dw}$ (Figure 3.4a), brGDGT concentrations from 0.03 to 3.09 $\mu g/g_{dw}$ (Figure 3.5a) and lignin concentrations from 1.7 to 283.9 $\mu g/g_{dw}$ (Figure 3.6a).

FA concentrations normalized to TOC content (Figure 3.4b) range between 0.40 and 2.55 mg/g_{OC}, showing relatively constant values along the Inn and Danube (average, 0.96 ±0.40 mg/g_{OC}). BrGDGT concentrations normalized to TOC (Figure 3.5b) increase along the Inn River from 7.7 to 29.1 $\mu g/g_{OC}$ and remain at roughly constant levels along the Danube mainstem, though differing between sampling campaigns (2013 average, 51.8 ±16.6 $\mu g/g_{OC}$; 2014 average, 103.3 ±35.5 $\mu g/g_{OC}$). In contrast to FAs and brGDGTs, lignin concentrations normalized to TOC (Figure 3.6b) show an increase from 0.48 mg/g_{OC} at the Inn River headwaters to 15.3 mg/g_{OC} upstream of the Iron Gates Reservoir, followed by decreasing values after the dams.

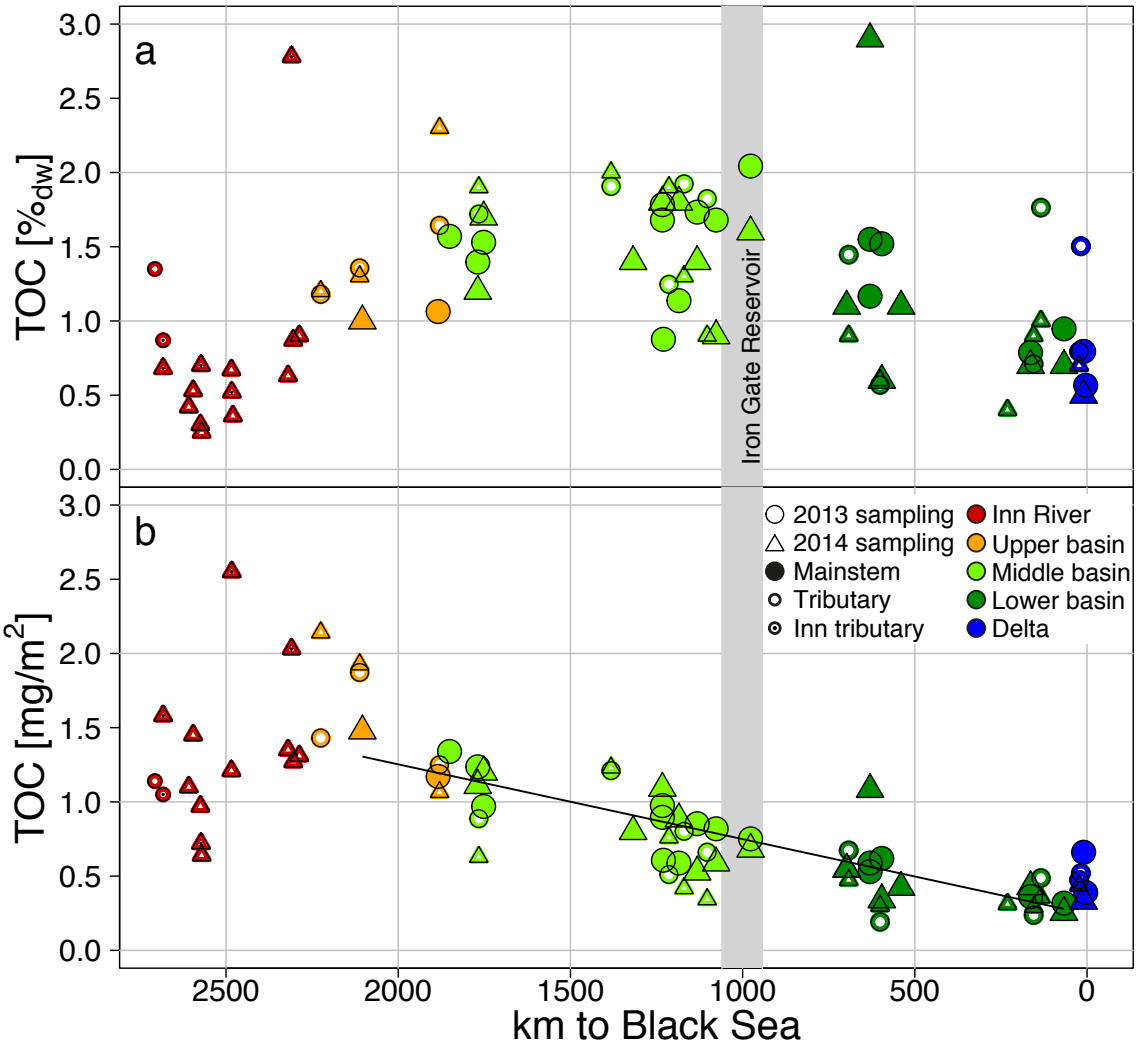

Figure 3.3. Evolution of TOC content along the river. (a) TOC ($\%_{dw}$), (b) TOC normalized to SA (mg_{OC}/m^2) as a function of distance to the Black Sea (2,500 km alpine tributary; 0 km river mouth(s) at the Black Sea). The regression line in panel b) corresponds to data from Danube mainstem sampling locations only (closed symbols). Symbol color and shape correspond to sampling locations in Figures 3.1 and 3.2. The vertical gray bar indicates the location of the Iron Gate reservoir.

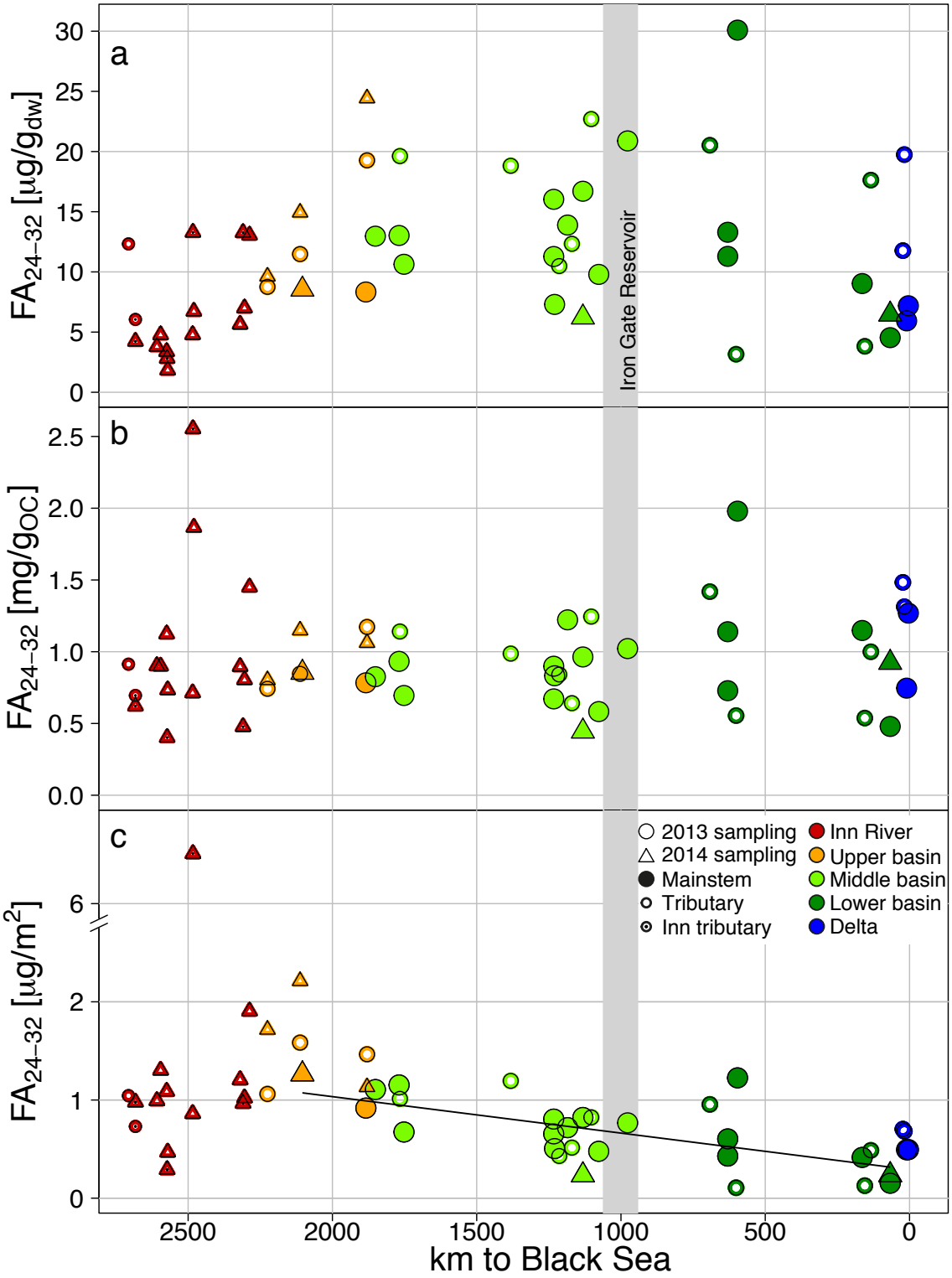

Figure 3.4. Evolution of long-chain (n-$C_{24–32}$) FAs along the river. (a) FA concentrations normalized to sediment weight ($\mu g/g_{dw}$), (b) FA concentrations normalized to TOC (mg/g_{OC}), (c) FA concentrations normalized to mineral-specific SA in $\mu g_{FA}/m^2$ at distance to the Black Sea. The regression line in panel (c) corresponds to Danube mainstem sampling locations only. Symbol color and shape correspond to sampling locations in Figures 3.1 and 3.2.

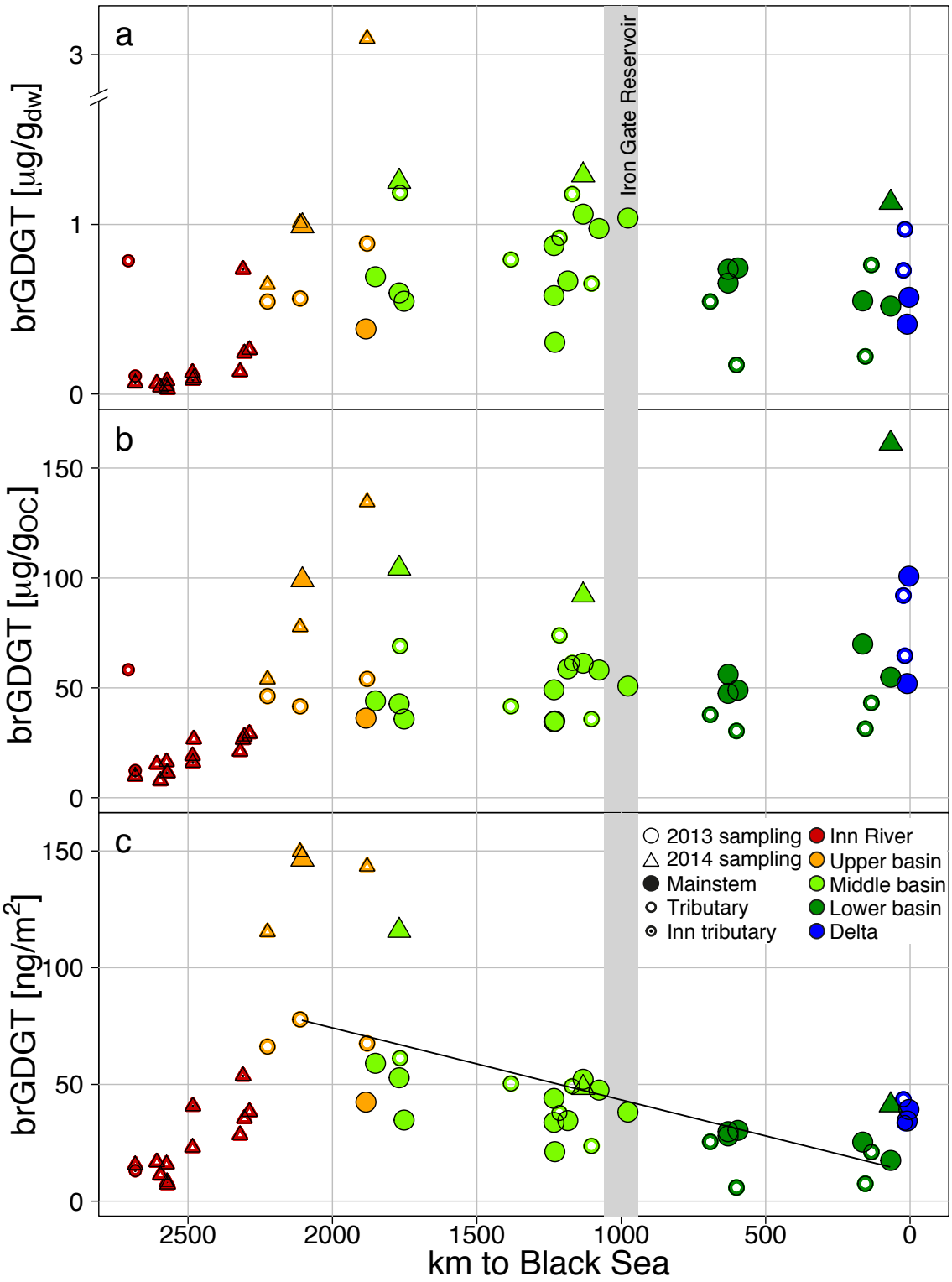

Figure 3.5. Evolution of brGDGTs along the river. (a) BrGDGT concentrations normalized to sediment weight in µg/g_{dw}, (b) brGDGT concentrations normalized to TOC in µg/g_{OC}, (c) brGDGT concentrations normalized to SA in ng/m^2 at distance to the Black Sea. The regression line in panel (c) corresponds to Danube mainstem sampling locations only. Symbol color and shape correspond to those in Figures 3.1 and 3.2.

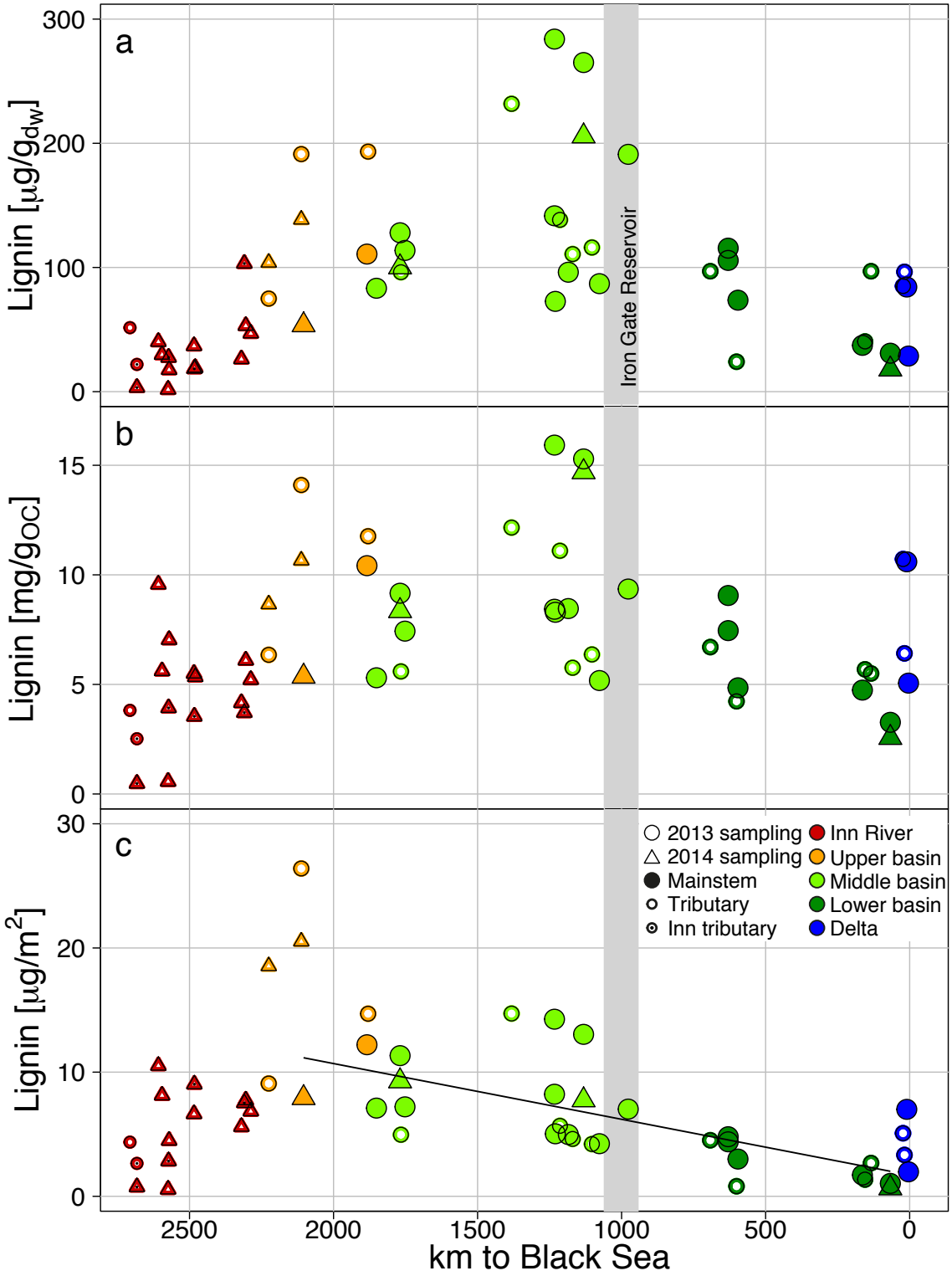

Figure 3.6. Evolution of lignin along the river. (a) Lignin concentrations normalized to sediment weight in µg/g_{dw}, (b) lignin concentrations normalized to TOC in mg/g_{OC}, (c) lignin concentrations normalized to SA in µg/m^2 at distance to the Black Sea. The regression line in panel (c) corresponds to Danube mainstem sampling locations only. Symbol color and shape correspond to those in Figures 3.1 and 3.2.

Normalizing TOC to SA (Figure 3.3b) reveals a linear decrease (r^2 = 0.76, p-value <0.05) in loadings along the Danube mainstem locations from the upper basin (1.48 mg_{OC}/m^2) to the lower basin (0.26 mg_{OC}/m^2). From the uppermost mainstem location in the upper basin to the most downstream location in the lower basin before the delta, TOC loadings decrease by 79%, corresponding to a loss of 50 $\mu g_{OC}/m^2$ per 100 km. Loadings along the Inn River range between 0.64 and 2.55 mg_{OC}/m^2 (average 1.32 ±0.48 mg_{OC}/m^2). Only considering the Inn mainstem, a weak and not significant trend (r^2 = 0.26, p-value = 0.13) of increasing OC loadings from the headwaters to the confluence of the Inn with the Danube is apparent.

FA (Figure 3.4c), brGDGT (Figure 3.5c) and lignin (Figure 3.6c) loadings of Danube mainstem sediments also exhibit a general decrease with distance along the river, albeit with greater scatter (r^2 = 0.46, 0.38 and 0.51, respectively; p-values <0.05). Calculated decreases from the uppermost mainstem location in the upper basin to the most downstream location in the lower basin are as follows: 70% for FAs (corresponding to -36 ng_{FA}/m^2 per 100 km); 81% for brGDGTs (-3.1 ng_{brGDGT}/m^2 per 100 km); 82% for lignin (-400 ng_{lignin}/m^2 per 100 km). The Inn River shows a weak trend to increasing FA and lignin loadings whereas the brGDGT loadings increase linearly (r^2 = 0.79, p-value <0.05, excluding the outlier at km = 2,707).

Cross-plotting TOC versus SA (Figure 3.7a), river sediments from the Inn and Danube yield an average TOC/SA ratio of 0.86 ±0.49 (stdv) mg_{OC}/m^2, and mostly fall into the range considered typical for river suspended sediments (0.4–1 mg_{OC}/m^2; Blair and Aller, 2012). Locations in the upper basin generally exhibit higher TOC loadings and are located outside of this window. Moving downstream to the middle basin and further to the lower basin, the TOC/SA ratio decreases while absolute values for both TOC and SA increase, and most of the locations in the lower basin fall below 0.4 mg_{OC}/m^2. The delta locations exhibit relatively low absolute TOC and SA values, but fall into the typical suspended sediment window. Thus, TOC/ SA values of river mainstem sediments appear to develop along an elliptical orbit (depicted in Figure 3.7e), moving clockwise from close to the origin in headwater samples and returning to similar coordinates in the plot for delta samples (Figure 3.7a). FA, brGDGT and lignin phenol concentrations when plotted against SA (Figure 3.7b-d) show a similar pattern to that of TOC, albeit with greater scatter and slightly varying "orbits" (Figure 3.7a–e).

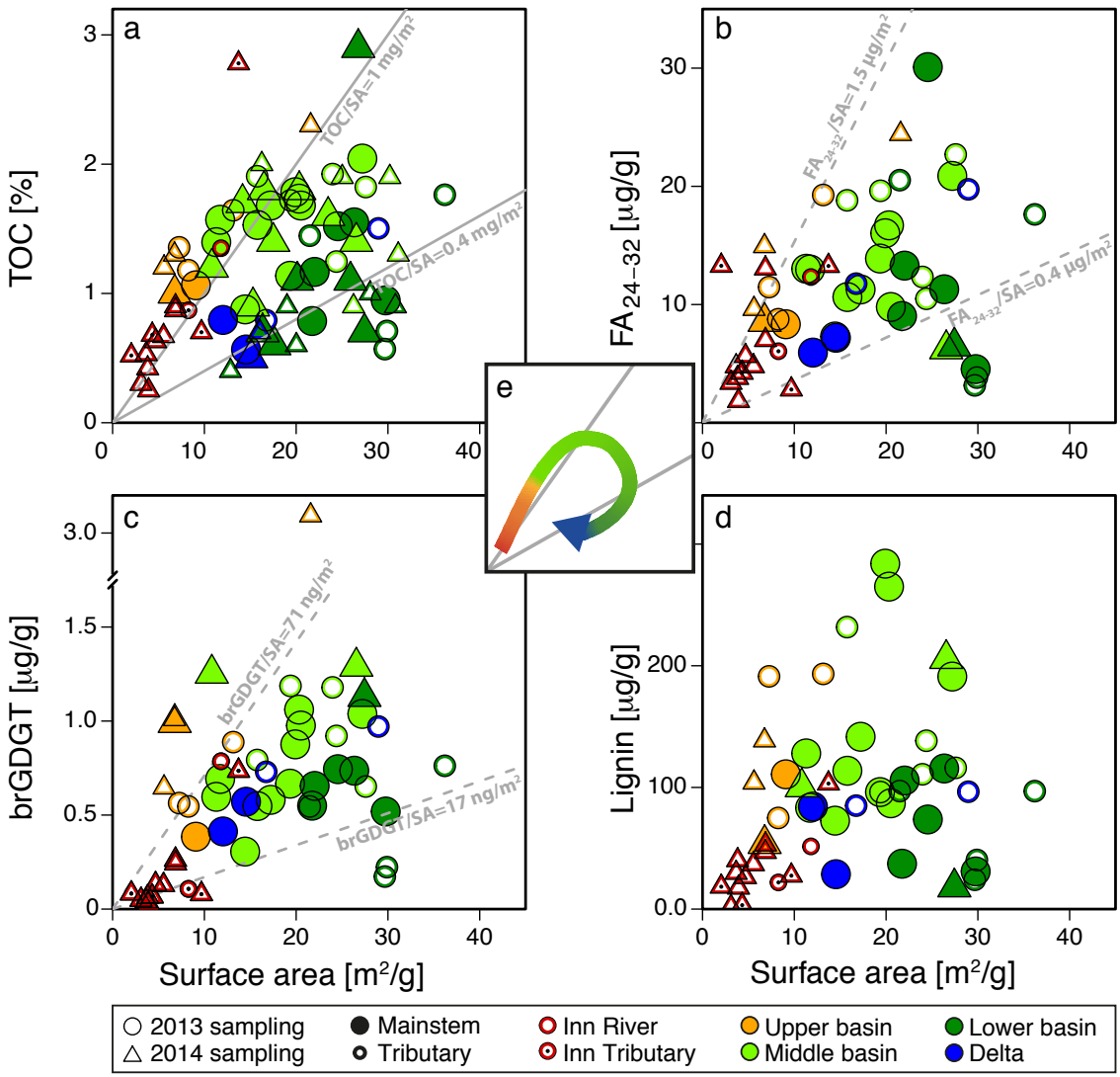

Figure 3.7. (a) TOC, (b) FA, (c) brGDGT and (d) lignin concentrations against SA. Gray lines in (a) correspond to the typical river suspended sediment range of 0.4–1 mg_{OC}/m^2, defined by Blair and Aller (2012). Dashed gray lines in (b) and (c) correspond to proposed "typical" river sediment biomolecular loading ranges of 0.4–1.5 $\mu g_{FA}/m^2$ and 17–71 ng_{brGDGT}/m^2. (e) Schematic evolution of the loadings from the upper basin (red, orange) to the delta (blue). Symbol color and shape correspond to sampling locations in Figures 3.1 and 3.2.

3.5 Discussion

3.5.1 Concept of mineral surface area normalization

OC and biomarker concentrations in fluvial and other sediments are typically normalized to sediment dry weight (dw), however, this approach does not account for changes in mineral composition and hydrological sorting effects in aquatic systems (Blair and Aller, 2012). For biomarker concentrations, this issue can be at least partially obviated by normalizing to TOC content, however quantitative information is lost concerning how OC and specific biomarker concentrations vary as a function of the overall suspended sediment load. By normalizing OC and biomarker concentrations to mineral SA, OC and biomarker loadings are created, taking the mineral composition as well as hydrological sorting effects into account. Coarse particles with little SA and low OC and biomarker concentrations result in similar OC/SA ratios as fine particles with high SA and high OC and biomarker concentration. Keil et al. (1997) used SA as a quasi-conservative property in order to study OM loss and replacement on mineral surfaces of riverine particulate matter in estuarine and deltaic systems. With the assumption that SA is a conservative parameter and that most particulate OC is associated with mineral surfaces, changes in TOC loading should reflect the net exchange of carbon on mineral surfaces (Keil et al., 1997). For this study, the river sediments were sieved to <63 μm with the goal of excluding any large plant debris (that may be derived from local riverbank erosion) and reducing grain size variations. Grain size variations within this clay/silt fraction do persist, as revealed by the gradual decrease in median GS towards the delta, together with a corresponding increase in SA (Figure 3.2). Our basin-wide quantification of phyllosilicate contents (i.e., illite + smectite; Supplementary Figure A.3.2) also shows an increase in the proportion of the high SA clay minerals illite + smectite relative to total sediment weight from the upper basin to the beginning of the lower basin. In general, mainstem sediments of a large river like the Danube River represent the sum of tributary inputs along the river, contributing to the sediment signal by adding mineralogical signals reflective of their respective catchments. Seen from the terminus of the river, the mineralogy of the exported river sediment and the corresponding SA represents an integrated signal of the evolving signal along the flow path (Martin and Meybeck, 1979). However, corresponding SA along a river potentially not only changes due to tributary inputs but could also be affected by different processes. The abrasion of coarse mineral grains during transport decreases with decreasing grain size. In large sand bed rivers, abrasion is generally small but might be more important in the uppermost parts of the catchment (Frings, 2008). Further, the formation of secondary phyllosilicates in temporary traps (e.g., bars and floodplains) would add new high SA particles to the sediment. This process is difficult to quantify, however, in case of the Danube, natural floodplains are scarce due to river regulation. In Danube tributaries sediments, both SA values (Figure

3.2a) and phyllosilicate concentrations (Supplementary Figure A.3.2) follow a similar increasing trend from the upper to the lower Danube basin and show a significant correlation ($r^2 = 0.62$, p-value <0.05). The increase in SA can mostly be explained by the increase in phyllosilicate content, suggesting that inputs from middle and lower basin tributaries are the main driver for the observed SA trend. Therefore, we suggest that SA serves as a useful property against which to assess potential variations in OM loading, and we argue that this property is likely to be more constant than others used for assessment of changes in OM concentrations.

3.5.2 Biomolecular loadings on river sediments

Blair and Aller (2012) adopted the concept of general ranges in SA normalized OC loadings of continental margin sediments that was first developed by Mayer (1994), and found a ratio of 0.4–1 mg_{OC}/m^2 to be representative of river-dominated continental margin sediments. We apply this concept to recent Danube River sediments, and find that they mostly plot within this "typical" river suspended sediment range, but follow a distinct pattern along the course of the river as described in the following, and also depicted in Figure 3.7e. Sediments with higher OC/SA ratio (at the upper end of the window) – defined by Blair and Aller (2012) as freshly deposited with short oxygen exposure time – are located in the upper basin and at the beginning of the middle basin of the catchment. Moving downstream, OC/SA ratios decrease and corresponding sediments plot towards the lower end of the window. Some sediments, mostly from the lower basin, have lower OC/SA ratios than the typical river suspended sediment window (i.e., <0.4 mg/m^2), which according to Blair and Aller (2012) would imply that the associated OM has been subject to protracted oxygen exposure.

Here, we extend this same concept with respect to the concentration of three established groups of biomolecular tracer compounds: FAs, brGDGTs and lignin-derived phenols. We find a similar clustering as for TOC, and similar headwater-to-delta evolutionary trajectories (Figure 3.7a–e). Based on these patterns, we propose windows reflecting "typical" river suspended sediment for FA and brGDGT loadings for the Danube River system (Figure 3.7b and c). The Danube TOC loading (TOC/SA) data is fitted by a log-normal distribution and the range of characteristic river loadings is defined as covering 68% around the mean of the fitted distribution (1σ). With this definition, Danube sediments are characterized by a TOC loading ranging from 0.4 mg_{OC}/m^2 to 1.3 mg_{OC}/m^2, close to TOC loadings of Blair and Aller (2012) (0.4 mg/m^2 and 1 mg/m^2). The somewhat higher upper value found for the Danube (1.3 mg_{OC}/m^2) may reflect the fact that the sediments in the present study are actual river sediments and thus subject to less degradation than river-influenced continental margin sediments. Accordingly, windows for FAs and brGDGTs were defined similarly (dashed lines in Figure 3.7b and c). For long-chain (n-$C_{24–32}$) FAs, we therefore define 0.4–1.5 $\mu g_{FA}/m^2$ and for brGDGTs 17–71 ng_{brGDGT}/m^2 as ranges for Danube River biomarker

loadings (Figure 3.7b and c). Lignin-derived phenols display less systematic behavior, as indicated by greater scatter when concentrations are plotted with respect to SA (Figure 3.7d). We attribute this to the presence of lignin both as discrete (woody) debris and associated with mineral surfaces. Additionally, lignin as a structural polymer is present in the particulate as well as in the dissolved phase due to the weaker hydrophobicity than for example fatty acids or other long alkyl chain lipids, potentially further weakening the correlation between lignin and mineral surface area. The higher TOC- and SA-normalized lignin concentrations in the middle basin compared to the other biomarkers (Figure 3.6b and c) is consistent with enhanced deposition of litter/debris due to slower water velocity upstream of the Iron Gate dam.

3.5.3 Evolution of organic carbon loadings within the river basin

In the Inn tributary and Danube mainstem, organic carbon, as well as biomarker loadings evolve in a distinct pattern from the headwaters towards the Black Sea, which is further discussed below (Figures 3.3b, 3.4c, 3.5c and 3.6c).

From the alpine source in the upper basin (2,484 m a.s.l) to the confluence with the Danube (~300 m a.s.l), Inn River OC loadings increase, and this is followed by a linear decrease along the Danube mainstem to the delta that forms the interface to the Black Sea.

3.5.3.1 Loading increase along the alpine tributary

The initial increase in OM loadings is most pronounced for the brGDGT soil biomarkers (Figure 3.5c), and is consistent with the extent of soil coverage and formation. The highest elevations of the Inn catchment are devoid of soils, and transition to shallow, barely developed soils and then to thicker soil profiles with fully developed A, B and C horizons with decreasing elevation (Figure 3.1). Loadings of the higher plant markers (lignin-derived phenols and especially FAs; Figures 3.6c and 3.4c) and of TOC (Figure 3.3b) exhibit greater scatter. Lignin is presumably present in varying proportions as discrete woody debris in coarser fractions, as well as in dissolved, and mineral-bound form, likely accounting for the weaker correlation with mineral surface area compared to FAs, which are mainly associated with the mineral phase (Chen and Tarachitzky, 2009; Jex et al., 2014). In contrast to [mineral-bound] plant wax FAs (Wiesenberg et al., 2010), surface runoff of vegetation and litter may be an important vector for supply of lignin to the river (Feng et al., 2013). The scatter of FA loadings in the alpine sub-catchment likely partially reflects variability in tributary catchments, gradients in soil development (thickness), as well as higher erosion rates at higher elevations due to steeper slopes and therefore higher energy processes. Since the latter would limit timescales for formation of organo-mineral associations and enhance the export of coarser (rock) particles with low SA, a greater proportion of OC may be transported as discrete debris and not associated with mineral surfaces. Generally,

stochastic erosion processes in high elevations tend to induce a higher variability in signals (Smith et al., 2013). A further consideration is the gradient in vegetation abundance and type within the Inn catchment; Grasses predominate in the highest parts of the catchment above the tree line, and vegetation biomass increases down to the confluence with the Danube, potentially contributing to higher biomolecular and TOC loadings further downstream. Scatter in TOC loadings in the upper Inn catchment (Figure 3.3b) likely derive from a relatively OC-rich sedimentary rock formation the Inn incises (Bündnerschiefer; Waibel and Frisch, 1989). Erosion of this material may entrain fossil OC independent of grain size.

3.5.3.2 Loading decrease along the Danube mainstem

The Inn carries about 65% more water than the Danube mainstem at their confluence (Sommerwerk et al., 2009) and about five times more total suspended solids, which is mainly inorganic in content (ICPDR, 2008). The alpine tributary water mass mixes with the Danube River, with the latter sourced in the Black Forest at lower elevation (ca. 1,000 m a.s.l) and likely carrying a different organic carbon and biomarker signal. From this point onwards, the TOC, FA, brGDGT and lignin loadings decrease linearly with distance downstream (Figures 3.3b and 3.4c, 3.5c and 3.6c). Material from well-developed soils is continuously added to the river sediment load. In soils, fresh biomass is preferentially degraded while organic molecules sorbed to minerals, primarily phyllosilicates, are more persistent (von Lützow et al., 2006). However, although the clay content of topsoil in the catchment generally increases from the upper to the lower basin (Supplementary Figure A.3.3), the OM loadings on these minerals decrease. This trend is followed by tributaries, which exhibit lower loadings further downstream in the catchment (Figure 3.3b and 3.4c, 3.5c and 3.6c). This suggests that a more continental climate (ICPDR, 2005) and/or flatter topography in the lower reaches of the catchment (i.e., slower transfer times from the landscape into the river) enhance reworking and degradation of OM in soils, leading to more degraded OC contributing to fluvial sediments. Additionally, erosion of low OC/high SA loess or other pre-Holocene sedimentary rock deposits, mainly in the middle and lower basins (Kostic and Protic, 2000; Haase et al., 2007; Hatte et al., 2013; Zech et al., 2013; Jipa, 2014) likely contribute to the decreasing loadings in Danube sediments. In this context, the distinctive pattern exhibited by the Inn and Danube sediments in Figure 3.7 –with upper basin locations at the upper end of the 'typical river sediment' loading range, and lower basin locations at the lower loading end– implies that sediments along this large river transect can be envisioned as a gradient of short (fresher OC) to long (more degraded OC) exposure times of terrestrial OM to oxic conditions on the landscape (i.e., in soils) and/or during fluvial transport. Thus, projecting loadings within this type of graphical framework (Figure 3.7) may prove useful for examination of longitudinal trends in fluvial systems.

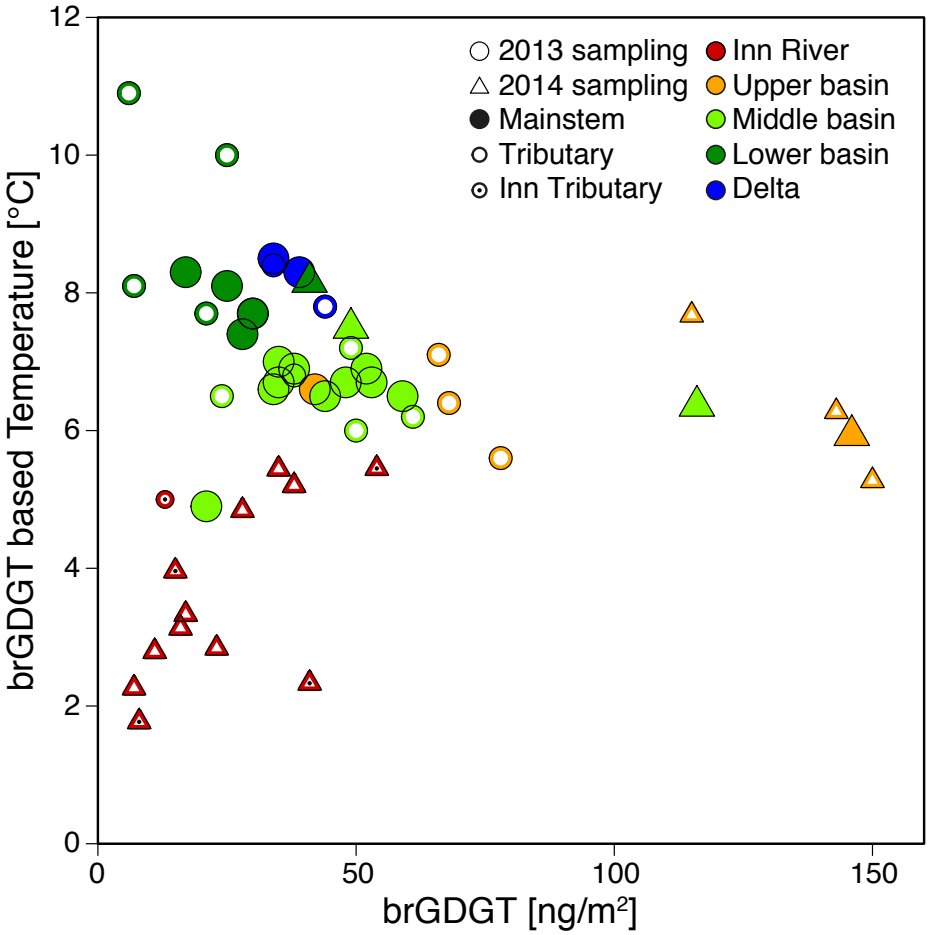

Figure 8. BrGDGT-based temperature in relation to brGDGT loading. BrGDGT-based temperature data from Freymond et al. (2017). In red, the initial buildup of brGDGT loadings with increasing temperature (and therefore decreasing altitude) is visible, followed by increasing temperatures with decreasing loadings along the Danube mainstem. Symbol color and shape correspond to those in Figures 1 and 2.

The addition of low OC/high SA loess material from middle and lower basin tributaries likely contributes to a decrease in the loadings of Danube mainstem sediments. However, in comparison to the Danube mainstem, the addition of sediment with low OC loadings from these tributaries (especially those in the lower basin) is too small to lower the mainstem loadings to the observed extent (Supplementary Figure A.3.4). Another process that potentially could lead to decreasing loadings is POC/DOC exchange and loss of POC into the DOC pool. However, the brGDGT-derived temperature signal in the river sediment changes in line with the local conditions at the sampling locations with no evidence for significant addition of in-river produced brGDGTs, as shown in Freymond et al. (2017). These local brGDGT proxy values in river sediment evolve together with the decrease in loadings (Figure 3.8), what speaks against POC/DOC exchange as main process. This rather implies that new material carrying local information is added to the sediment and therefore, at least a portion of the upstream signal has to be removed to produce such a local signal. Furthermore, it is unlikely that highly hydrophobic (and therefore particle-reactive) molecules such as

long-chain FAs will accumulate in the dissolved phase whereas it is clear that the mineral-associated concentration decreases. A local plant wax fatty acid signature corresponding to the altitude of the sampling location was also found in the Madre de Dios River, and was partly attributed to degradation and net loss of the upstream signal (Ponton et al., 2014). Therefore, we conclude that degradation processes contribute to the observed decrease in OC and biomarker loadings in the lower reaches. The large decrease of OC (70–80%) along the river system (Figures 3.3b and 3.4c, 3.5c and 3.6c) suggests that not only fresh and free organic carbon is remineralized, but mineral-associated carbon also seems to be degraded during transport. Radiocarbon measurement of TOC for sediment samples from the apex of the delta yielded a ^{14}C age of about 2,000 years (Supplementary Figure A.3.1e), consistent with protracted entrainment in deposition and resuspension cycles during fluvial transport accompanied by aging and degradation of OC and/or dilution with pre-aged, low OC loading loess material. The smaller decrease of FA loadings (70%) compared to brGDGTs (81%) suggests that FAs are more closely associated with SA. Therefore, while organo-mineral interactions likely suppress degradation and to some degree protect mineral-bound OM from remineralization, our findings show that organo-mineral associations within river systems are clearly dynamic and evolve throughout the river network. Further constraints on the composition, provenance and age of specific organic components in river sediment as well as suspended sediment are needed in order to shed further light on the evolution of OM during fluvial transport.

Our study ends at the terminus of the Danube River, and thus the fate of fluvially-derived sedimentary OM upon discharge to the Black Sea remains an open question. Nevertheless, the strong decrease in loading over a 2,000 km tract of one of the largest rivers on Earth implies that degradation of particulate OC is significant during transit, and that export of OM from terrigenous primary production to the ocean for such rivers may be dominated by lower basin inputs. In this context, OM preserved in river-dominated shelf sediments may not reflect integrated signals for the entire catchment, but rather is weighted towards its lower reaches, with implications for carbon budgets and interpretation of sedimentary archives.

Acknowledgements

This project was funded by the Swiss National Science Foundation ("CAPS-LOCK" and "CAPS-LOCK2"; #200021_140850). We thank colleagues who supported both sampling campaigns (Marilu Tavagna, Alissa Zuijdgeest, James Saenz, Stefan Eugen Filip, Silvia Lavinia Filip, Mihai, Clayton Magill, Michael Albani). Further thank goes to Daniel Montluçon, Negar Haghipour and Jennifer Anspach for valuable lab support and Lorena Fischer for ArcGIS-related work. Grain size measurements were performed in the limnogeology lab at ETH Zürich. FP acknowledges funding from ETH Fellowship FEL-36 11-1 and NWO-Veni 863.13.016. All data included in this manuscript can be found in Supplementary Tables B.3. This manuscript benefitted from feedback of three anonymous reviewers.

Associate Editor—Josef P. Werne

References

Baldock, J.A. and Skjemstad, J.O. (2000) Role of the soil matrix and minerals in protecting natural organic materials against biological attack. *Organic Geochemistry* 31, 697–710.

Bao, R., McIntyre, C., Zhao, M., Zhu, C., Kao, S.J. and Eglinton, T.I. (2016) Widespread dispersal and aging of organic carbon in shallow marginal seas. *Geology* 44, 791–794.

Bendle, J.A., Weijers, J.W.H., Maslin, M.A., Sinninghe Damsté, J.S., Schouten, S., Hopmans, E.C., Boot, C.S. and Pancost, R.D. (2010) Major changes in glacial and Holocene terrestrial temperatures and sources of organic carbon recorded in the Amazon fan by tetraether lipids. *Geochemistry Geophysichs Geosystems* 11, 1–13.

Bergmann, J. and Kleeberg, R. (1998) Rietveld analysis of disordered layer silicates. *Materials Science Forum* 278–281, 300–305.

Berner, R.A. (2006) GEOCARBSULF: A combined model for Phanerozoic atmospheric O_2 and CO_2. *Geochimica et Cosmochimica Acta* 70, 5653–5664.

Blair, N.E. and Aller, R.C. (2012) The fate of terrestrial organic carbon in the marine environment. *Annual Review of Marine Science* 4, 401–423.

Blair, N.E., Leithold, E.L. and Aller, R.C. (2004) From bedrock to burial: The evolution of particulate organic carbon across coupled watershed-continental margin systems. *Marine Chemistry* 92, 141–156.

Blöschl, G., Nester, T., Komma, J., Parajka, J. and Perdigao, R.A.P. (2013) The June 2013 flood in the Upper Danube Basin, and comparisons with the 2002, 1954 and 1899 floods. *Hydrology and Earth System Sciences* 17, 5197–5212.

Bröder, L., Tesi, T., Andersson, A., Eglinton, T.I., Semiletov, I.P., Dudarev, O.V., Roos, P. and Gustafsson, Ö. (2016a) Historical records of organic matter supply and degradation status in the East Siberian Sea. *Organic Geochemistry* 91, 16–30.

Bröder, L., Tesi, T., Salvado, J.A., Semiletov, I.P., Dudarev, O.V. and Gustafsson, Ö. (2016b) Fate of terrigenous organic matter across the Laptev Sea from the mouth of the Lena River to the deep sea of the Arctic interior. *Biogeosciences* 13, 5003–5019.

Burdige, D.J. (2005) Burial of terrestrial organic matter in marine sediments: A re-assessment. *Global Biogeochemical Cycles* 19.

Chen, Y. and Tarachitzky, J. (2009) Organo-mineral complexes and their effects on the physico-chemical properties of soils. *CMS Workshop Lectures* 16, 32–49.

Chiou, C.T., Lee, J.F. and Boyd, S.A. (1990) The surface area of soil organic matter. *Environmental Science and Technology* 24, 1164–1166.

Chotzen, R.A., Polubesova, T., Chefetz, B. and Mishael, Y.G. (2016) Adsorption of soil-derived humic acid by seven clay minerals: A systematic study. *Clays and Clay Minerals* 64, 628–638.

Christl, M., Vockenhuber, C., Kubik, P.W., Wacker, L., Lachner, J., Alfimov, V. and Synal, H.A. (2013) The ETH Zurich AMS facilities: Performance parameters and reference materials. *Nuclear Instruments and Methods in Physics Research B* 294, 29–38.

Coppola, L., Gustafsson, Ö., Andersson, P., Eglinton, T.I., Uchida, M. and Dickens, A.F. (2007) The importance of ultrafine particles as a control on the distribution of organic carbon in Washington Margin and Cascadia Basin sediments. *Chemical Geology* 243, 142–156.

Dogan, M., Dogan, A.U., Yesilyurt, F.I., Alaygut, D., Buckner, I. and Wurster, D.E. (2007) Baseline studies of The Clay Minerals Society special clays: Specific surface area by the Brunauer Emmett Teller (BET) method. *Clays and Clay Minerals* 55, 534–541.

Downie, A., Munroe, P. and Crosky, A. (2009) Characteristics of biochar: Physical and structural properties, in: Lehmann J. and Joseph S. (Eds.), Biochar for environmental management: Science and Technology. Earthscan, London and Sterling, VA, pp. 13–29.

Eglinton, T.I. and Eglinton, G. (2008) Molecular proxies for paleoclimatology. *Earth and Planetary Science Letters* 275, 1–16.

Feng, X.J., Vonk, J.E., van Dongen, B.E., Gustafsson, Ö., Semiletov, I.P., Dudarev, O.V., Wang, Z.H., Montluçon, D.B., Wacker, L. and Eglinton, T.I. (2013) Differential mobilization of terrestrial carbon pools in Eurasian Arctic river basins. *Proceedings of the National Academy of Science USA* 110, 14168–14173.

Freymond, C.V., Peterse, F., Fischer, L.V., Filip, F., Giosan, L. and Eglinton, T.I. (2017) Branched GDGT signals in fluvial sediments of the Danube River basin: Method comparison and longitudinal evolution. *Organic Geochemistry* 103, 88–96.

Frings, R.M. (2008) Downstream fining in large sand-bed rivers. *Earth-Science Reviews* 87, 39–60.

Galy, V., France-Lanord, C. and Lartiges, B. (2008) Loading and fate of particulate organic carbon from the Himalaya to the Ganga-Brahmaputra delta. *Geochimica et Cosmochimica Acta* 72, 1767–1787.

Galy, V., Eglinton, T., France-Lanord, C. and Sylva, S. (2011) The provenance of vegetation and environmental signatures encoded in vascular plant biomarkers carried by the Ganges-Brahmaputra rivers. *Earth and Planetary Science Letters* 304, 1–12.

Garzanti, E., Ando, S. and Vezzoli, G. (2009) Grain-size dependence of sediment composition and environmental bias in provenance studies. *Earth and Planetary Science Letters* 277, 422–432.

Goni, M.A. and Montgomery, S. (2000) Alkaline CuO oxidation with a microwave digestion system: Lignin analyses of geochemical samples. *Analytical Chemistry* 72, 3116–3121.

Goni, M.A., Teixeira, M.J. and Perkey, D.W. (2003) Sources and distribution of organic matter in a river-dominated estuary (Winyah Bay, SC, USA). *Estuarine Coastal and Shelf Science* 57, 1023–1048.

Goni, M.A., Yunker, M.B., Macdonald, R.W. and Eglinton, T.I. (2005) The supply and preservation of ancient and modern components of organic carbon in the Canadian Beaufort Shelf of the Arctic Ocean. *Marine Chemistry* 93, 53–73.

Goni, M.A., O'Connor, A.E., Kuzyk, Z.Z., Yunker, M.B., Gobeil, C. and Macdonald, R.W. (2013) Distribution and sources of organic matter in surface marine sediments across the North American Arctic margin. *Journal of Geophysical Research: Oceans* 118, 4017–4035.

Grams, C.M., Binder, H., Pfahl, S., Piaget, N. and Wernli, H. (2014) Atmospheric processes triggering the central European floods in June 2013. *Natural Hazards and Earth System Sciences* 14, 1691–1702.

Griepentrog, M., Eglinton, T.I., Hagedorn, F., Schmidt, M.W.I. and Wiesenberg, G.L.B. (2015) Interactive effects of elevated CO_2 and nitrogen deposition on fatty acid molecular and isotope composition of above- and belowground tree biomass and forest soil fractions. *Global Change Biology* 21, 473–486.

Haase, D., Fink, J., Haase, G., Ruske, R., Pecsi, M., Richter, H., Altermann, M. and Jager, K.D. (2007) Loess in Europe - its spatial distribution based on a European Loess Map, scale 1:2,500,000. *Quaternary Science Review* 26, 1301–1312.

Hatte, C., Gauthier, C., Rousseau, D.D., Antoine, P., Fuchs, M., Lagroix, F., Markovic, S.B., Moine, O. and Sima, A. (2013) Excursions to C4 vegetation recorded in the Upper Pleistocene loess of Surduk (Northern Serbia): An organic isotope geochemistry study. *Climate of the Past* 9, 1001–1014.

Hedges, J.I. and Keil, R.G. (1995) Sedimentary organic matter preservation: An assessment and speculative synthesis. *Marine Chemistry* 49, 81–115.

Hedges, J.I. and Stern, J.H. (1984) Carbon and nitrogen determinations of carbonate-containing solids. *Limnology and Oceanography* 29, 657–663.

Hemingway, J.D., Rothman, D.H., Rosengard, S.Z. and Galy, V.V. (2017) Technical note: An inverse method to relate organic carbon reactivity to isotope composition from serial oxidation. *Biogeosciences* 14, 5099–5114.

ICPDR (2005) The Danube River Basin District. Part A – Basin- wide Overview (Ed. U. Schmedtje). International Commission for the Protection of the Danube River, ICPDR.

ICPDR (2008) Joint Danube Survey 2. Final Scientific Report. International Commission for the Protection of the Danube River, ICPDR.

ICPDR (2014) Floods in June 2013 in the Danube River Basin. Brief Overview of Key Events and Lessons Learned. International Commission for the Protection of the Danube River, ICPDR.

ICPDR & ISRBC (2015) Floods in May 2014 in the Sava River Basin. Brief overview of key events and lessons learned. International Commission for the Protection of the Danube River, ICPDR and International Sava River Basin Commission, ISRBC.

JDS3 (2013) Danubis, the ICPDR information system – Danube river basin water quality database.

Jex, C.N., Pate, G.H., Blyth, A.J., Spencer, R.G.M., Hernes, P.J., Kahn, S.J. and Baker, A. (2014) Lignin biogeochemistry: From modern processes to Quaternary achieves. *Quaternary Science Review* 87, 46–59.

Jipa, D.C. (2014) The conceptual sedimentary model of the Lower Danube loess basin: Sedimentogenetic implications. *Quaternary International* 351, 14–24.

Kastner, T.P. and Goni, M.A. (2003) Constancy in the vegetation of the Amazon Basin during the late Pleistocene: Evidence from the organic matter composition of Amazon deep sea fan sediments. *Geology* 31, 291–294.

Kaufhold, S., Dohrmann, R., Klinkenberg, M., Siegesmund, S. and Ufer, K. (2010) N_2-BET specific surface area of bentonites. *Journal of Colloid and Interface Science* 349, 275–282.

Keil, R.G. and Mayer, L.M. (2014) Mineral matrices and organic matter, in: Turekian, K.K. (Ed.), Treatise on Geochemistry (second edition). Elsevier, Oxford, pp. 337–359.

Keil, R.G., Tsamakis, E., Fuh, C.B., Giddings, J.C. and Hedges, J.I. (1994) Mineralogical and textural controls on the organic composition of coastal marine sediments: Hydrodynamic separation using SPLITT-fractionation. *Geochimica et Cosmochimica Acta* 58, 879–893.

Keil, R.G., Mayer, L.M., Quay, P.D., Richey, J.E. and Hedges, J.I. (1997) Loss of organic matter from riverine particles in deltas. *Geochimica et Cosmochimica Acta* 61, 1507–1511.

Komada, T., Anderson, M.R. and Dorfmeier, C.L. (2008) Carbonate removal from coastal sediments for the determination of organic carbon and its isotopic signatures, delta C-13 and Delta C-14: Comparison of fumigation and direct acidification by hydrochloric acid. *Limnology and Oceanography: Methods* 6, 254– 262.

Kostic, N. and Protic, N. (2000) Pedology and mineralogy of loess profiles at Kapela-Batajnica and Stalac, Serbia. *Catena* 41, 217–227.

Ludwig, W., Probst, J.L. and Kempe, S. (1996) Predicting the oceanic input of organic carbon by continental erosion. *Global Biogeochemical Cycles* 10, 23–41.

Martin, J.M. and Meybeck, M. (1979) Elemental mass-balance of material carried by major world rivers. *Marine Chemistry* 7, 173–206.

Masiello, C.A. (2004) New directions in black carbon organic geochemistry. *Marine Chemistry* 92, 201–213.

Mayer, L.M. (1994) Surface-area control of organic-carbon accumulation in continental-shelf sediments. *Geochimica et Cosmochimica Acta* 58, 1271–1284.

Mayer, L.M., Macko, S.A. and Cammen, L. (1988) Provenance, concentrations and nature of sedimentary organic nitrogen in the Gulf of Maine. *Marine Chemistry* 25, 291–304.

McIntyre, C.P., Wacker, L., Haghipour, N., Blattmann, T.M., Fahrni, S., Usman, M., Eglinton, T.I. and Synal, H.A. (2016) Online 13C and 14C gas measurements by EA–IRMS–AMS at ETH Zürich. *Radiocarbon*, 1–11.

Nemec, M., Wacker, L. and Gaggeler, H. (2010) Optimization of the graphitization process at AGE-1. *Radiocarbon* 52, 1380–1393.

Nguyen, T.T. and Marschner, P. (2016) Sorption of water-extractable organic carbon in various clay subsoils: Effects of soil properties. *Pedosphere* 26, 55–61.

Noyan, H., Önal, M. and Sarikaya, Y. (2006) The effect of heating on the surface area, porosity and surface acidity of a bentonite. *Clays and Clay Minerals* 54, 375–381.

Pennell, K.D., Abriola, L.M. and Boyd, S.A. (1995) Surface area of soil organic matter reexamined. Soil *Science Society of America Journal* 59, 1012–1018.

Plesingerova, B., Sucik, G. and Fabian, M. (2011) Surface area change of kaolin causing annealing. *Acta Matallurgica Slovaca* 17, 169–176.

Ponton, C., West, A.J., Feakins, S.J. and Galy, V. (2014) Leaf wax biomarkers in transit record river catchment composition. *Geophysical Research Letters* 41, 6420–6427.

Ransom, B., Kim, D., Kastner, M. and Wainwright, S. (1998) Organic matter preservation on continental slopes: Importance of mineralogy and surface area. *Geochimica et Cosmochimica Acta* 62, 1329–1345.

R Core Team (2014) R: A Language and Environment for Statistical Computing. R Foundation for Statistical Computing, Vienna, Austria.

Saidy, A.R., Smernik, R.J., Baldock, J.A., Kaiser, K. and Sanderman, J. (2013) The sorption of organic carbon onto differing clay minerals in the presence and absence of hydrous iron oxide. *Geoderma* 209–210, 15–21.

Sanchi, L., Ménot, G. and Bard, E. (2014) Insights into continental temperatures in the northwestern Black Sea area during the Last Glacial period using branched tetraether lipids. *Quaternary Science Reviews* 84, 98–108.

Schefuss, E., Schouten, S. and Schneider, R.R. (2005) Climatic controls on central African hydrology during the past 20,000 years. *Nature* 437, 1003–1006.

Schiller, H., Miklos, D. and Sass, J. (2010) The Danube River and its basin physical characteristics, water regime and water balance, in: Mitja B. (Ed.), Hydrological processes of the Danube River Basin. Perspectives from the Danubian Countries. Springer, Dordrecht, Netherlands, pp. 25–77.

Schouten, S., Huguet, C., Hopmans, E.C., Kienhuis, M.V.M. and Sinninghe Damsté, J.S. (2007) Analytical methodology for TEX86 paleothermometry by high-performance liquid chromatography/atmospheric pressure chemical ionization-mass spectrometry. *Analytical Chemistry* 79, 2940–2944.

Schouten, S., Hopmans, E.C. and Sinninghe Damsté, J.S. (2013) The organic geochemistry of glycerol dialkyl glycerol tetraether lipids: A review. *Organic Geochemistry* 54, 19–61.

Singh, M., Sarkar, B., Biswas, B., Churchman, J. and Bolan, N.S. (2016) Adsorption-desorption behavior of dissolved organic carbon by soil clay fractions of varying mineralogy. *Geoderma* 280, 47–56.

Smith, J.C., Galy, A., Hovius, N., Tye, A.M., Turowski, J.M. and Schleppi, P. (2013) Runoff-driven export of particulate organic carbon from soil in temperate forested uplands. *Earth and Planetary Science Letters* 365, 198–208.

Sommerwerk, N., Hein, T., Scheider-Jakoby, M., Baumgartner, C., Ostojic, A., Paunovic, M., Bloesch, J., Sieber, R. and Tockner, K. (2009) The Danube River basin, in: Tockner, K., Uehlinger, U. and Robinson, C.T (Eds.), Rivers of Europe. Elsevier Science, London, pp. 59–112.

Sorensen, L.H. (1981) Carbon-nitrogen relationships during the humification of cellulose in soils containing different amounts of clay. *Soil Biology and Biochemistry* 13, 313–321.

Synal, H.A., Stocker, M. and Suter, M. (2007) MICADAS: A new compact radiocarbon AMS system. *Nuclear Instruments and Methods in Physics Research B* 259, 7–13.

Tao, S.Q., Eglinton, T.I., Montluçon, D.B., McIntyre, C. and Zhao, M.X. (2015) Pre-aged soil organic carbon as a major component of the Yellow River suspended load: Regional significance and global relevance. *Earth and Planetary Science Letters* 414, 77–86.

Tesi, T., Semiletov, I., Hugelius, G., Dudarev, O., Kuhry, P. and Gustafsson, Ö. (2014) Composition and fate of terrigenous organic matter along the Arctic land-ocean continuum in East Siberia: Insights from biomarkers and carbon isotopes. *Geochimica et Cosmochimica Acta* 133, 235–256.

Tesi, T., Semiletov, I., Dudarev, O., Andersson, A. and Gustafsson, Ö. (2016) Matrix association effects on hydrodynamic sorting and degradation of terrestrial organic matter during cross-shelf transport in the Laptev and East Siberian shelf seas. *Journal of Geophysical Research Biogeosciences* 121, 731–752.

Thevenot, M., Dignac, M.F. and Rumpel, C. (2010) Fate of lignins in soils: A review. *Soil Biology and Biochemistry* 42, 1200–1211.

Torn, M. S., Trumbore S. E., Chadwick O. A., Vitousek P. M. and Hendricks D. M. (1997) Mineral control of soil organic carbon storage and turnover. Nature 389, 170–173.

Valter M. and Plötze, M. (2013) Characteristics of variably saturated granular bentonite after long-term storage at near- field relevant temperatures. *Clay Minerals* 48, 343–361.

Vogel, C., Heister, K., Buegger, F., Tanuwidjaja, I., Haug, S., Schloter, M. and Kögel-Knabner, I. (2015) Clay mineral composition modifies decomposition and sequestration of organic carbon and nitrogen in fine soil fractions. *Biology and Fertility of Soils* 51, 427–442.

von Lützow, M., Kögel-Knabner, I., Ekschmitt, K., Matzner, E., Guggenberger, G., Marschner, B. and Flessa, H. (2006) Stabilization of organic matter in temperate soils: Mechanisms and their relevance under different soil conditions - a review. *European Journal of Soil Science* 57, 426–445.

Vonk, J.E., Giosan, L., Blusztajn, J., Montluçon, D., Pannatier, E.G., McIntyre, C., Wacker, L., Macdonald, R.W., Yunker, M.B. and Eglinton, T.I. (2015) Spatial variations in geochemical characteristics of the modern Mackenzie Delta sedimentary system. *Geochimica et Cosmochimica Acta* 171, 100–120.

Wacker, L., Nemec, M. and Bourquin, J. (2010) A revolutionary graphitisation system: Fully automated, compact and simple. *Nuclear Instruments and Methods in Physics Research B* 268, 931–934.

Waibel, A.F. and Frisch, W. (1989) The Lower Engadine Window: Sediment deposition and accretion in relation to the plate-tectonic evolution of the Eastern Alps. *Tectonophysics* 162, 229–241.

Wakeham, S.G., Canuel, E.A., Lerberg, E.J., Mason, P., Sampere, T.P. and Bianchi, T.S. (2009) Partitioning of organic matter in continental margin sediments among density fractions. *Marine Chemistry* 115, 211–225.

Weijers, J.W.H., Schefuss, E., Schouten, S. and Sinninghe Damsté, J.S. (2007) Coupled thermal and hydrological evolution of tropical Africa over the last deglaciation. *Science* 315, 1701–1704.

Wiesenberg, G.L.B., Dorodnikov, M. and Kuzyakov, Y. (2010) Source determination of lipids in bulk soil and soil density fractions after four years of wheat cropping. *Geoderma* 156, 267–277.

Zech, R., Zech, M., Markovic, S., Hambach, U. and Huang, Y. (2013) Humid glacials, arid interglacials? Critical thoughts on pedogenesis and paleoclimate based on multi-proxy analyses of the loess-paleosol sequence Crvenka, Northern Serbia. *Palaeogeography, Palaeoclimatology, Paleoecology* 387, 165–175.

Zhang, G.P., Germaine, J.T., Martin, R.T. and Whittle, A.J. (2003) A simple sample-mounting method for random powder X-ray diffraction. *Clays and Clay Minerals* 51, 218–225.

APPENDIX A.3 Supplementary information

A.3.1 Comparison of SPM and bank sediments

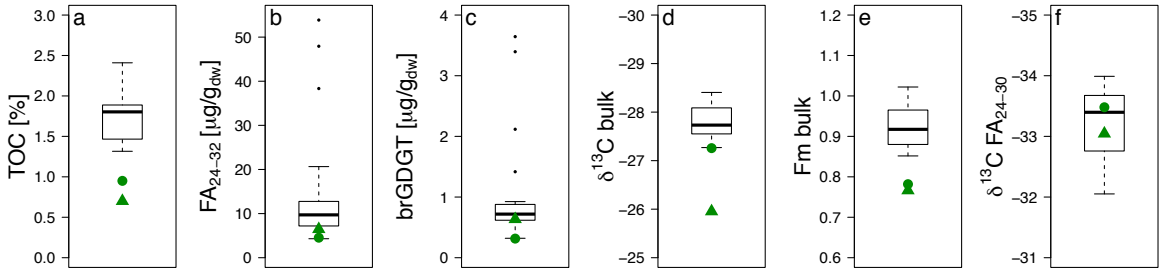

Figure A.3.1. Riverbank sediment – SPM comparison. Box-and-whisker plots of a) TOC, b) FA concentration, c) brGDGT concentration, d) bulk $\delta^{13}C$, e) bulk fraction modern (Fm) and f) FA $\delta^{13}C$. Values of the box-and-whisker plots are SPM samples from depth profiles across the river from the 2013 and 2014 sampling campaigns. The green circle and triangle correspond to riverbank sediment at the same location in 2013 and 2014, respectively.

A.3.2 Phyllosilicates along the Danube

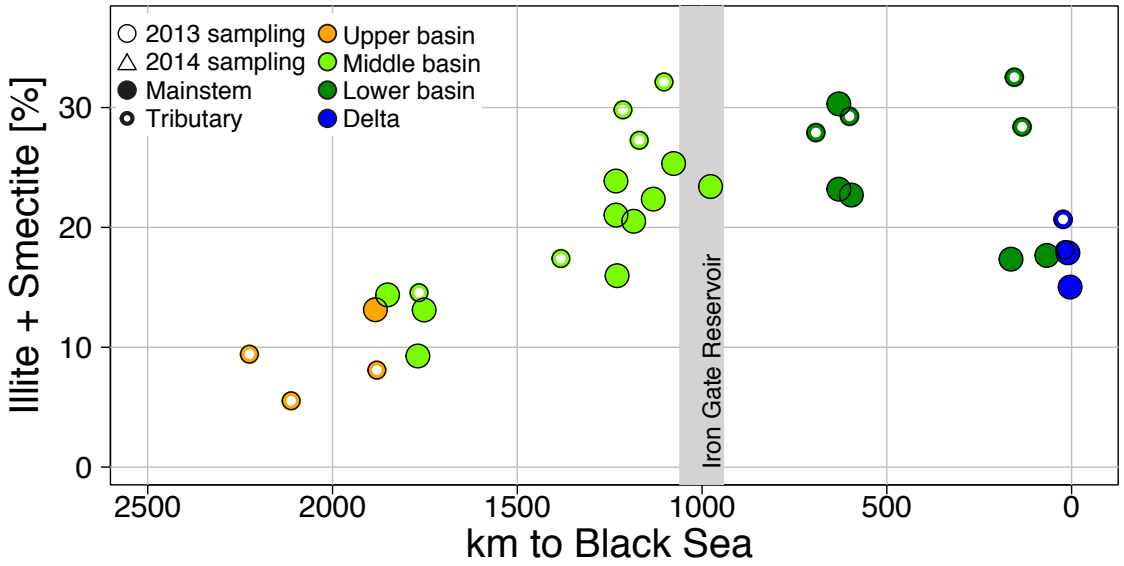

Figure A.3.2. Illite + smectite content along the river in weitht %. Symbol colors correspond to sub-basins (orange: upper Danube basin; light green: middle Danube basin; dark green: lower Danube basin; blue: delta region). Closed symbols correspond to Danube mainstem locations, open symbols to tributary locations from the 2013 sampling campaign. The gray bar indicates the location of the Iron Gate reservoir.

A.3.3 Soil clay content

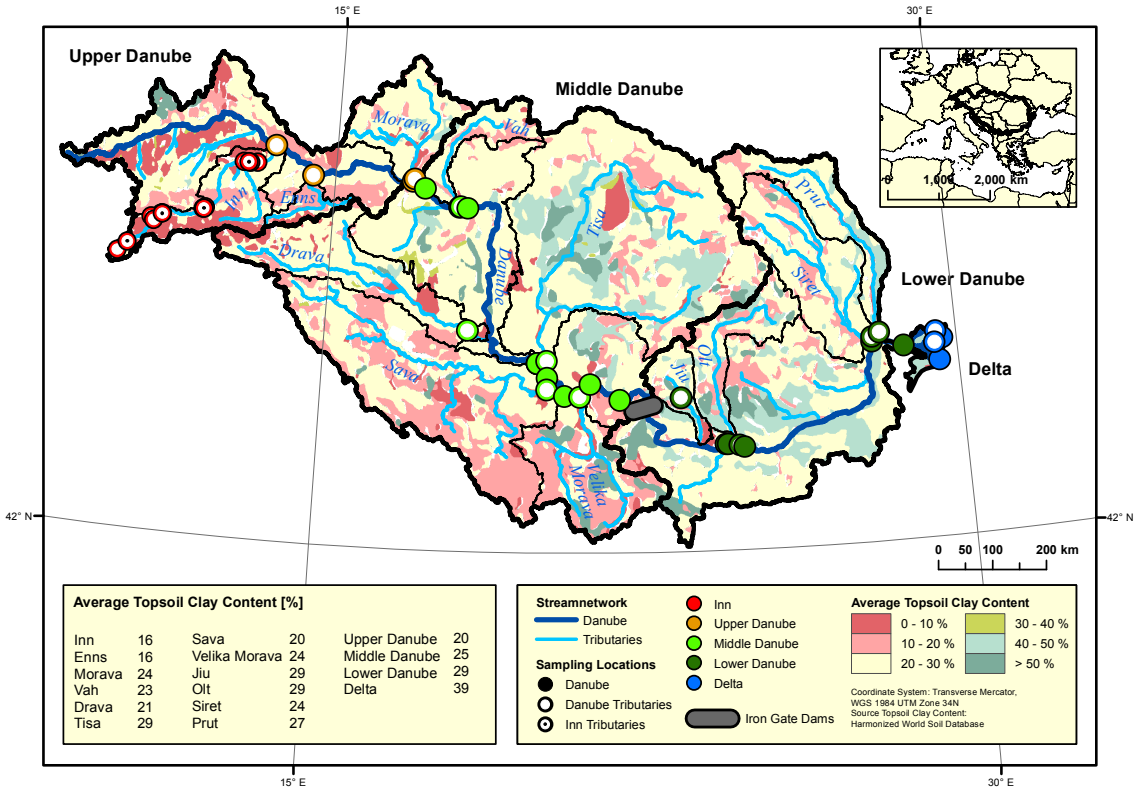

Figure A.3.3. Soil clay content in the Danube basin. Map of Danube basin topsoil clay content with calculated average clay content for sub-basins. Data from the Harmonized World Soil Database (HWSD, 2012).

A.3.4 Modeled tributary TOC loadings

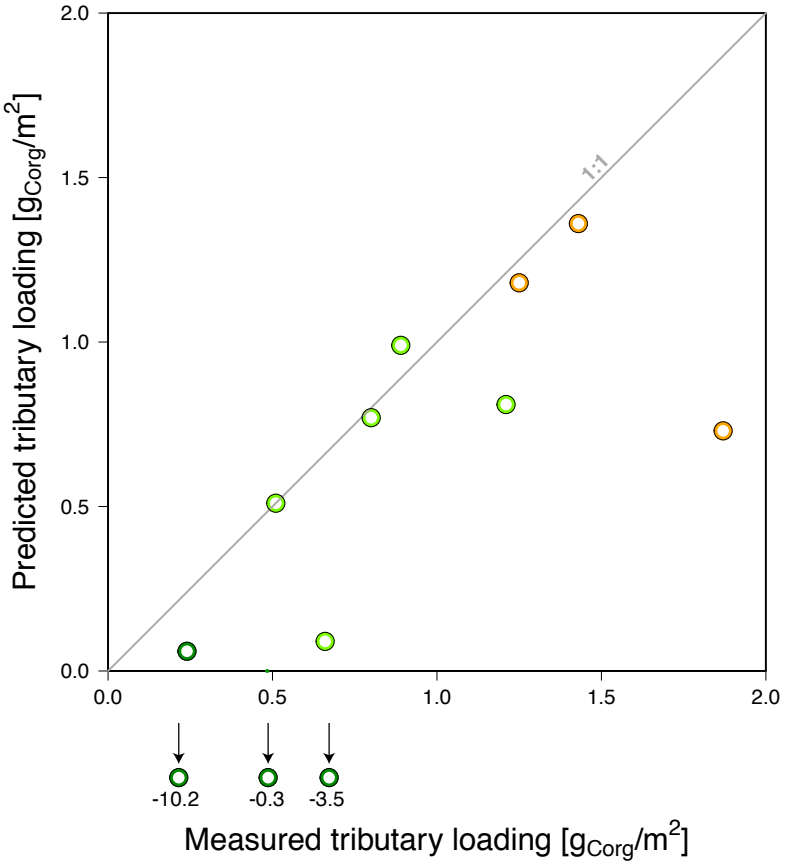

Figure A.3.4. Measuerd vs. predicted tributary TOC loading. Predicted TOC loadings: calculated values how tributary loadings should be to keep the Danube mainstem loadings on the regression line of Figure 3.3b (i.e. measured values). A mass balance calculation for each confluence was done as follows:

$$(Q_{upstream} \times L_{upstream}) + (Q_{tributary} \times L_{tributary}) = L_{downstream} \times (Q_{tributary} + Q_{upstream})$$

Q being the sediment discharge and L the sediment TOC loading.
Predicted values are approximated based on the water discharge of the corresponding tributary and Danube locations. Tributaries plotting below the 1:1 line (grey) should have lower loadings than were measured in this study to explain the observed decrease in Danube mainstem TOC loadings. Especially lower basin tributaries (dark green) would need much lower or even negative loadings to explain the decrease. This shows that, independent on the sediment load of these tributaries, dilution by low OC/high SA sediments in the middle and lower basins only plays a minor role in lowering the Danube mainstem TOC loading signal.
Symbol colors correspond to sub-basins (orange: upper Danube basin; light green: middle Danube basin; dark green: lower Danube basin; blue: delta region).

Reference

HWSD (2012) FAO/IIASA/ISRIC/ISS-CAS/JRC, Harmonized World Soil Database (version 1.2), FAO, Rome, Italy and IIASA, Laxenburg, Austria.

Appendix B.3 Data tables

Table B.3.1. Coordinates of sampling locations, fine fraction surface area and grain size.

Year	Name	N	E	SA [m^2/g]	median grain size [µm]
2013	Inn	48°34'15.0"	13°27'46.7"	8	13
2013	Enns	48°07'48.3"	14°28'15.1"	7	15
2013	D up Morava	48°08'45.9"	16°56'00.3"	9	
2013	Morava	48°11'10.6"	16°58'38.1"	13	11
2013	D d Morava	48°01'56.2"	17°14'57.2"	12	12
2013	D up Vah	47°45'01.0"	18°06'45.3"	11	13
2013	Vah	47°54'50.5"	18°00'43.6"	19	8
2013	D d Vah	47°43'57.7"	18°19'18.2"	16	9
2013	Drava	45°41'26.0"	18°24'59.7"	16	12
2013	D up Tisa 1	45°10'03.2"	20°04'46.6"	17	9
2013	D up Tisa 2	45°10'03.2"	20°04'46.6"	20	9
2013	D up Tisa 3	45°09'54.1"	20°06'34.3"	14	13
2013	Tisa	45°12'16.4"	20°18'44.7"	24	10
2013	D up Sava	44°55'24.5"	20°19'16.0"	19	9
2013	Sava	44°43'24.9"	20°18'34.7"	24	8
2013	D d Sava	44°39'56.7"	20°46'48.2"	20	10
2013	Velika Morava	44°36'21.0"	21°05'10.6"	28	8
2013	D d Velika Morava	44°49'01.0"	21°20'04.3"	21	10
2013	IG reservoir	44°33'06.6"	22°01'42.3"	27	8
2013	Jiu	44°34'09.8"	23°27'19.8"	21	8
2013	D up Olt 1	43°46'15.5"	24°30'50.2"	26	8
2013	D up Olt 2	43°46'16.3"	24°30'42.8"	22	9
2013	Olt	43°44'38.7"	24°46'43.0"	30	14
2013	D d Olt	43°42'46.3"	24°53'28.3"	25	7
2013	D up Siret	45°19'22.8"	28°00'07.9"	22	8
2013	Siret	45°23'56.8"	28°00'41.9"	30	7
2013	Prut	45°28'15.9"	28°11'53.3"	36	5
2013	Apex	45°12'55.3"	28°45'10.7"	30	11
2013	DD18	44°55'08.7"	29°33'24.7"	12	14
2013	DD9	45°16'44.9"	29°40'28.7"	15	21
2013	DD11	45°23'53.3"	29°31'48.3"	17	13
2013	DD5	45°12'55.8"	29°29'03.8"	29	12

Table B.3.1 (continued)

Year	Name	N	E	SA [m²/g]	median grain size [µm]
2014	Inn	48°34'15.0"	13°27'46.7"	6	18
2014	Enns	48°07'48.3"	14°28'15.1"	7	
2014	D d Enns	48°11'56.9"	14°36'38.6"	7	
2014	Morava	48°11'10.6"	16°58'38.1"	22	
2014	D up Vah	47°45'01.0"	18°06'45.3"	11	16
2014	Vah	47°54'50.5"	18°00'43.6"	30	
2014	D d Vah	47°43'57.7"	18°19'18.2"	14	
2014	Drava	45°41'26.0"	18°24'59.7"	16	
2014	D d Drava	45°17'03.8"	19°08'35.8"	17	
2014	D up Tisa 1	45°10'03.2"	20°04'46.6"	16	
2014	Tisa	45°12'16.4"	20°18'44.7"	25	
2014	D up Sava	44°55'24.5"	20°19'16.0"	20	
2014	Sava	44°43'24.9"	20°18'34.7"	31	
2014	D d Sava	44°39'56.7"	20°46'48.2"	27	6
2014	Velika Morava	44°36'21.0"	21°05'10.6"	26	
2014	D d Velika Morava	44°49'01.0"	21°20'04.3"	15	
2014	IG reservoir	44°33'06.6"	22°01'42.3"	23	
2014	D up Jiu	43°48'19.5"	23° 45' 1.38"	20	
2014	Jiu	44°34'09.8"	23°27'19.8"	19	
2014	D up Olt 1	43°46'15.5"	24°30'50.2"	27	
2014	Olt	43°44'38.7"	24°46'43.0"	20	
2014	D d Olt	43°42'46.3"	24°53'28.3"	18	
2014	D d Vedea	43°39'12.84"	25°31'43.56"	26	
2014	Ialomita	44°39'5.82"	27°49'9.78"	13	
2014	D up Siret	45°19'22.8"	28°00'07.9"	16	
2014	Siret	45°23'56.8"	28°00'41.9"	31	
2014	Prut	45°28'15.9"	28°11'53.3"	28	
2014	Apex	45°12'55.3"	28°45'10.7"	27	13
2014	DD20	45°09'37.9"	29°36'28.7"	15	
2014	DD11	45°23'53.3"	29°31'48.3"	16	
2014	Inn down Salzach	48°15'45.6"	13°02'12.5"	7	17
2014	Inn down Alz	48°14'44.0"	12°51'50.8"	7	15
2014	Inn up Alz	48°15'03.8"	12°41'44.0"	5	21
2014	Inn down Ziller	47°25'39.7"	11°51'55.3"		17
2014	Inn up Ziller	47°24'09.5"	11°49'26.3"	6	16
2014	Inn down Oetztaler Ache	47°14'26.6"	10°51'19.4"	4	18
2014	Inn up Oetztaler Ache	47°13'37.6"	10°49'18.4"	3	25
2014	Inn down Sanna	47°09'57.4"	10°35'29.5"	4	16
2014	Inn up Sanna	47°06'48.6"	10°39'19.7"	4	24
2013	Inn up Flaz	46°32'24.1"	09°53'07.7"	12	11
2014	Alz	48°14'53.5"	12°48'54.6"	14	12
2014	Ziller	47°24'06.3"	11°50'13.9"	2	20
2014	Oetztaler Ache	47°13'38.6"	10°51'21.6"	10	10
2013	Spoel	46°41'44.8"	10°06'07.1"	8	15
2014	Spoel	46°41'44.8"	10°06'07.1"	4	22

Abbreviations: D: Danube; D up: Danube upstream of...; D d: Danbue downstram of...; IG: Iron Gate; DD: Danube delta

Table B.3.2. TOC, FA, brGDGT and lignin concentrations normalized to (i) sediment weight; (ii) TOC; (iii) SA.

		Normalized to sediment weight				Normalized to TOC			Normalized to SA			
Year	Name	TOC wt%	FA n-C_{24-32} [µg/g]	brGDGTs [ng/g]	lignin [µg/g]	FA n-C_{24-32} [µg/g C_{org}]	brGDGTs [µg/g C_{org}]	lignin [mg/g C_{org}]	TOC [mg/m²]	FA n-C_{24-32} [µg/m²]	brGDGTs [ng/m²]	lignin [µg/m²]
2013	Inn	1.18	8.8	546	75	742.1	46	6.3	1.4	1.1	66	9.1
2013	Enns	1.36	11.5	564	191	846.1	42	14.1	1.9	1.6	78	26.4
2013	D up Morava	1.06	8.3	385	111	783.4	36	10.4	1.2	0.9	42	12.2
2013	Morava	1.64	19.3	888	193	1172.5	54	11.8	1.3	1.5	68	14.7
2013	D d Morava	1.57	13.0	692	83	826.0	44	5.3	1.3	1.1	59	7.1
2013	D up Vah	1.4	13.0	597	128	932.7	43	9.2	1.2	1.2	53	11.3
2013	Vah	1.72	19.6	1187	96	1140.8	69	5.6	0.9	1.0	61	5.0
2013	D d Vah	1.53	10.6	548	114	695.0	36	7.4	1.0	0.7	35	7.2
2013	Drava	1.91	18.8	793	232	986.9	42	12.2	1.2	1.2	50	14.7
2013	D up Tisa 1	1.68	11.3	581	142	671.3	35	8.4	1.0	0.7	34	8.2
2013	D up Tisa 2	1.78	16.0	876	284	898.9	49	15.9	0.9	0.8	44	14.3
2013	D up Tisa 3	0.88	7.3	306	73	832.4	35	8.3	0.6	0.5	21	5.0
2013	Tisa	1.25	10.5	921	138	841.2	74	11.1	0.5	0.4	38	5.7
2013	D up Sava	1.14	13.9	667	96	1222.1	59	8.5	0.6	0.7	35	5.0
2013	Sava	1.92	12.3	1179	111	641.3	61	5.8	0.8	0.5	49	4.6
2013	D d Sava	1.73	16.7	1061	265	963.5	61	15.3	0.9	0.8	52	13.0
2013	Velika Morava	1.82	22.7	652	116	1244.8	36	6.4	0.7	0.8	24	4.2
2013	D d Velika Morava	1.68	9.8	976	87	582.8	58	5.2	0.8	0.5	48	4.2
2013	IG reservoir	2.04	20.9	1038	191	1022.0	51	9.4	0.8	0.8	38	7.0
2013	Jiu	1.45	20.5	546	97	1418.6	38	6.7	0.7	1.0	25	4.5
2013	D up Olt 1	1.55	11.3	736	116	728.5	47	7.5	0.6	0.4	28	4.4
2013	D up Olt 2	1.17	13.3	655	106	1139.4	56	9.1	0.5	0.6	30	4.8
2013	Olt	0.57	3.2	173	24	555.0	30	4.2	0.2	0.1	6	0.8
2013	D d Olt	1.52	30.1	744	74	1979.4	49	4.8	0.6	1.2	30	3.0
2013	D up Siret	0.79	9.0	550	37	1148.0	70	4.7	0.4	0.4	25	1.7
2013	Siret	0.71	3.8	223	40	537.8	31	5.7	0.2	0.1	7	1.4
2013	Prut	1.76	17.6	762	97	999.6	43	5.5	0.5	0.5	21	2.7
2013	Apex	0.95	4.5	519	31	479.3	55	3.3	0.3	0.2	17	1.0
2013	DD18	0.8	5.9	413	84	746.2	52	10.6	0.7	0.5	34	7.0
2013	DD9	0.57	7.2	571	29	1268.8	101	5.1	0.4	0.5	39	2.0
2013	DD11	0.79	11.8	730	85	1483.3	92	10.7	0.5	0.7	44	5.1
2013	DD5	1.5	19.7	971	96	1313.5	65	6.4	0.5	0.7	34	3.3

Table B.3.2 (continued)

		Normalized to sediment weight				Normalized to TOC			Normalized to SA			
Year	Name	TOC wt%	FA n-C_{24-32} [µg/g]	brGDGTs [ng/g]	lignin [µg/g]	FA n-C_{24-32} [µg/g C_{org}]	brGDGTs [µg/g C_{org}]	lignin [mg/g C_{org}]	TOC [mg/m²]	FA n-C_{24-32} [µg/m²]	brGDGTs [ng/m²]	lignin [µg/m²]
2014	Inn	1.2	9.6	646	104	801.8	54	8.7	2.1	1.7	115	18.5
2014	Enns	1.3	14.9	1010	139	1148.6	78	10.7	1.9	2.2	150	20.5
2014	D d Enns	1	8.5	990	54	854.3	99	5.4	1.5	1.3	146	7.9
2014	Morava	2.3	24.4	3093		1061.8	134		1.1	1.1	143	
2014	D up Vah	1.2		1253	100		104	8.4	1.1		116	9.3
2014	Vah	1.9							0.6			
2014	D d Vah	1.7							1.2			
2014	Drava	2							1.2			
2014	D d Drava	1.4							0.8			
2014	D up Tisa 1	1.8							1.1			
2014	Tisa	1.9							0.8			
2014	D up Sava	1.8							0.9			
2014	Sava	1.3							0.4			
2014	D d Sava	1.4	6.2	1290	206	444.6	92	14.7	0.5	0.2	49	7.7
2014	Velika Morava	0.9							0.3			
2014	D d Velika Morava	0.9							0.6			
2014	IG reservoir	1.6							0.7			
2014	D up Jiu	1.1							0.5			
2014	Jiu	0.9							0.5			
2014	D up Olt 1	2.9							1.1			
2014	Olt	0.6							0.3			
2014	D d Olt	0.6							0.3			
2014	D d Vedea	1.1							0.4			
2014	Ialomita	0.4							0.3			
2014	D up Siret	0.7							0.4			
2014	Siret	0.9							0.3			
2014	Prut	1							0.4			
2014	Apex	0.7	6.5	1129	18	923.6	161	2.6	0.3	0.2	41	0.7
2014	DD20	0.5							0.3			
2014	DD11	0.7							0.4			

Table B.3.2 (continued)

		Normalized to sediment weight				Normalized to TOC			Normalized to SA			
		TOC	FA n-C_{24-32}	brGDGTs	lignin	FA n-C_{24-32}	brGDGTs	lignin	TOC	FA n-C_{24-32}	brGDGTs	lignin
Year	Name	wt%	[µg/g]	[ng/g]	[µg/g]	[µg/g C_{org}]	[µg/g C_{org}]	[mg/g C_{org}]	[mg/m²]	[µg/m²]	[ng/m²]	[µg/m²]
2014	Inn down Salzach	0.9	13.0	262	47	1449.7	29	5.2	1.3	1.9	38	6.8
2014	Inn down Alz	0.87	7.0	242	53	803.9	28	6.1	1.3	1.0	35	7.7
2014	Inn up Alz	0.63	5.6	132	26	895.5	21	4.2	1.4	1.2	28	5.6
2014	Inn down Ziller	0.36	6.7	96	19	1866.2	27	5.3				
2014	Inn up Ziller	0.67	4.8	128	37	712.9	19	5.5	1.2	0.9	23	6.6
2014	Inn down Oetztaler Ache	0.25	1.8	28	18	733.5	11	7.0	0.6	0.5	7	4.5
2014	Inn up Oetztaler Ache	0.3	3.4	49	2	1123.3	16	0.6	1.0	1.1	16	0.6
2014	Inn down Sanna	0.53	4.8	41	30	899.2	8	5.6	1.5	1.3	11	8.1
2014	Inn up Sanna	0.42	3.8	64	40	902.0	15	9.6	1.1	1.0	17	10.5
2013	Inn up Flaz	1.35	12.3	786	52	913.0	58	3.8	1.1	1.0		4.4
2014	Alz	2.78	13.3	735	103	477.0	26	3.7	2.0	1.0	54	7.5
2014	Ziller	0.52	13.3	83	18	2553.1	16	3.5	2.6	6.5	41	9.0
2014	Oetztaler Ache	0.7	2.8	79	27	401.4	11	3.9	0.7	0.3	8	2.8
2013	Spoel	0.87	6.0	108	22	695.2	12	2.5	1.1	0.7	13	2.7
2014	Spoel	0.68	4.2	67	3	621.0	10	0.5	1.6	1.0	15	0.7

Table B.3.3. Mineralogy data.

Year	Name	Anatase wt%	Anatase ±	Calcite wt%	Calcite ±	Chlorite wt%	Chlorite ±	Dolomite wt%	Dolomite ±	Hornblende wt%	Hornblende ±	Illite wt%	Illite ±
2013	Inn	0.5	0.2	10.6	0.6	9.4	1.3	17.7	0.8	2.6	0.5	2.9	0.5
2013	Enns	0.7	0.2	6.1	0.5	9.3	1.1	22.4	0.8	2.2	0.5	5.5	0.8
2013	D up Morava	0.4	0.2	8.8	0.5	7.6	1.1	17.3	0.9	1.9	0.5	10.4	1.8
2013	Morava	0.6	0.2	10.6	0.5	10.1	1.2	15.1	0.8	2.4	0.5	2.5	0.7
2013	D d Morava	0.4	0.2	12.1	0.5	9.0	1.1	16.8	0.8	0.8	0.5	10.3	1.5
2013	D up Vah	0.6	0.2	11.5	0.5	8.4	1.2	15.6	0.8	1.4	0.6	6.4	1.1
2013	Vah			11.2	0.5	13.3	1.4	12.3	0.8	1.3	0.8	8.5	1.6
2013	D d Vah	0.5	0.2	14.1	0.5	9.9	0.9	16.0	0.6	1.0	0.5	9.2	1.2
2013	Drava	0.5	0.2	3.6	0.5	8.9	1.4	7.2	0.8	1.9	0.6	13.2	2.1
2013	D up Tisa 1	0.6	0.2	12.7	0.6	4.7	1.1	9.1	0.8	0.8	0.5	12.2	2.5
2013	D up Tisa 2	0.4	0.3	8.4	0.5	7.1	1.1	9.8	0.7	0.8	0.3	11.9	1.9
2013	D up Tisa 3	0.3	0.2	6.4	0.5	5.7	1.0	10.2	0.7	1.0	0.5	12.8	1.8
2013	Tisa	0.5	0.2	3.0	0.4	3.4	0.8	2.4	0.4	0.7	0.3	13.1	2.0
2013	D up Sava	0.5	0.2	7.5	0.5	6.3	1.3	7.4	0.6	1.7	0.5	9.2	1.9
2013	Sava	0.5	0.2	12.9	0.6	4.1	1.0	3.5	0.7	2.2	0.5	3.5	0.6
2013	D d Sava	0.6	0.2	9.5	0.4	6.4	1.2	6.1	0.5	1.8	0.4	3.5	0.5
2013	Velika Morava	0.3	0.1	7.7	0.7	4.1	0.7	0.6	0.5	1.2	0.6	16.1	2.6
2013	D d Velika Morava	0.7	0.2	9.2	0.6	2.8	0.7	5.9	0.6	1.3	0.6	11.8	2.4
2013	IG reservoir	0.6	0.2	9.5	0.5	7.7	1.4	7.1	0.7	1.9	0.5	2.5	0.5
2013	Jiu			2.2	0.3	2.8	0.9	1.6	0.5	1.5	0.5	14.0	2.2
2013	D up Olt 1	0.5	0.2	6.4	0.5	2.9	0.6	5.1	0.6	0.9	0.5	13.5	2.4
2013	D up Olt 2	0.6	0.2	5.6	0.4	6.4	1.1	5.8	0.5	1.4	0.5	13.3	2.0
2013	Olt	0.4	0.2	1.3	0.3	2.9	0.8	0.5	0.4	1.5	0.6	12.4	2.3
2013	D d Olt	0.6	0.2	6.7	0.5	6.8	1.6	5.6	0.8	2.0	0.5	12.4	1.9
2013	D up Siret	0.6	0.2	7.1	0.5	5.7	1.4	5.9	0.6	1.9	0.8	9.3	2.1
2013	Siret			9.6	0.6	5.1	1.0	2.6	0.5	0.8	0.6	12.1	1.7
2013	Prut	0.4	0.3	7.3	0.6	6.3	1.6	2.8	0.6	1.2	0.5	14.5	2.1
2013	Apex	0.6	0.1	6.6	0.4	4.4	1.0	6.3	0.5	1.2	0.4	9.6	1.7
2013	DD18	0.4	0.2	7.0	0.5	5.3	1.1	5.6	0.6	0.6	0.3	10.0	1.7
2013	DD9	0.5	0.1	7.1	0.4	6.0	1.0	5.7	0.5	0.8	0.4	8.4	1.4
2013	DD11	0.4	0.2	7.0	0.5	3.5	0.8	6.3	0.6	0.9	0.5	10.2	1.5
2013	DD5	0.5	0.2	5.6	0.5	6.1	1.1	7.1	0.6	0.8	0.5	12.3	1.9

Table B.3.3 (continued)

Year	Name	Kaolinite wt%	Kaolinite ±	Muscovite wt%	Muscovite ±	Orthoclase wt%	Orthoclase ±	Plagioclase Albite wt%	Plagioclase Albite ±	Plagioclase Oligoclase wt%	Plagioclase Oligoclase ±
2013	Inn			12.4	1.1	1.2	0.8	11.5	0.7		
2013	Enns			18.0	0.9	0.9	0.4	11.4	0.7		
2013	D up Morava	0.3	0.3	9.6	1.0	2.6	0.6	6.4	1.1	5.1	1.0
2013	Morava	2.4	0.7	15.7	1.1	2.2	0.6	9.4	0.8		
2013	D d Morava	1.0	0.7	14.1	1.0	1.2	0.3	5.5	1.1	3.6	1.0
2013	D up Vah	0.9	0.7	13.0	1.0	3.3	0.6	7.8	1.1	3.8	1.1
2013	Vah	1.7	0.7	18.0	1.3	1.0	0.8	7.8	0.6		
2013	D d Vah	1.1	0.9	15.3	0.9	2.2	0.5	5.6	0.8	2.8	0.8
2013	Drava	3.5	1.1	13.9	1.1	0.5	0.5	12.5	0.7		
2013	D up Tisa 1	1.0	0.5	10.2	1.0	3.2	0.7	5.2	1.1	4.3	1.0
2013	D up Tisa 2	2.5	1.1	10.9	1.0	3.1	0.6	6.9	1.2	3.5	1.0
2013	D up Tisa 3	2.1	1.2	8.4	0.9	3.7	0.5	8.6	1.1	4.7	1.0
2013	Tisa	2.9	0.8	10.4	1.1	2.5	0.7	12.3	0.7		
2013	D up Sava	1.6	0.8	9.4	0.9	3.3	0.6	6.7	1.1	3.9	1.0
2013	Sava	3.2	1.0	9.8	1.2	1.8	0.6	8.1	0.6		
2013	D d Sava	2.4	0.8	10.3	0.9	2.6	0.5	6.9	1.0	3.6	1.0
2013	Velika Morava	4.4	1.1	8.7	1.0	3.2	0.6	7.6	1.4	5.2	1.1
2013	D d Velika Morava	2.0	1.0	10.0	0.9	3.0	0.6	8.2	1.2	3.6	1.0
2013	IG reservoir	3.0	1.7	10.2	0.9	3.5	0.6	6.8	1.1	3.9	1.0
2013	Jiu	8.0	5.1	8.4	1.1	3.9	0.7	16.1	1.3		
2013	D up Olt 1	2.6	1.1	10.9	1.0	3.5	0.6	8.5	1.0	3.5	0.9
2013	D up Olt 2	4.3	1.0	9.4	0.8	3.0	0.5	8.7	1.0	3.4	0.9
2013	Olt	2.6	0.8	9.2	1.0	2.1	0.8	15.8	0.8		
2013	D d Olt	3.8	1.2	9.9	1.1	2.8	1.0	7.6	1.3	3.9	1.1
2013	D up Siret	1.2	0.6	8.0	1.0	4.0	0.6	9.0	1.2	4.9	1.0
2013	Siret	3.0	1.6	9.7	1.3	2.3	0.6	8.3	0.6		
2013	Prut			10.4	1.3	1.9	0.7	7.3	0.8		
2013	Apex	0.6	0.4	6.4	0.8	3.1	0.5	8.7	1.0	5.8	0.9
2013	DD18	0.8	0.5	8.5	0.8	3.1	0.6	7.9	1.2	5.0	1.0
2013	DD9	1.7	0.7	7.7	0.7	3.4	0.5	9.0	1.1	4.9	1.0
2013	DD11	0.7	0.5	6.7	1.0	3.1	0.5	9.0	1.2	4.5	1.0
2013	DD5	3.8	1.1	8.8	1.0	3.4	0.6	8.7	1.2	4.3	1.0

Table B.3.3 (continued)

Year	Name	Quarz wt%	Quarz ±	Rutile wt%	Rutile ±	Smectite wt%	Smectite ±	Microcline wt%	Microcline ±
2013	Inn	20.4	0.7	0.6	0.2	6.6	2.2	3.7	0.9
2013	Enns	19.5	0.5	0.5	0.2	0.0	0.0	3.5	0.3
2013	D up Morava	26.5	0.7	0.4	0.2	2.7	1.3		
2013	Morava	18.2	0.6	0.7	0.3	5.6	2.5	4.5	0.8
2013	D d Morava	20.9	0.6	0.3	0.1	4.1	1.2		
2013	D up Vah	23.9	0.6	0.5	0.2	2.8	1.4		
2013	Vah	17.0	0.6	0.6	0.3	6.1	1.7	1.4	0.5
2013	D d Vah	18.1	0.5	0.4	0.2	3.9	1.1		
2013	Drava	27.7	0.9	0.6	0.3	4.2	2.0	2.0	1.4
2013	D up Tisa 1	24.1	0.9	0.3	0.2	11.7	2.4		
2013	D up Tisa 2	25.3	0.8	0.4	0.2	9.1	3.3		
2013	D up Tisa 3	32.5	1.0	0.5	0.3	3.2	1.4		
2013	Tisa	31.7	1.1	0.4	0.2	16.7	3.6		
2013	D up Sava	30.7	0.9	0.4	0.3	11.3	2.5		
2013	Sava	25.9	0.9	0.7	0.3	23.7	2.6		
2013	D d Sava	26.8	0.8	0.7	0.2	18.9	2.3		
2013	Velika Morava	24.6	1.2	0.3	0.2	16.0	4.5		
2013	D d Velika Morava	27.4	1.0	0.5	0.3	13.5	3.0		
2013	IG reservoir	22.0	0.8	0.5	0.2	20.9	2.2		
2013	Jiu	27.3	1.7	0.3	0.2	13.9	3.3		
2013	D up Olt 1	24.7	0.8	0.4	0.2	16.8	2.1		
2013	D up Olt 2	27.9	0.8	0.5	0.2	9.9	3.0		
2013	Olt	31.6	1.1	0.7	0.2	16.9	3.0	2.3	0.8
2013	D d Olt	27.1	0.8	0.6	0.2	10.3	2.3		
2013	D up Siret	34.1	1.0	0.5	0.2	8.1	2.7		
2013	Siret	25.9	1.0	0.3	0.2	20.4	3.3		
2013	Prut	31.2	1.1	0.2	0.3	13.9	3.0	2.8	0.8
2013	Apex	38.4	0.9	0.4	0.2	8.1	2.4		
2013	DD18	37.4	1.0	0.5	0.2	7.9	1.9		
2013	DD9	37.6	0.7	0.6	0.2	6.6	1.8		
2013	DD11	37.1	1.0	0.3	0.2	10.5	2.3		
2013	DD5	32.6	1.0	0.3	0.2	5.8	2.9		

Chapter 4

Loss or Loess? Investigating factors modulating organic carbon evolution along a river system

Chantal V. Freymond[a], Maarten Lupker[a], Nicole Kündig[a], Björn Buggle[a], Francien Peterse[a,b], Negar Haghipour[a], Cameron McIntyre[c,d], S. Nemiah Ladd[e], Carsten Schubert[e], Florin Filip[f,g], Liviu Giosan[h] and Timothy I. Eglinton[a]

[a] Geological Institute, ETH Zurich, Switzerland
[b] Department of Earth Sciences, Utrecht University, Netherlands
[c] Laboratory for Ion Beam Physics, ETH Zürich, Switzerland
[d] Scottish Universities Environmental Research Centre, University of Glasgow, UK
[e] Department of Surface Waters Research & Management, Eawag, Switzerland
[f] Department of Geography, University of Bucharest, Romania
[g] Fabrica de Cercetare, Romania
[h] Woods Hole Oceanographic Institution, USA

Abstract

Rivers move large amounts of sediment and with it organic carbon (OC) from the continents to the ocean. OC ultimately buried in continental margin sediments acts as active carbon sink and contributes to the continuous record of environmental conditions. In this context, the fate of OC as it is transported within a river catchment is of broad interest. Here, a detailed basin-wide investigation of river sediments is performed along the Danube River and its major tributaries, which is the second largest river system in Europe. Stable and radiocarbon analysis of the bulk sediment fine fraction and of plant wax fatty acids associated with this fraction are used to investigate the evolution of the OC composition during transit and to better constrain the different mechanisms that lead to the OC composition of sediment that is finally exported to the Black Sea. To our knowledge, this is the first in-depth investigation where radiocarbon characteristics of specific components have been determined along the course of a river system. We report a transport time along the Danube of 2,130 years for total organic carbon and 2,790 years for fatty acids. Considering source contributions, we find that significant addition of loess in the middle and lower basins lead to an overprint of the upstream OC signal. However, with the data available in this study, it is not possible to fully disentangle transport time related OC aging, loss due to degradation and the contribution of local OC sources. We conclude that the OC that is exported by the Danube shows a lower basin dominated signal and therefore, source analysis of OC is key for more complete interpretation of the sedimentary archive on ocean margins.

4.1 Introduction

The transport of organic matter (OM) from terrigenous carbon pools (biosphere, soils, sedimentary rocks) and its delivery to, and sequestration in marine sediments is mainly driven by erosion processes on land and subsequent riverine transport. Given that OM deposition and preservation on continental margins accounts for the vast majority of oceanic carbon burial globally (Hedges and Keil, 1995), terrigenous OM has been suggested to comprise one third of the organic matter being buried in modern marine sediments (Burdige, 2005). Correspondingly, variations in terrigenous OM burial may influence the global carbon budget on glacial-interglacial, as well as longer, and potentially shorter timescales (Burdige, 2005; Eglinton, 2008). However, the sources and fate of terrigenous OM as it is transported within and exported beyond river basins are still poorly constrained. Much of the OM exported by rivers is likely prone to degradation during export and across-shelf transport (Burdige, 2005; Blair and Aller, 2012; Bröder et al., 2016b). Both the mode and timescales of terrigenous OM transport are potentially of key importance in dictating its ultimate fate (Blair and Aller, 2012). In addition to improved understanding of the role of these parameters in carbon cycling on

regional to global scales, such information is crucial for informed interpretation of sedimentary records in the context of paleo-environmental reconstructions.

Eroded soil is a major source of OM to the total OM load of rivers (e.g. Gordon and Goni, 2003), consisting of fresh and partly degraded plant material, microbial biomass and parent rock derived minerals. Soil OM typically reflects the $\delta^{13}C$ signature of the vegetation building up the C stock and often shows increasing ages with depth due to modern litter input at the surface and subsequent aging in underlying horizons (Marschner et al., 2008; Trumbore, 2009). The occurrence of organo-mineral interactions in soils inhibits degradation of organic molecules due to their association with primarily fine-grained, high surface area (SA) minerals (i.e., phyllosilicates) (Baldock and Skjemstad, 2000; Keil and Mayer, 2014; Doetterl et al., 2015). These associations evolve during erosion and movement across the landscape (Doetterl et al., 2016), still acting to protect organic matter from decomposition. Due to its hydrodynamic characteristics, organic matter hosted on fine-grained mineral particles has the potential to be transported over long distances upon mobilization and transfer to fluvial networks (Blair and Aller, 2012; Tesi et al., 2016b). Another component of the river OM load constitutes of fresh plant debris directly washed into rivers (Goni et al., 2005; Doetterl et al., 2016), and carries a $\delta^{13}C$ signature reflective of the primary vegetation and contains modern ^{14}C. This is in contrast to the signature of the third major component of river sediment load, i.e. petrogenic organic carbon originating from sedimentary rock erosion, which is "radiocarbon dead" by virtue of its geologic age, and may exhibit variable $\delta^{13}C$ compositions (Lewan, 1986). Finally, OM introduced to rivers from the landscape can be augmented by that derived from aquatic productivity, with the latter being particularly significant in rivers with low suspended loads (Martinelli et al., 1999; Blair et al., 2003) and in the marine realm (e.g. Keil et al., 1997). Due to characteristic ranges of stable and radiocarbon isotopic signatures of different OM sources, $\delta^{13}C$ in combination with the radiocarbon ^{14}C composition of bulk particulate organic carbon (OC) is often used to disentangle contributions from recent C3/C4 vegetation, soil-, petrogenic- and aquatic *in situ*-produced OC in rivers (Gordon and Goni, 2003; Alin et al., 2008; Hilton et al., 2010) and river-dominated margin sediments (Goni et al., 2008; Karlsson et al., 2011; Cathalot et al., 2013; Toussaint et al., 2013; Bröder et al., 2016a; Tesi et al., 2016b). Such bulk isotope mixing models help to quantify different carbon sources if all end members are distinct, invariant and well-constrained. However, sedimentary $\delta^{13}C$ and ^{14}C signals always encompass complex mixtures of various compounds contributing to the observed signal. An additional layer of information can be given by analyzing source specific compounds. Drenzek et al. (2009), for example, studied the stable and radiocarbon isotopic composition of long chain fatty acids (FA) derived from terrestrial higher plant waxes (Eglinton and Hamilton, 1967; Eglinton and Eglinton, 2008) in Eel River margin sediments. They showed that the terrigenous OM makes up the majority of the OC in

these sediments and that the stored FAs were "pre-aged" over several millennia through temporary storage in terrigenous sinks such as soils or floodplains, before burial on the continental margin (Drenzek et al., 2009). Combining compound-specific $\delta^{13}C$ as well as the hydrogen isotopic ($\delta^{2}H$) composition of plant waxes in river sediments, Galy et al. (2011) could detect the increasing contribution of C4 vegetation along the Ganges-Brahmaputra River system, suggesting that these plant waxes ultimately stored in river fan sediments allow reconstructing climate and hydrological conditions within the river basin. Feakins et al. (2016) further showed that plant wax $\delta^{2}H$ follows the hydrogen isotope elevation gradient of the Andes-Amazon system, implying that molecular isotopic signatures have value as provenance indicators.

If sediment exported by rivers is not buried immediately in intermediate reservoirs, as for example during flood events where several tons of sediment can be deposited in a very short time (Cathalot et al., 2010) or in delta systems with very high accumulation rates (Galy et al., 2007), it can be further transported along the continental margin. Bröder (2016) calculated a cross-shelf transport time of 3,900 ±300 years for 600 km distance over the East Siberian Arctic shelf, based on compound-specific ^{14}C ages of long-chain FAs in surface sediments. Additionally, they observed that 85% of terrigenous OC exported by the Lena River is degraded during across-shelf lateral transport (Bröder, 2016). Global estimates on the degradation of fluvial derived OC suggest that up to 70% of the terrigenous particulate OC is remineralized on the continental margins (Hedges et al., 1997; Burdige, 2005).

Freymond et al. (2018) found that total organic carbon (TOC) and biomarker (plant wax lipids, branched glycerol dialkyl glycerol tetraethers (GDGTs) and lignin phenols) loadings on mineral surfaces (in $g_{Corg\ or\ biomarker}/m^2$) of Danube River sediments decrease by 70–80% along the 2,000 km flow path from the upper to the lower basin. This decrease in loading is either due to addition of high SA/low OC sediments in the lower basin or due to degradative losses, which would imply that the lower part of the basin is the dominant source region for OM reaching the delta (Freymond et al., 2018).

The aim of this study is to better understand the sources and evolution of terrigenous OC composition in Danube River sediment as it is transported within the catchment. Therefore, the bulk and compound-specific fatty acid stable and radiocarbon isotopic composition of Danube River sediment is investigated on a basin scale. The evolution of the isotopic signals from the upper basin to the Black Sea is discussed in the context of different potential scenarios that could lead to the observed decrease in OC loadings that was shown by Freymond et al. (2018).

4.2 Study area

The Danube river basin, with a catchment area of 801,463 km^2, is the second largest in Europe (Figure 4.1). In the upper basin, the Danube sources in the Black Forest in southern Germany at 1,000 m a.s.l. After about 600 km, the Inn River, sourcing at ~2,500 m a.s.l in the Swiss Alps, joins and more than doubles the discharge of the Danube. The upper Danube basin ends at the Gate of Devin where the foothills of the Eastern Alps and the Small Carpathians meet (ICPDR, 2005). At the beginning of the middle basin, the Danube changes direction, and heads southward. After crossing the Pannonian sedimentary basin, the Danube changes its direction again, shifting to the east and four large tributaries (Drava, Tisa, Sava, Velika Morava) enter the Danube before it reaches the >100 km long Iron Gate gorge where the Danube cuts the Carpathian Mountains. Two large hydropower dams, Iron Gate I (built in 1972) and Iron Gate II (1986) form a huge reservoir, reducing the sediment load of the Danube by approximately 50% (McCarney-Castle et al., 2012). In the lower basin downstream of the Iron Gates, the Danube passes the Romanian/Bulgarian plain, turns northwards where the two tributaries Siret and Prut join, and then turns to east again before the mainstem divides into the three main branches of the Danube delta (area of 675,000 ha; ICPDR, 2005).

The climate in the Danube basin changes from an Atlantic climate with high precipitation in the western part to a continental climate with dryer and colder winters and higher summer temperatures in the eastern part (ICPDR, 2005). The southwest portion of the basin, i.e. the Drava and Sava catchments, is partly influenced by a Mediterranean climate with less precipitation in summer (ICPDR, 2005; McCarney-Castle et al., 2012). Following the climate gradient, vegetation changes from exclusively C3 plants in the upper basin to up to 20% C4 vegetation in the lower basin (Still et al., 2003).

About one third of the area drained by the Danube is occupied by mountains (Schiller et al., 2010). The Mesozoic Alpine mountain system, including the Alps, Dinaric Mountains, Carpathians and the Balkan Mountains, mostly consists of crystalline rocks, limestone, flysch and molasses. The other two thirds of the basin are hills and plains, with the Pannonian basin and the lower Danube plain constituting the two largest inter-mountain plains. Remnants of higher Palaeozoic mountain ranges, mostly of crystalline rock, are located in the upper basin and to a smaller extent in the lower basin (Schiller et al., 2010). In the Inn River catchment in the upper Danube basin, Bündnerschiefer including partially thermally altered organic carbon-rich flysch-like sediments crops out in the Engadiner and the Tauern windows (Demeny and Kreulen, 1993).

Pleistocene loess deposits cover large areas of the intermountain plains and plateaus, mainly in the middle and lower basin. These deposits consist of aeolian loess, loess derivates (i.e. loess that was modified through processes like soil formation) and

alluvial loess that was further transported and re-distributed by rivers (Haase et al., 2007). Loess and loess-like deposits are often thickest close to the Danube mainstem, at some locations exceeding 50 m thickness (Jipa, 2014).

Soil thickness and composition varies with bedrock type, precipitation, temperature, vegetation cover and relief (Schiller et al., 2010). In steep, high-mountain areas, virgin soils (consisting of A and C horizons) with only a thin humus layer predominate. At lower elevations, deeper Brown soils and water influenced Gray soils are developed. At low altitudes, deep soils have developed on loose sediment deposits and floodplain soils have evolved in river valleys and plains. With the more continental climate, OC rich Black soils forming on loess deposits predominate in the plains of the lower basin (Schiller et al., 2010).

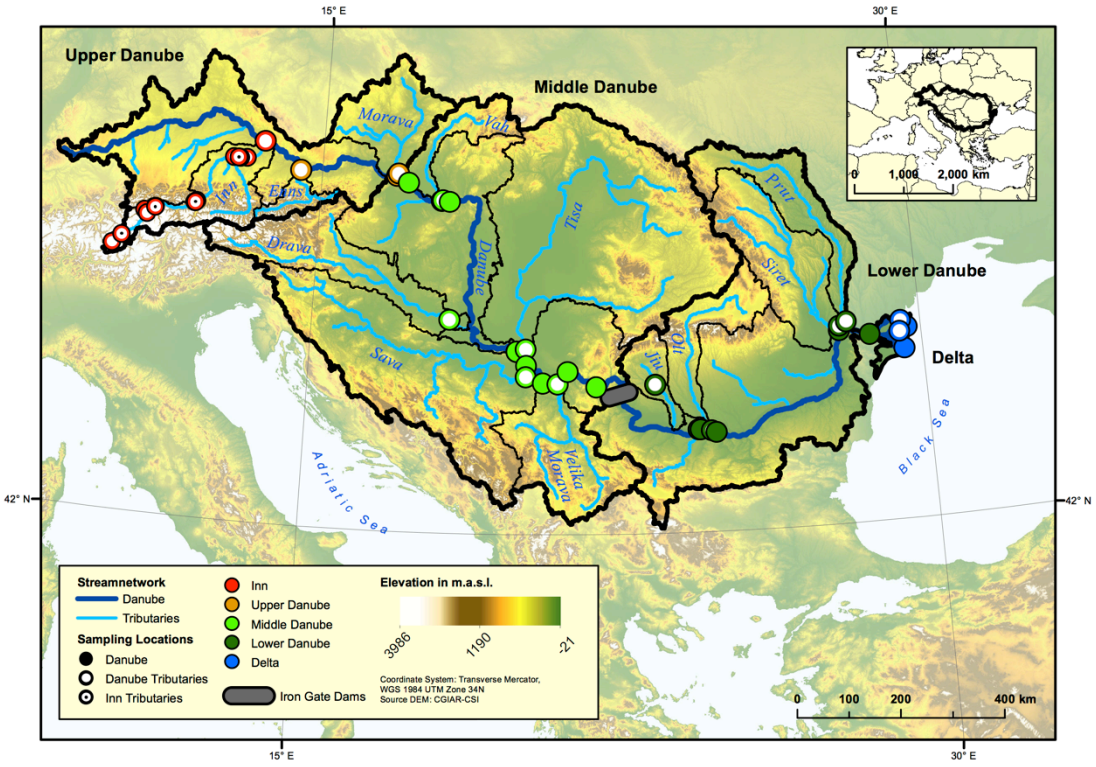

Figure 4.1. The Danube River basin. Topographic overview map of the Danube catchment showing the Danube mainstem and its major tributaries. Thick black lines represent the catchment border and subdivision into upper, middle, lower basins and delta. Thin black lines are tributary catchment borders. The largest hydropower dams are shown with one gray bar. Sampling locations are shown with closed symbols for locations at the Danube and open symbols for tributaries. The color coding refers to the sub-catchments (red: Inn River; orange: upper basin; light green: middle basin; dark green: lower basin; blue: delta).

4.3 Methods

4.3.1 Sample collection

Sampling took place during two campaigns in May/June 2013 and 2014, immediately following the maximum discharge in the yearly hydrograph (Belz and Goda, 2004). About 2 kg freshly deposited fine-grained (<2 mm) river sediments were collected from riverbanks or in quiescent, shallow water settings from the 12 largest tributaries to the Danube (Inn, Enns, Morava, Vah, Drava, Tisa, Sava, Velika Morava, Jiu, Olt, Siret and Prut) and 18 sites along the Danube mainstem between Passau (Germany) and the Black Sea (Figure 4.1). Danube mainstem locations were chosen immediately upstream and >5 km after the confluence of the tributaries. In 2014, the sampling was extended and 10 locations along the Inn River and 4 tributaries to the Inn River were sampled additionally (Kündig, 2014). Beginning of June 2013, heavy rainfall in southern Germany and Austria caused a 100-year flood in the upper and middle basin (Blöschl et al., 2013; Grams et al., 2014; ICPDR, 2014), which made it impossible to find fine river sediment at several mainstem locations. Another 100-year flood event, this time in the middle basin, occurred shortly before the 2014 sampling campaign, but did not affect the sampling (ICPDR&ISRBC, 2015; Vidmar et al., 2016). In addition to the sediment samples, 2 ml river surface water was filtered over a 0.22 µm filter (Sterivex GP Millipore) for water isotope (δ^2H, $\delta^{18}O$) measurement. The sediment and water samples were kept frozen until further processing at ETH Zürich.

4.3.2 Sample preparation

Bulk river sediments were wet-sieved with milliQ water over 200 µm and 63 µm sieves on a shaking table. The resulting <63 µm fraction was freeze-dried and kept frozen.

4.3.3 Bulk TOC, $\delta^{13}C$ and ^{14}C measurements

Aliquots of river sediment fine fraction (<63 µm) were de-carbonated in pre-combusted Ag boats by fumigation with HCl vapors in a desiccator (60 °C, 3 days), followed by a neutralization period with NaOH pellets (60 °C, 3 days) (Hedges and Stern, 1984; Komada et al., 2008). After neutralisation, the de-carbonated samples and the silver boats were wrapped in tin boats prior to combustion in the elemental analyzer.

For Danube samples from the first sampling campaign (2013) and Inn River samples, TOC and $\delta^{13}C$ were measured with a FlashEA 1112 Elemental Analyzer (EA) coupled to an isotope ratio mass spectrometer (IRMS; Isoprime, Vision). For ^{14}C measurement, the de-carbonated sediment was combusted in an EA and the resulting CO_2 collected and graphitized with an Automated Graphitisation Equipment system (AGE; Nemec et al., 2010; Wacker et al., 2010). ^{14}C contents of the graphite samples were measured on a MIni radioCArbon DAting System (MICADAS) at the Laboratory for Ion Beam Physics at ETH Zürich (Synal et al., 2007; Christl et al., 2013). TOC, $\delta^{13}C$

and ^{14}C of de-carbonated Danube 2014 samples were measured with an on-line EA-IRMS-AMS system (McIntyre et al., 2016).

For ten samples, ^{14}C was measured with both methods for comparison. The results correlate linearly with an $r^2 = 0.93$. Values measured with the AGE-system were on average 0.4% (35 yr) lower than measured with the EA-IRMS-AMS and are considered to be comparable for this study.

4.3.4 Plant wax fatty acid extraction

Fatty acid extraction and purification are described in detail in Freymond et al. (2018). In short, a total lipid extract was obtained by microwave extraction (30–50 g for Danube and tributary samples; 5 g for Inn samples) of the <63 µm fraction with dichloromethane:methanol (DCM:MeOH 9:1 v:v, 25 min at 100 °C). After saponification with KOH in MeOH (0.5 M, 2 h at 70 °C) and the addition of 5 ml MilliQ water with NaCl, the neutral phase was extracted with hexane (Hex). After acidification of the residue to pH 2 with HCl, the acid fractions was extracted with Hex:DCM (4:1 v:v) and methylated with MeOH:HCl (95:5 v:v, 12–18 h at 70 °C) to get fatty acid methyl esters (FAMEs). FAMEs were purified first over a SiO_2 column with $NaSO_4$ (eluting with (1) Hex, (2) DCM:Hex (2:1 v:v) and (3) DCM), followed by an $AgNO_3$-SiO_2 column (eluting with (1) DCM and (2) ethyl acetate). Measurement and quantification of FAs was done on a GC-FID (Gas chromatograph with a flame ionization detector, Agilent Technologies 7890A) with an external FAME standard (Supelco, saturated *n*-$C_{4\text{-}24}$ even-carbon-numbered FAMEs).

4.3.5 Compound-specific $\delta^{13}C$ and $\delta^{2}H$ measurements

Stable carbon isotopic analysis ($\delta^{13}C$) of the purified FAs (5% aliquots of Danube and tributary samples; entire sample for Inn samples) was performed using a gas chromatograph (GC, Thermo Scientific Trace GC Ultra, equipped with a Agilent VF-1ms column, 60 m x 250 µm ID, film thickness: 0.25 µm) coupled to an isotope ratio mass spectrometer (GC-IRMS, Thermo Scientific Delta-V Plus). The $\delta^{13}C$ values were corrected for the carbon added to the molecules during methylation and reported as ‰ units compared to VPDB.

The hydrogen isotopic composition of the FAs ($\delta^{2}H=(^{2}H/^{1}H_{Sample})/(^{2}H/^{1}H_{VSMOW})+1$) was measured by GC-IRMS (GC: Trace 1310, Thermo Scientific; IRMS: Delta V Advantage, Thermo Scientific) at EAWAG in Kastanienbaum, Switzerland. The GC was equipped with a split/splitless inlet operated in splitless mode at 280 °C and an InertCap 5MS/NP column (0.25 mm x 30 m x 0.25 µm) (GL Sciences). The oven temperature program was set as follows: at 40 °C/min from 80 °C to 130 °C, then at 6 °C/min to 300 °C and hold at 300 °C for 20 min. Eluting compounds were converted to H_2 in a pyrolysis reactor at 1,420 °C and transferred to the IRMS for compound specific $\delta^{2}H$ measurement via a Conflow IV interface (Thermo Scientific). Samples were measured in

duplicate. The H_3^+ factor was determined at the beginning of each sequence, being stable with an average of 5.98 (stdv = 0.004). δ^2H values were corrected for hydrogen atoms added during the methylation step using isotopic mass balance. The values were calibrated to the VSMOW scale with *n*-C_{25}-, *n*-C_{27}-, *n*-C_{29}-, and *n*-C_{32}-alkane standards (Arndt Schimmelmann) that were run at the beginning and end of each sequence and after every 6 samples (standard deviations: 2.6‰ (*n*-C_{25}, n=36), 2.4‰ (*n*-C_{27}, n=36), 6.9‰ (*n*-C_{29}, n=36), 7.1‰ (*n*-C_{32}, n=36)). Additional standards of *n*-C_{27}-alkane (Arndt Schimmelmann) and *n*-C_{29}-alkane (laboratory standard) were run in varying concentrations throughout the sequence and had standard deviations of 3.9‰ (*n*-C_{27}, n=37) and 2.4‰ (*n*-C_{29}, n=7).

4.3.6 Compound-specific ^{14}C measurements

FAs for compound specific ^{14}C analysis were isolated by preparative capillary gas chromatography (PCGC; Eglinton et al., 1996). The system consisted of a GC (Agilent Technologies 7890A) equipped with a flame ionization detector (FID) and an Agilent VF-1 ms column (30 m x 530 µm ID x 0.5 µm film thickness), and a seven-port fraction collector (Gerstel Preparative Fraction Collector). The oven temperature ramped at 40 °C/min from 45 °C to 120 °C and then at 6 °C/min to 320 °C where the temperature stayed for 5 min. 10% of the sample went to the detector for purity, concentration and retention time control and 90% were transferred to the fraction collector where single peaks (FA *n*-C_{16}, *n*-C_{18}, *n*-C_{24}, *n*-C_{26}, *n*-C_{28}, *n*-C_{30}) were collected in single glass U-tube traps. Each sample was injected 50–100 times to get sufficient amounts of carbon for reliable ^{14}C measurements (20–100 µgC). The traps were rinsed with Hex:DCM (9:1 v:v) to transfer the samples to 1 ml vials and the purity of the compounds was tested on a GC-FID. The samples were passed over a 1 cm SiO_2 column with 1 mL DCM to remove any column bleed, and subsequently transferred to 9 mm quartz tubes and dried over a stream of high-purity N_2 gas. Pre-combusted CuO was added to the dried samples before the quartz tubes were fixed to a vacuum line, cooled with butyl acetate (-77 °C), evacuated to $<2\times10^{-3}$ mbar, and sealed with a torch. The samples were combusted at 850 °C for 5 h and the resulting CO_2 was purified with a cool trap (butyl acetate), quantified and transferred to 4 mm Pyrex tubes in a vacuum line. ^{14}C on the CO_2 was measured on a MICADAS at the Laboratory for Ion Beam Physics at ETH Zürich. ^{14}C fraction modern (Fm) was blank corrected with a processing blank (Tao et al., 2015) and corrected for the carbon atoms added during methylation of the FAs. Fm was converted to $\Delta^{14}C$ with the following equation where λ = 1/8,267 and y stands for the year of measurement (Sternström et al., 2011).

(4.1) $$\Delta^{14}C = (Fm \times e^{\lambda(1950-y)} - 1) \times 1000$$

4.4 Results

4.4.1 Bulk fine fraction

4.4.1.1 $\delta^{13}C_{org}$ values of Danube sediments

$\delta^{13}C$ values (Figure 4.2) of bulk organic carbon of Danube mainstem sediment are relatively constant along the river, ranging from -28.4‰ to -25.9‰ with an average of -27.4‰ (excluding the outlier at km 1,077 with a $\delta^{13}C$ value of -35.2‰). The tributaries of the Danube (including the site at the Inn close to the confluence with the Danube, but excluding the upstream locations along the Inn and its tributaries) are slightly more ^{13}C-enriched than the Danube mainstem, ranging from -28.4‰ to -24.6‰ with an average of -26.8‰. Locations along the Inn River and the tributaries to the Inn show more scatter, ranging from -29.6‰ to -23.6‰ with an average of -26.4‰.

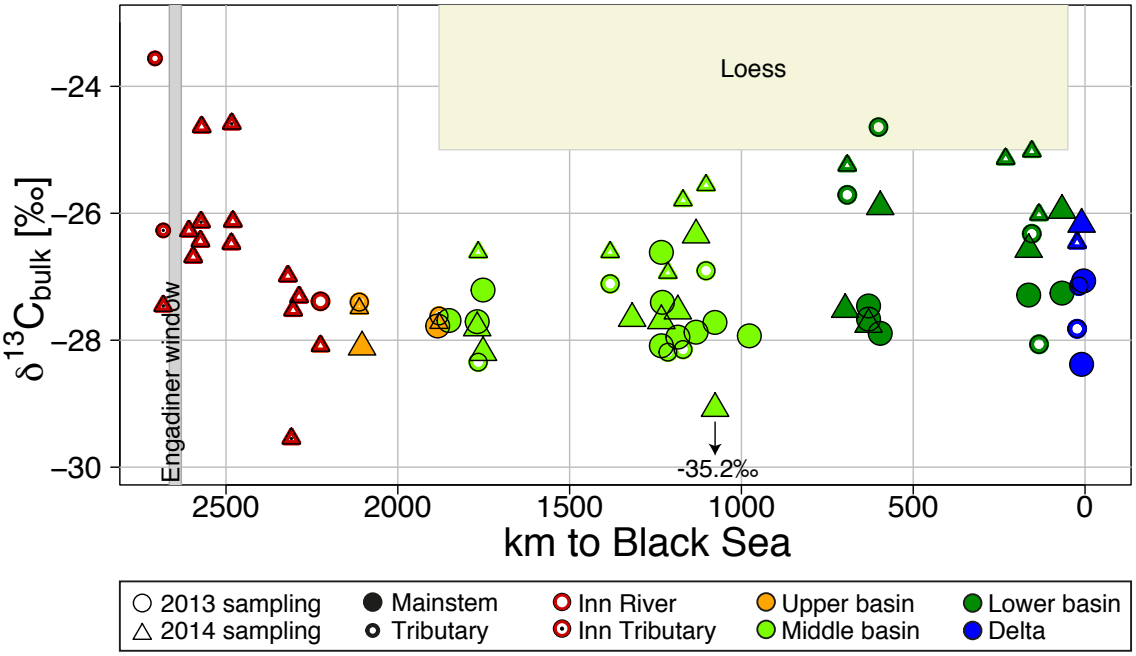

Figure 4.2. Bulk fine fraction $\delta^{13}C_{org}$ along the Danube. Samples from the 2013 sampling campaign are shown in circles, samples from the sampling in 2014 in triangles. Filled symbols are Danube mainstem locations, open symbols are locations at tributaries and open symbols with a black dot are tributaries to the Inn River. Symbol color refers to the sub basins (red: Inn River; orange: upper basin; light green: middle basin; dark green: lower basin; blue: delta). The location of the Engadiner window is shown with the gray bar. $\delta^{13}C$ values of the organic rich Bündnerschiefer in the Tauern Window east of the Engadiner window range from -14 – -21‰ (Demeny and Kreulen, 1993). The location and range of $\delta^{13}C$ values for loess are shown with the beige rectangle. Published $\delta^{13}C$ values for loess in Serbia range from -22.5 – -25‰ (Hatte et al., 2013; Zech et al., 2013). An outlier value (Danube downstream Velika Morava) is included with its $\delta^{13}C$ value of -35.2‰.

4.4.1.2 Bulk fine fraction ^{14}C characteristics

Bulk $\Delta^{14}C$ values (Figure 4.3) of organic carbon in the fine fraction of the Inn River and its tributaries range from -77 to -364‰, with the lowest values generally in the upper half and highest values in the lower half of the catchment. The Danube mainstem shows $\Delta^{14}C$ values ranging from -36 to -316‰, with an average of -83‰ in the upper and middle basin. Below the Iron Gate reservoir, $\Delta^{14}C$ values decrease to a minimum of -316‰ near the mouth of the river. The tributaries (excluding the locations along the Inn River) show variable $\Delta^{14}C$ values, ranging from -32 to -449‰ and follow the decreasing trend of the mainstem. Some tributaries, mainly in the lower part of the middle basin and the lower basin, show significantly lower values than the Danube mainstem.

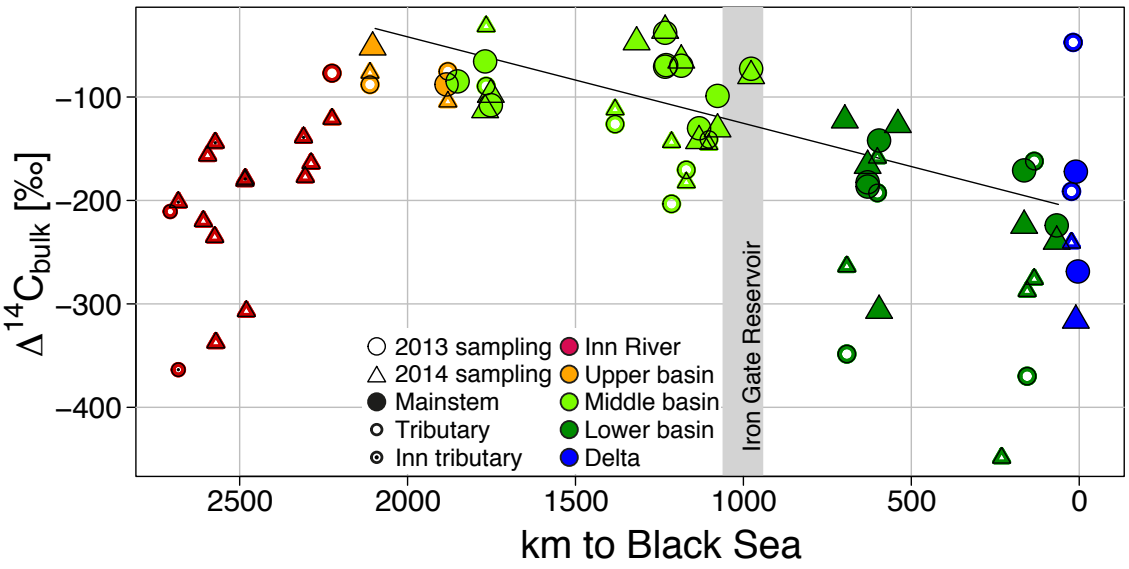

Figure 4.3. Bulk (<63 µm) $\Delta^{14}C$ along the river. The regression line was fitted to Danube mainstem locations only. Errors are within the symbol size. The gray bar indicates the location of the Iron Gate reservoir. Symbol color and shape correspond to Figure 4.1 & 4.2.

4.4.2 Long-chain plant wax fatty acids

4.4.2.1 Fatty acid $\delta^{13}C$

Weighted mean average $\delta^{13}C$ values of long-chain (n-C_{24-30}) plant wax fatty acids in Danube mainstem, tributaries and Inn River sediment samples range between -35.1‰ and -32.1‰ with an average of -33.5‰ (excluding the outlier from close to the source of the Inn with a $\delta^{13}C$ value of -29.0‰; Figure 4.4). From the highest elevations in the Inn catchment down to the beginning of the middle basin, FA $\delta^{13}C$ values show a decreasing trend, whereas from the second half of the middle basin to the delta, the values remain approximately constant, with an average of -33.4‰. Tributaries generally follow the mainstem trend, apart from the lower basin where three tributaries show more enriched values and one shows a more depleted value than the mainstem.

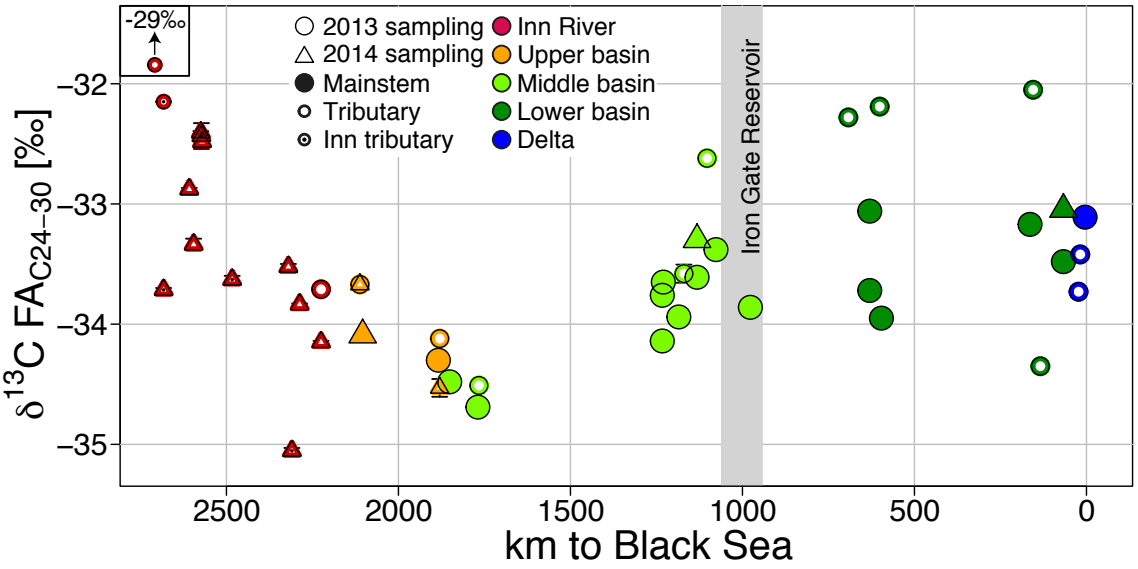

Figure 4.4. Compound-specific $\delta^{13}C$ of long chain (n-C_{24-30}) fatty acids along the river. Error bars correspond to the standard deviation of duplicate measurements and are mostly within the symbol size. Colors and symbol shape corrspond to Figure 4.1 & 4.2.

4.4.2.2 Fatty acid $\Delta^{14}C$

Long-chain fatty acid (n-C_{24-30}) $\Delta^{14}C$ values (Figure 4.5) of Danube mainstem sediment fine fraction decreases linearly from modern values in the upper basin to -208‰ at the mouth of the river (r^2 = 0.93). Tributaries generally follow this decreasing trend, with two tributaries in the middle basin (Drava, Sava) and one in the lower basin (Siret) showing lower values than the general trend. One tributary in the lower basin (Prut) and one delta location reveal higher $\Delta^{14}C$ values than the mainstem trend line.

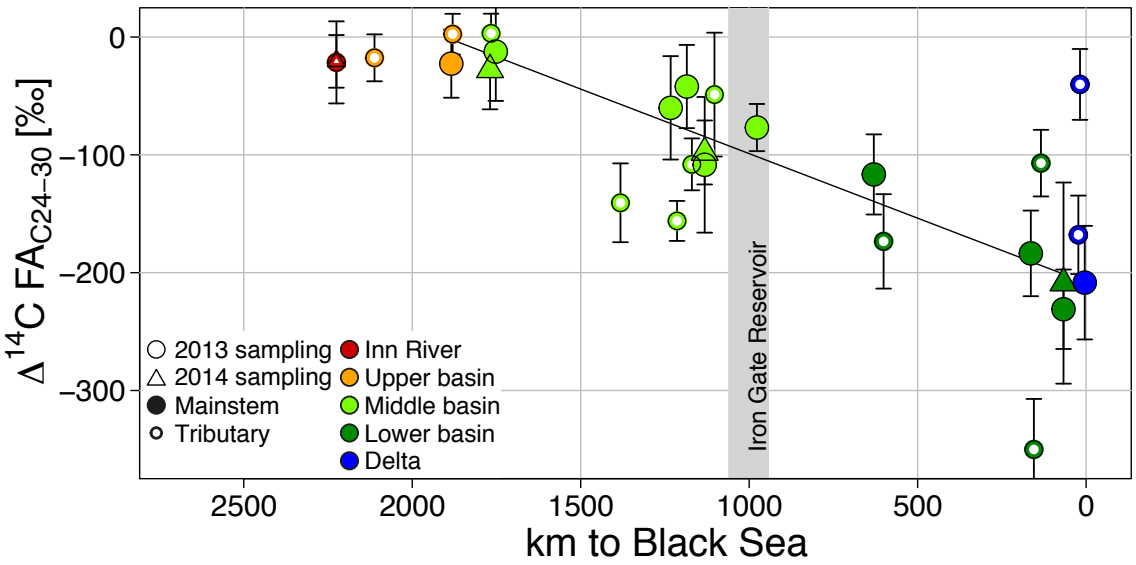

Figure 4.5. Compound-specific $\Delta^{14}C$ of long chain fatty acids (n-$C_{24\text{-}30}$). The regression line corresponds to Danube mainstem locations only. Symbol color and shape correspond to the ones in Figure 4.1 & 4.2.

4.4.2.3 Fatty acid δ^2H

FA hydrogen isotope values (δ^2H; Figure 4.6) range from -199 – -169‰. They show a slight trend from more depleted values along the Inn and the upper basin (average of -186‰) to more enriched values in the middle and lower basins (average of -178‰). For the 2014 sampling, only samples from the Inn River and the upper and beginning of the middle basin were measured. These samples show slightly less depleted values (3–11‰ difference) than the 2013 samples. Error bars show the standard deviation from duplicate measurements.

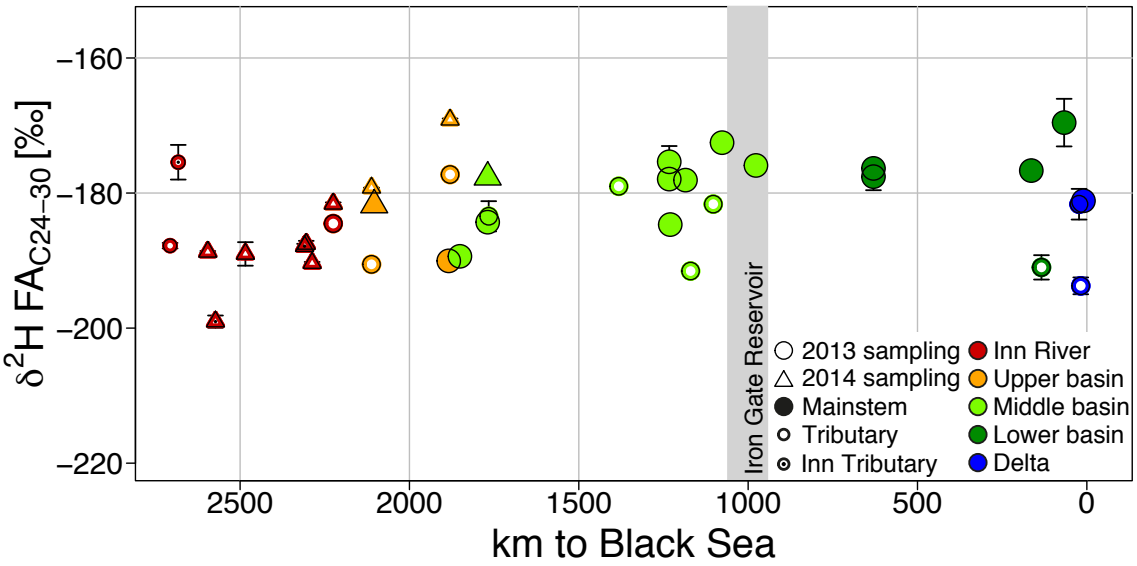

Figure 4.6. Fatty acid δ^2H along the Danube. Error bars correspond to the standard deviation from duplicate measurements. Symbol color and shape correspond to the ones in Figure 4.1 & 4.2.

4.5 Discussion

Previously, we have found a 70–80% decrease in mineral surface area-normalized TOC and terrestrial biomarker (plant wax FA, brGDGTs, lignin-derived phenols) loadings along the course of Danube (Freymond et al., 2018). The same trend is evident after normalization of bulk OC and biomarkers to the summed sedimentary abundance of phyllosilicates (illite + smectite; Freymond et al., 2018). This systematic change in organic matter loadings with river distance may reflect one or more processes including: (i) loss of OC during transport and (ii) addition of OC-poor, high-SA sediment along the course of the river system. These different scenarios have contrasting implications with respect to the nature and dynamics of organo-mineral interactions during fluvial transport.

4.5.1 Comparison of the two sampling years

The sample set shown in this study includes very special hydrological conditions. During the first sampling campaign in May/June 2013, heavy rainfall in southern Germany and Austria caused a 100-year flood from the confluence of the Inn River and Danube on (Supplementary Figure A.4.1) (Grams et al., 2014; ICPDR, 2014). Samples in the lower basin and the lower part of the middle basin (including the tributaries Tisa, Sava, Velika Morava) were collected before the flood peak reached this part of the basin. However, water level was already high during sampling in the middle basin. All samples upstream of the Drava River were collected after the flood peak had passed. The Danube basin experienced a second 100-year flood only one year later, in May 2014 (ICPDR & ISRBC, 2015; Vidmar et al., 2016). This time, the Sava River in the middle basin reached a >100 year high water stage, resulting in flooding of the Sava and the Danube in the middle basin from the confluence with the Sava on. Samples taken in the upper and lower Danube basins were not affected by this flood. Therefore, a complete comparison of flood vs. non-flood sediment deposits is not possible. Only for the upper Danube basin both 'normal' and flood condition samples are available. All lower basin samples were not affected by both floods.

Such flood events mobilize and discharge large amounts of sediment and OC (Cathalot et al., 2010; Smith et al., 2013). Both, stable $\delta^{13}C$ values from high to low flow conditions (Cathalot et al., 2013) and changing isotopic composition of the suspended particulate matter during a flood event (Cathalot et al., 2010) have been shown for the Rhône River. Drenzek et al. (2009) conclude that although OC discharge increases during flood events at the Eel River, the corresponding relative contribution of pre-aged soil and petrogenic OC remains constant. Considering the extreme events sampled in the Danube basin, it seems surprising that sedimentological characteristics (i.e. mineral surface area; Freymond et al., 2018) as well as organic bulk fine fraction and compound-specific parameters (i.e. bulk and FA $\delta^{13}C$ and ^{14}C, FA $\delta^{2}H$) show comparable values for

the two sampling years (Figure 4.2–4.6). This suggests that the relative source contributions stay constant over normal and high discharge conditions.

4.5.2 *Soils as the primary source of fluvially-transported sediments*

In a previous study, we found that *in situ* brGDGT production in the Danube river is minor and therefore, brGDGTs in sediments are mainly soil derived (Freymond et al., 2017). The increase in FA concentration with increasing brGDGT concentration (Figure 4.7) indicates that these two markers have a common main source, or at least, a comparable relative proportion of different sources (soil, litter, in-river production) between sampling locations. Moreover, due to the correlations of FA $\delta^{13}C$ vs. bulk $\delta^{13}C$, and especially FA $\Delta^{14}C$ and bulk $\Delta^{14}C$ (Figure 4.8), it can be assumed that soil is not only the primary source of brGDGTs and FAs but probably of TOC in Danube river sediment in general. The tight coupling of OC, FA and brGDGT concentrations with SA and phyllosilicate content further supports the hypothesis that the sediment load of the Danube is primarily related to mineral soil input (Freymond et al., 2018). However, large areas of the middle and lower basins are covered by loess, which serves as parent material for soils in this area (Haase et al., 2007). Although loess generally has a low TOC content (0.2–0.5%; Hatte et al., 2013), it has to be considered as significant OC source to Danube sediments because of its widespread occurrence, the numerous outcrops in the middle and lower basins and its high erodibility.

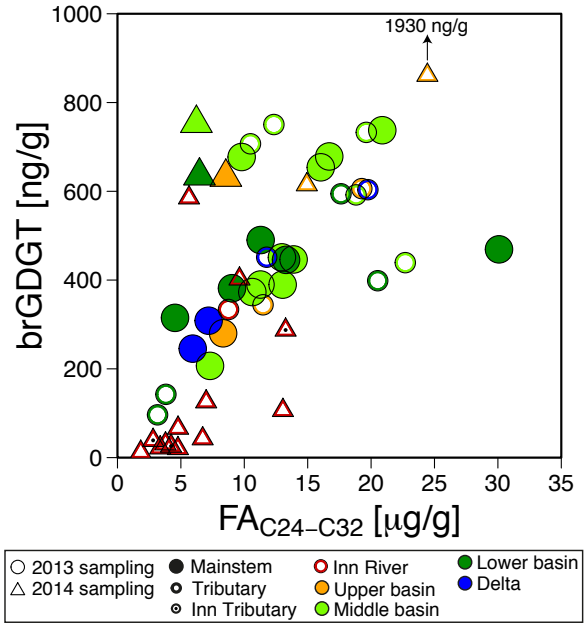

Figure 4.7. FA vs. brGDGT concentration of the Inn and Danube River sediment fine fraction. Symbols and colors correspond to the sampling locations in Figure 4.1 & 4.2.

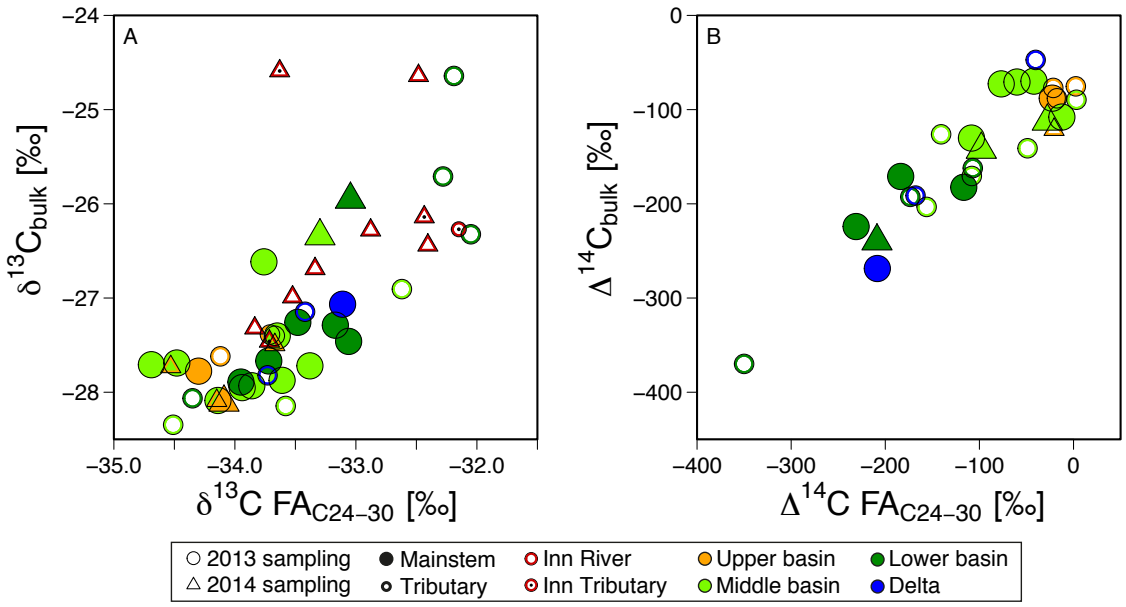

Figure 4.8. Bulk vs. FA carbon isotopic composition of Inn and Danube River sediment fine fraction. A) $\delta^{13}C$ bulk vs. FA and B) $\Delta^{14}C$ bulk vs. FA. Symbols and colors correspond to the sampling locations in Figure 4.1 & 4.2.

4.5.3 *Locally-sourced versus basin-integrated signals*

Studying the evolution of the brGDGT composition along the Danube, it was found that brGDGT distributions reflect the local temperature at each sampling location. It was therefore concluded that the signal exported to the Black Sea reflects the lower basin rather than an integration of the entire Danube basin (Freymond et al., 2017). Comparing the Danube sediment brGDGT composition and evolution of the signal to available brGDGT data from two loess sequences in the middle Danube basin reveals that BIT, MBT/MBT', CBT/CBT' and resulting MAT and pH values are in the same range (Zech et al., 2012; Schreuder et al., 2016; Freymond et al., 2017). However, because the brGDGT signal in tributaries draining loess areas is mostly not different than of the Danube mainstem just upstream of these tributaries, it cannot be concluded that the local character is loess derived.

The evolution of the organic matter signal along the river is also reflected in the stable and radiocarbon isotopic composition of the river sediment. These data support the continuous addition of organic carbon along the course of the river as suggested by the brGDGTs and as further discussed below. Given that overall TOC and biomarker loadings are decreasing (Freymond et al., 2018) implies that there must be significant loss of upstream soil OM and/or that the soil OM emanating from downstream catchments –while sufficient to dilute the upstream signal– is poorly loaded on its mineral host.

4.5.3.1 C3 vs. C4 vegetation contribution

Sediment $\delta^{13}C$ values are often used for example to track vegetation changes from a C3 to a C4 (or vice versa) dominated system (e.g. Hatte et al., 2013; Contreras et al., 2016) or to determine the fraction of each plant type contributing to sediment (e.g. Galy et al., 2008). This is possible because of the different CO_2 fixation pathways of C3 and C4 plants, resulting in distinct $\delta^{13}C$ values (C3: ~ -24 to -32‰; C4: ~ -11 to -16‰; Oleary, 1988). The vegetation in the Danube basin changes from C3 vegetation only in the upper basin to up to 10–20% C4 vegetation in some areas in the middle and lower basins (Still et al., 2003). The $\delta^{13}C$ of Danube mainstem sediment is on average -27.7‰, indicating a clear C3 vegetation signal. Tributaries in the middle and lower basins show slightly less depleted values than the Danube mainstem (Figure 4.2). With a simple two end member mass balance, the contribution of C3 and C4 vegetation (fraction C3 (f_{C3}) and C4 (f_{C4})) to middle and lower basin tributaries can be calculated. The Danube mainstem $\delta^{13}C$ average value of -27.7‰ is taken as the C3 and -14‰ as the C4 end member signal (Oleary, 1988). Resulting C4 plant contribution of Danube tributary sediments (average of 2013 and 2014 samples) in the middle and lower basins is 1–22% (Table 4.1). These values are in the range, and for some tributaries at the upper limit of the range, of the C4 vegetation cover (Still et al., 2003). However, the calculated f_{C4} seems too high, especially for tributaries coming from the Carpathian Mountains (Olt, Jiu) where less C4 vegetation would be expected at higher elevations. Therefore, the two end member mixing model does not seem to resolve the OC composition to a satisfactory degree.

Table 4.1. Modelled C3 and C4 vegetation contribution to tributary sediment OC based on the binary mixing model. Values show the average of 2013 and 2014 samples.

Tributary	f_{C3} [‰]	f_{C4} [‰]
Vah	98	2
Drava	94	6
Tisa	99	1
Sava	95	5
Velika Morava	89	11
Jiu	84	16
Olt	78	22
Ialomita	81	19
Siret	85	15
Prut	95	5

4.5.3.2 Local elevation effect on FA $\delta^{13}C$ values

FA $\delta^{13}C$ values for sediments from the Inn River to the upper part of the middle basin show a trend from more enriched values in the Alps to more depleted values along the Danube and its tributaries (Figure 4.9). These enriched values cannot be explained by a C4 contribution because the vegetation in this environment is exclusively C3. ^{13}C enrichment of bulk C3 plant leaves with increasing elevation was found globally for regions not experiencing drought stress (e.g. Körner et al., 1988). However, for the Inn-Danube continuum the enrichment with elevation is +3.4‰ per 1,000 m, which is almost a factor of three higher than described for the global average (Körner et al., 1988).

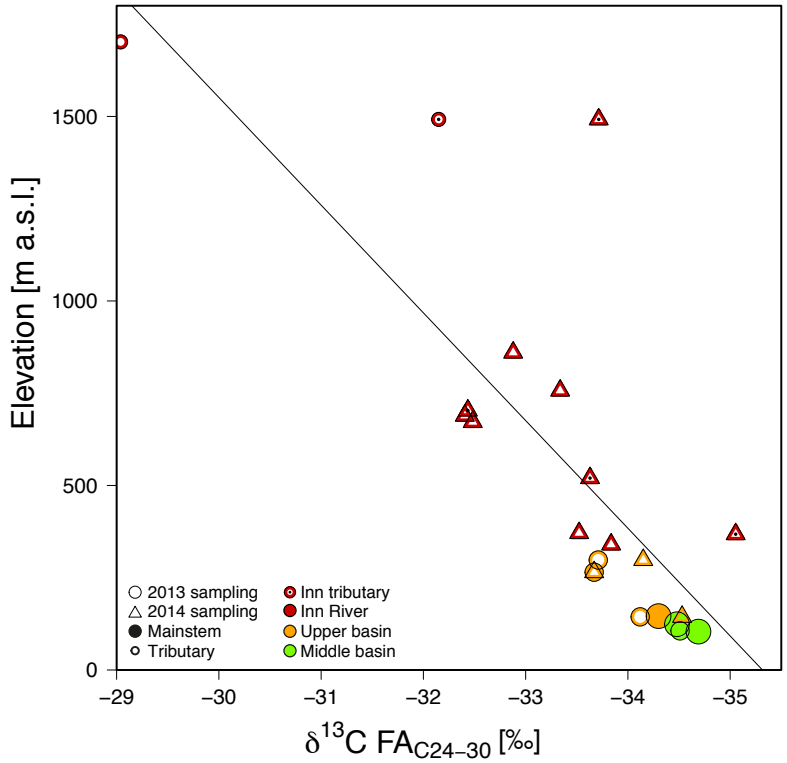

Figure 4.9. Long chain FA $\delta^{13}C$ against elevation of the sampling location. Only sampling locations from the upper and the beginning of the middle basins are shown. The linear regression shows an $r^2 = 0.61$. Symbol color and shape correspond to the ones in Figure 4.1 & 4.2.

Downstream of the upper part shown in Figure 4.9, FA $\delta^{13}C$ values increase in the middle basin and stay at an approximately constant level with an average of -33.4‰. Along this stretch, there is almost no elevation gradient along the Danube mainstem (from 100–0 m a.s.l.) and therefore no elevation effect in FA $\delta^{13}C$ values can be expected. However, it has to be noted here that the tributaries in this part of the basin have their source in mountain regions as well (see Figure 4.1). Their slightly more enriched FA $\delta^{13}C$ values could therefore reflect an altitude effect emanating from their

headwaters. On the other hand, we see at the Inn River that the FA $\delta^{13}C$ shows a local signal. Close to the confluence with the Danube, the more enriched signal from higher elevations is overprinted with the downstream signal. Therefore, we would not expect to see an elevation-derived $\delta^{13}C$ signal close to the Danube in middle and lower basin tributaries. Alternatively, the relative ^{13}C enrichment downstream could either derive from a C4 plant contribution (section 4.5.3.1) and/or from a substantial loess input from the lower reaches of these tributaries. However, there are no reports of the isotopic composition of FAs in loess in the Danube region, which makes it impossible to constrain a potential loess-derived FA contribution.

4.5.3.3 Evolution of FA δ^2H signatures

FA δ^2H along the Danube shows an increase of about 10‰ from the upper basin to the delta (Figure 4.6). This gradual enrichment along the Danube mainstem is in the same range as the enrichment of the river water (Supplementary Figure A.4.2). However, in the Inn catchment, river water and precipitation δ^2H in the upper Alpine region is about 30‰ more depleted than at its terminus. A corresponding depletion of FA δ^2H with increasing elevation would be expected but was not observed. Therefore, a local influence on the river sediment signal is only partly reflected in FA δ^2H.

In summary, the stable isotope composition in river sediment shows a changing signal along the Danube that suggests local biospheric carbon input.

4.5.4 Evolution of organic matter ages

A river system like the Danube is moving large amounts of sediments in space and time. Freymond et al. (2018) shows that the observed decrease in OC/SA ratio along the course of the river cannot be explained only due to the local tributary addition of low OC/high SA sediments, i.e. loess, to the mainstem. However, besides the addition of loess also a temporal aspect, i.e. transport time along the river, variable residence time of OC in soils within the river basin, and artificial aging due to preferential degradation of more refractory fresh OC, can at least partially explain the downstream decrease in the OC/SA ratio.

Bulk and FA ^{14}C both show a generally systematic change with river distance (Figures 4.3 & 4.5). The heterogeneity of bulk OC in the Inn River catchment ($\Delta^{14}C$ values from -360‰ to about -100‰) can be attributed to varying petrogenic carbon input. Only considering the Danube mainstem, bulk $\Delta^{14}C$ decreases systematically from -50‰ to about -240‰ and FA $\Delta^{14}C$ from -20‰ to -230‰. These linear decreases ($r^2_{bulk} = 0.51$, $r^2_{FA} = 0.92$) can be translated into an approximate aging of $\Delta^{14}C$ of -8‰ (80 yr) and -11‰ (100 yr) per 100 kilometers for TOC and FA, respectively.

The increase in age coincides with a continuous decrease of OC and biomarker loadings on mineral surfaces (Freymond et al., 2018). This results in high loadings with

young OC in the upper basin and poorly loaded sediment with aged OC in the lower basin (Figure 4.10). This pattern can be the result of three different processes: (i) Preferential unloading and degradation of young and labile compounds resulting in 'artificial aging'; (ii) carbon aging and degradation during transport; and (iii) dilution with sediments characterized by low OC-loading and old ages.

In the following discussion, these different scenarios that could lead to the observed 'aging' along the river are discussed.

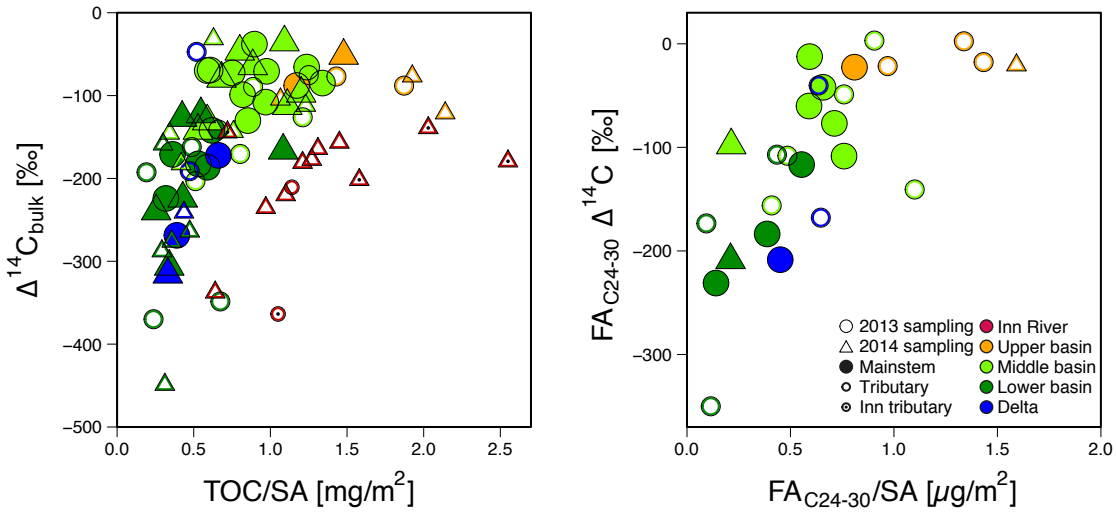

Figure 4.10. $\Delta^{14}C$ against loading on mineral surface area. Left panel: TOC; right panel: FA. Symbol color and shape correspond to the ones in Figure 4.1 & 4.2.

4.5.4.1 Preferential removal of young organic carbon

Some compounds are more easily degraded than others due to their chemical composition and structure (von Lützow et al., 2006). During the first stages of decomposition, the relative lability of each compound influences the composition of OC that enters the longer-term OC pool of soils. However, on a long-term view, the composition of soil OC is mainly driven by other parameters like the activity of and accessibility to decomposers of the OC (e.g. sorption to surfaces, enclosure in small pores) (Schmidt et al., 2011). In a river system, the preferential removal of young, well accessible OC would lead to an artificial aging of the total OC and FAs during transit. On a compound-specific scale, one would, additionally to increasing age, expect a change in FA composition. More degradation would result in an increasing even over odd predominance of the FAs, which can be quantified in the carbon preference index (CPI). However, the CPI does not change significantly along the Danube but stays rather constant (Supplementary Table B.4.2), and is therefore no clear sign for degradation. Preferential degradation can also be recognized by the evolution of the $\delta^{13}C$ value as a result of the natural preference for isotopically light carbon. Indeed, alkanes in

soils showed a slight increase in $\delta^{13}C$ of about 1–2‰ during early decomposition (Wang et al., 2016; Li et al., 2017). Also the FA $\delta^{13}C$ values along the Danube show an increase of about 1‰ from the upper to the middle basin (Figure 4.4). However, next to degradation, also other factors, like replacement with a local signal, can explain this signal.

4.5.4.2 Aging during transport

Prior to entering a river, OC can be pre-aged due to intermediate storage in soils. OC pre-aging in soils potentially varies within the catchment, and may be higher in well-developed, deep soils in the lower reaches with flat topography compared to less deep soils in the upstream part with steeper topography and more erosion. However, this aspect may lose importance assuming that mainly recent topsoil is eroded and contributes to the river load. Nevertheless, extreme events causing deeper mineral soil erosion can still occur. Second, further aging of OC occurs during river transport, when it likely experiences several cycles of deposition and re-suspension. The ageing of OC during the deposition and re-suspension cycles goes hand in hand with the degradation processes mentioned in the previous paragraph (4.5.4.1). The co-occurrence of the two processes makes it hard to separate the influence of preferential degradation and aging during transport.

4.5.4.3 Degradation and aging during transport

The relation between aging and degradation of OC with decreasing OC loading has previously been studied on the East Siberian Arctic Shelf (ESAS; Bröder, 2016). The ESAS serves as natural transport and degradation laboratory, as it has one point source of terrigenous OC, the Lena River, followed by lateral transport of the riverine sediment across the shelf. Bröder (2016) found that the FA ^{14}C age in ESAS surface sediment linearly increased with increasing water depth following

(4.2) $\text{age [kyr]} = a \times \text{waterdepth [m]} + b$

From this trend, transport time was calculated according to

(4.3) $\text{Transport time [kyr]} = \text{age [kyr]} - b\ \text{[kyr]} = a\ \text{[kyr/m]} \times \text{waterdepth [m]}$

This resulted in an exponential decrease of terrigenous OC/SA and biomarker/SA ratios with transport time. An exponential function of the following form was fitted to this dataset

(4.4) $C(t) = C(0) \times e^{-kt} + R$

where C(t) is the OC loading at time t, C(0) the initial OC loading, k the degradation rate (where smaller values represent slower degradation), and R an asymptotic constant for $t \longrightarrow \infty$, representing a recalcitrant fraction. With this, the degradation rate for

terrigenous OC (TerrOC; 2.2 ±0.6 kyr^{-1}) and FAs (3.8 ±0.9 kyr^{-1}) on the ESAS and recalcitrant fractions of 15 ±6% and 5 ±2% for TerrOC and FAs, respectively, were calculated. The transport time from the mouth of the Lena River to the deepest sampling location was determined to be 3,900 ±300 yr (Bröder, 2016).

Here, we apply this same method to Danube mainstem TOC and FAs (replacing water depth with km along the river) to estimate the transport time of TOC and FAs for this river. We hereby assume a 'pipeline'-like transport of OC, where soil OC enters the Danube at its source, followed by a linear transport pathway along a distance of 2,700 km. Nevertheless, ^{14}C ages from the locations along the Danube are included in the model with the value that was measured, therefore including OC that was added by tributaries to the mainstem during the transport.

Following the above set of equations (Equations 4.2–4.4), the resulting transport time of TOC for the 2,700 km along the Inn and Danube is 2,130 yr, the degradation rate is k = 0.90 kyr^{-1} and the recalcitrant fraction is 4% (Figure 4.11A). The transport time for the FAs is 2,790 yr, the degradation rate is k = 1.01 kyr^{-1} and the recalcitrant fraction is 18% (Figure 4.11B). These transport times correspond to transport velocities of 80 yr/100 km and 100 yr/100 km (or 1.25 km/yr and 1.0 km/yr) for TOC and FAs, respectively (as already shown in section 4.5.4). Compared to the transport time of 6.5 yr/km for TerrOC on the ESAS (= 0.15 km/yr)(Bröder, 2016), OC transport is >6 times faster in the Danube. This is easily explained by the unidirectional flow and high velocity of the river water compared to continental shelf environments. In contrast, the degradation rate k is smaller for the OC in the Danube sediment (k = 0.90 kyr^{-1}) than for TerrOC on the ESAS (k = 2.2 ±0.6 kyr^{-1}), implying slower degradation of OC in the Danube River. However this is opposite of what we would expect and probably not the correct interpretation of these values. Sediment on the ESAS undergoes several oxic-suboxic burial and re-suspension cycles (Bröder, 2016), which may slow down degradation rates compared to the mainly oxic conditions in the Danube river. Another explanation for the offset in degradation rates is the complexity of a river system, with steady sediment input to the mainstem. The addition of OC that has not yet experienced the longitudinal transport as the OC that is already in the mainstem at this point artificially slows down degradation. The ESAS biomarker study in comparison is much closer to a real 'pipeline' transport system because the only source of terrestrial biomarkers like long chain plant wax fatty acids is the Lena River.

The recalcitrant fraction of the OC carried by the Danube, i.e. the OC that is not degraded after infinite time, is much smaller for TOC than for FAs (4 and 18%, respectively). As TOC is a mixture of fresh, pre-aged, and fossil OC with a large labile fraction, which is mostly rapidly degradable, only a small percentage of more recalcitrant molecules is left behind. In contrast, plant wax fatty acids in a river are mostly soil derived, and have already undergone degradation and soil formation processes. In soils, associations to mineral surfaces are formed that have been reported

to slow down degradation of FAs (Kleber et al., 2015; Tesi et al., 2016b). In general, FAs are known to be relatively persistent against degradation due to their molecular structure (Eglinton and Eglinton, 2008) and indeed, FAs buried in continental margin sediments after river discharge have been used for paleo-climate reconstructions (e.g. Kusch et al., 2010; Bröder et al., 2016a). However, the assumption that there is a recalcitrant fraction even for time $\longrightarrow \infty$ is questionable. Therefore, two slightly different models are tested for the Danube that do not include a recalcitrant fraction. For TOC loadings, a linear model ($r^2 = 0.74$) (dashed line in Figure 4.11A) and for FA loadings an exponential model with the asymptotic value 0 (dashed line in Figure 4.11B) was fitted. With the linear model, TOC loadings reach 0 after 2,700 yr. The second exponential model for FAs theoretically never reaches 0, conserving an infinitely small amount of FAs. Loadings reaching 0 or quasi 0 imply that degradation in the river is transport time limited and that with longer residence time in the catchment, all OC could be decomposed. For the Danube, the transport time for TOC was calculated to be 2,130 yr and total degradation to occur at a transport time >2,700 yr. Therefore, it seems reasonable that the largest part of the OC entering the river in the uppermost part is degraded by the time it reaches the river mouth. The OC signal exported to the ocean is therefore enriched in carbon that entered the river in the lower basin, as was already suggested by Freymond et al. (2017) based on the brGDGT signature in the same Danube sediments.

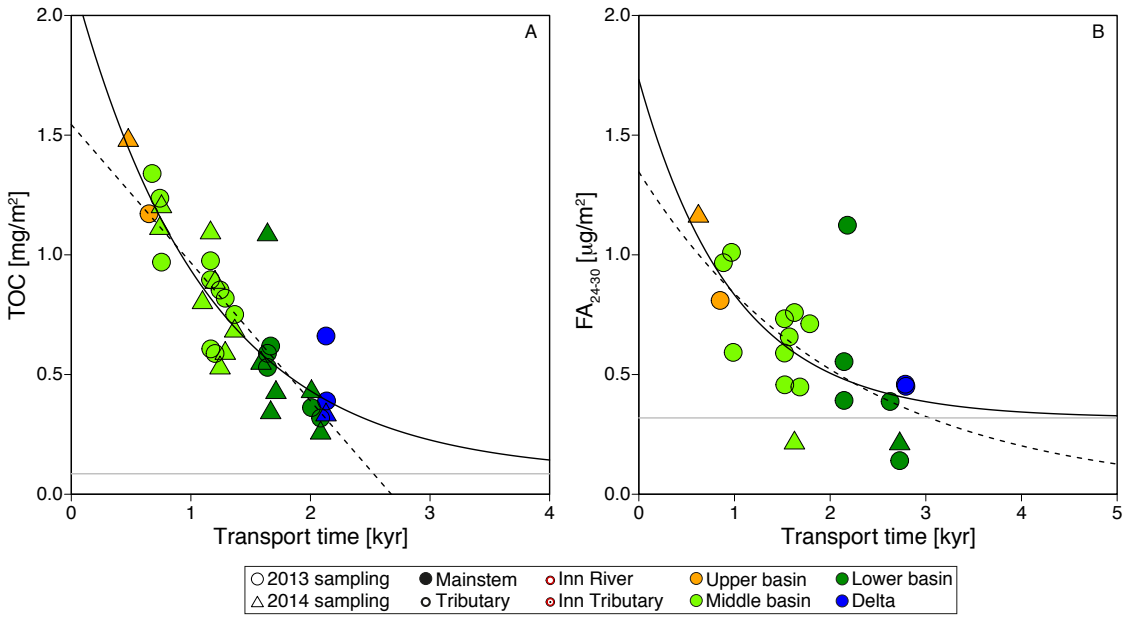

Figure 4.11. SA loading decrease of A) TOC and B) FA during transport along the Danube mainstem. The black curves correspond to an exponential function of the form $C(t) = C(0) \times e^{-kt} + R$. The horizontal gray lines show the asymptotic value, corresponding to the recalcitrant fraction of 4% for TOC and 18% for FAs. The dashed line in A) shows a linear model fitted to the dataset of the form $y = ax + b$. The dashed curve in B) shows an exponential curve of the form $C(t) = C(0) \times e^{-kt}$, assuming no recalcitrant fraction. Symbol color and shape correspond to the ones in Figure 4.1 & 4.2.

4.5.4.4 Loess as a significant carbon source

Continuous addition of sediment with high surface area, low OC loading and high ^{14}C age is a possible scenario to explain the observed loadings and ^{14}C trends. Following, the binary model from above (section 4.5.3.1), considering a C3 and a C4 vegetation dominated biospheric end member, is expanded to a ternary mixing model including loess (Figure 4.12). To solve the resulting three end member mass balance, bulk $\Delta^{14}C$ is included as additional dimension to the equation system.

(4.5) $\Delta^{14}C_{bulk} = (f_{C3} \times \Delta^{14}C_{C3}) + (f_{C4} \times \Delta^{14}C_{C4}) + (f_{loess} \times \Delta^{14}C_{loess})$

(4.6) $\delta^{13}C_{bulk} = (f_{C3} \times \delta^{13}C_{C3}) + (f_{C4} \times \delta^{13}C_{C4}) + (f_{loess} \times \delta^{13}C_{loess})$

(4.7) $1 = f_{C3} + f_{C4} + f_{loess}$

where f_{C3}, f_{C4} and f_{loess} are the fractional abundance of C3, C4 and loess, respectively. For $\Delta^{14}C_{C3}$ and $\Delta^{14}C_{C4}$ ($\Delta^{14}C$ of C3 and C4 vegetation derived OC, respectively), a value of -30‰ is assumed to represent a mixture of modern plant detritus and soil OC. In general, soil $\Delta^{14}C$ values can span a wide range from modern to pre-aged and generally decrease with depth (Marschner et al., 2008; Trumbore, 2009; Marwick et al., 2015; van der Voort et al., 2017). However, for this mass balance, it is assumed that surface soil and the upper part of the mineral soil is preferentially eroded. Together with recent plant material, this results in a near-modern $\Delta^{14}C$ value for this end member. Loess found in the Danube basin was deposited in the Pleistocene (Fitzsimmons et al., 2012). Hatte et al. (2013) describe a loess-paleosol sequence in Northern Serbia, reporting ^{14}C ages of 6,400 to >53,000 yr that underlays the modern soil. Beyond the ^{14}C dating limitations, the section was further dated to 120,700 yr in 19.4 m depth with infrared simulated luminescence dating. In regions where the thickest loess cover exists (northern Serbia and southeastern Romania), lower to mid Pleistocene loess is reported below the modern flood plain (Fitzsimmons et al., 2012). Such loess deposits, characterized by ^{14}C ages that range from ~6,000 yr to radiocarbon-dead thus represent a 'semi-petrogenic' end-member. Here, an average $\Delta^{14}C$ of -800‰ is assumed for the mass balance calculation, representing about the top 5 m, depending on the location (Supplementary Figure A.4.3). A sensitivity analysis on the $\Delta^{14}C$ value of loess shows that ±100‰ would result in a *relative* change of about ±10% in the resulting loess contribution. Reported $\delta^{13}C$ values of loess in Serbia range from -22.5 – -25‰ (Hatte et al., 2013; Zech et al., 2013). Based on these reported data, a $\delta^{13}C$ value of -23.5‰ is assigned to the loess end member. $\delta^{13}C$ values for C3 and C4 end members are -27.7‰ and -14‰, respectively, as described above.

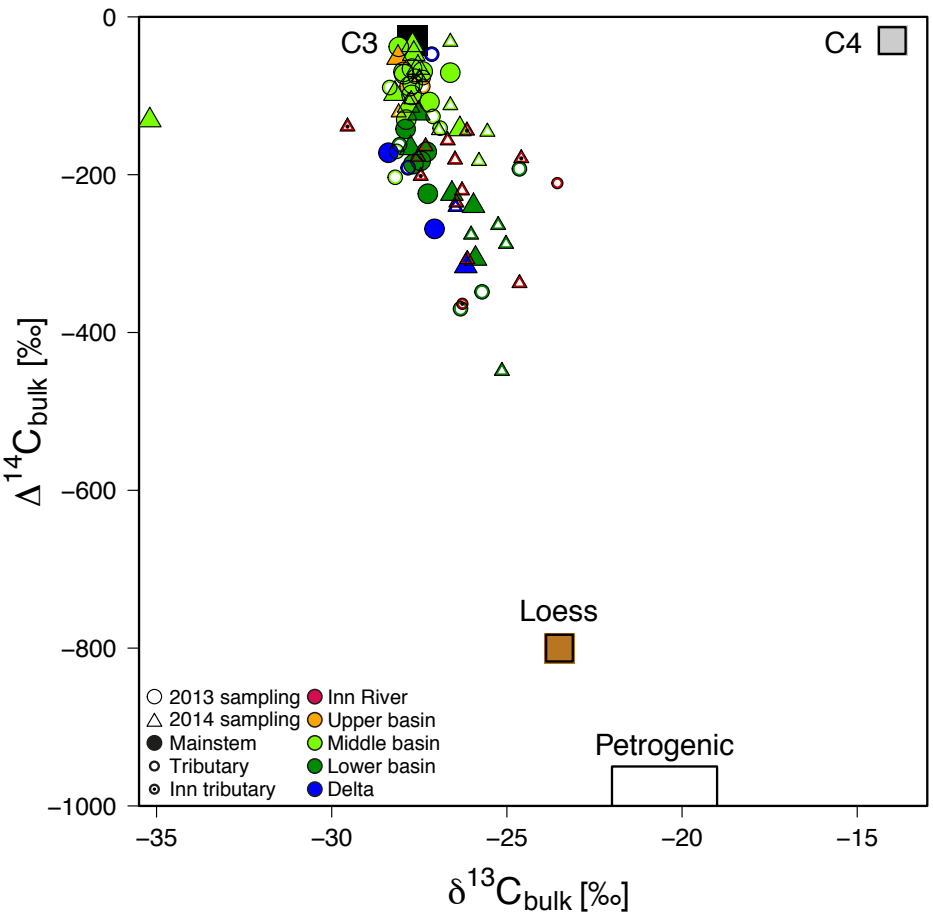

Figure 4.12. $\Delta^{14}C$ vs. $\delta^{13}C$ of Danube and tributary locations. The boxes show $\Delta^{14}C$ and $\delta^{13}C$ values of OC sources to the river sediment (white: petrogenic OC, brown: loess derived OC, light gray: C4 plant derived biospheric OC, black: C3 plant derived biospheric OC). Symbol color and shape of the samples correspond to the ones in Figure 4.1 & 4.2.

Measured $\Delta^{14}C$ and $\delta^{13}C$ values generally fall in the range defined by the end members (Figure 4.12). Values outside of the definition range could possibly be influenced by aquatic OC production leading to more depleted $\delta^{13}C$ values, or artificially fall outside of the definition range by assuming average $\Delta^{14}C$ and $\delta^{13}C$ values for the end members rather than ranges. This problem will be addressed with a Monte Carlo based mixing model approach in the future (e.g. Tesi et al., 2016a). The low $\delta^{13}C$ value of -29.6‰ measured in a tributary to the Inn River (the Alz River) can be explained by high contribution of aquatic *in situ* OC production (52%; Kündig, 2014) as this river forms the outlet of an alpine lake. The highly ^{13}C-depleted sample at one Danube mainstem location in the middle basin from the second sampling campaign (Danube downstream Velika Morava 2014; $\delta^{13}C$ -35.2‰) is suspected to be an outlier since the $\delta^{13}C$ value from the first sampling campaign is -27.7‰ and Danube mainstem locations upstream and downstream of this location show $\delta^{13}C$ values of -26.3 – -29.3‰ with no indication of a plausible OC source that could result in such a depleted signal. This value is therefore excluded from the mass balance calculation.

Due to the fact that significant C4 vegetation cover is only present in the middle and lower basin (Still et al., 2003), the model with the three defined end members (C3, C4, loess) is only applicable in the middle and lower basin. The upper basin with its alpine tributaries is best described by binary mixing of a C3 plant-derived biospheric OC source (fresh plant material plus soil OC) and a petrogenic OC source of eroded sedimentary rock. Loess is also present, in the non-Alpine region of the upper Danube basin (Haase et al., 2007). However, it is not considered in the source calculations here because the bio, semi-petro (i.e. loess) and petro end member plot on a line in the $\delta^{13}C$ vs. $\Delta^{14}C$ plot (Figure 4.12), therefore not allowing a meaningful calculation of these three fractions. Because the Inn River increases the suspended sediment load of the Danube by about a factor of 6 at their confluence (ICPDR, 2008), it is assumed that the Alpine petrogenic end member is dominant over the semi-petro end member in this part of the Danube catchment. For the Inn River and Danube locations in the upper basin, a binary mixing model considering C3-derived biospheric and petrogenic carbon was therefore applied using $\Delta^{14}C$ of -30‰ for biospheric (as described above) and $\Delta^{14}C$ of -1,000‰ for radiocarbon-dead petrogenic OC.

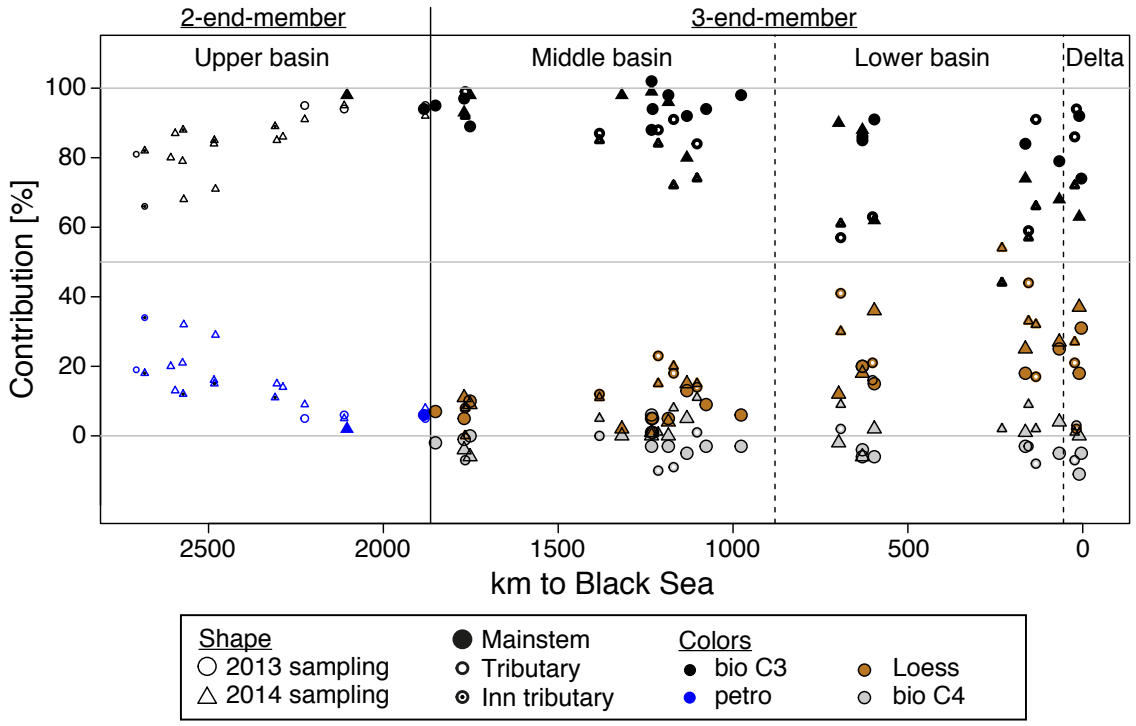

Figure 4.13. Contribution of OC sources to the river sediment. The contributions of a petrogenic (blue), loess (brown), C3 (black) and C4 (light gray) vegetation-derived OC sources along the Danube. The upper and middle basins are separated with a solid line because two different models (two and three end members, respectively) were applied. Middle and lower basins and the delta are separated with dashed lines. Symbol shapes correspond to the ones in Figure 4.2.

Biospheric OC (f_{bio}), including fresh plant debris and soil OC, is the main source of OC to Inn and Danube River and tributary sediments (Figure 4.13) as also found for other river systems (e.g. Gordon and Goni, 2003). The Inn River in the upper Danube basin shows f_{bio} values from 66–88% in the upper reaches, reflecting the heterogeneity of slopes and vegetation cover in the alpine region. In the lower reaches of the Inn River, f_{bio} increases to 93% (average of the sampling campaigns 2013 and 2014) close to the confluence with the Danube, following the increasing vegetation cover. The contribution of petrogenic OC to the river sediment (f_{petro}) mirrors the f_{bio} trend in this binary mixing model and decreases from 12–34% in the upper reaches to about 7% at its terminus (Figure 4.13).

From the middle basin on, the mixing model is adjusted to the increasing loess cover and upcoming C4 vegetation (Figure 4.13). Instead of the petrogenic end member, a semi-petrogenic end member is included and the biospheric OC source is split into a C3 and C4 vegetation derived end member. The C3-derived biospheric fraction (f_{C3}) stays at about 94% in the upper part of the middle basin. C4 contribution (f_{C4}) shows negative values and is supposed to be 0%, leaving about 6% of sedimentary OC to originate from a semi-petro loess source (f_{loess}). Although accompanied with significant scatter, the f_{C3} decreases further downstream to 63–92% with f_{loess} mirroring the trend increasing towards the delta to 18–37%. f_{C4} is ≤0 in the upper basin and at the majority of Danube mainstem locations in the middle and lower basins and the delta, reflecting a very small contribution of C4 vegetation to the river sediment, compared to the binary mixing that does not include loess (section 4.5.3.1). However, negative f_{C4} derive from non-ideal definition of end members and missing end members. A modern and ^{13}C depleted OC source like microbial production and a radiocarbon dead petrogenic source, that both can not be included in this model, can cause the negative f_{C4} values that compensate for the missing end members.

To test the influence of the Alpine petrogenic OC that is exported from the upper basin to the lower reaches, $\Delta^{14}C$ values of mainstem locations in the middle and lower basin were roughly corrected for the amount of Alpine radiocarbon dead OC. Therefore, the f_{petro} calculated with the binary mixing model that is exported from the upper basin (Figure 4.13) was converted to an approximate amount of Alpine OC_{petro} (in tons per year) using sediment flux data that was extracted from a figure by Habersack et al. (2013) (Supplementary Figure A.4.4) and an estimated TOC of 1%. With that, the $\Delta^{14}C$ values of the middle and lower basins were corrected as

$$\Delta^{14}C_{corr} = \Delta^{14}C \times Q / (Q - Q_{Alpine\ OCpetro}) \quad (4.8)$$

where $\Delta^{14}C$ is the measured value at the location, Q is the sediment flux in t/yr and $Q_{Alpine\ OCpetro}$ is the calculated Alpine petrogenic OC exported from the upper basin. The ternary mixing model (Equations 4.5–4.7) was re-calculated with the $\Delta^{14}C_{corr}$ values and the resulting f_{C3}, f_{C4} and f_{loess} were compared with the values of the not Alpine OC_{petro}

corrected values shown in Figure 4.13. This sensitivity analysis shows that incorporating the Alpine OC_{petro} changes the f_{loess} in the per mill scale and therefore, excluding the petrogenic OC source does not change the source contributions.

4.6 Summary and Conclusions

Loess vs. Loss seem to be two important parameters to constrain to understand the evolution of OC and the signal that is exported to the Black Sea. In a provenance study of suspended sediment in the Yellow River, loess and soil were combined in one pre-aged sediment source, resulting in a contribution of 55% pre-aged and 10–30% radiocarbon dead OC (Tao et al., 2015). The different end member definition of these two studies highlights the difficulty of a semi-petro OC source with ages that range from about 6,000 yr to radiocarbon dead. Whereas in the example of the Yellow River, deeper parts of the loess (>26,000 yr) are considered as fossil OC, therefore underestimating the loess content in the river sediment, the fossil OC source was not considered in the Danube study, leading to an undefined, but probably insignificant, overestimation of the loess content.

Even though loess contribution and the transport time through the river basin were quantified for the Danube, unknowns remain. The ternary mixing model, including C3 and C4 vegetation derived biospheric OC and a semi-petro OC source, results in source contributions to the sediment not taking a temporal aspect into account. Not including the transport time leads to an overestimation of the oldest source, the loess. However, this overestimation is probably not much because the loess is significantly older than the time range of the transport. Therefore, small amounts of 'extra' loess would correct for the missing aging. The transport time and loss calculations after Bröder (2016) on the other hand that is based on ^{14}C measurements along the Danube mainstem include tributary sediment and loess addition. The dilution with old carbon on the way leads to an overestimation of the transport time and degradative loss during transport.

Furthermore, assuming a transport time of about 2,100 years, the studied time window spans a time of high anthropogenic alteration of the river system, including deforestation and construction of numerous dams and river regulations that significantly altered the sediment transport along the Danube (Giosan et al., 2012; McCarney-Castle et al., 2012).

Considering (i) the local character of the stable isotopic composition of the river sediment, (ii) loss due to decomposition and estimated transport time through the basin, and (iii) loess contribution of about 18–37% at the terminus of the river – although most likely accompanied by large errors–, we conclude that significant addition of poorly loaded high SA loess in the middle and lower basins dominate the OC signal that finally reaches the delta. For a more accurate quantification of source contributions, the end members (i.e. loess and soils) would have to be better

constrained. Nevertheless, the data shows that the observed decrease in loading is not entirely explained by addition of tributary sediment only, implying that degradative loss and transport time on the continent are processes that significantly shape the OC signal exported to the Black Sea. Therefore, aging and degradation also have to be considered for the interpretation of down core sedimentary archives. The OC discharged to the ocean seems to represent a lower basin signal and most of the signal from the upper reaches is lost or overprinted, therefore reducing the basin area for reconstructions to the lower reaches. Provenance studies of OC deposited in ocean margin sediments are therefore key for paleo-environmental reconstructions.

Acknowledgements

This project was funded by the Swiss National Science Foundation ("CAPS-LOCK" and "CAPS-LOCK2"; #200021_140850). We want to thank the two fieldwork crews on both sampling campaigns (Marilu Tavagna, Alissa Zuijdgeest, James Saenz, Stefan Eugen Filip, Silvia Lavinia Filip, Mihai, Thomas Blattmann, Clayton Magill, Michael Albani). Further thanks goes to Daniel Montluçon for lab support and advice, Lorena Fischer for the ArcGIS based Danube basin map, Hannah Gies for the help on the prepGC and Thomas Blattman and Valier Galy (WHOI) for fruitful discussions. Radiocarbon measurements were done in the laboratory of Ion Beam Physics at ETH Zürich.

References

Alin, S.R., Aalto, R., Goni, M.A., Richey, J.E. and Dietrich, W.E. (2008) Biogeochemical characterization of carbon sources in the strickland and fly rivers, Papua New Guinea. *Journal of Geophysical Research* 113.

Baldock, J.A. and Skjemstad, J.O. (2000) Role of the soil matrix and minerals in protecting natural organic materials against biological attack. *Organic Geochemistry* 31, 697–710.

Belz, J.U. and Goda, L. (2004) Das Abflussregime der Donau und ihres Einzugsgebietes: Aktualisierung des Kapitels II der Donaumonographie. Deutsches Nationalkomitee für das International Hydrological Programme (IHP) der UNESCO, Koblenz.

Blair, N.E. and Aller, R.C. (2012) The fate of terrestrial organic carbon in the marine environment. *Annual Review of Marine Science* 4, 401–423.

Blair, N.E., Leithold, E.L., Ford, S.T., Peeler, K.A., Holmes, J.C. and Perkey, D.W. (2003) The persistence of memory: The fate of ancient sedimentary organic carbon in a modern sedimentary system. *Geochimica et Cosmochimica Acta* 67, 63–73.

Blöschl, G., Nester, T., Komma, J., Parajka, J. and Perdigao, R.A.P. (2013) The June 2013 flood in the Upper Danube Basin, and comparisons with the 2002, 1954 and 1899 floods. *Hydrology and Earth System Sciences* 17, 5197–5212.

Bröder, L. (2016) Transport, degradation and burial of organic matter released from permafrost to the East Sierian Arctic Shelf, Applied Environmental Science. PhD thesis, Stockholm University, Stockholm, Sweden.

Bröder, L., Tesi, T., Andersson, A., Eglinton, T.I., Semiletov, I.P., Dudarev, O.V., Roos, P. and Gustafsson, Ö. (2016a) Historical records of organic matter supply and degradation status in the East Siberian Sea. *Organic Geochemistry* 91, 16–30.

Bröder, L., Tesi, T., Salvado, J.A., Semiletov, I.P., Dudarev, O.V. and Gustafsson, Ö. (2016b) Fate of terrigenous organic matter across the Laptev Sea from the mouth of the Lena River to the deep sea of the Arctic interior. *Biogeosciences* 13, 5003–5019.

Burdige, D.J. (2005) Burial of terrestrial organic matter in marine sediments: A re-assessment. *Global Biogeochemical Cycles* 19.

Cathalot, C., Rabouille, C., Pastor, L., Deflandre, B., Viollier, E., Buscail, R., Gremare, A., Treignier, C. and Pruski, A. (2010) Temporal variability of carbon recycling in coastal sediments influenced by rivers: Assessing the impact of flood inputs in the Rhone River prodelta. *Biogeosciences* 7, 1187–1205.

Cathalot, C., Rabouille, C., Tisnerat-Laborde, N., Toussaint, F., Kerherve, P., Buscail, R., Loftis, K., Sun, M.Y., Tronczynski, J., Azoury, S., Lansard, B., Treignier, C., Pastor, L. and Tesi, T. (2013) The fate of river organic carbon in coastal areas: A study in the Rhone River delta using multiple isotopic (delta C-13, Delta C-14) and organic tracers. *Geochimica et Cosmochimica Acta* 118, 33–55.

Christl, M., Vockenhuber, C., Kubik, P.W., Wacker, L., Lachner, J., Alfimov, V. and Synal, H.A. (2013) The ETH Zurich AMS facilities: Performance parameters and reference materials. *Nuclear Instruments and Methods in Physics Research B* 294, 29–38.

Contreras, S., Werne, J.P., Brown, E.T., Anderson, R.S. and Fawcett, P.J. (2016) A molecular isotope record of climate variability and vegetation response in southwestern North America during mid-Pleistocene glacial/interglacial cycles. *Palaeogeography, Palaeoclimatology, Palaeoecology* 459, 338–347.

Demeny, A. and Kreulen, R. (1993) Carbon isotope ratios of graphites in the Bündnerschiefer series of the Tauern window and the Köszeg-Rechnitz windows (Austria and western Hungary): Origin of organic matter and sedimentary facies crrelation. *Geologica Carpathica* 44, 3–9.

Doetterl, S., Berhe, A.A., Nadeu, E., Wang, Z.G., Sommer, M. and Fiener, P. (2016) Erosion, deposition and soil carbon: A review of process-level controls, experimental tools and models to address C cycling in dynamic landscapes. *Earth-Science Reviews* 154, 102–122.

Doetterl, S., Stevens, A., Six, J., Merckx, R., van Oost, K., Pinto, M.C., Casanova-Katny, A., Munoz, C., Boudin, M., Venegas, E.Z. and Boeckx, P. (2015) Soil carbon storage controlled by interactions between geochemistry and climate. *Nature Geoscience* 8, 780–783.

Drenzek, N.J., Hughen, K.A., Montlucon, D.B., Southon, J.R., dos Santos, G.M., Druffel, E.R.M., Giosan, L. and Eglinton, T.I. (2009) A new look at old carbon in active margin sediments. *Geology* 37, 239–242.

Eglinton, G. and Hamilton, R.J. (1967) Leaf Epicuticular Waxes. *Science* 156, 1322–1335.

Eglinton, T.I. (2008) Carbon cycle tempestuous transport. *Nature Geoscience* 1, 727–728.

Eglinton, T.I., Aluwihare, L.I., Bauer, J.E., Druffel, E.R.M. and McNichol, A.P. (1996) Gas chromatographic isolation of individual compounds from complex matrices for radiocarbon dating. *Analytical Chemistry* 68, 904–912.

Eglinton, T.I. and Eglinton, G. (2008) Molecular proxies for paleoclimatology. *Earth and Planetary Science Letters* 275, 1–16.

Feakins, S.J., Bentley, L.P., Salinas, N., Shenkin, A., Blonder, B., Goldsmith, G.R., Ponton, C., Arvin, L.J., Wu, M.S., Peters, T., West, A.J., Martin, R.E., Enquist, B.J., Asner, G.P. and Malhi, Y. (2016) Plant leaf wax biomarkers capture gradients in hydrogen isotopes of precipitation from the Andes and Amazon. *Geochimica et Cosmochimica Acta* 182, 155–172.

Fitzsimmons, K.E., Markovic, S.B. and Hambach, U. (2012) Pleistocene environmental dynamics recorded in the loess of the middle and lower Danube basin. *Quaternary Science Reviews* 41, 104–118.

Freymond, C.V., Kündig, N., Stark, C., Peterse, F., Buggle, B., Lupker, M., Plötze, M., Filip, F., Giosan, L. and Eglinton, T. (2018) Evolution of biomolecular loadings along a major river system. *Geochimica et Cosmochimica Acta* 223, 389–404.

Freymond, C.V., Peterse, F., Fischer, L.V., Filip, F., Giosan, L. and Eglinton, T.I. (2017) Branched GDGT signals in fluvial sediments of the Danube River basin: Method comparison and longitudinal evolution. *Organic Geochemistry* 103, 88–96.

Galy, V., Eglinton, T., France-Lanord, C. and Sylya, S. (2011) The provenance of vegetation and environmental signatures encoded in vascular plant biomarkers carried by the Ganges-Brahmaputra rivers. *Earth and Planetary Science Letters* 304, 1–12.

Galy, V., France-Lanord, C., Beyssac, O., Faure, P., Kudrass, H. and Palhol, F. (2007) Efficient organic carbon burial in the Bengal fan sustained by the Himalayan erosional system. *Nature* 450, 407–410.

Galy, V., France-Lanord, C. and Lartiges, B. (2008) Loading and fate of particulate organic carbon from the Himalaya to the Ganga-Brahmaputra delta. *Geochimica et Cosmochimica Acta* 72, 1767–1787.

Giosan, L., Coolen, M.J.L., Kaplan, J.O., Constantinescu, S., Filip, F., Filipova-Marinova, M., Kettner, A.J. and Thom, N. (2012) Early anthropogenic transformation of the Danube-Black Sea system. *Scientific Reports* 2, 1–6.

Goni, M.A., Monacci, N., Gisewhite, R., Crockett, J., Nittrouer, C., Ogston, A., Alin, S.R. and Aalto, R. (2008) Terrigenous organic matter in sediments from the Fly River delta-clinoform system (Papua New Guinea). *Journal of Geophysical Research* 113.

Goni, M.A., Yunker, M.B., Macdonald, R.W. and Eglinton, T.I. (2005) The supply and preservation of ancient and modem components of organic carbon in the Canadian Beaufort Shelf of the Arctic Ocean. *Marine Chemisry* 93, 53–73.

Gordon, E.S. and Goni, M.A. (2003) Sources and distribution of terrigenous organic matter delivered by the Atchafalaya River to sediments in the northern Gulf of Mexico. *Geochimica et Cosmochimica Acta* 67, 2359–2375.

Grams, C.M., Binder, H., Pfahl, S., Piaget, N. and Wernli, H. (2014) Atmospheric processes triggering the central European floods in June 2013. *Natural Hazards and Earth System Sciences* 14, 1691–1702.

Haase, D., Fink, J., Haase, G., Ruske, R., Pecsi, M., Richter, H., Altermann, M. and Jager, K.D. (2007) Loess in Europe - its spatial distribution based on a European Loess Map, scale 1:2,500,000. *Quaternary Science Reviews* 26, 1301–1312.

Habersack, H., Jäger, E. and Hauer, C. (2013) The status of the Danube River sediment regime and morphology as a basis for future basin management. *International Journal of River Basin Management* 11, 153–166.

Hatte, C., Gauthier, C., Rousseau, D.D., Antoine, P., Fuchs, M., Lagroix, F., Markovic, S.B., Moine, O. and Sima, A. (2013) Excursions to C-4 vegetation recorded in the Upper Pleistocene loess of Surduk (Northern Serbia): An organic isotope geochemistry study. *Climate of the Past* 9, 1001–1014.

Hedges, J.I. and Keil, R.G. (1995) Sedimentary organic-matter preservation - an assessment and speculative synthesis. *Marine Chemistry* 49, 81–115.

Hedges, J.I., Keil, R.G. and Benner, R. (1997) What happens to terrestrial organic matter in the ocean? *Organic Geochemistry* 27, 195–212.

Hedges, J.I. and Stern, J.H. (1984) Carbon and nitrogen determinations of carbonate-containing solids. *Limnology and Oceanography* 29, 657–663.

Hilton, R.G., Galy, A., Hovius, N., Horng, M.J. and Chen, H.E. (2010) The isotopic composition of particulate organic carbon in mountain rivers of Taiwan. *Geochimica et Cosmochimica Acta* 74, 3164–3181.

ICPDR (2005) The Danube River Basin District. Part A – Basin-wide overview, in: Schmedtje, U. (Ed.). International Commission for the Protection of the Danube River, ICPDR.

ICPDR (2008) Joint Danube Survey 2 - Final Scientific Report ICPDR - International Commission for the Protection of the Danube River, Vienna, Austria.

ICPDR (2014) Floods in June 2013 in the Danube River Basin – Brief overview of key events and lessons learned.

ICPDR&ISRBC (2015) Floods in May 2014 in the Sava River Basin - Brief overview of key events and lessons learned.

Jipa, D.C. (2014) The conceptual sedimentary model of the Lower Danube loess basin: Sedimentogenetic implications. *Quaternary International* 351, 14–24.

Karlsson, E.S., Charkin, A., Dudarev, O., Semiletov, I., Vonk, J.E., Sanchez-Garcia, L., Andersson, A. and Gustafsson, Ö. (2011) Carbon isotopes and lipid biomarker investigation of sources, transport and degradation of terrestrial organic matter in the Buor-Khaya Bay, SE Laptev Sea. *Biogeosciences* 8, 1865–1879.

Keil, R.G. and Mayer, L.M. (2014) Mineral matrices and organic matter, in: Turekian, K.K. (Ed.), Treatise on Geochemistry (Second Edition). Elsevier, Oxford, pp. 337–359.

Keil, R.G., Mayer, L.M., Quay, P.D., Richey, J.E. and Hedges, J.I. (1997) Loss of organic matter from riverine particles in deltas. *Geochimica et Cosmochimica Acta* 61, 1507–1511.

Kleber, M., Eusterhues, K., Keiluweit, M., Mikutta, C., Mikutta, R. and Nico, P.S. (2015) Chapter one - mineral–organic associations: Formation, properties, and relevance in soil environments, in: Donald, L.S. (Ed.), Advances in Agronomy. Academic Press, pp. 1–140.

Komada, T., Anderson, M.R. and Dorfmeier, C.L. (2008) Carbonate removal from coastal sediments for the determination of organic carbon and its isotopic signatures, delta C-13 and Delta C-14: Comparison of fumigation and direct acidification by hydrochloric acid. *Limnology and Oceanography: Methods* 6, 254–262.

Körner, C., Farquhar, G.D. and Roksandic, Z. (1988) A global survey of carbon isotope discrimination in plants from high altitude. *Oecologia* 74, 623–632.

Kündig, N. (2014) Composition and provenance of terrestrial biomarkers within the Inn River drainage basin. Master thesis, ETH Zürich, Zürich, Switzerland.

Kusch, S., Rethemeyer, J., Schefuss, E. and Mollenhauer, G. (2010) Controls on the age of vascular plant biomarkers in Black Sea sediments. *Geochimica et Cosmochimica Acta* 74, 7031–7047.

Lewan, M.D. (1986) Stable carbon isotopes of amorphous kerogens from phanerozoic sedimentary-rocks. *Geochimica et Cosmochimica Acta* 50, 1583–1591.

Li, R.C., Fan, J., Xue, J.T. and Meyers, P.A. (2017) Effects of early diagenesis on molecular distributions and carbon isotopic compositions of leaf wax long chain biomarker n-alkanes: Comparison of two one-year-long burial experiments. *Organic Geochemistry* 104, 8–18.

Marschner, B., Brodowski, S., Dreves, A., Gleixner, G., Gude, A., Grootes, P.M., Hamer, U., Heim, A., Jandl, G., Ji, R., Kaiser, K., Kalbitz, K., Kramer, C., Leinweber, P., Rethemeyer, J., Schaeffer, A., Schmidt, M.W.I., Schwark, L. and Wiesenberg, G.L.B. (2008) How relevant is recalcitrance for the stabilization of organic matter in soils? *Journal of Plant Nutrition and Soil Science* 171, 91–110.

Martinelli, L.A., Ballester, M.V., Krusche, A.V., Victoria, R.L., de Camargo, P.B., Bernardes, M. and Ometto, J.P.H.B. (1999) Landcover changes and delta C-13 composition of riverine particulate organic matter in the Piracicaba River Basin (southeast region of Brazil). *Limnology and Oceanography* 44, 1826–1833.

Marwick, T.R., Tamooh, F., Teodoru, C.R., Borges, A.V., Darchambeau, F. and Bouillon, S. (2015) The age of river-transported carbon: A global perspective. *Global Biogeochemical Cycles* 29, 122–137.

McCarney-Castle, K., Voulgaris, G., Kettner, A.J. and Giosan, L. (2012) Simulating fluvial fluxes in the Danube watershed: The 'Little Ice Age' versus modern day. *Holocene* 22, 91–105.

McIntyre, C.P., Wacker, L., Haghipour, N., Blattmann, T.M., Fahrni, S., Usman, M., Eglinton, T.I. and Synal, H.-A. (2016) Online 13C and 14C Gas Measurements by EA-IRMS–AMS at ETH Zürich. *Radiocarbon*, 1–11.

Nemec, M., Wacker, L. and Gaggeler, H. (2010) Optimization of the graphitization process at AGE-1. *Radiocarbon* 52, 1380–1393.

Oleary, M.H. (1988) Carbon Isotopes in Photosynthesis. *Bioscience* 38, 328–336.

Schiller, H., Miklós, D. and Sass, J. (2010) The Danube River and its basin physical characteristics, water regime and water balance, in: Mitja, B. (Ed.), Hydrological Processes of the Danube River Basin. Perspectives from the Danubian Countries. Springer, Dordrecht, Netherlands, pp. 25–77.

Schmidt, M.W.I., Torn, M.S., Abiven, S., Dittmar, T., Guggenberger, G., Janssens, I.A., Kleber, M., Kögel-Knabner, I., Lehmann, J., Manning, D.A.C., Nannipieri, P., Rasse, D.P., Weiner, S. and Trumbore, S.E. (2011) Persistence of soil organic matter as an ecosystem property. *Nature* 478, 49–56.

Schreuder, L.T., Beets, C.J., Prins, M.A., Hatte, C. and Peterse, F. (2016) Late Pleistocene climate evolution in Southeastern Europe recorded by soil bacterial membrane lipids in Serbian loess. *Palaeogeography, Palaeoclimatology, Palaeoecology* 449, 141–148.

Smith, J.C., Galy, A., Hovius, N., Tye, A.M., Turowski, J.M. and Schleppi, P. (2013) Runoff-driven export of particulate organic carbon from soil in temperate forested uplands. *Earth and Planetary Science Letters* 365, 198–208.

Sternström, K.E., Skog, G., Georgiadou, E., Genberg, J. and Johansson, A. (2011) A guide to radiocarbon units and calculations. Lund University.

Still, C.J., Berry, J.A., Collatz, G.J. and DeFries, R.S. (2003) Global distribution of C-3 and C-4 vegetation: Carbon cycle implications. *Global Biogeochemical Cycles* 17.

Synal, H.A., Stocker, M. and Suter, M. (2007) MICADAS: A new compact radiocarbon AMS system. *Nuclear Instruments and Methods in Physics Research B* 259, 7–13.

Tao, S.Q., Eglinton, T.I., Montluçon, D.B., McIntyre, C. and Zhao, M.X. (2015) Pre-aged soil organic carbon as a major component of the Yellow River suspended load: Regional significance and global relevance. *Earth and Planetary Science Letters* 414, 77–86.

Tesi, T., Muschitiello, F., Smittenberg, R.H., Jakobsson, M., Vonk, J.E., Hill, P., Andersson, A., Kirchner, N., Noormets, R., Dudarev, O., Semiletov, I. and Gustafsson, O. (2016a) Massive remobilization of permafrost carbon during post-glacial warming. *Nature Communications* 7.

Tesi, T., Semiletov, I., Dudarev, O., Andersson, A. and Gustafsson, Ö. (2016b) Matrix association effects on hydrodynamic sorting and degradation of terrestrial organic matter during cross-shelf transport in the Laptev and East Siberian shelf seas. *Journal of Geophysical Research Biogeosciences* 121, 731–752.

Toussaint, F., Tisnerat-Laborde, N., Cathalot, C., Buscail, R., Kerherve, P. and Rabouille, C. (2013) Depositional processes of organic matter in the Rhone River Delta (Gulf of Lions, France) traced by density fractionation coupled with delta C-14 and delta C-13. *Radiocarbon* 55, 920–931.

Trumbore, S. (2009) Radiocarbon and soil carbon dynamics. *Annual Review of Earth and Planetary Sciences* 37, 47–66.

van der Voort, T.S., Zell, C.I., Hagedorn, F., Feng, X., McIntyre, C.P., Haghipour, N., Graf Pannatier, E. and Eglinton, T.I. (2017) Diverse soil carbon dynamics expressed at the molecular level. *Geophysical Research Letters* 44, 840–850.

Vidmar, A., Globevnik, L., Koprivsek, M., Secnik, M., Zabret, K., Durovic, B., Anzeljc, D., Kastelic, J., Kobold, M., Susnik, M., Borojevic, D., Kupusovic, T., Kupusovic, E., Vihar, A. and Brilly, M. (2016) The Bosna River floods in May 2014. *Natural Hazards and Earth System Sciences* 16, 2235–2246.

Von Lützow, M., Kögel-Knabner, I., Ekschmitt, K., Matzner, E., Guggenberger, G., Marschner, B. and Flessa, H. (2006) Stabilization of organic matter in temperate soils: Mechanisms and their relevance under different soil conditions - a review. *European Journal of Soil Science* 57, 426–445.

Wacker, L., Nemec, M. and Bourquin, J. (2010) A revolutionary graphitisation system: Fully automated, compact and simple. *Nuclear Instruments and Methods in Physics Research B* 268, 931–934.

Wang, X.X., Huang, X.Y., Sachse, D., Hu, Y., Xue, J.T. and Meyers, P.A. (2016) Comparisons of lipid molecular and carbon isotopic compositions in two particle-size fractions from surface peat and their implications for lipid preservation. *Environmental Earth Sciences* 75.

Zech, R., Gao, L., Tarozo, R. and Huang, Y. (2012) Branched glycerol dialkyl glycerol tetraethers in Pleistocene loess-paleosol sequences: Three case studies. *Organic Geochemistry* 53, 38–44.

Zech, R., Zech, M., Markovic, S., Hambach, U. and Huang, Y. (2013) Humid glacials, arid interglacials? Critical thoughts on pedogenesis and paleoclimate based on multi-proxy analyses of the loess-paleosol sequence Crvenka, Northern Serbia. *Palaeogeography, Palaeoclimatology, Palaeoecology* 387, 165–175.

Appendix A.4 Supplementary information

A.4.1 Precipitation in the upper Danube basin causing the flood in 2013

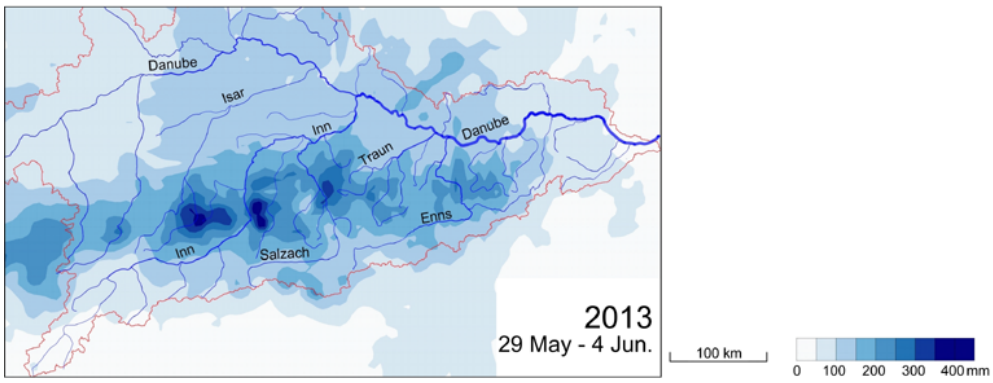

Figure A.4.1. Precipitation map of the rain event in the upper Danube and Inn basin that caused the 100-year flood in 2013. Figure from Blöschl et al. (2013).

A.4.2 River water isotopic composition

Water isotope measurement

$\delta^{2}H$ and $\delta^{18}O$ values of filtered river water was measured on a Picarro cavity ring down spectrometer L2120-i. Each sample was measured 7 times, of which the last 4 measurements were used to calculate the average isotope values. Calibration was done using 3 in-house standards that are calibrated against the VSMOV scale. Results are shown in ‰ units.

Danube water isotopic composition

Danube water isotope values mainly represents the isotopic composition of precipitation and change due to evaporation is minor (Rank et al., 2009). In general, the elevation effect leads to depletion of precipitation with increasing elevation and the continental effect leads to more depleted values with increasing distance to the Atlantic Ocean (Rank et al., 2009). Additionally to moisture from the Atlantic, moisture from the Mediterranean Sea leads to more enriched precipitation (Blöschl et al., 2013).

River water $\delta^{2}H$ along the Inn and Danube from the two sampling campaigns in 2013 and 2014 mirror the elevation of the sampling location and show the altitude effect of more depleted values in higher elevations (Figure A.4.2). The Sio channel, joining the Danube at km 1,496, is the outflow of the shallow Lake Balaton and shows a very enriched value due to evaporation.

Comparing the two sampling years

The heavy rain event that caused the flood in 2013 is reflected in the δ^2H values in the upper basin. In 2014, upper basin δ^2H are comparable to values from Rank et al. (2009) and represent 'normal' low water conditions. In 2013, the Inn River is 10‰ and the Danube River 5‰ more depleted. A simple mixing calculation of the Danube upstream of the confluence with the Inn and the Inn itself using δ^2H values shows that during normal conditions as in 2014, the Inn contributed 45% to the total Danube signal (downstream of the Inn), where as in 2013, the contribution of the Inn was 35%.

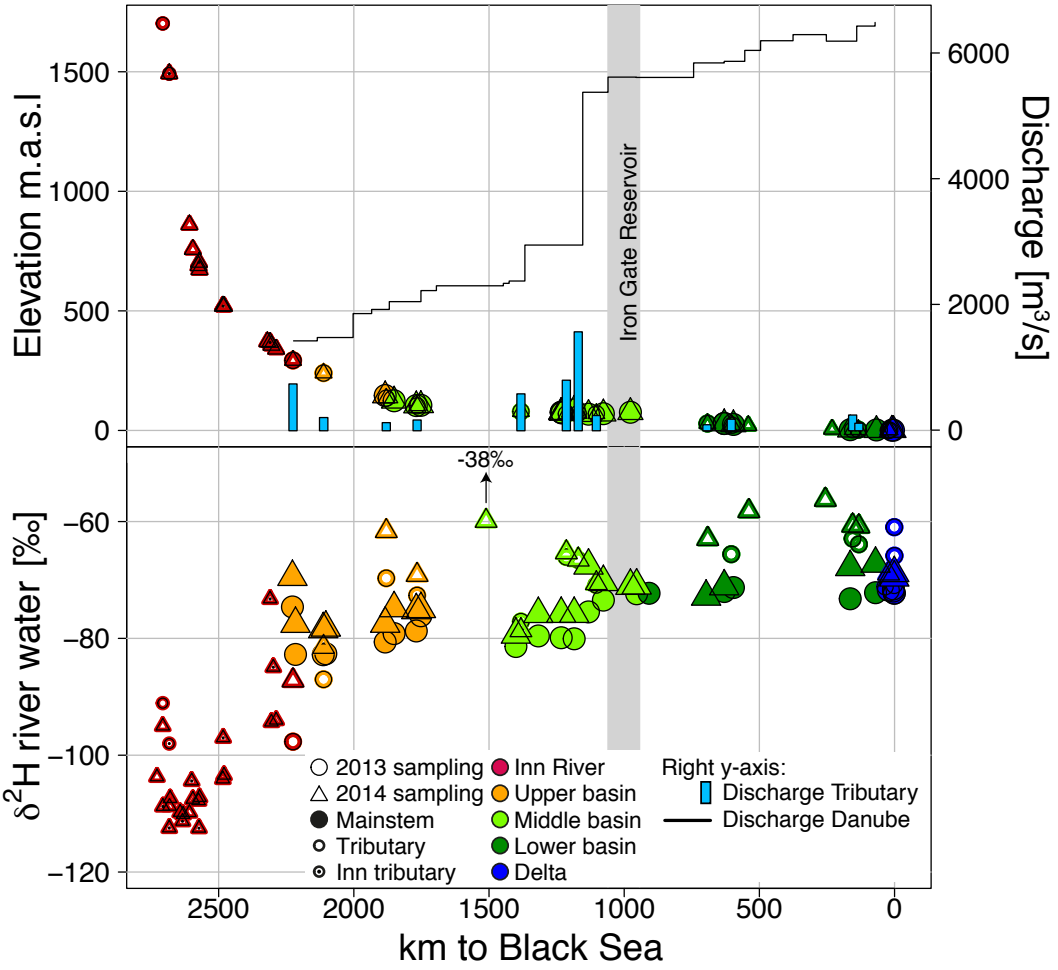

Figure A.4.2. Upper panel: Elevation (m a.s.l) of sampling locations along the Danube and the tributaries in the usual symbols and colors referring to sampling year and sub-basins (left y-axis). On the right y-axis, the average discharge along the Danube mainstem is shown with the solid line. Additionally, average tributary discharge values are shown with bars in light blue at the corresponding location where they join the Danube.

Lower panel: River water δ^2H from the 2013 and 2014 sampling campaign.

A.4.3 Stratigraphy and age model of the Surduk loess sequence, Serbia

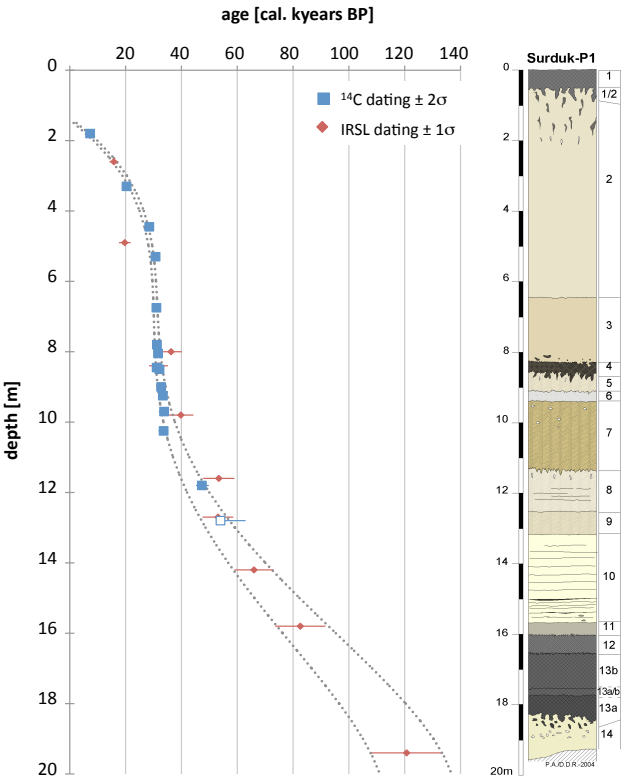

Figure A.4.3. Radiocarbon daing of loess in Serbia showing the age increase with depth. Figure from Hatte et al. (2013).

A.4.4 Suspended sediment load in the Danube mainstem

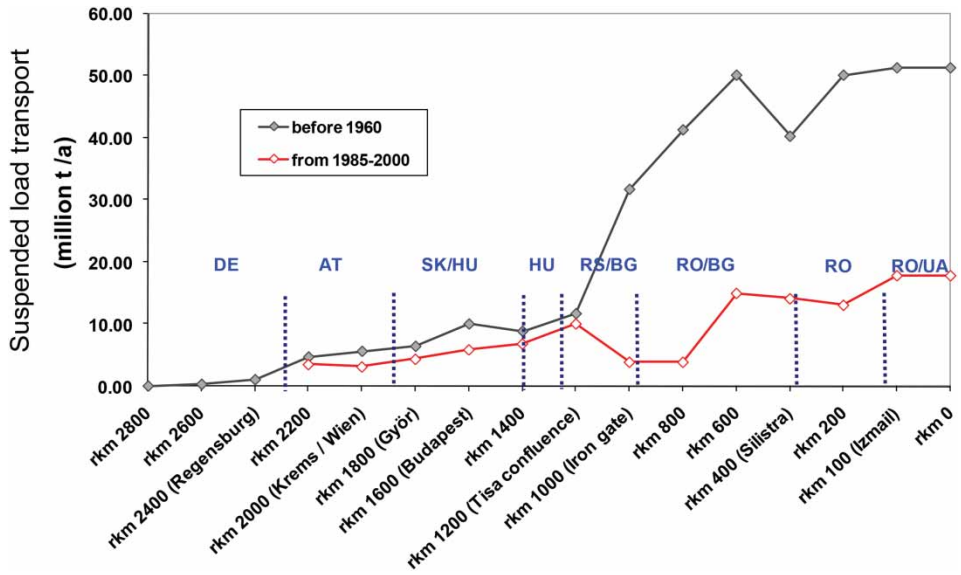

Figure A.4.4. Suspended sediment load transport along the Danube before and after the construction of Iron Gate I (1972) and Iron Gate II (1986). Figure from Habersack et al. (2013).

References

Blöschl, G., Nester, T., Komma, J., Parajka, J. and Perdigao, R.A.P. (2013) The June 2013 flood in the Upper Danube Basin, and comparisons with the 2002, 1954 and 1899 floods. *Hydrology and Earth System Sciences* 17, 5197–5212.

Habersack, H., Jäger, E. and Hauer, C. (2013) The status of the Danube River sediment regime and morphology as a basis for future basin management. *International Journal of River Basin Management* 11, 153–166.

Hatte, C., Gauthier, C., Rousseau, D.D., Antoine, P., Fuchs, M., Lagroix, F., Markovic, S.B., Moine, O. and Sima, A. (2013) Excursions to C-4 vegetation recorded in the Upper Pleistocene loess of Surduk (Northern Serbia): an organic isotope geochemistry study. *Climate of the Past* 9, 1001–1014.

Rank, D., Papesch, W., Heiss, G. and Tesch, R. (2009) Isotopic composition of river water in the Danube basin – Results from the Joint Danube Survey 2 (2007). *Austrian Journal of Earth Sciences* 102, 170–180.

Appendix B.4 Data tables

Table B.4.1. Sediment fine fraction (<63 μm) characteristics. Distance to the Black Sea in km, ^{13}C and ^{14}C values and CPI value of long chain (n-C_{24-30}) fatty acids.

Year	Name	km	$\delta^{13}C$ [‰]	$\Delta^{14}C$ [‰]	$\Delta^{14}C \pm$ [‰]	^{14}C age [yr]	Age ± [yr]
2013	Inn	2225	-27.4	-77	4	582	38
2013	Enns	2112	-27.4	-88	5	679	40
2013	D up Morava	1884	-27.8	-88	4	677	36
2013	Morava	1880	-27.6	-75	4	568	32
2013	D d Morava	1851	-27.7	-85	4	651	32
2013	D up Vah	1769	-27.7	-66	4	484	32
2013	Vah	1766	-28.3	-90	4	692	32
2013	D d Vah	1752	-27.2	-108	4	856	36
2013	Drava	1382	-27.1	-126	4	1022	32
2013	D up Tisa 1	1233	-26.6	-71	4	528	32
2013	D up Tisa 2	1233	-28.1	-38	4	249	31
2013	D up Tisa 3	1230	-27.4	-69	4	515	32
2013	Tisa	1214	-28.2	-203	3	1764	33
2013	D up Sava	1185	-28.0	-70	4	520	32
2013	Sava	1170	-28.1	-170	3	1440	32
2013	D d Sava	1132	-27.9	-130	4	1059	32
2013	Velika Morava	1103	-26.9	-141	4	1160	32
2013	D d Velika Morava	1077	-27.7	-99	4	776	32
2013	IG reservoir	977	-27.9	-73	4	545	36
2013	Jiu	692	-25.7	-348	3	3380	34
2013	D up Olt 1	630	-27.7	-187	3	1597	32
2013	D up Olt 2	630	-27.5	-182	4	1557	36
2013	Olt	601	-24.6	-193	4	1658	37
2013	D d Olt	596	-27.9	-142	4	1169	36
2013	D up Siret	164	-27.3	-171	4	1445	36
2013	Siret	155	-26.3	-370	3	3649	38
2013	Prut	134	-28.1	-162	3	1359	32
2013	Apex	67	-27.3	-224	3	1977	36
2013	DD18	10	-28.4	-172	3	1457	32
2013	DD9	4	-27.1	-269	3	2452	33
2013	DD11	23	-27.8	-191	3	1644	32
2013	DD5	18	-27.1	-47	4	328	35

Table B.4.1 (continued)

Year	Name	rkm	$\delta^{13}C$ [‰]	$\Delta^{14}C$ [‰]	$\Delta^{14}C \pm$ [‰]	^{14}C age [yr]	Age ± [yr]
2014	Inn	2225	-28.1	-121	9	974	80
2014	Enns	2112	-27.5	-77	9	576	77
2014	D d Enns	2104	-28.1	-52	9	364	73
2014	D up Morava	1884					
2014	Morava	1880	-27.7	-105	14	823	121
2014	D d Morava	1851					
2014	D up Vah	1769	-27.8	-113	9	895	79
2014	Vah	1766	-26.6	-32	14	195	117
2014	D d Vah	1752	-28.2	-98	8	761	69
2014	Drava	1382	-26.6	-112	14	891	125
2014	D d Drava	1318	-27.7	-47	13	322	108
2014	D up Tisa 1	1233	-27.7	-36	13	228	107
2014	Tisa	1214	-26.9	-144	13	1182	117
2014	D up Sava	1185	-27.5	-64	13	471	107
2014	Sava	1170	-25.8	-183	12	1557	120
2014	D d Sava	1132	-26.3	-142	12	1170	114
2014	Velika Morava	1103	-25.6	-146	14	1201	126
2014	D d Velika Morava	1077	-35.2	-131	9	1064	81
2014	IG reservoir	977		-80	13	602	111
2014	D up Jiu	698	-27.5	-122	9	985	79
2014	Jiu	692	-25.2	-264	12	2397	126
2014	D up Olt	630	-27.8	-166	12	1397	114
2014	Olt	601		-159	12	1325	114
2014	D d Olt	596	-25.9	-306	12	2876	132
2014	D d Vedea	540		-127	12	1026	111
2014	Ialomita	231	-25.1	-449	11	4722	152
2014	D up Siret	164	-26.6	-224	12	1976	123
2014	Siret	155	-25.0	-288	12	2662	128
2014	Prut	134	-26.0	-276	12	2532	127
2014	Apex	67	-26.0	-240	12	2137	124
2014	DD20	10	-26.2	-316	13	2986	146
2014	DD11	23	-26.5	-241	13	2151	141
2014	Inn d Salzach	2287	-27.3	-164		1379	
2014	Inn d Alz	2305	-27.5	-177		1506	
2014	Inn up Alz	2320	-27.0				
2014	Inn d Ziller	2480	-26.1	-307		2885	
2014	Inn up Ziller	2484	-26.5	-181		1542	
2014	Inn d Ötztaler Ache	2571	-24.6	-338		3246	
2014	Inn up Ötztaler Ache	2574	-26.4	-235		2094	
2014	Inn d Sanna	2595	-26.7	-157		1306	
2014	Inn up Sanna	2608	-26.3	-220		1934	
2013	Inn up Flaz 2013	2707	-23.6	-211		1838	
2014	Alz	2310	-29.6	-139		1141	
2014	Ziller	2483	-24.6	-179		1525	
2014	Ötztaler Ache	2573	-26.1	-144		1189	
2013	Spöl	2683	-26.3	-364		3568	
2014	Spöl	2683	-27.5	-202		1747	

Table B.4.2. Concentrations of brGDGT and long chain fatty acid (n-C_{24-32}) and the carbon preference index (CPI) of long chain (n-C_{24-30}) fatty acids.

Year	Name	brGDGT [ng/g]	FA [µg/g]	CPI
2013	Inn	334	8.8	4.2
2013	Enns	344	11.5	3.9
2013	D up Morava	280	8.3	4.7
2013	Morava	606	19.3	4.4
2013	D d Morava	451	13.0	4.3
2013	D up Vah	390	13.0	4.6
2013	Vah	733	19.6	4.7
2013	D d Vah	373	10.6	4.5
2013	Drava	592	18.8	4.4
2013	D up Tisa 1	390	11.3	4.6
2013	D up Tisa 2	654	16.0	4.3
2013	D up Tisa 3	207	7.3	4.0
2013	Tisa	707	10.5	4.6
2013	D up Sava	446	13.9	4.3
2013	Sava	750	12.3	4.1
2013	D d Sava	679	16.7	4.0
2013	Velika Morava	439	22.7	4.2
2013	D d Velika Morava	677	9.8	4.0
2013	IG reservoir	738	20.9	4.3
2013	Jiu	399	20.5	4.1
2013	D up Olt 1	490	11.3	4.3
2013	D up Olt 2	446	13.3	4.1
2013	Olt	96	3.2	4.1
2013	D d Olt	469	30.1	4.5
2013	D up Siret	382	9.0	4.3
2013	Siret	143	3.8	3.6
2013	Prut	594	17.6	4.4
2013	Apex	315	4.5	4.2
2013	DD18	246	5.9	4.3
2013	DD9	308	7.2	4.2
2013	DD11	451	11.8	4.5
2013	DD5	604	19.7	4.9

Table B.4.2 (continued)

Year	Name	brGDGT [ng/g]	FA [µg/g]	CPI
2014	Inn	403	9.6	6.7
2014	Enns	615	14.9	5.4
2014	D d Enns	632	8.5	6.5
2014	Morava	1930	24.4	5.5
2014	D up Vah	788		5.6
2014	D d Sava	753	6.2	
2014	Apex	635	6.5	
2014	Inn d Salzach	106	13.0	
2014	Inn d Alz	126	7.0	
2014	Inn up Alz	585	5.6	
2014	Inn d Ziller	43	6.7	
2014	Inn up Ziller	66	4.8	
2014	Inn d Ötztaler Ache	12	1.8	
2014	Inn up Ötztaler Ache	22	3.4	
2014	Inn d Sanna	21	4.8	
2014	Inn up Sanna	31	3.8	
2013	Inn up Flaz 2013		12.3	
2014	Alz	287	13.3	
2014	Ziller		13.3	
2014	Ötztaler Ache	38.88	2.8	
2013	Spöl		6.0	
2014	Spöl	25.96	4.2	

Table B.4.3. Compound-specific $\delta^{13}C$ of long chain (n-C_{24-30}) fatty acids. The average value is the concentration weighted average of n-C_{24-30}.

		FA n-C_{24}		FA n-C_{26}		FA n-C_{28}		FA n-C_{30}		Average FA n-C_{24-30}	
Year	Name	$\delta^{13}C$ [‰]	Stdv	$\delta^{13}C$ [‰]	Stdv	$\delta^{13}C$ [‰]	Stdv	$\delta^{13}C$ [‰]	Stdv	$\delta^{13}C$ [‰]	Stdv
2013	Inn	-32.6	0.14	-33.6	0.13	-34.3	0.06	-35.2	0.05	-33.7	0.04
2013	Enns	-32.4	0.04	-33.7	0.10	-34.3	0.02	-35.2	0.01	-33.7	0.01
2013	D up Morava	-33.3	0.03	-34.0	0.06	-34.8	0.02	-35.4	0.06	-34.3	0.01
2013	Morava	-32.9	0.04	-34.0	0.03	-34.9	0.03	-35.3	0.02	-34.1	0.01
2013	D d Morava	-33.5	0.14	-34.2	0.18	-35.1	0.18	-35.3	0.07	-34.5	0.06
2013	D up Vah	-33.8	0.19	-34.6	0.08	-35.2	0.03	-35.4	0.24	-34.7	0.03
2013	Vah	-33.5	0.05	-34.4	0.12	-35.2	0.06	-35.4	0.04	-34.5	0.03
2013	D up Tisa 1	-32.4	0.02	-33.7	0.18	-34.7	0.08	-34.9	0.15	-33.8	0.02
2013	D up Tisa 2	-33.0	0.07	-33.9	0.03	-34.7	0.06	-35.5	0.41	-34.1	0.02
2013	D up Tisa 3	-32.9	0.21	-33.6	0.05	-34.3	0.04	-34.1	0.04	-33.7	0.02
2013	D up Sava	-32.6	0.04	-33.7	0.09	-34.7	0.07	-35.2	0.15	-33.9	0.03
2013	Sava	-33.1	0.15	-33.7	0.13	-34.2	0.12			-33.6	0.08
2013	D d Sava	-32.6	0.02	-33.4	0.02	-34.4	0.03	-34.7	0.10	-33.6	0.01
2013	Velika Morava	-31.5	0.05	-32.0	0.03	-33.6	0.11	-34.3	0.17	-32.6	0.03
2013	D d Velika Morava	-32.2	0.03	-33.2	0.09	-34.3	0.17	-34.9	0.10	-33.4	0.03
2013	IG reservoir	-32.5	0.02	-33.8	0.12	-34.9	0.09	-34.9	0.19	-33.9	0.02
2013	Jiu	-30.6	0.10	-32.1	0.12	-33.0	0.04	-33.7	0.01	-32.3	0.01
2013	D up Olt 1	-32.5	0.11	-33.5	0.25	-34.6	0.14	-34.4	0.05	-33.7	0.04
2013	D up Olt 2	-31.8	0.09	-32.9	0.21	-34.0	0.11	-33.9	0.03	-33.1	0.03
2013	Olt	-30.7	0.08	-32.1	0.02	-32.8	0.18	-33.3	0.11	-32.2	0.02
2013	D d Olt	-32.9	0.21	-33.8	0.19	-34.7	0.06	-34.4	0.05	-34.0	0.04
2013	D up Siret	-32.0	0.13	-33.0	0.02	-34.3	0.06	-33.6	0.07	-33.2	0.02
2013	Siret	-31.3	0.09	-32.0	0.09	-32.5	0.06	-33.2	0.08	-32.1	0.04
2013	Prut	-33.4	0.03	-34.1	0.06	-34.7	0.01	-35.1	0.26	-34.4	0.01
2013	Apex	-32.3	0.05	-33.4	0.09	-34.5	0.02	-34.0	0.05	-33.5	0.01
2013	DD9	-32.0	0.03	-32.9	0.03	-33.9	0.11	-33.8	0.05	-33.1	0.02
2013	DD11	-32.9	0.18	-33.7	0.08	-34.3	0.06	-34.1	0.21	-33.7	0.04
2013	DD5	-33.0	0.27	-33.3	0.14	-33.9	0.02			-33.4	0.02
2014	Inn	-33.0	0.13	-33.8	0.01	-34.8	0.70	-35.6	0.07	-34.2	0.01
2014	Enns	-32.3	0.00	-33.4	0.03	-34.4	0.09	-35.2	0.04	-33.7	0.00
2014	D d Enns	-33.0	0.11	-33.8	0.18	-34.9	0.03	-35.1	0.04	-34.1	0.02
2014	Morava	-33.2	0.15	-34.1	0.12	-35.6	0.18	-35.4	0.16	-34.5	0.07
2014	D up Vah	-33.3	0.10	-34.1	0.01	-34.7	0.17	-35.4	0.04		
2014	D d Sava	-32.1	0.09	-33.1	0.13	-34.0	0.08	-34.4	0.05	-33.3	0.04
2014	Apex	-32.0	0.00	-32.8	0.02	-33.6	0.01	-33.8	0.04	-33.0	0.00
2014	Inn d Salzach	-32.8	0.05	-33.7	0.07	-34.3	0.01	-35.2	0.11	-33.8	0.01
2014	Inn up Alz	-32.3	0.07	-33.6	0.04	-34.1	0.06	-34.8	0.04	-33.5	0.02
2014	Inn d Ötztaler Ache	-31.3		-32.6		-33.0		-33.3		-32.5	
2014	Inn up Ötztaler Ache	-31.4	0.03	-32.5	0.06	-32.9	0.12	-33.1	0.01	-32.4	0.01
2014	Inn d Sanna	-32.8	0.51	-33.3	0.06	-33.5	0.19	-34.0	0.08	-33.3	0.05
2014	Inn up Sanna	-31.5	0.01	-33.2	0.08	-33.5	0.05	-33.9	0.03	-32.9	0.01
2013	Inn up Flaz	-27.4	0.01	-28.2	0.07	-31.1	0.16	-32.5	0.01	-29.0	0.01
2014	Alz	-34.9	0.10	-34.4	0.03	-35.2	0.07	-35.8	0.19	-35.1	0.02
2014	Ziller	-31.9	0.08	-34.0	0.04	-34.4	0.31	-35.6	0.12	-33.6	0.03
2014	Ötztaler Ache	-31.7	0.42	-33.4	0.85	-33.3	0.21	-31.7	0.13	-32.4	0.11
2013	Spöl	-30.8	0.16	-32.6	0.06	-33.2	0.00	-33.1	0.01	-32.1	0.00
2014	Spöl	-32.7	0.04	-33.9	0.02	-34.2	0.08	-34.2	0.19	-33.7	0.02

Table B.4.4. Compound-specific radiocarbon dating of fatty acids. Single compound (chain lengts n-C_{16}, n-C_{18}, n-C_{24}, n-C_{26}, n-C_{28}, n-C_{30}) fraction modern (Fm) and concentration weighted average (n-C_{24-30}) Fm, ^{14}C age and $\Delta^{14}C$.

		FA C16		FA C18		FA C24		FA C26		FA C28		FA C30		Average FA n-C_{24-30}		Average FA n-C_{24-30}		Average FA n-C_{24-30}	
Year	Name	Fm	Fm ±	Fm	Fm ±	Fm	Fm ±	Fm	Fm ±	Fm	Fm ±	Fm	Fm ±	Fm	Fm ±	^{14}C age [yr]	Age ± [yr]	$\Delta^{14}C$ [‰]	$\Delta^{14}C$ ± [‰]
2013	Inn	1.01	0.05	1.01	0.12	1.01	0.07	0.99	0.07	0.97	0.06	0.97	0.10	0.99	0.03	112	280	-22	35
2013	Enns	0.99	0.03	1.01	0.06	1.00	0.03	0.99	0.04	0.99	0.04	0.98	0.06	0.99	0.02	79	160	-18	20
2013	D up Morava	1.06	0.07			1.02	0.06	1.05	0.07	0.95	0.05	0.94	0.07	0.99	0.03	127	232	-23	29
2013	Morava	1.04	0.02	1.02	0.02	1.03	0.03	1.05	0.03	0.98	0.04	0.95	0.06	1.01	0.02	-78	139	2	17
2013	Vah	1.00	0.02	1.05	0.04	1.04	0.03	1.05	0.03	0.97	0.03	0.97	0.05	1.01	0.02	-84	134	3	17
2013	D d Vah	0.99	0.02	1.03	0.11									1.00	0.04	36	336	-12	42
2013	Drava	0.94	0.03	0.97	0.05	0.95	0.06	0.85	0.06	0.81	0.07	0.83	0.10	0.87	0.03	1169	269	-141	33
2013	D up Tisa 1	1.02	0.02	1.03	0.07	0.98	0.07	0.95	0.09	0.93	0.09	0.92	0.13	0.95	0.04	436	352	-60	44
2013	Tisa	0.97	0.02	0.99	0.04	0.90	0.03	0.85	0.03	0.82	0.03	0.78	0.11	0.85	0.02	1307	136	-156	17
2013	D up Sava	1.01	0.04	0.91	0.03	0.98	0.05	0.97	0.07	0.91	0.08	1.04	0.17	0.97	0.04	288	284	-42	35
2013	Sava	0.97	0.02	1.01	0.03	0.96	0.03	0.90	0.04	0.84	0.05	0.84	0.07	0.90	0.02	868	177	-108	22
2013	D d Sava	0.97	0.02			0.96	0.09	0.91	0.13	0.86	0.11	0.82	0.15	0.90	0.06	872	462	-108	58
2013	Velika Morava	0.99	0.03	1.02	0.06	0.98	0.10							0.96	0.05	340	422	-49	53
2013	IG reservoir	0.98	0.04	1.04	0.03	0.98	0.03	0.96	0.04	0.87	0.04	0.88	0.07	0.93	0.02	590	161	-77	20
2013	D up Olt 2	1.02	0.04	0.99	0.06	0.97	0.05	0.86	0.06	0.84	0.06	0.86	0.24	0.89	0.03	948	273	-117	34
2013	Olt	0.96	0.02	0.89	0.14	0.85	0.11							0.83	0.04	1466	322	-173	40
2013	D up Siret	0.97	0.03	0.98	0.09	0.84	0.08	0.84	0.07	0.82	0.06	0.77	0.11	0.82	0.04	1570	292	-184	36
2013	Siret	0.98	0.04	0.96	0.16									0.66	0.04	3397	344	-350	43
2013	Prut	0.98	0.02	0.93	0.16	0.93	0.06	0.90	0.06	0.89	0.05	0.88	0.07	0.90	0.03	846	227	-107	28
2013	Apex	0.99	0.04	0.99	0.08	0.86	0.06	0.77	0.07	0.74	0.06	0.70	0.11	0.78	0.03	2068	271	-231	34
2013	DD18	1.03	0.07	0.90	0.09			0.86	0.07	0.86	0.06	0.77	0.09						
2013	DD9	0.99	0.04	0.24	0.03	0.94	0.06	0.50	0.19	0.76	0.10	0.69	0.24	0.80	0.05	1985	387	-208	48
2013	DD11	0.99	0.03	0.97	0.09	0.90	0.06	0.84	0.06	0.83	0.06	0.75	0.11	0.84	0.03	1424	268	-168	33
2013	DD5	1.02	0.06	1.02	0.13	0.99	0.06	0.97	0.05	0.96	0.06	0.89	0.17	0.97	0.03	269	241	-40	30
2014	Inn	0.97	0.07	1.02	0.03	0.98	0.03	1.00	0.05	0.98	0.04	0.99	0.06	0.99	0.02	104	180	-21	22
2014	D up Vah	1.01	0.04	1.03	0.06	1.01	0.06	0.99	0.07	0.96	0.06	0.93	0.13	0.98	0.03	166	269	-28	34
2014	D d Sava	1.04	0.02	1.03	0.02	0.96	0.04	0.92	0.06	0.87	0.06	0.85	0.09	0.91	0.03	772	218	-98	27
2014	Apex	0.96	0.19											0.80	0.09	1817	686	-209	85

Table B.4.5: Compound-specific hydrogen isotope data of fatty acids. The average values is the concentration weighted average.

		FA n-C_{24}		FA n-C_{26}		FA n-C_{28}		FA n-C_{30}		Average n-C_{24-30}	
Year	Name	δ^2H [‰]	Stdv	δ^2H [‰]	Stdv	δ^2H [‰]	Stdv	δ^2H [‰]	Stdv	δ^2H [‰]	Stdv
2013	Inn	-183		-189		-182				-185	
2013	Enns	-177	1.75	-191	4.36	-201	3.62	-202	0.67	-191	0.56
2013	D up Morava	-178	0.69	-190	2.05	-200	0.33	-193	3.26	-190	0.21
2013	Morava	-173	0.29	-185	3.19	-171	8.59	-183	7.51	-177	0.11
2013	D d Morava	-176	1.61	-186	1.35	-194	8.14	-206	9.81	-189	0.97
2013	D up Vah	-177	3.72	-185	1.52	-187	19.22	-189	6.32	-184	1.31
2013	Vah	-176	2.63	-188	6.12	-185	13.13	-187	13.40	-183	2.24
2013	Drava	-173		-186		-175		-185		-179	
2013	D up Tisa 1	-172	4.16	-182	3.29	-164	10.25	-188	10.33	-175	2.34
2013	D up Tisa 2	-166	1.45	-182	4.54	-174	4.68	-197	1.18	-178	0.84
2013	D up Tisa 3	-170	2.73	-187	0.90	-198	0.20	-188	9.07	-185	0.09
2013	D up Sava	-172	1.99	-182	0.73	-172	2.11	-190	0.50	-178	0.36
2013	Sava	-181	4.02	-188	0.34	-188	1.82	-227	22.62	-192	0.23
2013	Velika Morava	-180	0.39	-185	1.71	-173	7.74	-192	12.42	-182	0.31
2013	D d Velika Morava	-169		-183		-165		-175		-173	
2013	IG reservoir	-179	8.78	-178	0.42	-171	6.00	-177	8.60	-176	0.36
2013	D up Olt 1	-171	2.64	-178	4.49	-168	5.61	-201	16.43	-178	2.01
2013	D up Olt 2	-171	1.96	-179	0.75	-177	0.25	-180	0.54	-176	0.15
2013	D up Siret	-167	0.89	-181	0.77	-167	1.58	-204	5.88	-177	0.51
2013	Prut	-175	3.44	-182	3.93	-186	2.80	-223	12.07	-191	1.80
2013	Apex	-169	7.85	-169	6.12	-164	5.62	-180		-170	3.52
2013	DD18	-172	1.34	-181	0.47	-179	10.59	-197	1.00	-181	0.35
2013	DD11	-170	5.90	-184	3.32	-167	4.54	-218	9.34	-182	2.27
2013	DD5	-183	1.80	-191	2.21	-196	4.05	-208	9.05	-194	1.24
2014	Inn	-176	0.32	-188	1.15	-181	0.58			-182	0.21
2014	Enns	-176	0.53	-184	0.20	-179	0.82			-179	0.03
2014	D d Enns	-179	0.36	-188	0.25	-180	0.28			-182	0.11
2014	Morava	-168	0.80	-175	0.29	-165	0.97			-169	0.19
2014	D up Vah	-174	0.22	-185	1.44	-175	0.19			-178	0.04
2014	Inn d Salzach	-187	0.28	-194	0.79	-191	2.48			-190	0.17
2014	Inn d Alz	-188	0.82	-190	1.10	-185	0.75			-188	0.46
2014	Inn up Ziller	-195	10.18	-186	2.65	-185	2.55			-189	1.74
2014	Inn d Ötztaler Ache	-216		-188							
2014	Inn d Sanna	-190	9.06	-183	0.23	-187	2.06	-196		-189	0.13
2013	Inn up Flaz	-180	0.68	-196	1.47	-192	0.64			-188	0.41
2014	Alz	-191	0.46	-193	6.76	-180	0.80			-188	0.35
2014	Ziller	-243	2.20	-189	1.16						
2014	Ötztaler Ache	-216	23.83	-185	0.96	-188				-199	0.90
2013	Spöl	-171	11.61	-185	4.83	-184	3.32	-163		-175	2.57

Table B.4.6. $\delta^{2}H$ and $\delta^{18}O$ values of river water and corresponding standard deviations.

Year	Name	$\delta^{18}O$ [‰]	Stdv.	$\delta^{2}H$ [‰]	Stdv.
2013	D up Inn	-10.68	0.05	-74.62	0.37
2013	Inn	-13.66	0.03	-97.68	0.44
2013	D d Inn	-11.85	0.04	-82.75	0.22
2013	D up Enns	-11.81	0.03	-82.80	0.48
2013	Enns	-12.43	0.05	-87.02	0.40
2013	D d Enns	-11.87	0.03	-82.63	0.29
2013	D up Morava	-11.66	0.04	-80.62	0.28
2013	Morava	-10.17	0.05	-69.70	0.34
2013	D d Morava	-11.53	0.04	-79.18	0.33
2013	D up Vah	-11.49	0.09	-78.73	0.12
2013	Vah	-10.64	0.05	-72.64	0.19
2013	D d Vah	-10.70		-76.13	
2013	D up Drava	-11.53		-81.39	
2013	Drava	-11.22		-77.12	
2013	D d Drava	-11.44		-79.58	
2013	D up Tisa	-11.36		-79.89	
2013	Tisa	-9.72		-66.06	
2013	D up Sava	-11.64	0.10	-80.07	0.25
2013	Sava	-10.35	0.07	-66.59	0.16
2013	D d Sava	-11.20	0.04	-75.47	0.31
2013	Velika Morava	-10.38	0.09	-70.87	0.14
2013	D d Velika Morava	-10.83	0.05	-73.45	0.30
2013	IG reservoir	-10.61	0.08	-72.36	0.72
2013	D d Iron Gate	-10.25	0.07	-72.28	0.22
2013	D up Olt	-10.43	0.03	-71.98	0.10
2013	Olt	-9.59	0.09	-65.59	0.41
2013	D d Olt	-10.36	0.08	-71.30	0.28
2013	D up Siret	-10.57	0.08	-73.22	0.31
2013	Siret	-8.87	0.06	-62.92	0.08
2013	Prut	-9.28	0.04	-63.89	0.23
2013	DD1	-10.36	0.07	-71.17	0.19
2013	DD5	-9.94	0.03	-68.90	0.21
2013	DD6	-10.41	0.05	-71.89	0.34
2013	DD7	-8.44	0.06	-60.96	0.28
2013	DD8	-10.34	0.06	-71.54	0.30
2013	DD10	-10.40	0.02	-71.74	0.46
2013	DD13	-9.56	0.03	-65.85	0.13
2013	DD16	-10.43	0.08	-70.93	0.52
2013	DD17	-10.66	0.05	-72.25	0.39
2013	DD20	-10.60	0.07	-72.27	0.45

Table B.4.6 (continued)

Year	Name				
2014	D up Inn	-10.02	0.06	-69.49	0.26
2014	Inn	-12.44	0.08	-87.22	0.24
2014	D d Inn	-11.02	0.06	-77.52	0.11
2014	D up Enns	-11.18	0.04	-78.43	0.16
2014	Enns	-11.80	0.05	-81.48	0.20
2014	D d Enns	-11.23	0.03	-78.16	0.28
2014	D up Morava	-11.06	0.03	-77.50	0.31
2014	Morava	-8.74	0.05	-61.64	0.28
2014	D d Morava	-10.66	0.15	-74.85	0.86
2014	D up Vah	-10.81	0.08	-75.18	0.44
2014	Vah	-9.96	0.22	-68.85	0.79
2014	D d Vah	-10.57	0.26	-74.34	0.97
2014	Sio	-4.67	0.02	-37.96	0.70
2014	D up Drava	-11.41	0.02	-79.37	0.04
2014	Drava	-11.28	0.05	-78.63	0.10
2014	D d Drava	-10.76	0.10	-75.83	0.19
2014	D up Tisa	-10.79	0.03	-75.81	0.29
2014	Tisa	-9.52		-65.29	
2014	D up Sava	-10.91	0.07	-75.82	0.10
2014	Sava	-9.92	0.09	-66.53	0.17
2014	D d Sava	-9.77	0.10	-67.54	0.43
2014	Velika Morava	-10.37	0.08	-70.57	0.43
2014	D d Velika Morava	-10.28	0.10	-70.36	0.32
2014	IG reservoir	-10.44	0.06	-71.01	0.08
2014	D up Jiu	-10.56	0.05	-72.87	0.21
2014	Jiu	-9.40	0.09	-62.98	0.25
2014	D up Olt	-10.31	0.03	-71.10	0.29
2014	Vedea	-8.17	0.07	-58.22	0.43
2014	Ialomita	-8.61	0.05	-56.28	0.23
2014	D up Siret	-9.91	0.04	-67.80	0.24
2014	Siret	-9.02	0.04	-60.70	0.35
2014	Prut	-8.68	0.06	-60.85	0.38
2014	Apex	-10.93	0.04	-77.56	0.17
2014	DD1	-9.08	0.03	-62.20	0.35
2014	DD3	-9.02	0.04	-61.90	0.19
2014	DD5	-8.47	0.03	-59.43	0.32
2014	DD6	-9.59	0.04	-65.25	0.26
2014	DD7	-8.39	0.03	-59.07	0.32
2014	DD8	-9.53	0.02	-65.11	0.21
2014	DD10	-9.49	0.07	-65.71	0.18
2014	DD11	-9.60	0.27	-68.92	0.81
2014	DD12	-8.06	0.08	-57.86	0.30
2014	DD14	-9.63	0.02	-65.45	0.34
2014	DD16	-9.51	0.06	-63.83	0.13
2014	DD17	-10.07	0.05	-69.59	0.37
2014	DD18	-9.52	0.06	-64.18	0.26
2014	DD19	-7.92	0.03	-55.15	0.29
2014	DD20	-10.06	0.02	-68.83	0.31
2014	DD32	-7.35	0.04	-52.30	0.28
2014	DD33	-7.63	0.02	-54.34	0.16
2014	middle profile 0m	-9.65	0.07	-65.80	0.23
2014	middle profiel 26m	-9.70	0.06	-66.56	0.27

Chapter 5

Constraining instantaneous fluxes and integrated compositions of fluvially-discharged organic matter

Chantal V. Freymond[a], Maarten Lupker[a], Francien Peterse[a,b], Negar Haghipour[a], Lukas Wacker[c], Florin Filip[d,e], Liviu Giosan[f] and Timothy I. Eglinton[a]

[a] Geological Institute, ETH Zürich, Switzerland
[b] Department of Earth Sciences, Utrecht University, Netherlands
[c] Ion Beam Physics, ETH Zürich, Switzerland
[d] Department of Geography, University of Bucharest, Romania
[e] Fabrica de Cercetare, Romania
[f] Woods Hole Oceanographic Institution, USA

Abstract

Fluvial export of organic carbon (OC) and burial in ocean sediments comprises an important carbon sink, but fluxes remain poorly constrained, particularly for specific organic components. Here, OC and lipid biomarker contents and isotopic characteristics of suspended matter determined in depth profiles across an active channel close to the terminus of the Danube River are used to constrain instantaneous OC and biomarker fluxes and integrated compositions during high to moderate discharge. During high (*moderate*) discharge, the total Danube exports 8 (*7*) kg/s OC, 7 (*3*) g/s higher plant-derived long-chain fatty acids (LCFA), 34 (*21*) g/s short-chain fatty acids (SCFA) and 0.5 (*0.2*) g/s soil bacterial membrane lipids (brGDGTs). Integrated stable carbon isotopic compositions were TOC: -28.0 (*-27.6*)‰, LCFA: -33.5 (*-32.8*)‰; and $\Delta^{14}C$ TOC: -129 (*-38*)‰; LCFA: -134 (*-143*)‰, respectively. Such estimates will aid in establishing quantitative links between production, export and burial of OC from the terrestrial biosphere.

5.1 Introduction

Rivers are the most important conduits for transfer of sediment eroded on continents to ocean basins. Globally, rivers discharge about 19 billion tons of sediment per year to the coastal ocean (Milliman and Farnsworth, 2011), entraining and exporting about 200 Mt/yr particulate organic carbon (POC) (Galy et al., 2015). Once deposited on continental margins, the OC may be stored on long timescales, and corresponding sedimentary sequences thus serve both as long-term sink for terrigenous OC and as continuous archives of palaeoenvironmental change in the adjacent river catchments.

Global estimates for riverine discharge of suspended particulate matter (SPM) are not well constrained because of variable sampling strategies and frequencies over different hydrological conditions (Milliman and Farnsworth, 2011). Often, such estimates stem from measurement of near-surface SPM close to the river axis, and assumptions are then made concerning the homogeneity of the suspended load in order to derive an integrated flux. However, the vertical distribution of SPM in a river is influenced by hydrodynamic sorting, which causes coarser and higher density sediment to be transported closer to the riverbed, whereas finer and low-density particles are more homogeneously distributed over the water column (Bouchez et al., 2011; Lupker et al., 2011). Several studies have explored variations in the distribution and the mineral and inorganic geochemical characteristics of SPM across depth and cross-sections of rivers in order to derive integrated SPM fluxes (e.g. Armijos et al., 2017; Bouchez et al., 2011; Lupker et al., 2011). In contrast, the lateral and vertical variability in bulk OC (Bouchez et al., 2014; Galy et al., 2008; Goni et al., 2005; Guinoiseau et al., 2016) and molecular (biomarker) (Feng et al., 2016) composition and corresponding isotopic

(stable and radiocarbon) characteristics are significantly less well known. This is in part due to logistical challenges associated with sampling and analysis for trace organic constituents, hindering our ability to place robust constraints on the characteristics and fluxes of POC and biomarkers discharged to the oceans.

In a recent study, the existence of a POC-rich and particulate lignin-rich suspended sediment layer just above the riverbed was observed in the Madre de Dios River, and was attributed to high proportions of plant debris at this particular depth (Feng et al., 2016). In contrast, soil OC is thought to be mainly associated with fine-grained phyllosilicates (Baldock and Skjemstad, 2000; Doetterl et al., 2015; Freymond et al, 2018), that is well dispersed throughout the water column and therefore more uniform vertical distributions are expected (Bouchez et al., 2011).

In this study, SPM was characterized from several depth-profiles that serve as a "picket fence" spanning one of the two main branches of the Danube River at the apex prior of the delta. Bulk OC and biomarker concentrations as well as corresponding stable and radiocarbon isotopic compositions of SPM samples collected on campaigns during two different years were determined, and compared to adjacent river sediment deposits. Focus was placed on long-chain fatty acids (LCFA) and branched glycerol dialkyl glycerol tetraethers (brGDGTs) as tracers of higher plant-derived material (Eglinton and Eglinton, 2008) and soil OC (Schouten et al., 2013), respectively, in order to constrain the instantaneous export flux of OC and these source-specific biomarkers to the Black Sea. Extrapolating bulk and compound-specific isotope signatures as well as proxy values to the river cross-section, we assess heterogeneity in organic matter (OM) associated with SPM and potential uncertainties associated with extrapolation of single-point measurements to derive estimates of fluvial discharge.

5.2 Site description

The Danube River, with a catchment area of 817,000 km^2, including parts of the Eastern Alps, the Carpathian, Dinaric and Balkan mountains, and large sedimentary basins (Vienna basin, Pannonian and lower Danubian plains; Schiller et al., 2010), is the second largest fluvial system in Europe. Mean annual discharge to the Black Sea is 6,850 m^3/s (Schiller et al., 2010) and present-day total sediment export (SPM and bed load) is 25–35 Mt/yr, of which about 18 Mt/yr is in the suspended fraction (Habersack et al., 2016). At the beginning of its delta, the Danube mainstem splits into two main branches – the northern Chilia branch and southern Tulcea branch. The Tulcea branch further splits into the Sulina and Sf. Gheorge branches (Supplementary Figure A.5.1).

5.3 Methods

5.3.1 Sample collection

Samples were collected on the Tulcea branch that accounts for 45% of the total water flux (Torica, 2006), shortly downstream of the diffluence (<2 km) (Supplementary Figure A.5.1) in early June 2013 and early September 2014 during decreasing water level (Supplementary Figure A.5.2). For political reasons, depth profiles could not be taken across the entire Danube mainstem before its main diffluence as it coincides with the Romanian – Ukrainian border. However, it is assumed given its proximity to the mainstem that the SPM is representative of material entering from the river to the delta. Furthermore, the sampling location is >50 km downstream of the last large tributary confluence, and therefore, the river is expected to be well mixed. Water depth, bathymetry, velocity and total discharge were determined by deployment of an Acoustic Doppler Current Profiler (ADCP). Based on the ADCP river cross-sections, optimal locations for the depth profiles and large-volume water sampling were determined (Supplementary Figure A.5.4). Water samples were collected with a 5-liter horizontal, open ended, sampling bottle equipped with a pneumatic closing mechanism (Lupker et al., 2011). The depth of the sampling bottle was controlled with an echo sounder. In 2013, about 30 L of water was sampled for each depth at the middle profile and about 10 L at the left and right profiles, as well as the near shore surface water locations. In 2014, >60 L water was sampled for every profile and depth. Water samples were filtered over pre-combusted and pre-weighted glass fiber filters (90 mm, 0.7 μm GF/F filters, Whatman). About 10 L of each sample was filtered over membrane filters (90 mm, 0.22 μm PES filters, Membrane Solutions) but not examined in this study. Filters were stored at -20 °C until they were freeze-dried. At the location of the sampling transect, fine-grained (<1 mm) sediment that was recently deposited on the riverbanks was collected from the shore (Freymond et al., 2017). Subsequently, the term 'river sediment' is used for these fresh deposits.

5.3.2 ADCP acquisition and data processing

The ADCP (Rio Grande, 1200 kHz) was mounted to the side of a boat ca. 0.1 m below the water surface (e.g. Muste et al., 2004). Riverbed geometry, water discharge and velocity profiles were determined with multiple river crossings perpendicular to the flow in bottom track mode with a vertical resolution of 0.1/0.25 m (2013/2014 respectively).

In 2014, a GPS unit was connected to the ADCP to record the exact transect position. Comparison between the bottom and GPS-referenced velocity did not reveal the presence of a moving bed (Callede et al., 2000). Four transects in the direct vicinity of the sediment sampling points were averaged using the USGS Velocity Mapping Toolbox (Parsons et al., 2013). These transects closely agree and the discharge calculated for each individual transect does not vary by more than 10%. In 2013, no GPS was

available, making precise transect averaging impossible. A single river transect was selected (out of seven; discharge estimates varied by <6%) based on data quality and proximity to the 2013 water sampling points, and used for calculations.

The velocity data was further processed in R (R Core Team, 2014). Missing discharge data was interpolated based on the average of neighboring velocity profiles. The top and bottom discharge data that cannot be resolved by the ADCP was extrapolated based on a power law fit to the available velocity data (Chen, 1991) (Supplementary Figure A.5.4). Discharge was calculated based on the velocity data and corrected for the difference between ship and water flow direction.

Concentration and proxy data from the depth profiles were extrapolated to the river cross-section using an inverse distance method. This extrapolated data was then combined with the water discharge profiles to derive discharge-weighted proxy average values and instantaneous fluxes of OC and biomarkers.

5.3.3 Bulk measurements: SPM concentration, TOC, $\delta^{13}C$, ^{14}C

To determine SPM concentrations, pre-combusted filters were weighted before and after filtering a known amount of water and subsequent freeze-drying. SPM concentrations are reported in mg/L.

For total organic carbon (TOC), $\delta^{13}C$ and ^{14}C measurement, filter pieces of known diameter and river sediments were de-carbonated as described in Freymond et al. (2018). Blank filters were treated with the same method. The measurement was performed on a coupled EA-IRMS-AMS (elemental analyzer, isotope ratio mass spectrometer, accelerator mass spectrometer) system (McIntyre et al., 2016) and corrected for procedural blank values.

5.3.4 FA and brGDGT extraction and quantification

Freeze-dried filters were cut in pieces whereas river sediments were sieved to <63 µm prior to microwave extraction. BrGDGTs were extracted as described in Freymond et al. (2017) and measured on a UHPLC–APCI–MS system (Ultra High Performance Liquid Chromatograph, Agilent 1290, coupled to a quadrupole Mass Spectrometer, Agilent 6310) at Utrecht University following the settings of Hopmans et al. (2016). For proxy calculations see Supplementary Equations A.5.1, Supplementary Figure A.5.3.

FAs were extracted as described in Freymond et al. (2018) from the same total lipid extract as for the brGDGTs and quantified against an external standard (*n*-$C_{4\text{-}24}$ even carbon saturated FAMEs; Supelco) on a gas chromatograph equipped with a flame ionization detector (GC-FID; Agilent 7890A). Results are reported as sum of even C-number long-chain FA (*n*-$C_{24\text{-}30}$; LCFA) and short-chain FA (*n*-$C_{16\text{-}18}$; SCFA) concentrations.

5.3.5 LCFA $\delta^{13}C$ measurement

LCFA $\delta^{13}C$ determination was performed in duplicate measurements with a GC-IRMS (gas chromatograph, Thermo Trace GC Ultra, coupled to an isotope ratio mass spectrometer, Thermo Delta V Plus). The $\delta^{13}C$ values were calibrated using an external fatty acid methyl ester standard calibrated to the VPDB scale, and corrected for carbon atoms that were added during methylation. Results are shown as concentration weighted average values (n-$C_{24\text{-}30}$) with standard deviations ranging from 0.12–0.97.

5.3.6 Compound-specific FA ^{14}C measurement

Due to the low abundance of LCFAs (generally <1 µg/L), samples from different depths and profiles were combined in order to obtain sufficient C required for ^{14}C measurement (typically >10 µgC) (Supplementary Figure A.5.5). Separation and isolation of FAs was achieved using a PCGC (preparative capillary gas chromatograph; Eglinton et al., 1996). FAs n-C_{16}, n-C_{18} and n-$C_{24\text{-}30}$ were collected in three separate traps. Two blank runs with the same amount of single runs and the same time windows of collection as for samples were run to determine the processing blank. The single compounds were converted to CO_2 with pre-combusted CuO in evacuated quartz tubes (850 °C, 5 h). ^{14}C on the CO_2 was measured with a MICADAS (MIni radioCArbon DAting System; Christl et al., 2013; Synal et al., 2007;) at the Laboratory for Ion Beam Physics at ETH. Fraction modern (Fm) values were corrected for the processing blank (Tao et al., 2015) and for carbon atoms added during methylation. Fm values were subsequently converted to $\Delta^{14}C$ values (Sternström et al., 2011).

5.4 Results

5.4.1 Depth profiles

SPM concentrations range from 25–70 mg/L and do not show a clear variation with depth (Figure 5.1). However, SPM concentrations are higher in the middle profile than in the right and left profiles in 2014, whereas the opposite is the case in 2013. TOC contents, ranging between 1.3–2.4%, show a maximum at mid depth, which is most pronounced in the middle profile in 2014. LCFA, SCFA and brGDGT concentrations are higher in 2013 than 2014, ranging from 0.37–0.98 µg/L and 0.19–0.54 µg/L for LCFAs, 1.91–5.40 µg/L and 1.22–4.64 µg/L for SCFAs and 26.59–62.55 ng/L and 12.83–40.56 ng/L for brGDGTs in 2013 and 2014, respectively. LCFA and brGDGT concentrations are strongly correlated (0.95, Pearson correlation coefficient). Bulk $\delta^{13}C$ values are relatively constant over different locations along the river cross-section, depths and years with a statistical (i.e., not discharge-weighted) average value of -27.8‰ (±0.34‰, n = 23) after excluding two outliers (2013 right 5 m = -36.3‰, and 2014 middle surface = -19.1‰). Bulk $\Delta^{14}C$ values are relatively homogeneous in 2013,

ranging from -155 to -90‰ (average -126‰ ±18‰, n = 12). In 2014, bulk $\Delta^{14}C$ values were higher and slightly more variable, ranging from -127 to +14‰ (average -41‰ ±38‰, n = 13), with highest values in the middle profile. Compound-specific LCFA $\delta^{13}C$ values of the left, middle and right profile surface water are similar for both years with an average of -33.7‰ (±0.06‰, n = 6), although surface water from close to the left and right shores show more ^{13}C-enriched values than mid channel in 2014. In 2013, depth profiles exhibit relatively constant LCFA $\delta^{13}C$ values whereas in 2014, values are about 1‰ more enriched at 7–26 m depth than at the surface. LCFA average chain length (ACL) is constant with depth, but shows differences across the river. The middle profile in 2013 shows an average of 26.5 whereas the left and right profiles show an average of 25.7 and 25.5, respectively. In 2014, ACL is only slightly higher in the middle profile (averages: middle = 26.3, left = 26.1, right = 26.0). BrGDGT-derived proxies are generally constant with depth. BIT and CBT' show distinct values between the two years, however, the differences are small and corresponding isomer ratio (IR) and $\#rings_{tetra}$ values fall in the same range in 2013 and 2014 (Figure 5.1).

In general, no significant correlations were found between sample depth and geochemical parameters. BrGDGT and LCFA concentrations only display weak correlations with SPM concentration of 0.65 and 0.57, respectively (Pearson correlation coefficients).

5.4.2 Discharge-weighted average and instantaneous fluxes

Extrapolated and discharge-weighted average bulk and biomarker proxy values for the 2013 and 2014 samplings are shown in Table 5.1 (Supplementary Figures A.5.6 & A.5.7). Between years, average TOC (1.6/1.8%) and bulk $\delta^{13}C$ (-28.0/-27.6‰; 2013/2014, respectively) are very comparable. Bulk $\Delta^{14}C$ values are more variable, and imply a higher proportion of fossil or pre-aged OC in 2013 ($\Delta^{14}C$ = -129‰) compared to 2014 ($\Delta^{14}C$ = -38‰). The distinct changes in LCFA $\delta^{13}C$ values with depth between the two years result in a slightly lower average value in 2013 than 2014 (-33.5/-32.8‰), whereas average LCFA $\Delta^{14}C$ values for 2013 and 2014 samples are comparable. Similarly, average brGDGT-derived proxy values show little variation between the two sampling periods (Table 5.1).

Discharge-weighted instantaneous SPM, OC and biomarker fluxes for the two sampling periods are shown in Figure 5.2, Supplementary Table A.5.1.

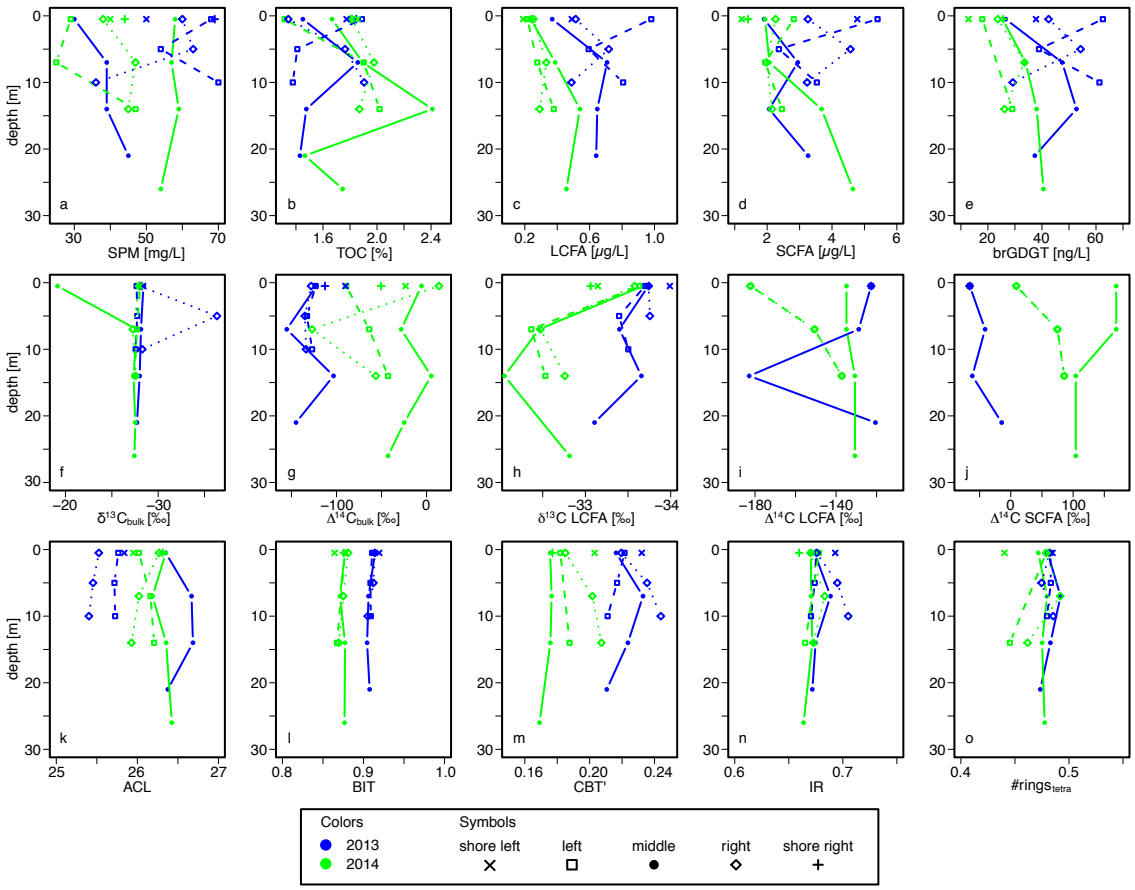

Figure 5.1. Concentration and proxy values in depth profiles. Solid lines show the middle; dashed lines the left and right profiles.

5.4.3 *River sediment composition*

River sediment deposits at the location of the depth profiles are characterized by lower TOC content (0.9/0.7; 2013/2014, respectively) and lower bulk (-224‰/-240‰) and LCFA $\Delta^{14}C$ values (-231‰/-209‰) compared to cross-section SPM. Stable isotope and proxy values, except CBT' that shows significantly lower values in river sediments, are comparable to the ones in SPM samples (Table 5.1).

Table 5.1. Discharge-weighted average OC and biomarker proxy values in SPM and river sediments.

	River cross section SPM		River bar sediment	
	2013	2014	2013	2014
TOC [%]	1.6	1.8	0.9[a]	0.7[a]
Bulk $\delta^{13}C$ [‰]	-28.0	-27.6	-27.3	-26.0
Bulk $\Delta^{14}C$ [‰]	-129	-38	-224	-240
LCFA $\delta^{13}C$ [‰]	-33.5	-32.8	-33.5	-33.0
LCFA $\Delta^{14}C$ [‰]	-134	-143	-231	-209
SCFA $\Delta^{14}C$ [‰]	-52	99	-18	-46
ACL	26.1	26.2	27.1	27.5
BIT	0.91	0.87	0.91[b]	0.89
CBT'	0.22	0.18	0.03[b]	0.06
MATmr [°C]	9.2	9.9	8.4[b]	8.3
pH	7.5	7.4	7.2[b]	7.2
IR	0.68	0.67	0.55	0.57
$\#rings_{tetra}$	0.48	0.47	0.50	0.47

[a] Data from Freymond et al., 2018

[b] Data from Freymond et al., 2017

5.5 Discussion

5.5.1 SPM composition and fluxes

The identification of only small variations in concentrations and proxy values with depth and among different profiles across the channel shows that the SPM in the river is well mixed at the sampling location (Figures 5.1, A.5.6 & A.5.7). Only SPM concentration and ACL show systematic differences across the river. In 2014, SPM is higher in the middle of the river, where the water velocity is highest and thus theoretically coarser-grained particles can be retained in suspension. However, in 2013, SPM concentration is lower in the middle profile compared to the left and right ones. In 2013, ACL in the middle profile is higher compared to profiles on the river flanks, potentially indicating different LCFA sources. However, such a difference is not reflected in corresponding LCFA $\delta^{13}C$ values. In the vertical direction, an increase of SPM with depth is only observed in the middle profile in 2013. The typical hydrodynamic sorting of sediments leading to an increase in the average grain-size towards the bottom of the water column, as observed in other large rivers (Bouchez et al., 2011; Feng et al., 2016; Lupker et al., 2011), does not seem to occur here. The OM composition, expressed in bulk $\delta^{13}C$, LCFA $\delta^{13}C$, LCFA $\Delta^{14}C$, ACL, and brGDGT proxy values (Table 5.1), remains fairly constant between years. The minor compositional changes between 2013 and 2014 are well within the range of inter- and intra-annual fluctuations reported for e.g. the Tagus, Congo and Yellow Rivers (Hemingway et al.,

2017; Tao et al., 2017; Zell et al., 2014). Given that sampling in 2013 and 2014 was in early and in late summer, respectively, observed minor differences likely reflect seasonal variations. However, given the generally homogenous characteristics as a function of location, depth and time, these data can be considered representative of the SPM composition in the Danube during yearly high-water conditions.

BrGDGTs are ubiquitously produced in soils (Peterse et al., 2012; Weijers et al., 2007), and hence may serve as tracers for soil OC during fluvial transport, even though *in situ* production in lake and river waters has also been documented (De Jonge et al., 2014b; Tierney and Russell, 2009; Weber et al., 2015). Although the high BIT index values for Danube SPM (0.91/0.87 in 2013/2014, respectively, Table 5.1) suggest that brGDGTs are mainly soil-derived (Schouten et al., 2013), these high BIT values may also be the result of a large contribution of in-river produced brGDGTs (De Jonge et al., 2014b). To identify such a potential *in situ* contribution, the IR, which is the fractional abundance of 6-methyl-isomer brGDGTs compared to all 5- and 6-methyl-isomers brGDGTs (Supplementary Equations A.5.1 & Supplementary Figure A.5.3), may be used, where high values relate to relatively more aquatic brGDGTs (De Jonge et al., 2014b). The IR for the SPM (0.68/0.67 for 2013/2014, Table 5.1) is slightly higher than for the river sediments (0.55/0.57 for 2013/2014, Table 5.1), indicating potential *in situ* production. Indeed, SPM IR values are in the same range as for Danube sediments upstream of the Iron Gate dams, where lower water velocities may have enhanced *in situ* brGDGT production, albeit to a minor extent (Freymond et al., 2017). Nevertheless, considering the comparable brGDGT composition in the SPM close to the Black Sea with that in fluvial sediment deposits upstream (Freymond et al., 2017), the vast majority of the brGDGTs appears to be derived from soils with a minor in-river brGDGT contribution. This interpretation of predominantly soil (as opposed to aquatic) source is supported by the strong correlation between brGDGT and LCFA concentrations (0.95, Pearson correlation coefficient) in the SPM.

Water discharge was higher in 2013, and correspondingly SPM, TOC and biomarker fluxes were also higher than in 2014 (Figure 5.2). The SPM and TOC fluxes appear to increase in concert with the water flux (factor 1.3, 1.4 and 1.2 higher in 2013 for water, SPM and TOC, respectively), whereas LCFA, SCFA and brGDGT fluxes increase by factors of 2.5, 1.6 and 2.0, respectively, with higher discharge (Figure 5.2). This relative enhancement in SCFA and brGDGT compared to LCFA fluxes at lower discharge might indicate in-river production during more quiet conditions. Correspondingly, the higher SCFA and bulk $\Delta^{14}C$ values with lower discharge in 2014 may in turn reflect a greater contribution of fresh terrestrial or aquatic biomass relative to pre-aged soil or a smaller contribution of fossil OC (Table 5.1). On the other side, lower bulk $\Delta^{14}C$ values during higher discharge in 2013, indicate proportionally higher inputs of (pre-aged) soil-derived OM (Cathalot et al., 2010; Rosenheim et al., 2013) and/or fossil OC with correspondingly lower in-river production. LCFA $\Delta^{14}C$ values are

relatively low (~1,160 ^{14}C years) not showing a significant difference between years or varying discharge, indicating that the LCFAs primarily derive from mineral-associated OC that is pre-aged in soils (Tao et al., 2015; van der Voort et al., 2017).

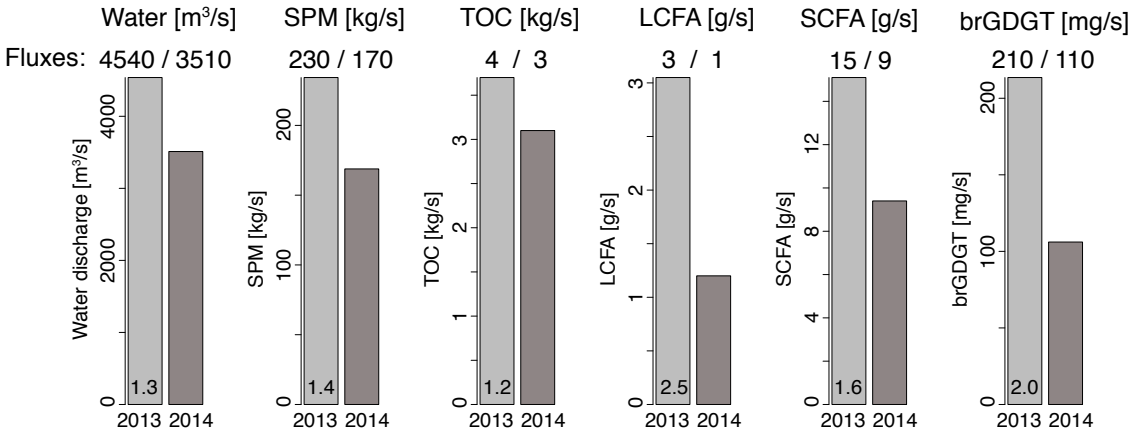

Figure 5.2. Instantaneous Danube River water, SPM, TOC and biomarker fluxes in 2013 and 2014. The number in the 2013 bar is the factor by which the 2013 flux is higher than in 2014.

5.5.2 Comparison of SPM to river sediments

TOC concentrations are significantly higher in SPM than in river sediments (Table 5.1), potentially reflecting hydrodynamic particle sorting during, or decomposition subsequent to, deposition. High-density coarse-grained particles (including mineral grains with little associated OC) are preferentially deposited compared to minerals in the clay and fine silt fraction that exhibit a high mineral-specific surface area (SA) available for organo-mineral interactions (Keil and Mayer, 2014). Additionally, low-density plant debris may preferentially remain in the suspended load. Greater contributions of plant debris to SPM relative to river sediments would also explain the higher bulk OC and LCFA Δ^{14}C values (i.e., fresher material) of the former (Table 5.1). Preferential post-depositional degradation of fresher and more labile non-mineral-associated OM in river sediments could also explain the lower TOC values and lower TOC and LCFA Δ^{14}C values (older ages) of river sediments. However, since LCFA δ^{13}C values show no indication for enrichment due to degradation (Li et al., 2017; Wang et al., 2016), suggesting a similar origin for LCFAs in SPM and river sediments, we suspect that preferential transport and deposition of mineral-associated LCFAs is the most likely explanation. The lower ACL values for SPM than river sediments is the only indication of additional sources of *n*-C_{24}-FAs to SPM, whereas brGDGT proxy values (BIT, #rings$_{tetra}$) are very comparable. One exception is the higher relative proportion of 6-methyl compared to 5-methyl brGDGT isomers in SPM (reflected in higher CBT' and slightly higher IR values) than in river sediments, suggesting a small additional aquatic

6-methyl brGDGT source in the river SPM (De Jonge et al., 2014b). On the other hand, corresponding MATmr and pH proxy values are only slightly higher for the SPM (0.8/1.6 °C, 0.3/0.2 pH units in 2013/2014, respectively), with these differences being well within the calibration uncertainty (errors: MATmr = 4.6 °C; pH = 0.5; De Jonge et al., 2014a). The broad similarity in brGDGT distributions is consistent with the finding of similar brGDGT distributions across different grain size classes in river sediments (Peterse and Eglinton, 2017).

Although the absolute concentration of TOC in SPM is higher than in river sediments, TOC may be comparable in SPM and river sediments when normalized to SA (Freymond et al., 2018). Although the limited sample sizes precluded SA determinations for Danube SPM, Bouchez et al. (2014) found that OC loadings on Amazon River SPM fall within a range typical for riverine suspended sediment (Blair and Aller, 2012). Assessments of loadings may therefore compensate for hydrological sorting processes during SPM deposition on (as well as erosion from) riverbanks.

Overall, taking into account all determined proxies as well as bulk and compound-specific stable and radiocarbon isotopes, we conclude that for a well-mixed large river such as the Danube close to its terminus, the composition of river sediments largely reflects the average SPM composition, albeit with some differences stemming from either hydrodynamic sorting or post-depositional degradation. Nevertheless, for accurate flux assessments, concentrations need to be measured on SPM samples given the significantly lower OC contents of river sediments.

5.5.3 Implications for OC export to the Black Sea

Taking into consideration that the Tulcea branch accounts for ~45% of the total Danube discharge, all fluxes were upscaled to 100% to derive fluxes for the entire river as it enters the delta. This results in a water discharge of 10,100/7,800 m^3/s (2013/2014, respectively), significantly above the average yearly discharge of 6,486 m^3/s in both years (Sommerwerk et al., 2009). In 2013, the discharge was close to the average annual flood discharge of 10,889 m^3/s. During these conditions, the total Danube is calculated to export 8/7 kg/s OC, 7/3 g/s LCFAs, 34/21 g/s SCFAs and 0.5/0.2 g/s brGDGTs (2013/2014, respectively, Supplementary Table A.5.1). Extrapolation of these instantaneous SPM fluxes to a yearly sediment discharge yields values of 16/12 Mt/yr of suspended sediment, which is close to the 18 Mt/yr estimated for the Danube (for 1985-2000) by Habersack et al. (2016).

Discharge-weighted SPM bulk $\delta^{13}C$ (-28.0/-27.6‰) and $\Delta^{14}C$ (-129/-38‰) values (Table 5.1) are respectively lower and higher than those of Black Sea surface sediments and coastal water SPM close to the outflow of the Sulina branch (Kusch et al., 2010; Saliot et al., 2002). Kusch et al. (2010) indicate that Black Sea sediment OC at 18 m water depth already comprises a substantial marine contribution, which is indicated by the lower BIT index (0.64) than for the Danube SPM (0.91/0.87 in 2013/2014,

respectively; Table 5.1). Also, the higher bulk $\delta^{13}C$ value (+2.1‰ on average) points towards a rapid marine overprint of the fluvial signal. Finally, higher bulk OC ages in the marine sediments are counter-intuitive but may be due to hydrological sorting and winnowing (Wakeham et al., 2009) and preferential accumulation of mineral-bound OC (soil or fossil OC) at the studied location (whereas fresh plant debris with lower density might be deposited further offshore) or to post-depositional (e.g., bioturbation) processes that vertically mix sediment of different ages. The discharge-weighted ^{14}C age of the LCFAs discharged in Danube SPM, which is similar for both years of sample collection (ave., 1,140 yr) is comparable to that in Black Sea surface sediments (FA n-$C_{26\text{-}30}$ = 1,649 yr; Kusch et al., 2010).

5.6 Conclusions

To our knowledge, this constitutes the first study that investigates cross-sectional variations in compound-specific stable and radiocarbon isotopic composition of SPM and reports corresponding estimates of biomarker discharge and discharge-weighted isotopic values.

Results show that Danube River SPM is well mixed with minor compositional changes with depth or across the river. Determining OC and biomarker fluxes from one point-sample compared to the picket fence approach would systematic biases of ±50% (Supplementary Figure A.5.8).

Comparing the discharge-weighted average composition of SPM to river sediments shows that lipid biomarker proxy values are generally similar. Therefore, although investigations spanning a broader range of fluvial systems are clearly needed, sampling of river sediments may serve as a convenient means to constrain the composition of suspended matter transported by river systems, including deriving detailed molecular isotopic signatures.

Ultimately, such constraints on fluvial fluxes of source-specific biomarkers associated with SPM may serve to establish quantitative links between OM production, export and burial at the molecular level.

Acknowledgements

This project was funded by the Swiss National Science Foundation SNF (“CAPS-LOCK” and “CAPS-LOCK2”; #200021_140850). We thank the sampling crews from both field campaigns (Björn Buggle, James Saenz, Alissa Zuijdgeest, Marilu Tavagna, Stefan Eugen Filip, Silvia Lavinia Filip, Mihai, Clayton Magill, Thomas Blattmann, Michael Albani), Daniel Montluçon for lab support and Hannah Gies for PCGC work.

References

Armijos, E., Crave, A., Espinoza, R., Fraizy, P., Dos Santos, A.L.M.R., Sampaio, F., De Oliveira, E., Santini, W., Martinez, J.M., Autin, P., Pantoja, N., Oliveira, M. and Filizola, N. (2017) Measuring and modeling vertical gradients in suspended sediments in the Solimoes/Amazon River. *Hydrological Processes* 31, 654–667.

Baldock, J.A. and Skjemstad, J. O. (2000) Role of the soil matrix and minerals in protecting natural organic materials against biological attack. *Organic Geochemistry* 31, 697–710.

Blair, N.E. and Aller, R.C. (2012) The Fate of Terrestrial Organic Carbon in the Marine Environment. *Annual Review of Marine Science* 4, 401–423.

Bouchez, J., Galy, V., Hilton, R.G., Gaillardet, J., Moreira-Turcq, P., Perez, M.A., France-Lanord, C. and Maurice, L. (2014) Source, transport and fluxes of Amazon River particulate organic carbon: Insights from river sediment depth-profiles. *Geochimica et Cosmochimica Acta* 133, 280–298.

Bouchez, J., Lupker, M., Gaillardet, J., France-Lanord, C. and Maurice, L. (2011) How important is it to integrate riverine suspended sediment chemical composition with depth? Clues from Amazon River depth-profiles. *Geochimica et Cosmochimica Acta* 75, 6955–6970.

Callede, J., Kosuth, P., Guyot, J.L. and Guimaraes, V. S. (2000) Discharge determination by Acoustic Doppler Current Profilers (ADCP): A moving bottom error correction method and its application on the River Amazon at Obidos. *Hydrological Sciences Journal* 45, 911–924.

Cathalot, C., Rabouille, C., Pastor, L., Deflandre, B., Viollier, E., Buscail, R., Gremare, A., Treignier, C. and Pruski, A. (2010) Temporal variability of carbon recycling in coastal sediments influenced by rivers: Assessing the impact of flood inputs in the Rhone River prodelta. *Biogeosciences* 7, 1187–1205.

Chen, C.I. (1991) Unified Theory on Power Laws for Flow Resistance. *Journal of Hydraulic Engineering* 117, 371–389.

Christl, M., Vockenhuber, C., Kubik, P.W., Wacker, L., Lachner, J., Alfimov, V. and Synal, H.A. (2013) The ETH Zurich AMS facilities: Performance parameters and reference materials. *Nuclear Instruments and Methods in Physics Research B* 294, 29–38.

De Jonge, C., Hopmans, E.C., Zell, C.I., Kim, J.H., Schouten, S. and Sinninghe Damsté, J.S. (2014a) Occurrence and abundance of 6-methyl branched glycerol dialkyl glycerol tetraethers in soils: Implications for palaeoclimate reconstruction. *Geochimica et Cosmochimica Acta* 141, 97–112.

De Jonge, C., Stadnitskaia, A., Hopmans, E.C., Cherkashov, G., Fedotov, A. and Sinninghe Damsté, J.S. (2014b) In situ produced branched glycerol dialkyl glycerol tetraethers in suspended particulate matter from the Yenisei River, Eastern Siberia. *Geochimica et Cosmochimica Acta* 125, 476–491.

Doetterl, S., Stevens, A., Six, J., Merckx, R., van Oost, K., Pinto, M.C., Casanova-Katny, A., Munoz, C., Boudin, M., Venegas, E.Z. and Boeckx, P. (2015) Soil carbon storage controlled by interactions between geochemistry and climate. *Nature Geoscience* 8, 780-783.

Eglinton, T.I., Aluwihare, L.I., Bauer, J.E., Druffel, E.R.M. and McNichol, A.P. (1996) Gas chromatographic isolation of individual compounds from complex matrices for radiocarbon dating. *Analytical Chemistry* 68, 904–912.

Eglinton, T.I. and Eglinton, G. (2008) Molecular proxies for paleoclimatology. *Earth and Planetary Science Letters* 275, 1–16.

Feng, X.J., Feakins, S.J., Liu, Z.G., Ponton, C., Wang, R.Z., Karkabi, E., Galy, V., Berelson, W.M., Nottingham, A.T., Meir, P. and West, A.J. (2016) Source to sink: Evolution of lignin composition in the Madre de Dios River system with connection to the Amazon basin and offshore. *Journal of Geophysical Research: Biogeosciences* 121, 1316–1338.

Freymond, C.V., Kündig, N., Stark, C., Peterse, F., Buggle, B., Lupker, M., Plötze, M., Blattmann, T.M., Filip, F., Giosan, L. and Eglinton, T.I. (2018) Evolution of biomolecular loadings along a major river system. *Geochimica et Cosmochimica Acta* 223, 389–404.

Freymond, C.V., Peterse, F., Fischer, L.V., Filip, F., Giosan, L. and Eglinton, T.I. (2017) Branched GDGT signals in fluvial sediments of the Danube River basin: Method comparison and longitudinal evolution. *Organic Geochemistry* 103, 88–96.

Galy, V., France-Lanord, C. and Lartiges, B. (2008) Loading and fate of particulate organic carbon from the Himalaya to the Ganga-Brahmaputra delta. *Geochimica et Cosmochimica Acta* 72, 1767–1787.

Galy, V., Peucker-Ehrenbrink, B. and Eglinton, T.I. (2015) Global carbon export from the terrestrial biosphere controlled by erosion. *Nature* 521, 204–207.

Goni, M.A., Cathey, M.W., Kim, Y.H. and Voulgaris, G. (2005) Fluxes and sources of suspended organic matter in an estuarine turbidity maximum region during low discharge conditions. *Estuarine Coastal and Shelf Science* 63, 683–700.

Guinoiseau, D., Bouchez, J., Gelabert, A., Louvat, P., Filizola, N. and Benedetti, M.F. (2016) The geochemical filter of large river confluences. *Chemical Geology* 441, 191–203.

Habersack, H., Hein, T., Stanica, A., Liska, I., Mair, R., Jager, E., Hauer, C. and Bradley, C. (2016) Challenges of river basin management: Current status of, and prospects for, the River Danube from a river engineering perspective. *Science of the Total Environment* 543, 828–845.

Hemingway, J.D., Schefuss, E., Spencer, R.G.M., Dinga, B.J., Eglinton, T.I., McIntyre, C. and Galy, V.V. (2017) Hydrologic controls on seasonal and inter-annual variability of Congo River particulate organic matter source and reservoir age. *Chemical Geology* 466, 454–465.

Hopmans, E.C., Schouten, S. and Sinninghe Damsté, J.S. (2016) The effect of improved chromatography on GDGT-based palaeoproxies. *Organic Geochemistry* 93, 1–6.

Keil, R.G. and Mayer, L.M. (2014) Mineral matrices and organic matter, in: Turekian, K.K. (Ed.), Treatise on geochemistry (second edition). Elsevier, Oxford, pp. 337-359.

Kusch, S., Rethemeyer, J., Schefuss, E. and Mollenhauer, G. (2010) Controls on the age of vascular plant biomarkers in Black Sea sediments. *Geochimica et Cosmochimica Acta* 74, 7031–7047.

Li, R.C., Fan, J., Xue, J.T. and Meyers, P.A. (2017) Effects of early diagenesis on molecular distributions and carbon isotopic compositions of leaf wax long chain biomarker n-alkanes: Comparison of two one-year-long burial experiments. *Organic Geochemistry* 104, 8–18.

Lupker, M., France-Lanord, C., Lave, J., Bouchez, J., Galy, V., Metivier, F., Gaillardet, J., Lartiges, B. and Mugnier, J.L. (2011) A Rouse-based method to integrate the chemical composition of river sediments: Application to the Ganga basin. *Journal of Geophysical Research: Earth Surface* 116.

McIntyre, C.P., Wacker, L., Haghipour, N., Blattmann, T.M., Fahrni, S., Usman, M., Eglinton, T.I. and Synal, H.-A. (2016) Online 13C and 14C Gas Measurements by EA-IRMS–AMS at ETH Zürich. *Radiocarbon*, 1–11.

Milliman, J. and Farnsworth, K. (2011) Runoff, erosion, and delivery to the coastal ocean, River discharge to the coastal ocean: A global synthesis. Cambridge University Press, Cambridge.

Muste, M., Yu, K. and Spasojevic, M. (2004) Practical aspects of ADCP data use for quantification of mean river flow characteristics; Part 1: moving-vessel measurements. *Flow Measurement and Instrumentation 15*, 1–16.

Parsons, D.R., Jackson, P.R., Czuba, J.A., Engel, F.L., Rhoads, B.L., Oberg, K.A., Best, J.L., Mueller, D.S., Johnson, K.K. and Riley, J.D. (2013) Velocity Mapping Toolbox (VMT): A processing and visualization suite for moving-vessel ADCP measurements. *Earth Surface Processes and Landforms* 38, 1244–1260.

Peterse, F. and Eglinton, T.I. (2017) Grain size associations of branched tetraether lipids in soils and riverbank sediments: Influence of hydrodynamic sorting processes. *Frontiers in Earth Science* 5.

Peterse, F., van der Meer, J., Schouten, S., Weijers, J.W.H., Fierer, N., Jackson, R.B., Kim, J.H. and Sinninghe Damsté, J.S. (2012) Revised calibration of the MBT-CBT paleotemperature proxy based on branched tetraether membrane lipids in surface soils. *Geochimica et Cosmochimica Acta* 96, 215–229.

R Core Team (2014) R: A language and environment for statistical computing. R Foundation for Statistical Computing, Vienna, Austria.

Rosenheim, B.E., Roe, K.M., Roberts, B.J., Kolker, A.S., Allison, M.A. and Johannesson, K.H. (2013) River discharge influences on particulate organic carbon age structure in the Mississippi/Atchafalaya River System. *Global Biogeochemical Cycles* 27, 154–166.

Saliot, A., Parrish, C.C., Sadouni, N., Bouloubassi, L., Fillaux, J. and Cauwet, G. (2002) Transport and fate of Danube Delta terrestrial organic matter in the Northwest Black Sea mixing zone. *Marine Chemistry* 79, 243–259.

Schiller, H., Miklós, D. and Sass, J. (2010) The Danube River and its basin physical characteristics, water regime and water balance, in: Mitja B. (Ed.), Hydrological processes of the Danube River basin. Perspectives from the Danubian Countries. Springer, Dordrecht, Netherlands, pp. 25–77.

Schouten, S., Hopmans, E.C. and Sinninghe Damsté, J.S. (2013) The organic geochemistry of glycerol dialkyl glycerol tetraether lipids: A review. *Organic Geochemistry* 54, 19–61.

Sommerwerk, N., Hein, T., Schneider-Jacoby, M., Baumgartner, C., Ostojic, A., Sieber, R., Bloesch, J., Paunovic, M. and Tockner, K. (2009) The Danube River basin, in: Tockner, K., Robinson, C.T., Uehlinger, U. (Eds.), Rivers of Europe. Elsevier Science, London, UK, pp. 59–112.

Sternström, K.E., Skog, G., Georgiadou, E., Genberg, J. and Johansson, A. (2011) A guide to radiocarbon units and calculations. Lund University.

Synal, H.A., Stocker, M. and Suter, M. (2007) MICADAS: A new compact radiocarbon AMS system. *Nuclear Instruments and Methods in Physics Research B* 259, 7–13.

Tao, S.Q., Eglinton, T.I., Montluçon, D.B., McIntyre, C. and Zhao, M.X. (2015) Pre-aged soil organic carbon as a major component of the Yellow River suspended load: Regional significance and global relevance. *Earth and Planetary Science Letters* 414, 77–86.

Tao, S.Q., Eglinton, T.I., Zhang, L., Yi, Z., Montluçon, D., McIntyre, C., Yu, M. and Zhao, M.X. (2017) Temporal variability in composition and fluxes of Yellow River particulate organic matter. *Limnology and Oceanography*.

Tierney, J.E. and Russell, J.M. (2009) Distributions of branched GDGTs in a tropical lake system: Implications for lacustrine application of the MBT/CBT paleoproxy. *Organic Geochemistry* 40, 1032–1036.

Torica, V. (2006) Physiography and climate, in: Tudorancea, C., Tudorancea, M.M. (Eds.), Danube delta: genesis and biodiversity. Backhuys, Leiden, Netherlands.

van der Voort, T.S., Zell, C.I., Hagedorn, F., Feng, X., McIntyre, C.P., Haghipour, N., Graf-Pannatier, E. and Eglinton, T.I. (2017) Diverse soil carbon dynamics expressed at the molecular level. *Geophysical Research Letters*.

Wakeham, S.G., Canuel, E.A., Lerberg, E.J., Mason, P., Sampere, T.P. and Bianchi, T.S. (2009) Partitioning of organic matter in continental margin sediments among density fractions. *Marine Chemistry* 115, 211–225.

Wang, X.X., Huang, X.Y., Sachse, D., Hu, Y., Xue, J.T. and Meyers, P.A. (2016) Comparisons of lipid molecular and carbon isotopic compositions in two particle-size fractions from surface peat and their implications for lipid preservation. *Environmental Earth Sciences* 75.

Weber, Y., De Jonge, C., Rijpstra, W.I.C., Hopmans, E.C., Stadnitskaia, A., Schubert, C.J., Lehmann, M.F., Sinninghe Damsté, J.S. and Niemann, H. (2015) Identification and carbon isotope composition of a novel branched GDGT isomer in lake sediments: Evidence for lacustrine branched GDGT production. *Geochimica et Cosmochimica Acta* 154, 118–129.

Weijers, J.W.H., Schouten, S., van den Donker, J.C., Hopmans, E.C. and Sinninghe Damsté, J.S. (2007) Environmental controls on bacterial tetraether membrane lipid distribution in soils. *Geochimica et Cosmochimica Acta* 71, 703–713.

Zell, C., Kim, J.H., Balsinha, M., Dorhout, D., Fernandes, C., Baas, M. and Sinninghe Damsté, J.S. (2014) Transport of branched tetraether lipids from the Tagus River basin to the coastal ocean of the Portuguese margin: Consequences for the interpretation of the MBT'/CBT paleothermometer. *Biogeosciences* 11, 5637–5655.

Appendix A.5 Supplementary information

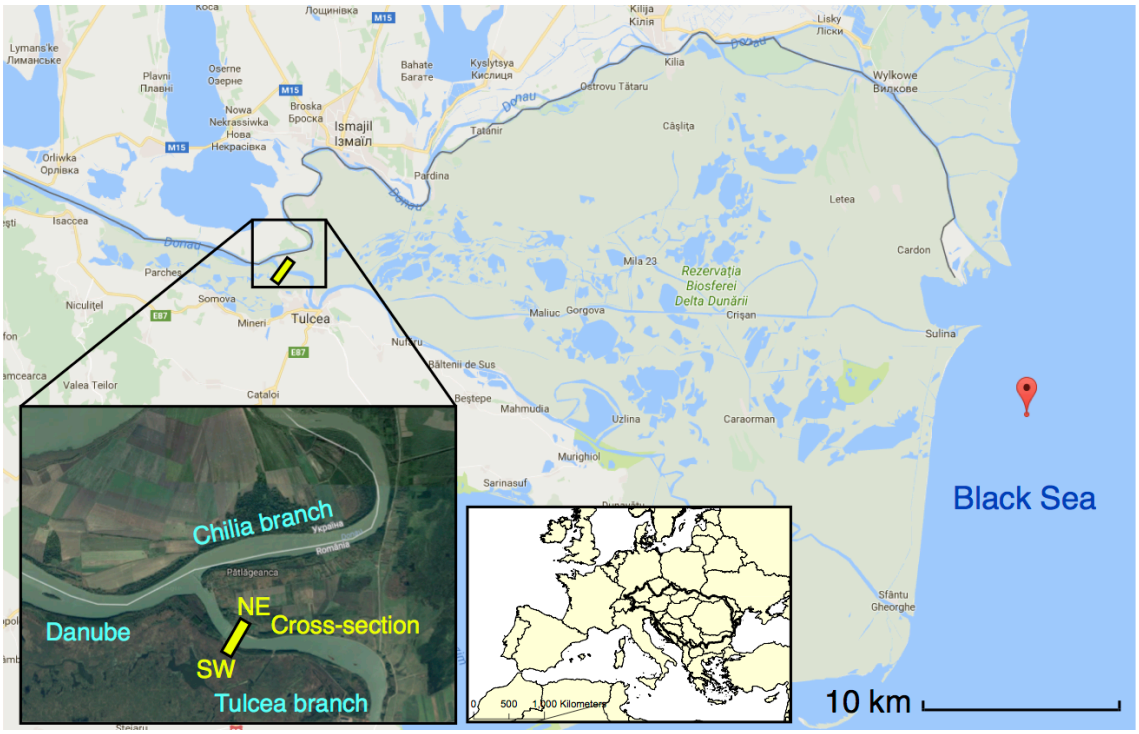

Figure A.5.1. Danube delta overview. The location of the river cross-section upstream of the city of Tulcea is marked with a yellow bar (N 45°12'56", E 28°45'18"). The red mark shows the Black Sea surface sediment location from Kusch et al. (2010). Source: Google.

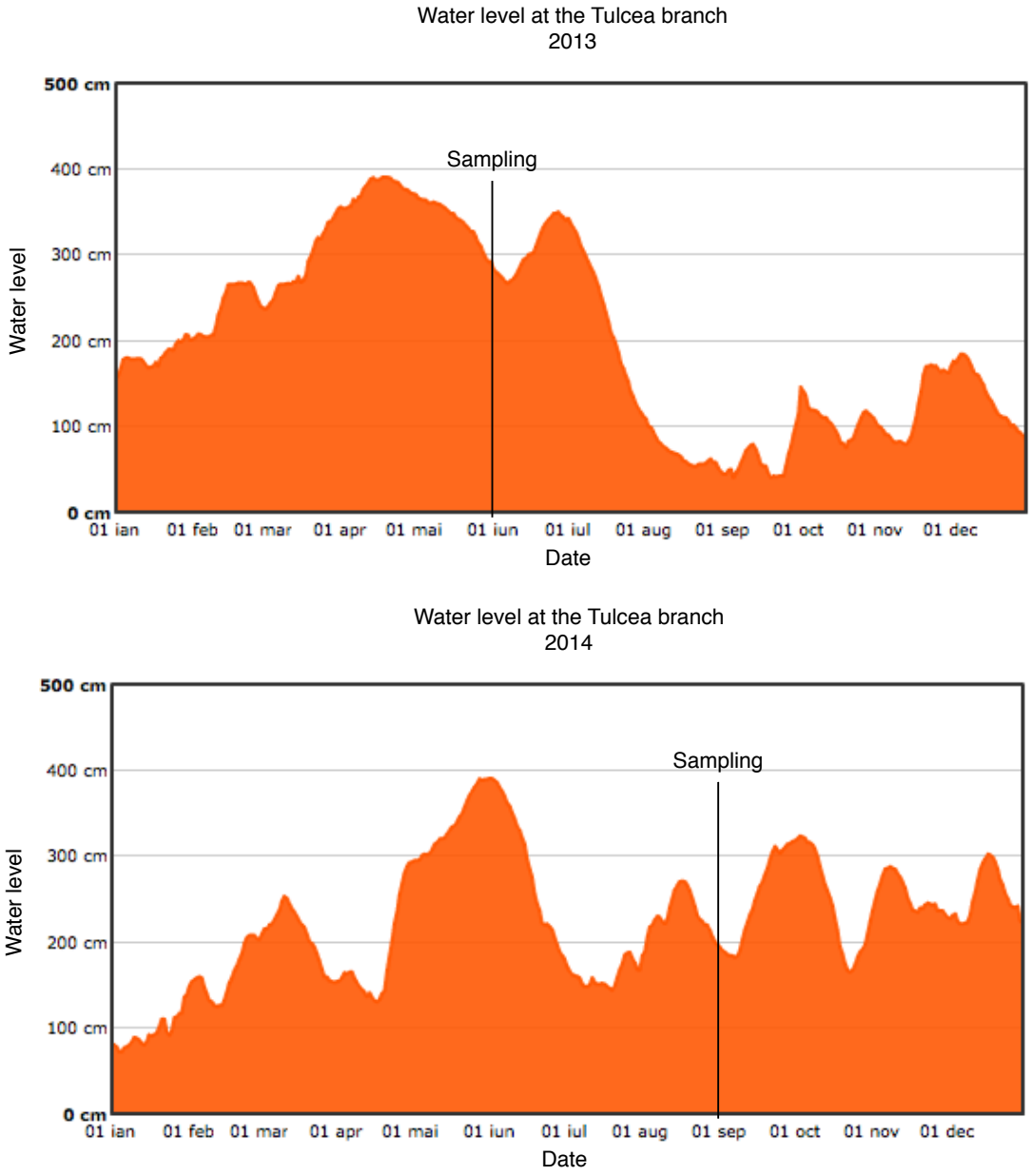

Figure A.5.2. Water level at the Tulcea branch in 2013 and 2014, measured at Tulcea city. The time of sampling is marked with black bars. Source: http://www.ghiduldelteidunarii.ro/cotele-apelor-dunarii-la-tulcea/.

Equations A.5.1: Proxy calculation

(1) $ACL_{C24\text{-}32} = \sum ([FA\ C24] \times 24 + \ldots + [FA\ C32] \times 32) / \sum ([FA\ C24] + \ldots + [FA\ C32])$

(2) $BIT = (IIIa + IIIa' + IIa + IIa' + Ia) / (IIIa + IIIa' + IIa + IIa' + Ia + Cren)$

(3) $MBT' = (Ia + Ib + Ic) / (Ia + Ib + Ic + IIa + IIb + IIc + IIIa)$

(4) $rel\text{-}x = x / (Ia + Ib + Ic + IIa + IIa' + IIb + IIb' + IIc + IIc' + IIIa + IIIa' + IIIb + IIIb' + IIIc + IIIc')$, x stands for one of the brGDGTs

(5) $CBT' = \log_{10}[(rel\text{-}Ic + rel\text{-}IIa' + rel\text{-}IIb' + rel\text{-}IIc' + rel\text{-}IIIa' + rel\text{-}IIIb' + rel\text{-}IIIc') / (rel\text{-}Ia + rel\text{-}IIa + rel\text{-}IIIa)]$

(6) $MAT_{mr} = 7.17 + (17.1 \times rel\text{-}Ia) + (25.9 \times rel\text{-}Ib) + (34.4 \times rel\text{-}Ic) - (28.6 \times rel\text{-}IIa)$

(7) $pH = 7.15 + 1.59 \times CBT'$

(8) $IR = (IIa'+b'+c' + IIIa'+b'+c') / (IIa+b+c + IIIa+b+c + IIa'+b'+c' + IIIa'+b'+c')$

(9) $\#rings_{tetra} = (rel\text{-}Ib + 2 \times rel\text{-}Ic) / (rel\text{-}Ia + rel\text{-}Ib + rel\text{-}Ic)$

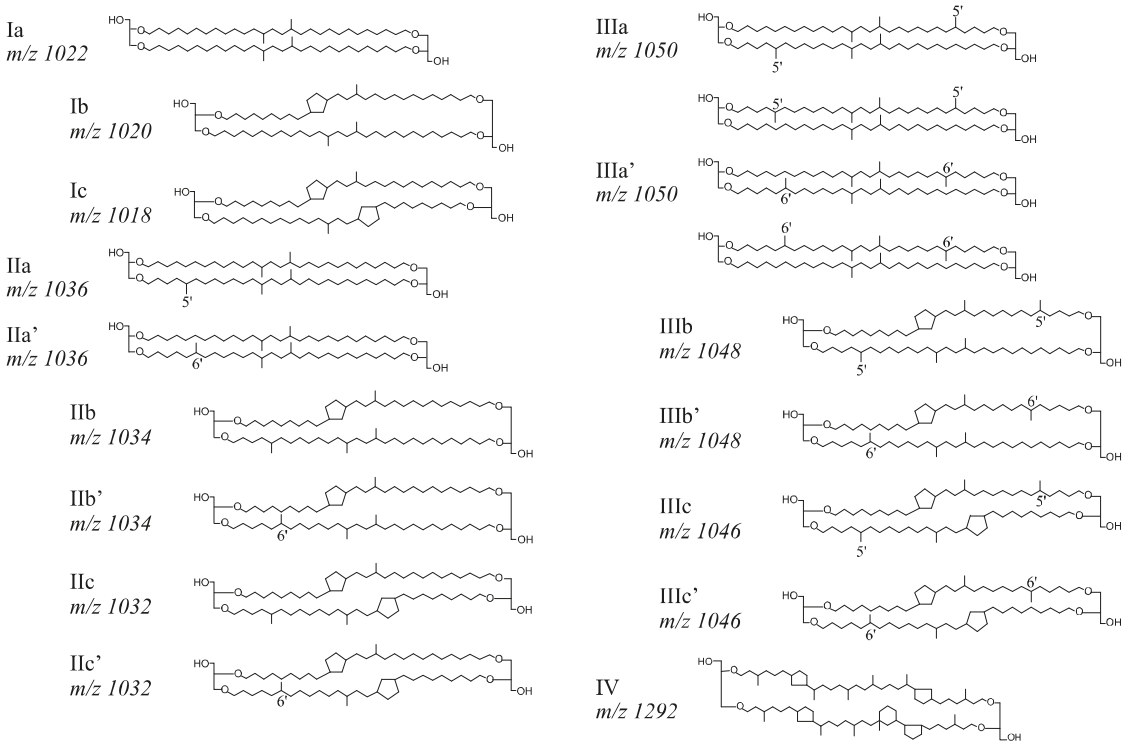

Figure A.5.3. Molecular structure of branched an isoprenoid GDGTs (De Jonge et al., 2014)).

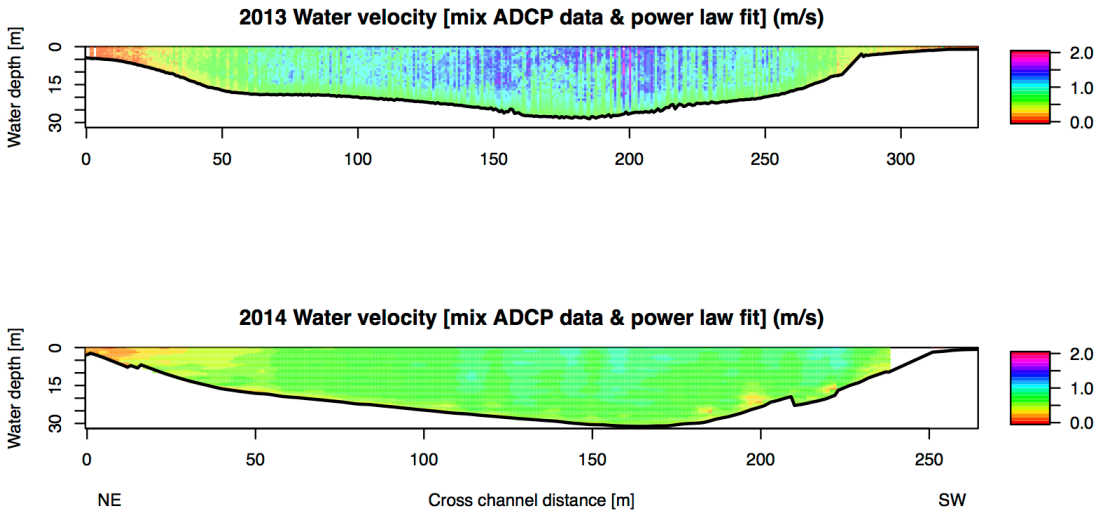

Figure A.5.4. Water velocity profiles based on ADCP data in 2013 and 2014. Missing ensembles were filled with the average of neighboring cells. Empty cells at the top of the profiles and close to the bottom were extrapolated with a power law fit.

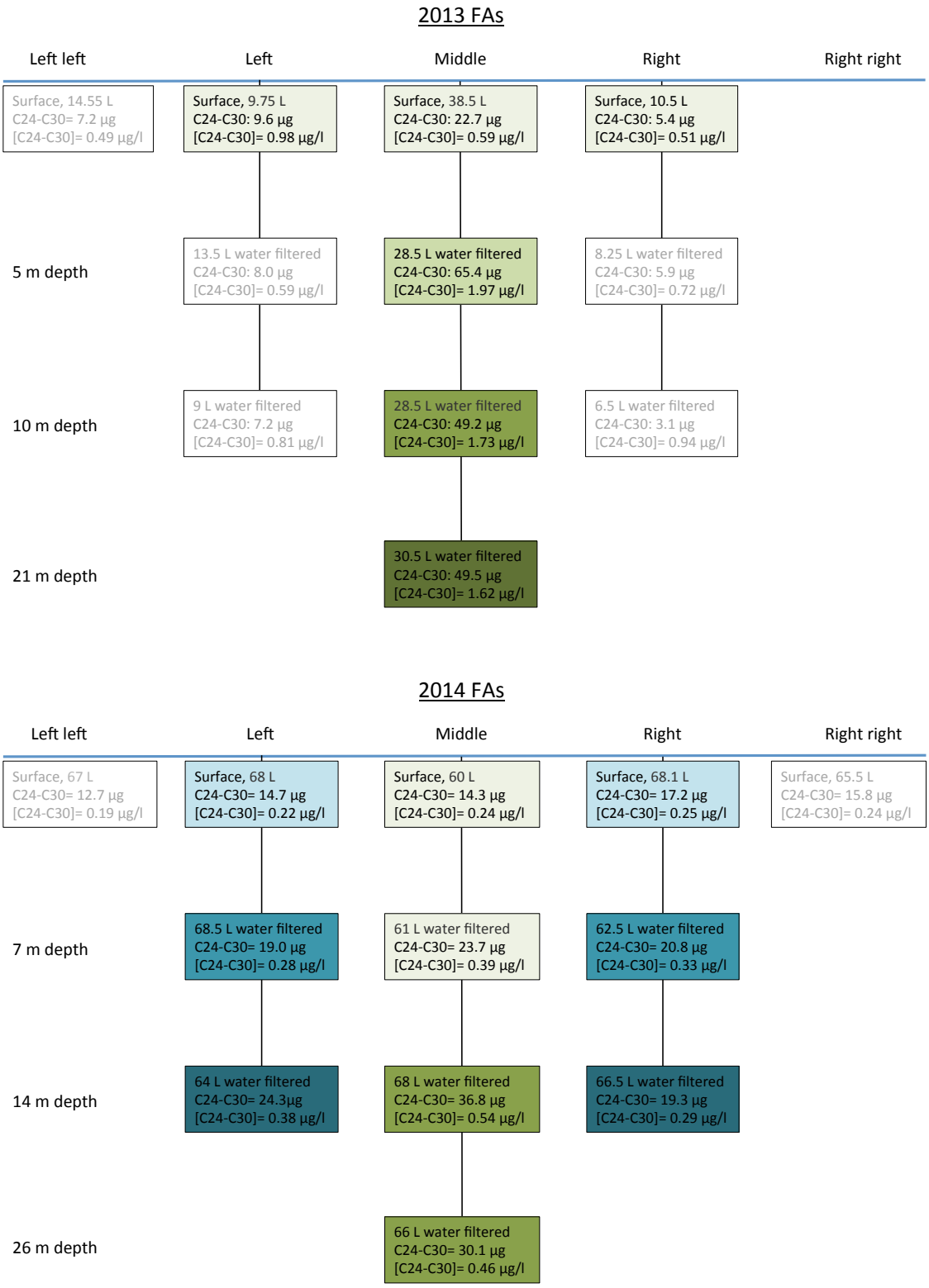

Figure A.5.5. Scheme of the samples for compound-specific fatty acid ^{14}C measurement in 2013 in the top panel and 2014 in the lower panel. Point samples with the same color were combined to result in large enough samples for subsequent separation and ^{14}C measurement.

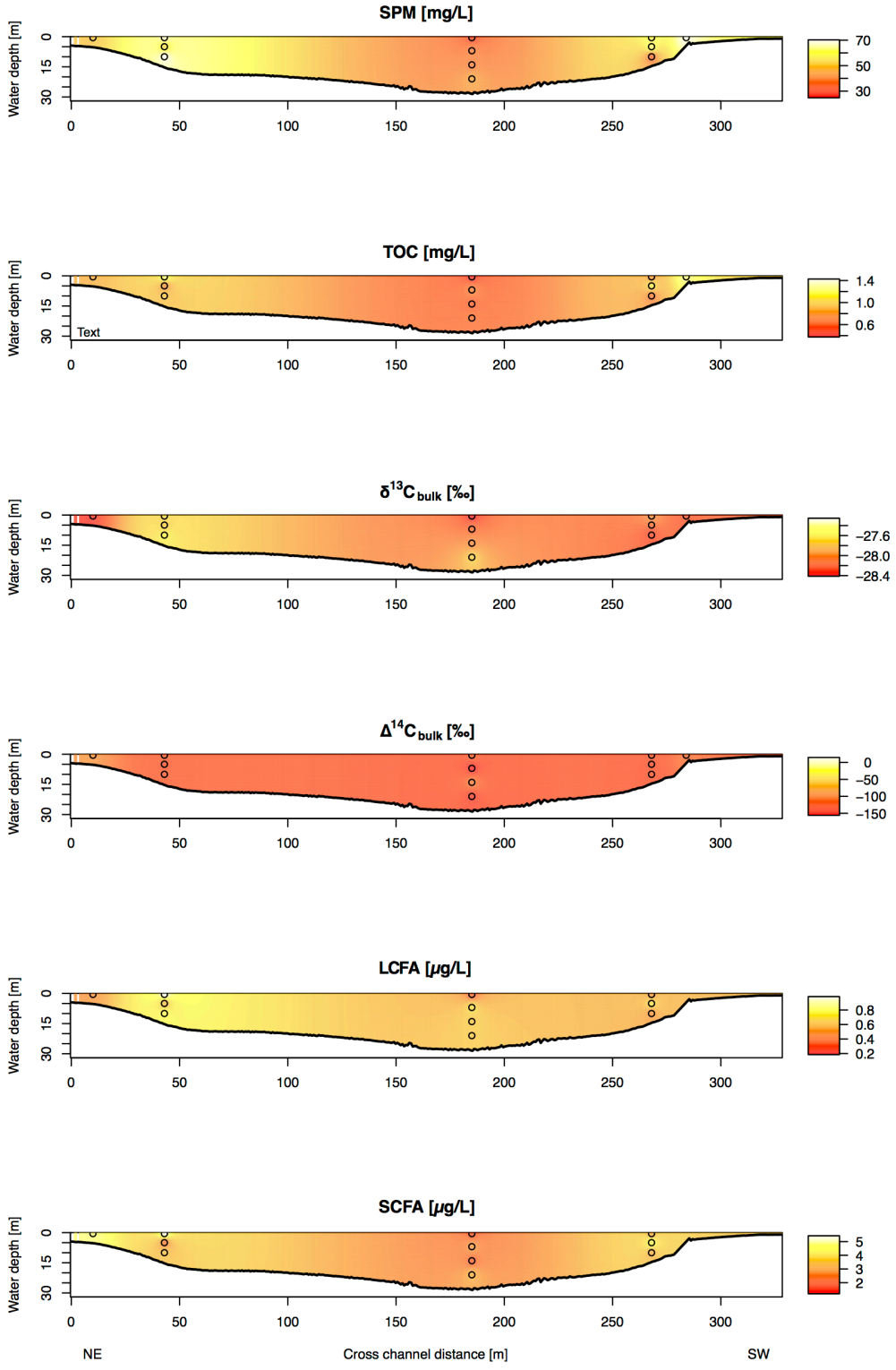

Figure A.5.6. Extrapolated SPM, TOC and biomarker concentrations and proxy values in 2013. The black circles show the locations of the point water sampling.

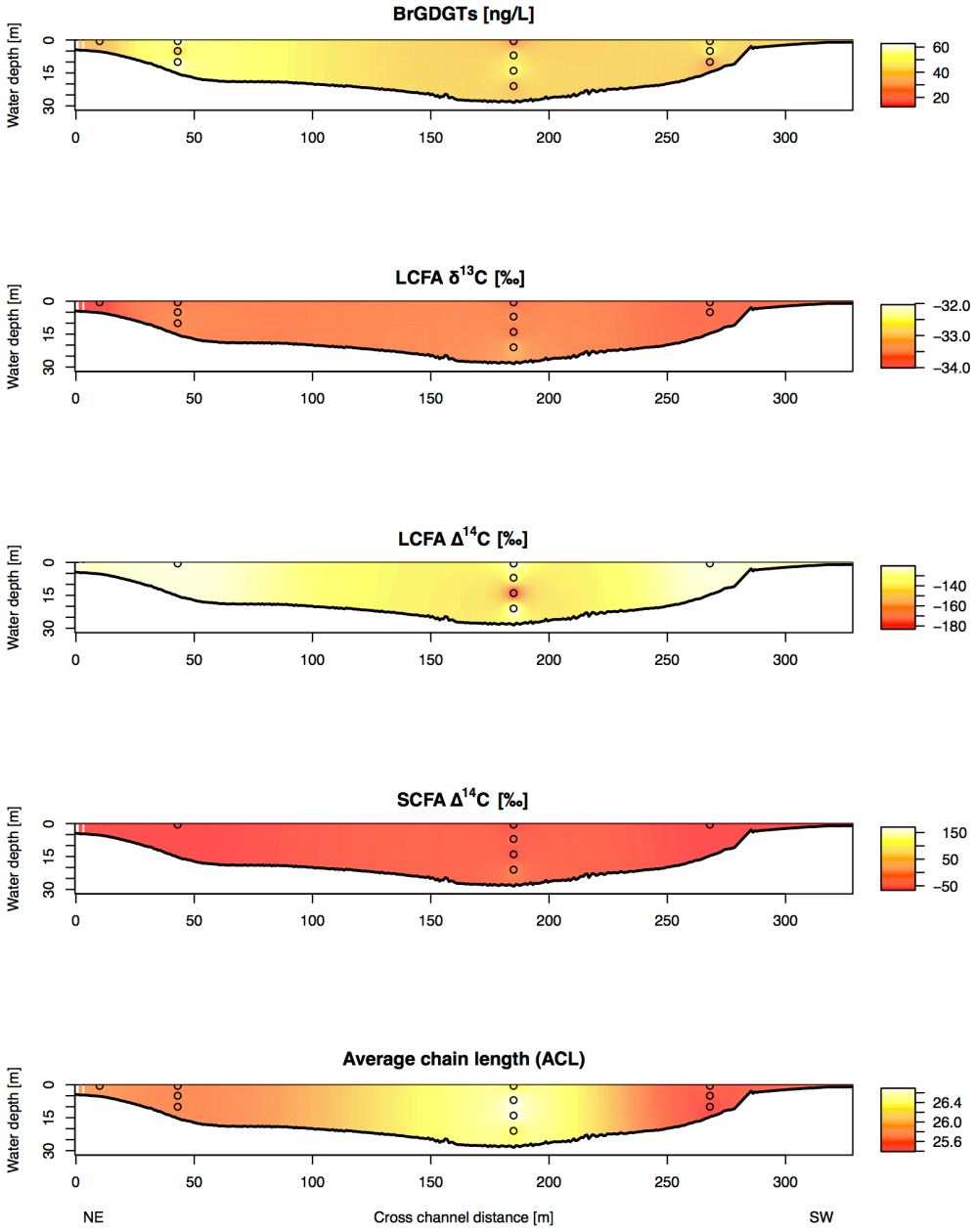

Figure A.5.6. Continued

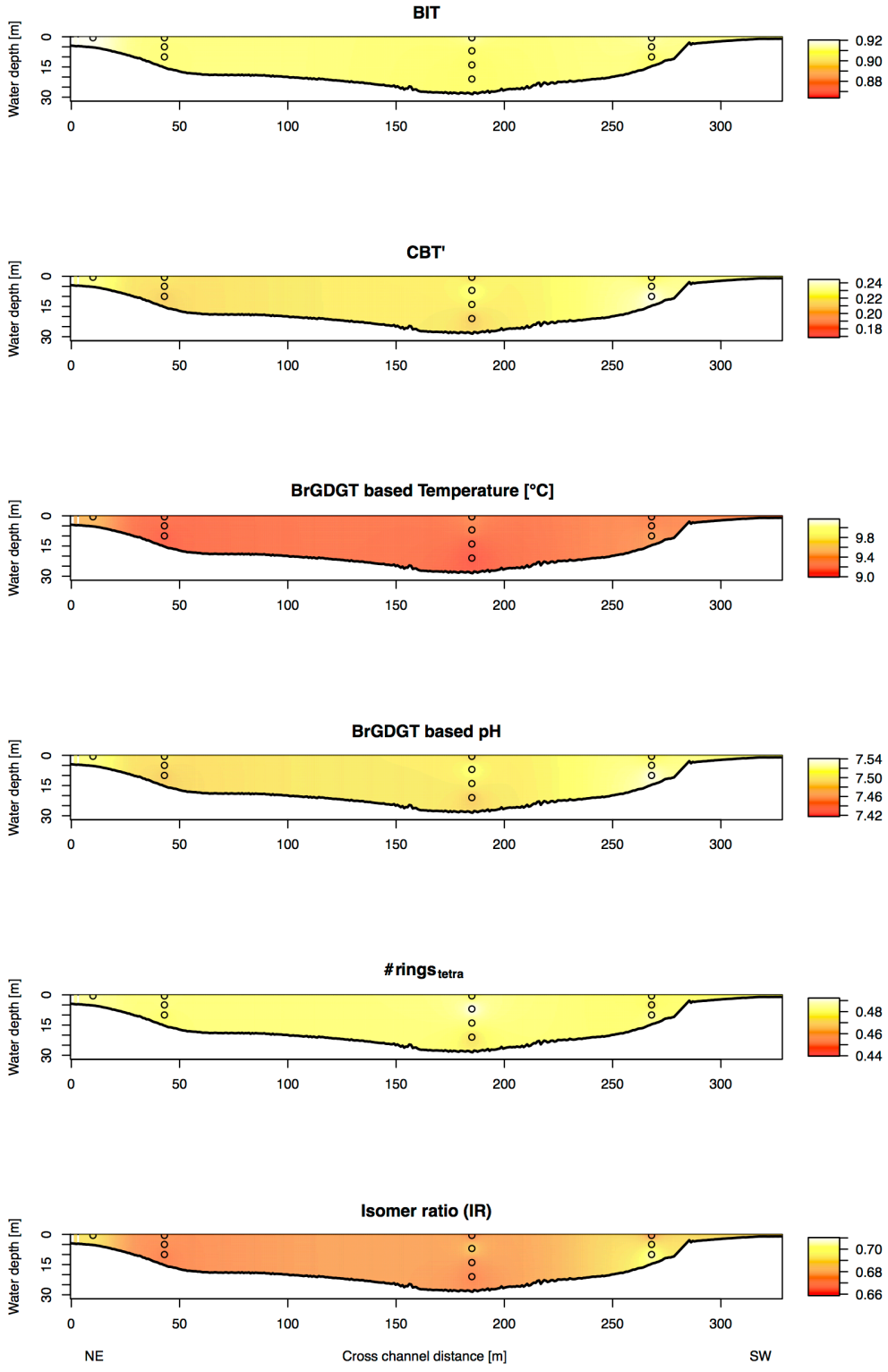

Figure A.5.6. Continued

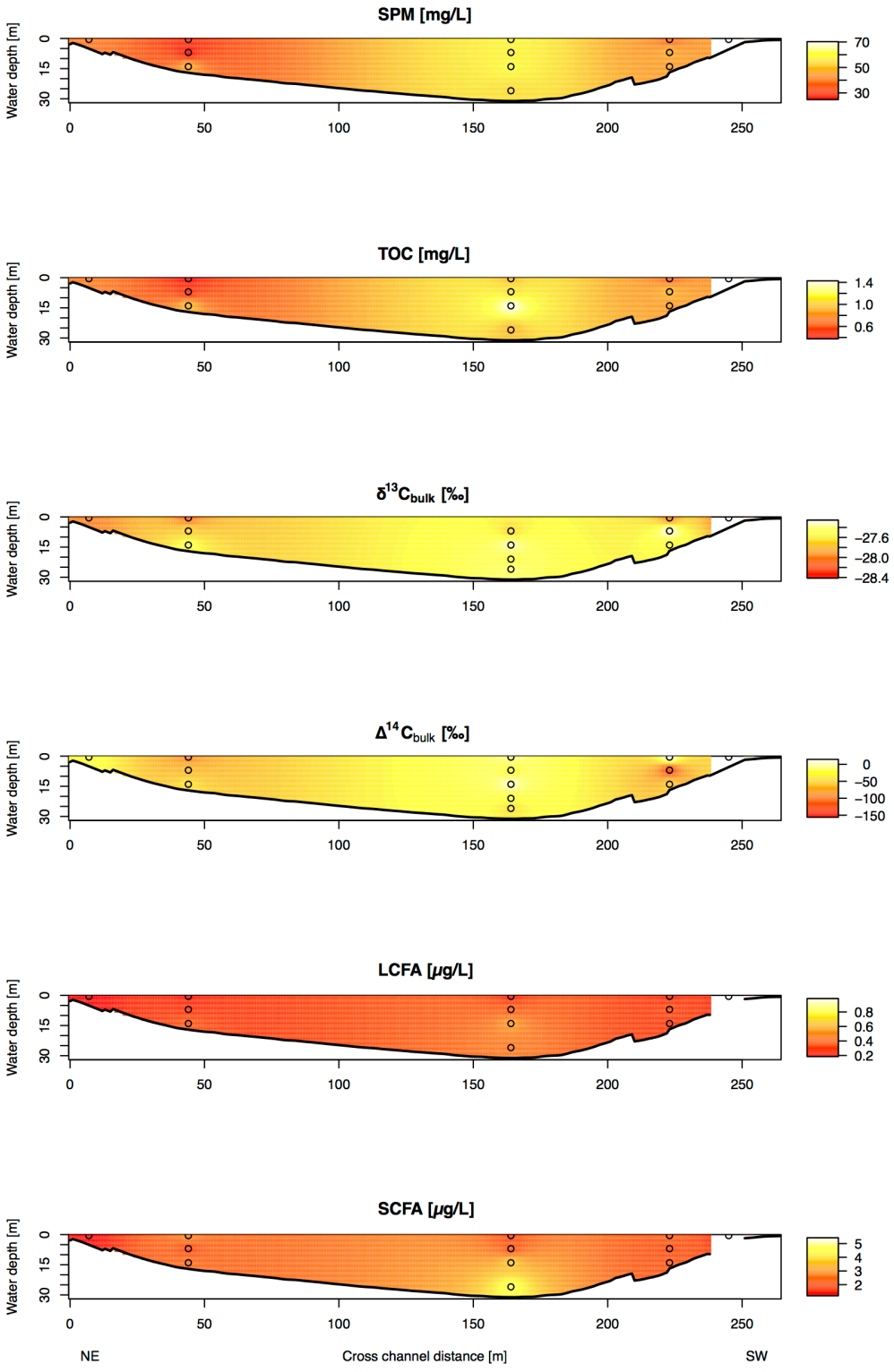

Figure A.5.7. Extrapolated SPM, TOC and biomarker concentrations and proxy values in 2014. The black circles show the locations of the point water sampling.

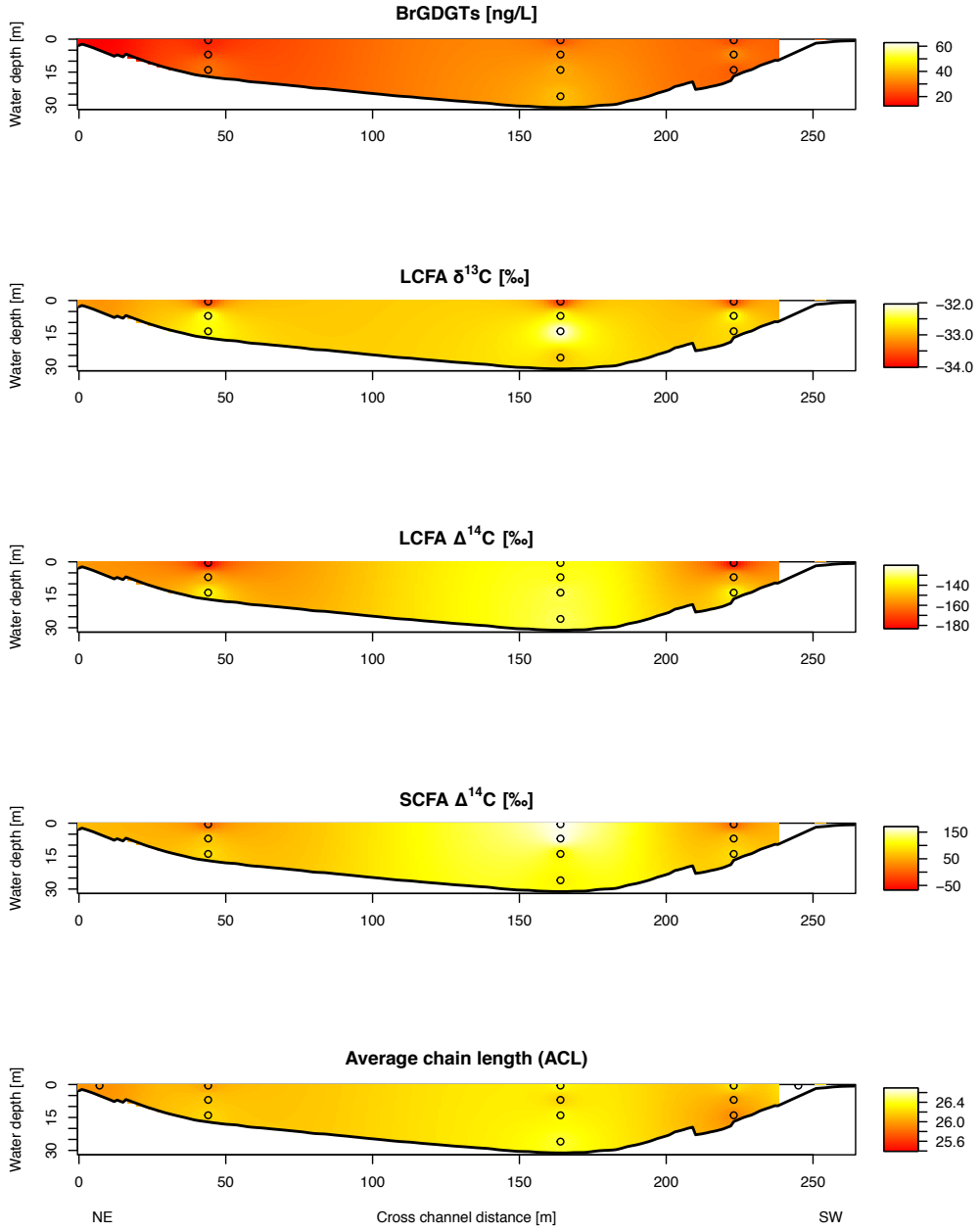

Figure A.5.7. Continued

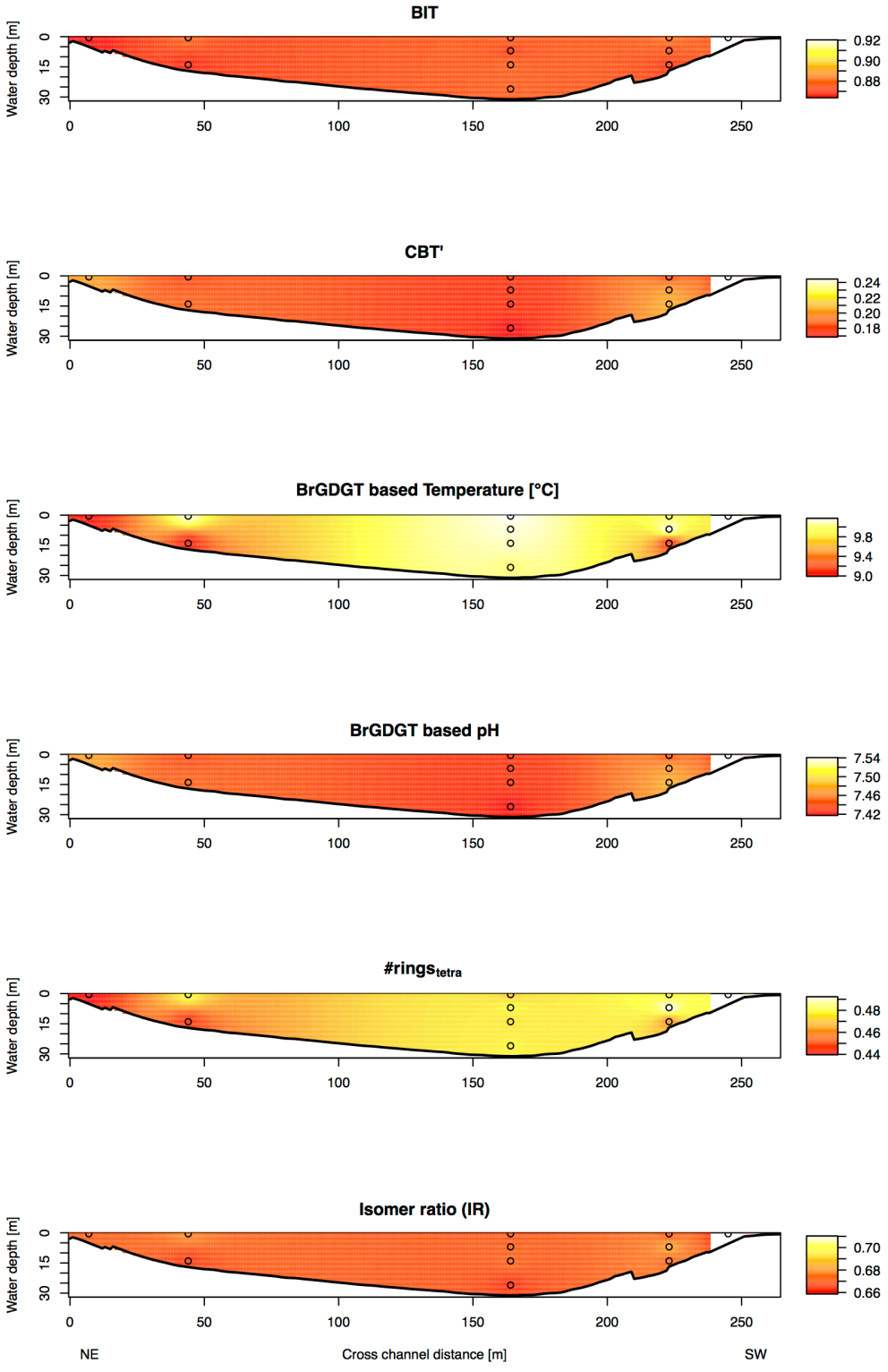

Figure A.5.7. Continued

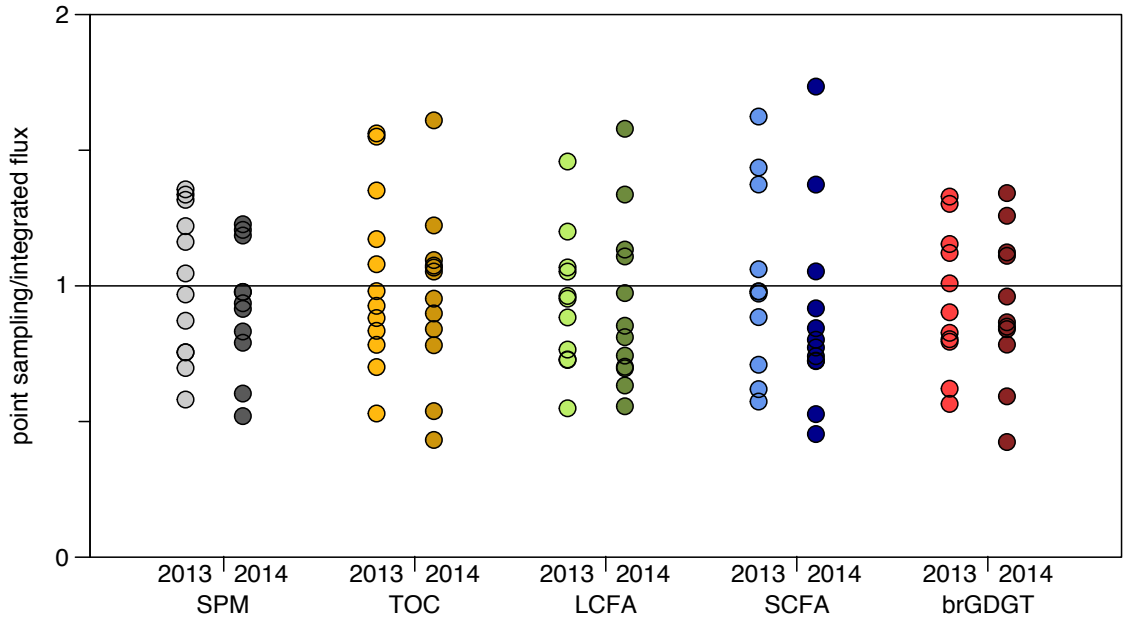

Figure A.5.8. Comparison of SPM, TOC and biomarker fluxes derived from point water sampling and picket fence sampling. The concentrations from every single sampling location in the depth profiles were used to calculate the corresponding flux by multiplying the concentration in this sample by water discharge. Subsequently, these fluxes were normalized to the extrapolated and discharge weighted fluxes derived from the depth profiles. The line at y=1 indicates the value where the fluxes derived from point sampling and the integrated fluxes result in the same value.

Table A.5.1. Water, suspended particulate TOC and biomarker fluxes in the Tulcea arm and extrapolated to the total Danube in 2013 and 2014.

	River cross section SPM		Total Danube	
	2013	2014	2013	2014
Water discharge [m^3/s]	4,538	3,511	10,084	7,802
SPM [kg/s]	234.3	168.8	521	375
TOC [kg/s]	3.7	3.1	8	7
LCFA [g/s]	3.1	1.2	7	3
SCFA [g/s]	15.1	9.4	34	21
BrGDGTs [mg/s]	214	106	476	236

Reference

De Jonge, C., Hopmans, E.C., Zell, C.I., Kim, J.H., Schouten, S. and Sinninghe Damsté, J.S. (2014) Occurrence and abundance of 6-methyl branched glycerol dialkyl glycerol tetraethers in soils: Implications for palaeoclimate reconstruction. *Geochimica et Cosmochimica Acta* 141, 97–112.

Appendix B.5 Data tables

Table B.5.1. Bulk characteristics of SPM in depth profiles from 2013 and 2014.

year	profile	depth [m]	dist. left shore [m]	total water depth [m]	TSS [mg/L]	TOC [%]	$\delta^{13}C$ bulk [‰]	$\Delta^{14}C$ bulk [‰]	$\Delta^{14}C$ ± [‰]	^{14}C Age [yr]	Age ± [yr]
2013	right right	0.5	290	5	69	1.85	-28.24	-113	11	896.18	102.50
2013	left left	0.5	10	5	50	1.78	-28.37	-90	13	692.63	112.26
2013	right	0.5	268	15	60	1.34	-28.00	-128	12	1036.53	112.54
2013	right	5	268	15	63	1.76	-36.34	-135	12	1100.58	108.98
2013	right	10	268	15	36	1.90	-28.28	-134	14	1087.99	129.28
2013	left	0.5	43	15	68	1.89	-27.67	-123	9	990.77	84.89
2013	left	5	43	15	54	1.41	-27.73	-133	14	1079.11	130.16
2013	left	10	43	15	70	1.38	-27.57	-127	16	1026.48	150.38
2013	middle	0.5	185	28	30	1.45	-28.41	-122	11	983.47	96.78
2013	middle	7	185	28	39	1.86	-28.14	-155	10	1289.77	94.35
2013	middle	14	185	28	39	1.48	-28.00	-103	10	810.82	92.19
2013	middle	21	185	28	45	1.43	-27.71	-145	10	1192.45	95.10
2014	right right	0.5	245	5	44	1.80	-28.09	-50	19	351.04	164.53
2014	left left	0.5	7	5	40	1.86	-27.99	-23	22	123.92	178.31
2014	right	0.5	223	17	38	1.82	-27.96	14	14	-175.47	107.69
2014	right	7	223	17	47	1.98	-27.27	-127	10	1026.27	95.77
2014	right	14	223	17	45	1.87	-27.55	-56	13	400.57	106.75
2014	left	0.5	44	17	29	1.32	-28.05	-89	12	685.53	108.15
2014	left	7	44	17	25	1.90	-27.70	-64	12	463.39	106.78
2014	left	14	44	17	47	2.02	-27.47	-43	12	285.43	99.54
2014	middle	0.5	164	32	58	1.67	-19.14	-6	11	-20.55	90.78
2014	middle	7	164	32	57	1.89	-27.67	-28	12	165.08	101.79
2014	middle	14	164	32	59	2.41	-27.34	5	11	-106.84	84.95
2014	middle	21	164	32		1.47	-27.52	-25	10	136.39	86.10
2014	middle	26	164	32	54	1.75	-27.43	-43	11	285.39	89.60

Table B.5.2. FA concentrations (single compounds and sum of n-C24-32) and average chain length (ACL) of SPM in depth profiles.

year	profile	depth [m]	FA n-C_{16} [µg/L]	FA n-C_{18} [µg/L]	FA n-C_{20} [µg/L]	FA n-C_{22} [µg/L]	FA n-C_{24} [µg/L]	FA n-C_{26} [µg/L]	FA n-C_{28} [µg/L]	FA n-C_{30} [µg/L]	FA n-C_{32} [µg/L]	FA n-C_{24-32} [µg/L]	ACL
2013	left left	0.5	4.26	0.52	0.10	0.18	0.22	0.15	0.09	0.03	0.01	0.50	25.84
2013	right	0.5	2.80	0.45	0.11	0.20	0.25	0.17	0.08	0.02	0.01	0.52	25.52
2013	right	5	3.88	0.70	0.16	0.28	0.37	0.23	0.10	0.02	0.01	0.73	25.45
2013	right	10	2.75	0.48	0.11	0.19	0.25	0.15	0.07	0.01	0.00	0.49	25.40
2013	left	0.5	4.68	0.73	0.19	0.35	0.46	0.31	0.16	0.05	0.02	1.00	25.77
2013	left	5	1.93	0.43	0.11	0.20	0.27	0.19	0.11	0.03	0.01	0.60	25.72
2013	left	10	2.90	0.63	0.15	0.27	0.36	0.26	0.15	0.04	0.01	0.82	25.73
2013	middle	0.5	1.62	0.29	0.06	0.11	0.15	0.10	0.08	0.04	0.02	0.39	26.35
2013	middle	7	2.46	0.48	0.11	0.19	0.25	0.19	0.17	0.10	0.05	0.75	26.67
2013	middle	14	1.66	0.40	0.10	0.18	0.24	0.17	0.15	0.09	0.05	0.69	26.69
2013	middle	21	2.58	0.68	0.12	0.21	0.26	0.17	0.13	0.08	0.04	0.68	26.38
2014	right right	0.5	1.20	0.22	0.04	0.07	0.10	0.07	0.05	0.03	0.01	0.25	26.31
2014	left left	0.5	1.05	0.16	0.03	0.05	0.08	0.06	0.04	0.01	0.00	0.19	25.95
2014	right	0.5	2.00	0.26	0.05	0.07	0.10	0.08	0.06	0.02	0.01	0.26	26.27
2014	right	7	1.58	0.40	0.06	0.09	0.15	0.10	0.06	0.03	0.01	0.34	26.02
2014	right	14	1.63	0.51	0.06	0.08	0.13	0.09	0.06	0.02	0.01	0.30	25.93
2014	left	0.5	2.56	0.26	0.04	0.07	0.09	0.07	0.04	0.02	0.01	0.22	26.02
2014	left	7	1.61	0.33	0.05	0.08	0.12	0.08	0.05	0.03	0.01	0.29	26.16
2014	left	14	2.05	0.41	0.07	0.10	0.16	0.11	0.07	0.04	0.02	0.40	26.21
2014	middle	0.5	1.67	0.27	0.04	0.07	0.10	0.07	0.05	0.03	0.01	0.25	26.35
2014	middle	7	1.71	0.36	0.07	0.10	0.16	0.11	0.08	0.04	0.02	0.40	26.19
2014	middle	14	3.04	0.64	0.11	0.15	0.22	0.15	0.11	0.06	0.03	0.57	26.35
2014	middle	26	3.71	0.94	0.09	0.12	0.18	0.13	0.10	0.05	0.02	0.48	26.43

Table B.5.3. Compound-specific $\delta^{13}C$ of long chain (n-C_{24-30}) fatty acids in depth profile SPM. The average value is the concentration weighted average of n-C_{24-30}.

year	profile	depth [m]	FA $\delta^{13}C$ n-C_{24} [‰]	FA $\delta^{13}C$ n-C_{24} Stdv	FA $\delta^{13}C$ n-C_{26} [‰]	FA $\delta^{13}C$ n-C_{26} Stdv	FA $\delta^{13}C$ n-C_{28} [‰]	FA $\delta^{13}C$ n-C_{28} Stdv	FA $\delta^{13}C$ n-C_{30} [‰]	FA $\delta^{13}C$ n-C_{30} Stdv	Average FA $\delta^{13}C$ n-C_{24-30} [‰]	Average FA $\delta^{13}C$ n-C_{24-30} Stdv
2013	left left	0.5	-33.1	0.03	-34.1	0.01	-36.0	0.48	-34.1	0.06	-34.0	0.49
2013	right	0.5	-33.1	0.48	-33.8	0.27	-35.5	0.06	-34.1	0.05	-33.7	0.55
2013	right	5	-32.9	0.03	-34.1	0.07	-36.0	0.23	-34.1	0.22	-33.8	0.33
2013	right	10										
2013	left	0.5	-32.9	0.01	-33.7	0.09	-35.8	0.06	-34.1	0.06	-33.7	0.12
2013	left	5	-32.4	0.06	-33.4	0.08	-35.6	0.21	-34.1	0.01	-33.4	0.23
2013	left	10	-32.5	0.01	-33.4	0.01	-35.9	0.15	-34.0	0.09	-33.5	0.17
2013	middle	0.5	-32.9	0.04	-33.7	0.02	-35.3	0.62	-34.1	0.18	-33.7	0.65
2013	middle	7	-32.7	0.37	-33.3	0.01	-34.5	0.06	-33.6	0.07	-33.4	0.39
2013	middle	14	-32.7	0.24	-33.5	0.12	-35.1	0.03	-34.0	0.04	-33.7	0.27
2013	middle	21	-32.1	0.02	-33.0	0.02	-34.8	0.07	-33.8	0.34	-33.1	0.35
2014	right right	0.5	-32.0	0.19	-32.7	0.04	-35.3	0.03	-33.8	0.02	-33.1	0.20
2014	left left	0.5	-32.1	0.08	-32.6	0.10	-35.5	0.45	-34.2	0.08	-33.1	0.47
2014	right	0.5	-32.9	0.17	-33.3	0.19	-35.2	0.12	-33.6	0.24	-33.6	0.37
2014	right	7	-31.3	0.04	-32.7	0.24	-34.3	0.44	-33.7	0.14	-32.5	0.53
2014	right	14	-31.8	0.29	-33.0	0.73	-34.3	0.03	-33.6	0.05	-32.8	0.79
2014	left	0.5	-33.1	0.14	-33.3	0.11	-35.3	0.36	-33.9	0.19	-33.6	0.44
2014	left	7	-31.4	0.01	-32.4	0.11	-33.9	0.16	-33.6	0.09	-32.4	0.21
2014	left	14	-31.6	0.27	-32.4	0.03	-34.2	0.41	-33.5	0.20	-32.5	0.53
2014	middle	0.5	-33.5	0.38	-33.3	0.04	-34.6	0.16	-33.7	0.17	-33.7	0.45
2014	middle	7	-31.4	0.03	-32.3	0.02	-34.2	0.39	-33.8	0.03	-32.5	0.39
2014	middle	14	-31.1	0.05	-31.9	0.05	-33.4	0.13	-33.5	0.07	-32.1	0.17
2014	middle	26	-32.0	0.28	-32.6	0.08	-34.1	0.28	-33.7	0.17	-32.8	0.44

Table B.5.4. Compound-specific FA ^{14}C in depth profile SPM. $\Delta^{14}C$ of combined n-$C_{24\text{-}30}$ FAs.

year	profile	depth [m]	$\Delta^{14}C$ n-$C_{24\text{-}30}$ [‰]	$\Delta^{14}C$ ± [‰]
2013	right+middle+left	0.5	-123	31
2013	middle	7	-129	8
2013	middle	14	-183	8
2013	middle	21	-121	8
2014	right+left	0.5	-182	9
2014	right+left	7	-151	9
2014	right+left	14	-137	8
2014	middle	0.5+7	-135	8
2014	middle	14+26	-131	8

Table B.5.5. BrGDGT composition of SPM in depth profiles.

year	profile	depth [m]	brGDGT [ng/L]	isoGDGT [ng/L]	Cren. [ng/L]	BIT	MBT'	MATmr [°C]	CBT'	brGDGT-pH	IR	$\#rings_{tetra}$
2013	left left	0.5	37.8	10.2	2.3	0.92	0.25	9.6	0.23	7.5	0.69	0.48
2013	right	0.5	42.5	12.3	2.7	0.91	0.25	9.3	0.22	7.5	0.68	0.48
2013	right	5	54.3	15.6	3.6	0.91	0.25	9.3	0.24	7.5	0.69	0.47
2013	right	10	29.2	9.0	2.1	0.91	0.24	9.4	0.24	7.5	0.71	0.49
2013	left	0.5	62.5	18.2	4.4	0.91	0.25	9.2	0.22	7.5	0.68	0.48
2013	left	5	38.9	11.8	2.8	0.91	0.25	9.2	0.22	7.5	0.67	0.48
2013	left	10	61.3	18.5	4.4	0.91	0.25	9.1	0.21	7.5	0.67	0.48
2013	middle	0.5	26.6	7.4	1.8	0.91	0.25	9.3	0.22	7.5	0.67	0.48
2013	middle	7	47.5	14.7	3.5	0.91	0.25	9.3	0.23	7.5	0.69	0.49
2013	middle	14	52.8	16.4	4.0	0.90	0.24	9.1	0.22	7.5	0.67	0.48
2013	middle	21	37.4	11.3	2.7	0.91	0.25	9.1	0.21	7.5	0.67	0.47
2014	right right	0.5	25.7	7.4	2.5	0.88	0.28	9.8	0.18	7.4	0.66	0.48
2014	left left	0.5	12.8	4.3	1.4	0.86	0.24	9.0	0.20	7.5	0.67	0.44
2014	right	0.5	23.7	6.8	2.2	0.88	0.30	10.0	0.19	7.4	0.67	0.48
2014	right	7	33.6	10.0	3.2	0.88	0.28	10.2	0.20	7.5	0.68	0.49
2014	right	14	26.2	8.7	2.8	0.87	0.25	9.1	0.21	7.5	0.67	0.46
2014	left	0.5	17.9	5.3	1.7	0.88	0.29	10.1	0.18	7.4	0.68	0.48
2014	left	7										
2014	left	14	29.0	9.7	3.1	0.87	0.25	9.0	0.19	7.4	0.67	0.45
2014	middle	0.5	25.4	7.6	2.4	0.88	0.29	10.2	0.18	7.4	0.67	0.47
2014	middle	7	34.0	10.8	3.4	0.87	0.29	10.1	0.18	7.4	0.67	0.48
2014	middle	14	38.0	11.6	3.6	0.88	0.29	10.1	0.18	7.4	0.67	0.48
2014	middle	26	40.6	12.5	3.9	0.88	0.31	10.0	0.17	7.4	0.66	0.48

Table B.5.6. Relative abundances of brGDGTs in depth profile SPM.

year	profile	depth [m]	rel-Ia	rel-Ib	rel-Ic	rel-IIa	rel-IIa'	rel-IIb	rel-IIb'	rel-IIc	rel-IIc'	rel-IIIa	rel-IIIa'	rel-IIIb	rel-IIIb'	rel-IIIc	rel-IIIc'
2013	left left	0.5	0.14	0.08	0.02	0.10	0.19	0.05	0.13	0.00	0.01	0.07	0.17	0.01	0.02	0.00	0.00
2013	right	0.5	0.14	0.08	0.02	0.10	0.19	0.05	0.11	0.01	0.01	0.08	0.17	0.01	0.02	0.00	0.00
2013	right	5	0.14	0.08	0.02	0.10	0.19	0.04	0.12	0.00	0.01	0.07	0.18	0.01	0.02	0.00	0.00
2013	right	10	0.14	0.08	0.02	0.10	0.19	0.05	0.12	0.00	0.01	0.08	0.18	0.00	0.02	0.00	0.00
2013	left	0.5	0.14	0.08	0.02	0.11	0.19	0.05	0.12	0.01	0.01	0.07	0.17	0.01	0.02	0.00	0.00
2013	left	5	0.14	0.08	0.02	0.11	0.19	0.05	0.11	0.01	0.01	0.08	0.18	0.01	0.02	0.00	0.00
2013	left	10	0.14	0.08	0.02	0.11	0.19	0.05	0.11	0.01	0.01	0.07	0.17	0.01	0.02	0.00	0.00
2013	middle	0.5	0.14	0.08	0.02	0.10	0.19	0.05	0.11	0.01	0.01	0.07	0.17	0.01	0.02	0.00	0.00
2013	middle	7	0.14	0.08	0.02	0.10	0.19	0.05	0.12	0.00	0.01	0.07	0.17	0.01	0.02	0.00	0.00
2013	middle	14	0.14	0.08	0.02	0.11	0.19	0.05	0.12	0.01	0.01	0.07	0.17	0.01	0.02	0.00	0.00
2013	middle	21	0.14	0.08	0.02	0.11	0.19	0.05	0.12	0.01	0.01	0.07	0.17	0.01	0.02	0.00	0.00
2014	right right	0.5	0.16	0.09	0.02	0.11	0.19	0.06	0.12	0.01	0.01	0.07	0.14	0.01	0.02	0.00	0.00
2014	left left	0.5	0.14	0.08	0.01	0.11	0.19	0.05	0.12	0.01	0.01	0.08	0.16	0.01	0.03	0.00	0.00
2014	right	0.5	0.16	0.09	0.02	0.10	0.19	0.05	0.13	0.01	0.01	0.07	0.14	0.01	0.02	0.00	0.00
2014	right	7	0.16	0.09	0.02	0.10	0.18	0.05	0.13	0.01	0.01	0.07	0.14	0.01	0.02	0.00	0.00
2014	right	14	0.15	0.08	0.02	0.11	0.20	0.05	0.12	0.01	0.01	0.07	0.15	0.01	0.02	0.00	0.00
2014	left	0.5	0.16	0.09	0.02	0.10	0.18	0.05	0.13	0.01	0.01	0.07	0.14	0.01	0.02	0.00	0.00
2014	left	7															
2014	left	14	0.15	0.08	0.01	0.11	0.19	0.05	0.13	0.01	0.01	0.07	0.15	0.01	0.02	0.00	0.00
2014	middle	0.5	0.17	0.09	0.02	0.10	0.18	0.05	0.12	0.01	0.01	0.07	0.14	0.01	0.02	0.00	0.00
2014	middle	7	0.16	0.09	0.02	0.10	0.18	0.05	0.13	0.01	0.01	0.07	0.14	0.01	0.02	0.00	0.00
2014	middle	14	0.17	0.09	0.02	0.11	0.19	0.05	0.12	0.01	0.01	0.07	0.14	0.01	0.02	0.00	0.00
2014	middle	26	0.17	0.09	0.02	0.11	0.18	0.06	0.12	0.01	0.01	0.06	0.13	0.01	0.02	0.00	0.00

Chapter 6

Conclusions and Outlook

6.1 Conclusions

In this thesis, the composition of organic carbon (OC) in river sediment was studied along the course of the Danube River. Key aspects that were addressed to better constrain the amount and composition of OC that is ultimately exported to the ocean are (i) the sources contributing to the OC load in river sediment, (ii) the evolution of the OC signal as it evolves during transport within the catchment, and (iii) the timescale of transportation from the biological source to the sedimentary sink.

Finding that about 8 kg OC per second in the suspended particulate matter (SPM) load of the Danube are exported during high water conditions shows that rivers constitute an active conveyor belt, exporting significant amounts of OC from the continents to the ocean that has to be considered in the global carbon cycle.

6.1.1 Sources of OC to Danube sediments

The structural distribution of branched glycerol dialkyl glycerol tetraethers (brGDGTs) in river sediment that was recently deposited on riverbanks as well as in SPM shows that brGDGTs are mainly soil derived with a minor contribution of in-river produced brGDGTs. This *in situ* contribution was not found to significantly alter the total brGDGT-derived signal and therefore it is concluded that brGDGTs can be used as marker compounds for soil derived OC in Danube sediments.

The long chain plant wax fatty acid (FA) concentration evolves in line with the brGDGT concentration and therefore it is suggested that these two biomarkers have a common main source (i.e. soil) or a constant relative contribution of different sources (including soil, *in situ* production and fresh plant input). The strong relationship of FAs, brGDGTs and total organic carbon (TOC) content to mineral specific surface area (SA) and the systematic evolution of these concentrations normalized to SA along the river reveals that the majority of the OC is associated with the mineral phase. This further supports the finding that the OC in the river sediment was stored in a reservoir such as soil, where organo-mineral interactions were formed prior to erosion and transport to the river system. Lignin on the other hand shows less association to minerals, implying that a higher proportion of lignin is transported as discrete plant debris.

With a mixing model based on bulk $\delta^{13}C$ and $\Delta^{14}C$, C3 plant derived biospheric carbon was shown to be the main contributor of OC to the river sediment. Loess, i.e. abundant fine-grained sediment in the middle and lower basin, was included as possible carbon source and shows significant contribution of up to 37% at the mouth of the river. C4 plant derived biospheric carbon as well as petrogenic OC are minor contributors to the total OC in Danube sediments. However, the presence of loess as a significant OC source with ages that span from about 6,000 years to more than radiocarbon dead complicates the quantification of sources based on ^{14}C measurements.

6.1.2 Timescale of OC transport

Ages of bulk OC and FAs increase along the Danube while there is a 70–80% linear decrease in TOC, FA and brGDGT loadings on mineral surfaces (i.e. concentrations normalized to SA). Following these trends, the transport time for TOC and FAs in the Danube catchment is determined to 2,130 and 2,790 years, respectively. On such timescales, degradation leads to a net OC loss and potential preferential removal of young and more labile carbon leads to increasing overall ages. Therefore, degradation and the constant addition of pre-aged carbon along the way most likely lead to an overestimation of the calculated transport time. Although quantification of loss due to degradation is not possible with the data available, it is concluded that aging and degradation are significant and influence the OC signal exported to the Black Sea.

6.1.3 A basin integrating OC signal?

The brGDGT-derived mean annual temperature as well as compound-specific FA $\delta^{13}C$ and $\delta^{2}H$ follow the trends of local conditions along the river. Together with decreasing TOC, FA and brGDGT loadings on mineral surfaces, we conclude that most of the upstream signal is lost by the time it would reach the terminus of the river. Hence, the significant addition of high SA, low TOC loess leads to continuous dilution and replacement of the OC in the river sediment by a local signal. The OC that is finally exported to the Black Sea is therefore dominated by lower basin input and the area for down core paleo-environmental reconstructions in Black Sea sediments is limited to the lower reaches of the Danube basin.

6.1.4 OC exported to the Black Sea

Analyzing SPM in depth profiles across the Danube close to its terminus shows that the river is well mixed with minor variations in composition with depth, across the river and between years. Only bulk OC ages were significantly higher with higher discharge, reflecting the higher relative contribution of pre-aged material. FAs exported to the Black Sea show an average age of 1,166 years, which is comparable to FAs in Black Sea surface sediments close to the Danube. Finally, instantaneous fluxes to the Black Sea were determined to 8 kg/s TOC, 7 g/s long-chain FAs (n-$C_{24\text{-}30}$; LCFA), 34 g/s short-chain FAs (n-$C_{16\text{-}18}$; SCFA) and 0.5 g/s brGDGTs in 2013 and 7 kg/s TOC, 3 g/s LCFAs, 21 g/s SCFAs and 0.2 g/s brGDGTs in 2014, making a step towards the quantification of OC and biomarker fluxes from continents to oceans.

6.2 Outlook

This thesis gives detailed insight on the composition and evolution of organic carbon in Danube River sediments and contributes to the overall understanding of rivers as important land to ocean transport mechanism for terrigenous organic carbon. Nevertheless, the understanding of riverine OC transport is still in its infancy (Diefendorf and Freimuth, 2017) and many open questions remain. As for the Danube, sources of OC and the loss due to degradation would have to be better constrained.

6.2.1 Organic carbon sources

Most provenance studies, including this thesis, investigating OC sources to river sediments conclude that soil is the main contributor. Loess has not been included as discrete source in mass balance calculations in previous studies although it is abundant in semi-arid grassland or steppe regions in many parts of the world, including e.g. Eastern Europe, Russia, China (Pécsi, 1990). Localization and quantification of loess erosion and better constraints on the loess composition is needed to assess the significance of loess input to the river system. By analyzing organic carbon and biomarker characteristics as well mineralogical parameters of loess it might be possible to define a more loess-specific parameter than ^{14}C composition that is independent from the wide timespan of deposition.

Apart from studying loess, it would be interesting to study the evolution of OC in the sediment of a river that is not influenced by loess input. In such a setting, the evolution of OC and biomarker loadings on mineral surfaces should be investigated and compared to loadings observed in Danube sediments. This would give information about the influence of loess input on the decreasing loadings trend along the Danube. Furthermore, it would in general be interesting to see if the biomarker loading ranges as proposed in chapter 3 of this thesis are applicable to other rivers.

Radiocarbon dating of brGDGTs (Birkholz et al., 2013) and comparison of the brGDGT and FA radiocarbon evolution along the river would give another layer of information about the common (soil) source. Furthermore, brGDGT ^{14}C data could give insights to whether the brGDGTs show a pre-aged signal as would be expected for soil input or modern for *in situ* produced brGDGTs.

A further approach to investigate sources of OC in soils is based on the chain lengths distribution of fatty acids as described by Schäfer et al. (2016). They find that deciduous forest soils are often dominated by *n*-C_{28} FAs, conifer forests by *n*-C_{24} FAs and grasslands by *n*-C_{32} and *n*-C_{34} FAs. Three indices are proposed to represent the contribution of these different vegetation types (Schäfer et al., 2016) and could be tested for application in river sediments.

6.2.2 OC loss due to degradation during transport

The identification and quantification of OC loss due to degradation during transport along the river is an unsolved problem in provenance studies and needs further investigation. One possible approach would be to perform soil incubation experiments with river water to investigate the persistence of organo-mineral associations in the aquatic environment and the change in concentration and composition of different biomarkers with time, as done in Peterse et al. (2015) for the GDGT distribution in soils, in Karlsson et al. (2015) for OC in the marine environment and in Ward et al. (2016) with ^{13}C labeled substrate.

A second approach is to use a biomarker that enters the river system at a point source and to follow this marker along the river. A possibility would be biomarkers that are specific for conifers, i.e. abietic and dehydroabietic acid with the degradation product retene (Buggle et al., 2015). In the Danube basin, conifers are present in higher elevations in the Alps and Carpathian Mountains serving as two point sources of conifer markers. However, only considering the abundance of conifer markers would again lead to the problem of dilution with downstream carbon and complicate loss quantification. Therefore, the $\delta^{13}C$ signal of these compounds should additionally be followed along the river that might show enrichment due to preferential degradation of more depleted carbon.

6.2.3 Determination of OC and biomarker fluxes to the Black Sea

In chapter 5 of this thesis, OC and biomarker fluxes close to the Black Sea were determined during high water conditions. Determining fluxes at low water conditions as well would be key to approximate yearly fluxes of these compounds. Additionally, including OC and biomarker concentrations of bed load sediments as the lowest data point in the extrapolation would improve the extrapolation to the river cross-section and make it more robust.

SA measurements on SPM would be useful to compare loadings of OC/SA ratio in bank sediments and SPM. Since large amounts of sample (up to about 1 g) are needed for SA measurements with the facilities in the Biogeoscience lab at ETH, we will have to find a possibility to measure SA on smaller samples as was for example done on SPM of the Madre de Dios River by Feng et al. (2016) with sample sizes of 0.1–0.3 g. An alternative to SA measurements would be to measure Al/Si ratios on riverbank sediments and test the correlation to SA as suggested by Bouchez et al. (2014). If these two parameters correlate well, Al/Si ratio could as well be measured on SPM and used to approximate SA.

To investigate if lipid biomarker proxies of SPM and recent sediment deposits on riverbanks are also comparable in upstream regions, SPM on filters from along the Danube that were collected during the same field campaigns could be analyzed and compared to the trends shown for river sediments.

As a less time consuming alternative to filtering, chemical precipitation of SPM as used in wastewater treatment plants (e.g. Rashed et al., 2013) could be tested. Due to the addition of a coagulant like alum, suspended matter flocculates and precipitates. This precipitate would have to be analyzed for TOC and biomarker composition as well as SA to see if it is comparable to SPM collected on filters.

6.2.4 Looking back

Having studied the evolution of OC in the modern Danube River, the next step would be to go back in time and study the lipid distribution in sediment cores from the Danube delta and possibly from the Iron Gate reservoir. In such records, human perturbations on the sediment discharge could be studied, i.e. the erection of large dams in the catchment, deforestation and enhanced land use (e.g. Li et al., 2015), and compared to the findings of Giosan et al. (2012). On a larger timescale, SA and OC/SA ratios could give insight in variations in loess discharge and potentially the beginning of loess deposition.

6.2.5 Further analysis of already available samples

During the two sampling campaigns, additional samples were taken that have not been analyzed so far due to time constraints. These sample sets are listed below for a complete overview of the available samples from this project.

- Over two days and in six hour sampling intervals, SPM on the Danube mainstem was collected during the 100-year flood in 2013. This time series spans the flood peak from rising to decreasing water level and can give insights on the amount and composition of OC at maximum discharge.
- At locations along the Danube where fine-grained river sediment was not available (mainly due to coarse flood deposits), SPM was collected on filters. The evolution of SPM OC and biomarker signals along the Danube could be compared to the evolution of the signal in river sediments to further investigate if river sediment composition is a good representative for SPM from the headwaters to the delta.
- In 2014, sampling of bed load in the middle of the river at the location of the depth profiles was achieved with a bed load sampler built at ETH. TOC and lipid composition of this bed load could be included in the extrapolation of SPM composition in the river cross-section (chapter 5).
- Water samples for ^{14}C measurements on dissolved organic and inorganic carbon were taken during the sampling in the upper and middle basins and in the delta in 2014.
- During both sampling campaigns in the Danube delta, river sediment from more locations than were used in this thesis were collected and could be analysed for a more complete picture of processes in the delta wetlands.

- In the delta and along the Danube and its tributaries, water samples were collected for (i) nutrient and (ii) major and trace element analysis after the WHOI sampling scheme (www.whoi.edu/rivergroup/volunteer).

References

Birkholz, A., Smittenberg, R.H., Hajdas, I., Wacker, L. and Bernasconi, S.M. (2013) Isolation and compound specific radiocarbon dating of terrigenous branched glycerol dialkyl glycerol tetraethers (brGDGTs). *Organic Geochemistry* 60, 9–19.

Bouchez, J., Galy, V., Hilton, R.G., Gaillardet, J., Moreira-Turcq, P., Perez, M.A., France-Lanord, C. and Maurice, L. (2014) Source, transport and fluxes of Amazon River particulate organic carbon: Insights from river sediment depth-profiles. *Geochimica et Cosmochimica Acta* 133, 280–298.

Buggle, B., Wiesenberg, G.L.B., Eglinton, T.I. and Lucke, B. (2015) Molecular proxies in Late Holocene soils and sediments of Jordan – Priciples, potentials and perspectives. *Erlanger Geographische Arbeiten* 42, 163–182.

Diefendorf, A.F. and Freimuth, E.J. (2017) Extracting the most from terrestrial plant-derived n-alkyl lipids and their carbon isotopes from the sedimentary record: A review. *Organic Geochemistry* 103, 1–21.

Feng, X.J., Feakins, S.J., Liu, Z.G., Ponton, C., Wang, R.Z., Karkabi, E., Galy, V., Berelson, W.M., Nottingham, A.T., Meir, P. and West, A.J. (2016) Source to sink: Evolution of lignin composition in the Madre de Dios River system with connection to the Amazon basin and offshore. *Journal of Geophysical Research: Biogeosciences* 121, 1316–1338.

Giosan, L., Coolen, M.J.L., Kaplan, J.O., Constantinescu, S., Filip, F., Filipova-Marinova, M., Kettner, A.J. and Thom, N. (2012) Early anthropogenic transformation of the Danube-Black Sea system. *Scientific Reports* 2, 1–6.

Karlsson, E.S., Bruchert, V., Tesi, T., Charkin, A., Dudarev, O., Semiletov, I. and Gustafsson, Ö. (2015) Contrasting regimes for organic matter degradation in the East Siberian Sea and the Laptev Sea assessed through microbial incubations and molecular markers. *Marine Chemistry* 170, 11–22.

Li, D., Yao, P., Bianchi, T.S., Zhao, B., Pan, H.H., Zhang, T.T., Wang, J.P., Xu, B.C. and Yu, Z.G. (2015) Historical reconstruction of organic carbon inputs to the East China Sea inner shelf: Implications for anthropogenic activities and regional climate variability. *Holocene* 25, 1869–1881.

Pécsi, M. (1990) Loess is not just the accumulation of dust. *Quaternary International* 7–8, 1–21.

Peterse, F., Moy, C.M. and Eglinton, T.I. (2015) A laboratory experiment on the behaviour of soil-derived core and intact polar GDGTs in aquatic environments. *Biogeosciences* 12, 933–943.

Rashed, I.G.A.A., El-Morsy, A. and Ayoub, M. (2013) A new approach for upgrading of sewage treatment plants to accommodate excess organic and hydraulic loads. *Journal of Water Sustainability* 3, 153–163.

Schäfer, I.K., Lanny, V., Franke, J., Eglinton, T.I., Zech, M., Vyslouzilova, B. and Zech, R. (2016) Leaf waxes in litter and topsoil along a European transect. *Soil* 2, 551–564.

Ward, N.D., Bianchi, T.S., Sawakuchi, H.O., Gagne-Maynard, W., Cunha, A.C., Brito, D.C., Neu, V., Valerio, A.D., da Silva, R., Krusche, A.V., Richey, J.E. and Keil, R.G. (2016) The reactivity of plant-derived organic matter and the potential importance of priming effects along the lower Amazon River. *Journal of Geophysical Research: Biogeosciences* 121, 1522–1539.

Acknowledgements

First of all, I would like to express my sincere gratitude to my supervisor Tim Eglinton for giving me the opportunity and confidence to work on this project. This project and me as a person benefitted a lot from the fruitful discussions and meetings and I very much enjoyed the time you spent with me in the Danube delta. It was always a pleasure to work in such a friendly and positive atmosphere.

Special thank goes to my second supervisor Francien Peterse for your support and guidance and the opportunity to visit and perform measurements at the University of Utrecht. It was a pleasure to work with you at ETH and especially during the first sampling campaign in 2013 – with you and Björn, this was the best field trip ever.

I want to thank Maarten Lupker for his expertise in any modeling question and for being part of my thesis committee. Further thank goes to Thomas Bianchi who joins the examination board as external examiner.

This work would not have been possible without the funding of the Swiss National Science Foundation for the projects "CAPS-LOCK" and "CAPS-LOCK2" (#200021_140850).

The Laboratory of Ion Beam Physics is thanked for the possibility to use their labs including support and troubleshooting during radiocarbon measurements. I further want to thank Michael Plötze from the Clay Lab who gave me insights into the world of clay minerals.

Negar Haghipour is thanked for the time we spent together exploring the labs and methods when we both joined the Biogeoscience group, and later on, for her time and support in the lab. In the same category, Daniel Montluçon is thanked for the guidance in the lab and support with all chemistry and sampling related methodological questions.

Special thanks goes to the fieldwork crews of both field trips, including Björn, Alissa, James, Marilu, Clay, Thomas, Michael, Maarten, Francien, Liviu, Felipe, Silvia, Stephan, Nicole and Tim who invested a lot of effort and time in filtering.

I thank my lab and office mates Julia, Fränzi, Usman, Sascha, Reto, Thomas, Hannah, Tessa, Alissa, Lorena, Jenny, Bao and the rest of the Biogeoscience group, especially Kathrin, for the fun time we spent together.

Further thank goes to Derek Vance and Brandi Revels for giving me the opportunity to join the Amazon fieldwork and Julia for the time in Ethiopia.

I want to thank my parents Doris and Markus for their endless love and support, for giving me a secure base and wings to fly.

Great thank goes to my best friends and neighbors Katharina, Fabian and Emanuel for being part of the family, keeping me alive with uncountable dinner invitations, regular distraction with Lego and physical and mental support in every situation.

And last but not least, I want to warmly thank my girlfriend Bianca for your love, support and the wonderful time together.